19th International Conference on Sustainable Energy Technologies

16th to 18th August 2022, Turkey

Sustainable Energy Technologies 2022

Conference Proceedings – Volume 4

Reference to a conference paper:

To cite a paper published in these conference proceedings, please substitute the highlighted sections of the reference below with the details of the article you are referring to:

Author(s) Surname, Author(s) Initial(s), 2022. 'Title of paper'. In: Riffat, Su,. ed., **Sustainable Energy Technologies**: Proceedings of the 19th International Conference on Sustainable Energy Technologies, 16th – 18th August 2022, Turkey. University of Nottingham: Buildings, Energy & Environment Research Group. Pp XX-XX. Available from: nottingham-repository.worktribe.com/ [Last access date].

CONTENTS

#27: Performance evaluation of an HVAC system in a university building

Sadiye Birce ONGUN[1*], Hacer SEKERCI[2], Nurdan YILDIRIM[3]

[1]Faculty of Engineering, Department of Energy Systems Engineering, Yasar University, 35100 Izmir Turkey, birce.ongun@yasar.edu.tr
[2]Faculty of Engineering, Department of Electrical and Electronics Engineering, Yasar University, 35100 Izmir Turkey, hacer.sekerci@yasar.edu.tr
[3]Faculty of Engineering, Department of Mechanical Engineering, Yasar University, 35100 Izmir Turkey, nurdan.yildirim@yasar.edu.tr

Abstract: The aim of this study was to examine the parameters affecting energy consumption and indoor air quality in university buildings and to develop methods to improve these issues. Izmir was chosen as the target region for the research. Within the scope of the study, examinations were carried out in the selected classes in two different buildings of Yaşar University. In these classes, indoor air temperature, CO_2 concentration, and window opening data were measured and recorded at 15-minute intervals for 1 year. In addition, during the measurement process, the energy consumption data of buildings, operation conditions of the HVAC system, and occupancy data of the classes were collected. Analyses were made about the change of CO_2 concentration for the use of the measurement data collected during the lessons and exam periods. In these analyses, the effect of occupancy and window opening on the CO_2 concentration and indoor air temperature were investigated. A volume flow rate has been proposed in order for the CO_2 concentration to not exceed accepted levels, which should be 1000 ppm according to ASHRAE standards. In addition, the effect of outdoor air temperature and HVAC operating conditions on energy consumption was studied.

1. INTRODUCTION

In recent years, energy production and consumption have become among the most important issues of developed countries (Romano *et al.*, 2017). According to studies, the units that consume the most energy on a campus are buildings with more than 40% of the total energy consumed in Europe being by buildings (Li *et al.*, 2017). For this reason, increasing energy efficiency in buildings is one of the most important factors in reducing energy consumption. HVAC systems constitute approximately 50% of building energy consumption and this rate is expected to increase gradually (Yang *et al.*, 2019). Therefore, it has become an important issue to reduce the energy consumption of HVAC systems and increase the working efficiency. On the other hand, the energy consumption of buildings largely depends on the criteria used for the indoor environment (Olesen, 2007). Indoor environmental quality (IEQ) depends on many variables: temperature, relative humidity, CO_2 concentration, air flow rate, occupancy, etc. (Almeida *et al.*, 2014). These criteria significantly affect the health, comfort and performance of users. Indoor air quality (IAQ) is expressed as the temperature, humidity, ventilation and chemical substances of indoor air in non-industrial buildings such as schools, offices and hotels (Brown, 2019).

Educational buildings (school buildings and university campus buildings) are structures that require more attention in terms of indoor air quality and energy consumption compared to other buildings (Allab *et al.*, 2017). These structures have a higher number of users compared to home and office buildings (Chithra & Nagendra, 2012). There is a direct ratio between the number of users and energy consumption. IAQ and thermal comfort are the important parameters that affect the productivity and work efficiency of users. It is especially important to provide these conditions for students in educational buildings because IAQ parameters are of great importance to increase students' attention, perception and learning levels (Özdamar & Umaroğullari, 2018). High CO_2 concentration can negatively affect people's perception and cause health problems (Krawczyk *et al.*, 2016). However, when studies are examined (Dias *et al.*, 2016, Almeida *et al.*, 2014, Dias Pereira *et al.*, 2014), it can be seen that in many schools the CO_2 concentration exceeds the value specified in standards such as ASHRAE and ISO7730. As in the study of Rospi *et al.* (2017), many studies have been done to evaluate the indoor environment quality of the classrooms. When energy management is applied in buildings, energy consumption values and operating costs can be reduced (Y. Li *et al.*, 2017). In order to perform an energy audit, IAQ parameters must be measured and monitored regularly. The most up-to-date measurement method that can be used is to collect data on fixed sensor devices placed in the locations. These devices have a common cloud system and all data can be stored there.

In the detailed literature review, it was seen that the studies mainly focused on indoor air quality and reducing energy consumption. In this study, parameters such as temperature and CO_2 concentration values that affect indoor air quality in educational buildings were measured for a year and detailed analysis was made with simulations showing the change of these parameters over time in the Matlab program. The most important originality of this study was that it makes suggestions for increasing energy efficiency without disturbing the comfort conditions in the building types that are the subject of the research.

2. SYSTEM DESCRIPTION AND CURRENT OPERATION

In this study, two university buildings were compared with each other and with the classes within themselves. In this context, the parameters such as indoor temperature, humidity, CO_2 concentration and window opening that will affect the energy consumption and the comfort of the users have been examined. The effects of these parameters on energy consumption and indoor air quality are presented.

2.1. Characteristics of buildings and measured classrooms

Within the scope of the study, measurements were made in classes located on different floors and directions of 2 buildings (T and Y Buildings) of Yaşar University in Bornova/ Izmir. The locations and facade visuals of the university buildings are shown in Figure 1.
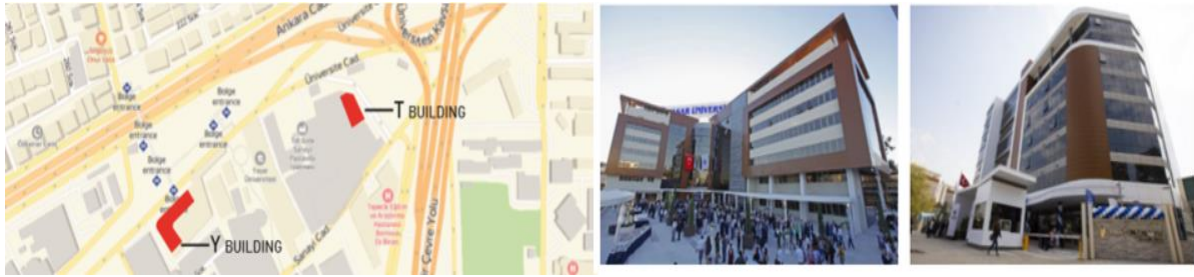
Figure 1: Monitored buildings (Y in the left, T in the right) and their locations

In Yaşar University Y Block, for an air conditioning system, a chiller was used for cooling and air handling unit and natural gas boilers for heating. In the T block, there was a VRF system which was a central system but could be used individually if desired. Capacity information of these air conditioning systems are given in Table 1.

Table 1: HVAC system information of the buildings

Y Building					T Building	
Type		Capacity [kW]	Type	Capacity [kW]	Type	Capacity [kW]
Air Handling Unit	Cooling	440.3	Chiller	750	VRF	590.832
	Heating	360.8	Boiler	5x100	Heat recovery system	673.91

2.2. Measurements and schedules

Temperature, wet bulb temperature, relative humidity, CO_2 concentration, atmospheric pressure, and open or closed windows were measured for 12 months in selected classes. The measurements made in this study focused on temperature, CO_2 intensity, and window opening. All measurements were made at 15 minutes intervals throughout the day and sent to the cloud system via Wi-Fi and recorded. The windows where the window opening were measured had approximately 1.30 m^2 area for the Y building and approximately 1.5 m^2 area for the T building. The windows open in top-hung outward type. The opening areas of the windows were approximately 0.15 m^2 and 0.1 m^2 for Y and T buildings, respectively.

Two academic semesters were examined to evaluate the times when the measured areas were used effectively. The study period of the semesters and the final exam period dates are as follows:

− Spring semester courses held between 4 February 2019 - 14 May 2019, spring semester final exams held between 20 May 2019 - 31 May 2019.
− Fall semester courses held between 16 September 2019 - 24 December 2019, fall semester final exams held between 2 January 2020 - 15 January 2020.

2.3. Energy consumption

Energy consumption information was not measured separately for each class. Information on the general amount of electricity consumed in the building Y can be accessed. Energy consumption information of the Y building was available as a monthly total consumption data. This total data included the electrical energy consumed by air handling units & fan coils and chiller (chiller, tower, pumps). In addition, the amount of natural gas used as fuel was converted into electrical energy and added to the monthly total. The monthly energy consumption of the Y building and the T building are shown in Figure 2. The consumption information in these graphs was calculated only with the electrical energy values used by the HVAC system. Averages of outside temperatures within working hours for the specified month are also shown. In addition, the mode of operation of the building's HVAC system for each building is also indicated on the graph.
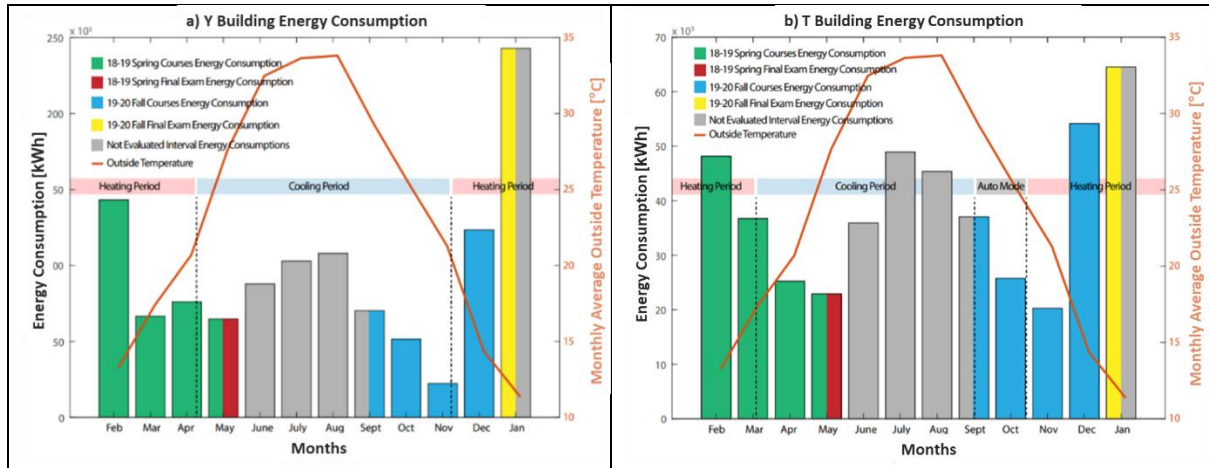
Figure 2: Monthly energy consumption of the Y building (a) and T building (b)

Since the first months of 2018-2019, the spring semester coincided with the months of February and March and it can be read from the graph that the energy consumption was high. In these months, it can be seen that the daily consumption value was generally higher than 1500 kWh. It was clearly seen that energy consumption decreased due to not using too much HVAC system in April and May. The HVAC system had not been used very effectively since the autumn climate conditions were experienced in September, October and early November, which are the first months of the 2019-2020 Fall semester. Therefore, while the energy consumption values were stable in the first months of the graph, energy consumption increased towards the last months. The HVAC system of both university buildings was operated as a central system. At certain times of the year, the technical team changed the operating conditions of the system and these changes were made throughout the building. The operating settings of the system were determined by the outside temperature or the returns from the users. There were 3 operating modes in HVAC operating settings: heating, cooling, and auto mode. The opening and closing hours of the air conditioner were registered into the system in auto mode with the system operating automatically at these hours. Operation charts are given periodically for all modes in Table 2. In these table, the operating mode information of the system and the allowable control set temperature range in that mode are given.

Table 2: Operation table of the HVAC system (18-19 spring and 19-20 fall) of the T building

	Changing date	Working mode	Control set temperature [°C]	Explanation
Spring	04.02.2019	Heating	23-25	The system starts automatically at 7:30 in the morning and closes at 17:30.
	18.03.2019	Heating	23-25	The automatic start of the system has been closed. It is controlled manually.
	25.04.2019	Cooling	23-25	The system is set to cooling mode. Automatic operation is not activated. It is controlled manually.
	21.05.2019	Cooling	23-25	The system starts automatically at 7:30 in the morning and closes at 17:30.
Fall	16.09.2019	Auto	20-23	The system starts automatically at 8:00 in the morning and closes at 17:30. Auto mode, heat 20 and cool 23 set value adjusted.
	25.10.2019	Cooling	20-23	The automatic start of the system has been closed. It is controlled manually.
	30.10.2019	Heating	24-27	The system starts automatically at 8:00 in the morning and closes at 17:30.

3. METHODOLOGY

3.1. Comfort conditions

In this study, while evaluating the effect of indoor air quality on comfort conditions, focus was placed on CO_2 concentration and temperature parameters. It was accepted that the indoor air temperature should be higher than 20°C in order to provide comfortable conditions (Lei *et al.*, 2017; Keun *et al.*, 2015). This condition is in the range of 20-24°C in some studies (Bernardo *et al.*, 2017; Johnson *et al.*, 2018). According to EN152151, heating operative temperature should be 20°C and cooling operative temperature should be 26°C (Olesen, 2007). In many studies in the literature, it has been emphasized that the most suitable CO_2 concentration for human health effects should be less than 1000 ppm (Krawczyk *et al.*, 2016; Kapalo *et al.*, 2014; Walker *et al.*, 2017; Heebøll *et al.*, 2018). Likewise, it has been stated that the CO_2 level for lecture classrooms in ASHRAE standards may be 539 ppm (970 mg / m³) more than the CO_2 concentration value outside (Persily, 2017). The CO_2 concentration in the outside air

is considered to be in the range of 400-450 ppm (Krawczyk *et al.*, 2016; Almeida and Freitas, 2014). In this case, the acceptable amount of CO_2 concentration in class rooms was approximately 1000 ppm. In some studies, it has been said that it is an acceptable level to increase this value up to 1500 ppm (Dias *et al.*, 2016; Almeida and Freitas, 2014; Bernardo *et al.*, 2017; Johnson *et al.*, 2018).

3.2. Data analysis

Measurement data were analysed in 2 different cases. These cases contained data in the final and course periods of the classes and are as follows: the relationship between CO_2, occupancy and window opening and the relationship between temperature, occupancy and window opening. In addition, the relationship between the energy consumption of the T building and the temperature was examined under the topic Energy consumption analysis. The reason why T building was preferred at this stage was that the building's HVAC system was VRF, and the analysers in the building could only access the electricity consumption data from the mechanical system. In this section, there is a general analysis of the measurements made during the spring and fall semesters. Mean, max, min, and standard deviation values of the measured parameters for all monitoring times are given. Thus, general information about the periods followed can be obtained. Table 3 contains the values of outdoor air, indoor air, and energy consumption.

The sum of average indoor air temperature and the standard deviation value was 25.20°C for the spring semester and 25.39°C for the fall semester. In this case, it can be said that the indoor air temperature was at a high level during the lesson times. The increase in outdoor temperatures that started after March 18 caused users to run the system less. Thus, the mean plus standard deviation value was 1.20°C degrees above the comfort condition and was at an acceptable level. However, in the fall period, 1.5 months of auto mode (16 September-30 October) and 2.5 months of heating mode (30 October-15 January) were active. Looking at this period, the mean plus standard deviation value was 5.38°C degrees above the 20°C comfort condition accepted for the winter months. Therefore, it could be predicted that a value higher than required for the heating mode had been set.

Table 3: Energy consumption, inside & outside temperature values for classes

	Spring Courses (04.02.19-14.05.19)				Spring Final Exams (20.05.19-31.05.19)			
	Mean	Max	Min	StDev	Mean	Max	Min	StDev
Outside Temp. [°C]	17.15	31.5	3.76	5.38	29.52	35.9	21.9	2.32
Inside Temp. [°C]	23.79	28.8	18.23	1.41	25.5	28.98	23.55	1.13
Energy Cons. [kWh]	884.07	2530.53	109.08	603.48	831.53	1179.03	176.76	323.80

	Fall Courses (16.09.19-24.12.19)				Fall Final Exams (02.01.20-15.01.20)			
	Mean	Max	Min	StDev	Mean	Max	Min	StDev
Outside Temp. [°C]	20.99	31.4	7	5.40	9.67	14.2	5	2.19
Inside Temp. [°C]	23.89	28.58	19.21	1.5	22.48	28.59	16.71	2.44
Energy Cons. [kWh]	836.02	2339.44	112.96	558.81	2092.02	3381.87	373.06	1039.34

3.3. CO_2 concentration calculation

CO_2 concentration value was measured in the classrooms. The CO_2 concentration in these measurements was supported by a mathematical model. This calculation was developed by the mass balance equation of CO_2 gas (Almeida and Freitas, 2014).

Equation 1: analytical solution achieved by mass balance equation of a ventilated area $C(t) = C_{ex} + \frac{G}{Q} + \left(C_0 - C_{ex} - \frac{G}{Q}\right)e^{-\left(\frac{Q}{V}\right)t}$

where:

- $C(t)$ = concentration of CO_2 at t (ppm)
- C_{ex} = the outdoor carbon dioxide concentration (ppm)
- C_0 = initial carbon dioxide concentration in zone (ppm)
- G = generation rate of carbon dioxide (m³/h)
- V = volume of the zone (m³)
- Q = volume flow rate into a zone (m³/h)

Equation was based on the calculation. The values obtained as a result of this formula were calculated using MATLAB software. By establishing a loop in MATLAB, CO_2 concentration change was found in the desired time interval. If there were no users to emit CO_2 in the environment during a test, the CO_2 concentration in the indoor and outdoor environment was expected to be close to each other. Thus, when the CO_2 production rate and the amount of outdoor CO_2 concentration were ignored, the equation can be simplified as follows:

Equation 2: the equation required to calculate the amount of ventilation in an environment $\frac{Q}{V} = n = \frac{ln\left(\frac{c_0}{c(t)}\right)}{t}$

Where:

- n is the air change rate (ACH).

In the calculation, the change of CO_2 concentration in the first condition over time was recorded and the slope of the linear graph of the change gave the number 'n'.

4. RESULT AND DISCUSSION

This study focused on examining the parameters of temperature, CO_2 concentration, and window opening. There were a total of 6 classrooms (2 in the Y building and 4 in the T building) where all of the environment parameters and the number of people in the classes could be recorded. For this reason, the data presented throughout the study were examined in these 6 classes. In this chapter, the measurement data collected were analysed. Secondly, the effect of the energy consumption data and the HVAC system operating modes were analysed in more detail. Finally, a detailed review was made on the CO_2 concentration parameter.

4.1. Measurement data

In this section, the measurement values of the classes examined are presented with graphics. The examinations were first made on a class basis. In the examinations made in the classrooms, the focus was on the values of CO_2 concentration, temperature, window opening, and occupancy.

While creating the graphics in this section, since the occupancy rate was known, it was primarily examined with the data of the final period. Only measurement data of the exam days were used. The occupancy rate of the Y214 class in the fall final semester was compared with the CO_2 density, indoor/outdoor temperatures and window opening data, respectively, and shown in Figure 3.
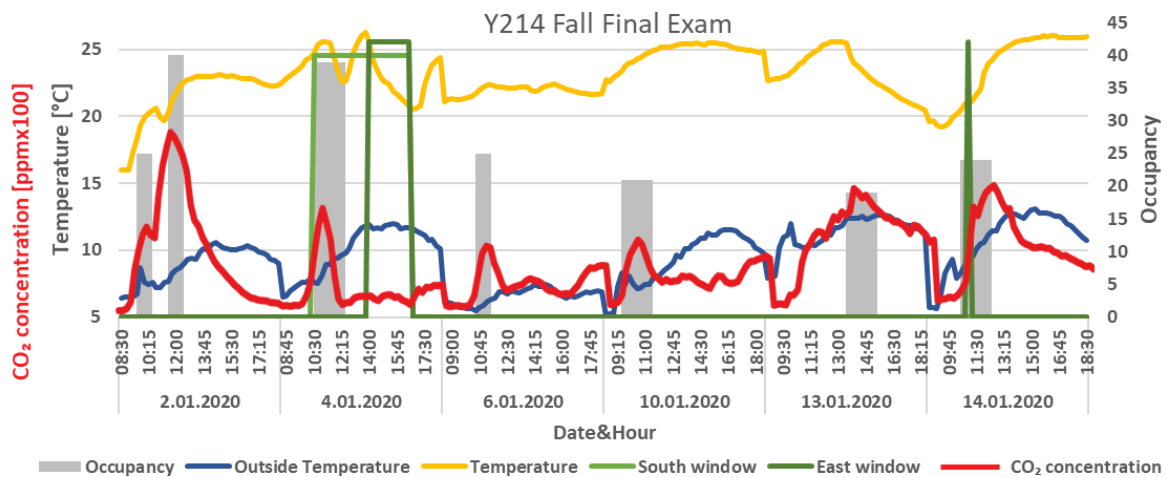
Figure 3: CO_2 concentration and classroom occupancy in Y214 for fall final exam period

In Figure 3, looking at the period when exams were held in the classroom, it was clearly seen that the concentration of CO_2 increased rapidly when there were students in the classroom. Since the examined dates were in January, the outside temperature was low and the windows are not opened very often. On the other days, the decrease in CO_2 intensity coincided with the middle of the occupancy block, and after a class evacuation, it proceeded with a

slow slope. This was due to the fact that there were more students in the classroom in the first minutes of the exams. However, when the days with window openings are examined, it was seen that there was a rapid decrease in CO_2 concentration by opening the window. For example, on 13.01.2020, it took approximately 3 hours for the CO_2 concentration, which increased to 1500 ppm during the exam, to fall back to 500 ppm. However, approximately 30 minutes was enough for the value, which reached 1300 ppm on 4.01.2020 with the windows open, to decrease to 500 ppm.

In addition, temperature measurement data were examined for the final and course periods of the classes with the data of indoor temperature changes with the effect of outdoor temperature, person density, and window opening being analysed. When Figure 3 is analysed, it can be seen that the indoor temperature created curves similar to the outdoor temperature. It can be said that the outside air temperature directly affected the indoor air conditions. At times when students were present in the classes, the temperature increased by an average of 3-4°C compared to the previous situation. As expected, a sudden drop in temperature was observed as soon as the window was opened. When the single window was opened, the decrease in temperature was 2-3°C, while in the scenario where the double window was open, this amount was 5-6°C.

4.2. Energy consumption analysis

Since the heating and cooling processes in the T building were provided by VRF system, a large part of the electricity consumption was caused by the HVAC system. The mechanical measurements of the analysers in the building showed the electrical energy consumed by the HVAC system. In this section, electricity consumption is examined according to the operating conditions. Figure 4 shows the energy consumption throughout the T building in a 2-week period - Monday to Friday. In the week starting on 11.03.2019, the mode of the HVAC system was programmed for automatic operation at 7:30 in the morning as in previous weeks. In the week beginning Monday, 18.03.2019, the automatic operation setting was closed and the system was controlled manually. The reason for this process was the increase in the average of outside temperature. When the daily consumption values were collected for both weeks without taking into account the weekends, the result were: 6848.81 kWh in the first week and 4363.55 kWh in the second week. In summary, just turning off the automatic operation setting of the system achieved a 36.2% reduction in energy consumption.
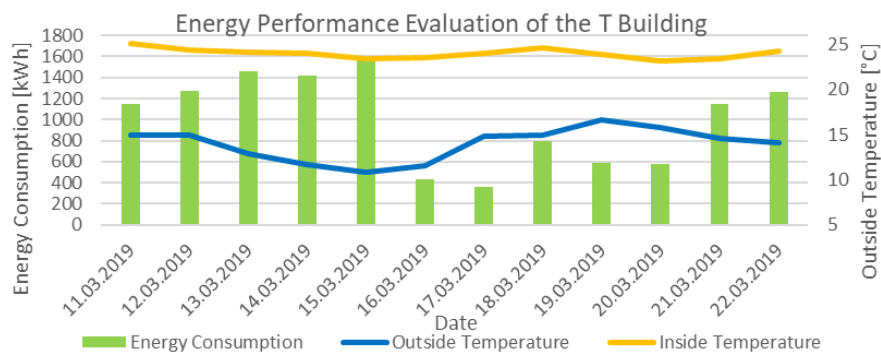
Figure 4: Energy performance evaluation according to heat mode change in the T building

Figure 4 summarizes the week after the automatic system was shut down for the first time. In this process, the increase of outside temperature also had an effect on the decrease of energy consumption. Table 4 examines 3 weeks before and after automatic operation was turned off.

Table 4: 6-week time monitoring of system activation mode change

	The day that week begins	Total weekly energy consumption [kWh]	Outside temp. average [°C]
Auto	25.02.2019	10734.53	8.77
	04.03.2019	6905.71	14.49
	11.03.2019	6848.81	13.06
Manuel	18.03.2019	4363.55	15.23
	25.03.2019	5404.11	13.44
	01.04.2019	4752.21	15.01

Looking at the dates of 15.03.2019 and 29.03.2019, it was observed that the outside temperature averages were very close for these two days. Energy consumption was 6848.81 kWh and 5404.11 kWh, respectively. In this case, it can be said that for the cases where the effect of the outside temperature factor impact was less, approximately 21% energy reduction was achieved by manually controlling the system.

4.3. CO_2 concentration analysis

Table 5 summarizes the CO_2 concentration analysis for the final exam period. Only the final exam times in the classrooms were used when creating the analysis table. It is clearly seen that when the volume and occupancy ratio decreased, the CO_2 concentration in the classrooms increased.

Table 5. CO_2 concentration analysis for the final exam period

	18-19 Spring Final Exam				19-20 Fall Final Exam			
	<1000 ppm	<1500 ppm	>1500 ppm	**Volume/ occupancy**	<1000 ppm	<1500 ppm	>1500 ppm	**Volume/ occupancy**
T214	45.74	64.89	35.11	**9.95**	69.23	90	10	**10.6**
Y214	79.84	98.45	1.55	**11.74**	41.18	90.20	9.80	**12.58**

A loop was created by using Equation 2 in MATLAB software. Thanks to this software, CO_2 concentration values in the classes have been estimated. A class with the same floor and direction was chosen from Y and T buildings (Y214 and T214). In the study, the air flow rate was not regularly measured and recorded. Therefore, the air flow rate was not known precisely. While modelling using Equation 2, the air flow rate and ACH were calculated. The number of people, one of the parameters that most affect the CO_2 concentration, was also not measured regularly. For this reason, examinations were carried out considering that most of the enrolled students would attend the final exam. However, students did not stay in the classroom during the entire exam period. Exams usually take 110 minutes and after about 45 min, 10% of the participants had left the class. In the last 15 minutes of the exam, only 10% of the class remained in the class. The number of people in the class was determined to fit the rates shown.

In each class, 3 exam times with the same number of people and with the same exam time were chosen on different days. The window opening situation was different in each of these 3 exams. Thus, the effect of window opening on the amount of CO_2 was examined. Date, time, number of users, window opening status and average CO_2 concentration values of the exams are given in Table 6.

According to Krawczyk *et al.* (2016) and Johnson *et al.* (2018), the air exchange rate (ACH) per hour in classes should be between 1 h^{-1} and 4 h^{-1}. First, the CO_2 concentration change charts were created by selecting the ACH value between 1 h^{-1} and 4 h^{-1} in the studied classes. Later, these curves were examined and ACH value was found to provide the level of CO_2 concentration in the standards. The fact that the number of open windows in the classrooms was different changed the amount of fresh air entering the interior environment. However, this situation varied according to the weather conditions. While creating all the graphs in this study, the weather conditions were considered constant and the values were calculated accordingly. Errors caused by outside weather conditions were neglected.

Table 6: Exam date, CO_2 concentration and window opening information in Y214 and T214 for 3 exams

Class	Exam Date	Exam Hour	Occupancy [ppm]	Window Condition	CO_2 Conc. Average [ppm]
Y214	21.05.2019	15:30-17:30	29	1 window open	795.12
	28.05.2019	14:30-16:30	29	no window open	1348.25
	29.05.2019	9:30-11:30	29	2 window open	619.5
T214	27.05.2019	11:00-12:30	29	1 window open	946.71
	23.05.2019	15:00-16:30	29	no window open	2118
	21.05.2019	15:00-16:30	30	2 window open	815.57

For the cases of T214 class 1 window open and 2 window open, ACH rate and CO_2 concentration change curves are given in Figure 5. The ACH value shown in red in the graphs examined is the value required for the CO_2 concentration of the class to remain at the limit level. For the T214 class, the optimum ACH value was found 2.8 h^{-1} in a 29-person exam. The 1000 ppm limit was not exceeded in cases where windows were open. However, where the CO_2 concentration initial value was greater than 1000 ppm, 1 hour was required to decrease to the limit level.
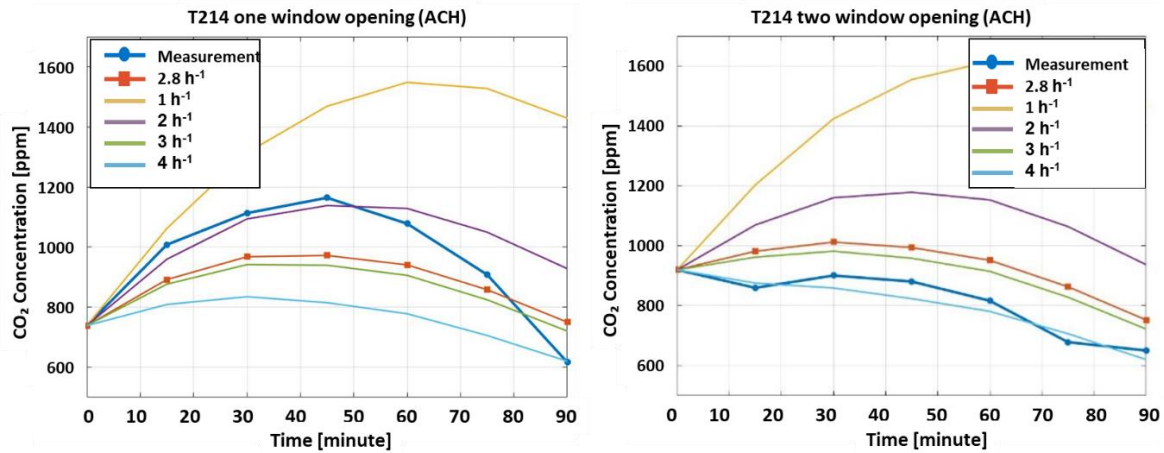
Figure 5: CO$_2$ curves for different ACH values (Occupancy=29)

A re-evaluation was made for the class named T214 from the examined classes. The reason for choosing T214 was that the ventilation system was located throughout the T building. Thus, the capacity adequacy of the ventilation system had been benchmarked. In the T214 class, there were 3 vents that blow fresh air inside and 3 exhaust the air inside. Each of these vents had an adjustable airflow rate from 200 m³/h to 500 m³/h. The air flow rate of the ventilation system in the class was modelled from the lowest level (600 m³/h) to the highest level (1500 m³/h). Curves showing the change of CO$_2$ concentration in the environment according to the air flow rate are given in Figure 6.
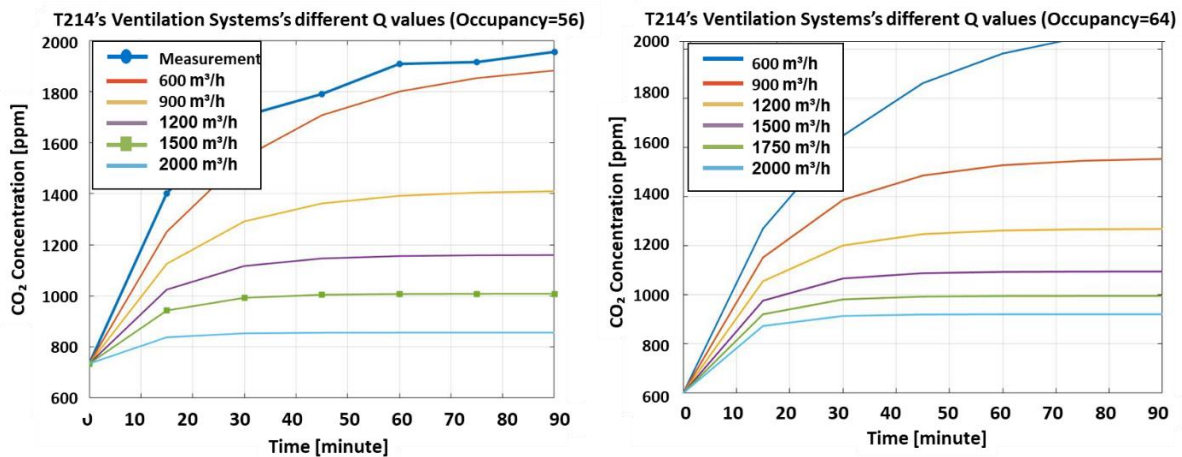
Figure 6: T214 Ventilation system's different Q values according to 56 and 64 user occupancy

In addition, an air flow rate (2000 m³/h) above the system capacity was shown in the graph to interpret the system capability. It was observed that the windows were closed during the 90-minute lesson. The CO$_2$ concentration measured in the classroom has exceeded 1800 ppm. However, when the curves were examined, it was seen that the CO$_2$ level conforms to the standards level when the system operates at full capacity. In addition, it was observed that when the ventilation system is operated at minimum flow rate, values close to the measurement data are formed. Considering this situation, it can be said that the ventilation system was in operation but it operated at low capacity. For the same class, the actual user capacity of the class was taken into account and CO$_2$ concentration change curves were modelled at different flow rates. These curves are shown in Figure 6. As a result of modelling, the number of people was fixed at 64, the windows were closed and the initial CO$_2$ concentration was 600 ppm, and the maximum capacity of the ventilation system was determined as 1500 m³/h. Looking at this value, it was seen that the air flow was not sufficient. When the air flow rate was 1500 m³/h, the CO$_2$ concentration had increased to a maximum of 1100 ppm. For some sources, this was an acceptable level (Almeida and Freitas, 2014, Johnson *et al.*, 2018, Bernardo *et al.*, 2017). The air flow rate required for the CO$_2$ level to not exceed 1000 ppm was found to be 1700 m³/s in conditions where the class chosen as the subject was 262 m³ and accommodated 64 people.

5. CONCLUSION

As a result of the rapidly increasing developments in the field of technology on a global scale, the energy needs of all countries will increase. Approximately more than half of the energy consumption in buildings arises from HVAC systems. In this study, examinations on energy consumption and indoor air quality in education buildings were conducted.

- It was observed that there was a 50% decrease in the level of CO_2 concentration by opening the windows when the occupancy was constant for the same class.
- It was observed that the indoor air temperature of the classes was generally 1-2°C above the specified standards. The indoor air temperature did not decrease below the comfort conditions when the windows were open. The absence of a decrease in temperature meant that the heating system was working more than necessary.
- When the automatic operation setting of the HVAC system was disabled and the system turned on and off manually, a 36% decrease in energy consumption was observed. The reason for this decrease was not only the change of the operating condition, but also the change in the outside temperature.
- For the weeks when the outside temperature was the same, by switching the HVAC operating condition to manual, a 21% energy decrease was achieved in the total weekly energy consumption.
- Classes with low volume/occupancy ratio were found to have a higher level of CO_2 concentration.
- Air change rates (ACH) were found for 2 sample classes (Y214 and T214) from each building to keep the CO_2 concentration below 1000 ppm. The ACH value was 2.2 h^{-1} for Y214 and 2.8 h^{-1} for T214.
- According to the CO_2 concentration estimation curves created by taking into account the total capacity of the class T214 (64 people), the capacity of the ventilation system in the class was not sufficient. This air flow rate was found to be 1750 m^3/h.

6. REFERENCES

Allab, Y., Pellegrino, M., Guo, X., Nefzaoui, E., & Kindinis, A. (2017). Energy and comfort assessment in educational building: Case study in a French university campus. *Energy and Buildings*, *143*(2017), 202–219.

Almeida, R. M. S. F. & Freitas, D. (2014). Indoor environmental quality of classrooms in Southern European climate. *Energy & Buildings*, *81*, 127–140. https://doi.org/10.1016/j.enbuild.2014.06.020

Bernardo, H., Henggeler, C., Gaspar, A., Dias, L., & Gameiro, M. (2017). An approach for energy performance and indoor climate assessment in a Portuguese school building. *Sustainable Cities and Society*, *30*, 184–194. https://doi.org/10.1016/j.scs.2016.12.014

Brown, N. J. (2019). Indoor air quality.

Chithra, V. S., & Nagendra, S. M. S. (2012). Indoor air quality investigations in a naturally ventilated school building located close to an urban roadway in Chennai , India. *Building and Environment, 54*, 159–167. https://doi.org/10.1016/j.buildenv.2012.01.016

Dias, L., Neto, L., Bernardoc, H., Carneiro, M., & Mark, C. (2016). An integrated approach on energy consumption and indoor environmental quality performance in six Portuguese secondary schools. *Energy Research & Social Science, 32*(2016), 23–43.

Dias Pereira, L., Raimondo, D., Corgnati, S. P., & Gameiro da Silva, M. (2014). Assessment of indoor air quality and thermal comfort in Portuguese secondary classrooms: Methodology and results. *Building and Environment*. https://doi.org/10.1016/j.buildenv.2014.06.008

Heebøll, A., Wargocki, P., & Toftum, J. (2018). Window and door opening behavior, carbon dioxide concentration, temperature, and energy use during the heating season in classrooms with different ventilation retrofits—ASHRAE RP1624. *Science and Technology for the Built Environment*, *24*(6), 626-637.

ISO, E. (2005). 7730. *Ergonomics of the thermal environment—analytical determination and interpretation of thermal comfort using calculation of the PMV and PPD indices and local thermal comfort criteria, Standards Norway, Oslo, Norway*.

Johnson, D. L., Lynchb, R. A., Floyda, E. L., Wanga, J., & Bartelsa, J. N. (2018). Indoor air quality in classrooms : Environmental measures and effective ventilation rate modeling in urban elementary schools. *Building and Environment, 136*(February).

Kapalo, P., Domnita, F., & Lojkovics, J. (2014). Methodology For Calculating The Fresh Air Ventilation Airflow Rate Based On. *An International Journal for Engineering and Information Sciences, 9*(2), 89–97. https://doi.org/10.1556/Pollack.9.2014.2.9

Keun, M., Baldini, L., Leibundgut, H., & Andre, J. (2015). A novel ventilation strategy with CO_2 capture device and energy saving in buildings. *Energy and Buildings. 87*, 134–141.

Krawczyk, D. A., Rodero, A., Gładyszewska-fiedoruk, K., & Gajewski, A. (2016). CO 2 concentration in naturally ventilated classrooms located in different climates — Measurements and simulations. *Energy & Buildings*, *129*, 491–498. https://doi.org/10.1016/j.enbuild.2016.08.003

Lei, Z., Liu, C., Wang, L., & Li, N. (2017). Effect of natural ventilation on indoor air quality and thermal comfort in dormitory during winter.*Building and Environment, 125*, 240–247. https://doi.org/10.1016/j.buildenv.2017.08.051

Li, Y., Donnell, J. O., García-castro, R., & Vega-sánchez, S. (2017). Identifying stakeholders and key performance indicators for district and building energy performance analysis. *Energy & Buildings*, *155*, 1–15. https://doi.org/10.1016/j.enbuild.2017.09.003

Olesen, B. W. (2007). The philosophy behind EN15251 : Indoor environmental criteria for design and calculation of energy performance of buildings. *Energy and Buildings, 39*, 740–749. https://doi.org/10.1016/j.enbuild.2007.02.011

Özdamar, M., & Umaroğullari, F. (2018). Thermal comfort and indoor air quality. *Int. J. Sci. Res. Innov. Technol,* 5(3), 90-109.

Persily, A., & de Jonge, L. (2017). Carbon dioxide generation rates for building occupants. *Indoor air*, *27*(5), 868-879.

Romano, A. A., Scandurra, G., Carfora, A., & Fodor, M. (2017). Renewable investments: The impact of green policies in developing and developed countries. *Renewable and Sustainable Energy Reviews*, 68, 738-747.

Rospi, G., Cardinale, N., & Negro, E. (2017). In the Mediterranean climate : A case study the schools of Matera city (I). *Energy and Buildings*, *152*, 52–60.

Standard, A. S. H. R. A. E. (2010). Standard 55-2010, Thermal environmental conditions for human occupancy. *American Society of Heating, Refrigerating and Air Conditioning Engineers.*

Walker, W. S.; Lombardi W.; Lesecq, S. (2017). ScienceDirect of Distributed Model Application of Distributed Model Application of Distributed Model Application of Distributed Model and Predictive Approaches to Temperature Predictive Approaches to Temperature and Predictive Approaches to Temperature an. *IFAC-PapersOnLine*, *50*(1), 2589–2594. https://doi.org/10.1016/j.ifacol.2017.08.107

Yang, X., Zhang, S., & Xu, W. (2019). Impact of zero energy buildings on medium-to-long term building energy consumption in China. *Energy Policy*, 129, 574-586.

#49: Theoretical evaluation of minimum superheat, energy, and exergy in a high-temperature heat pump system operating with low GWP refrigerants

Adam Y. SULAIMAN[*], Donal F. COTTER, Ming J. HUANG, Neil J. HEWITT

Centre for Sustainable Technologies, Belfast School of Architecture and The Built Environment, Ulster University, Shore Road, Newtownabbey, Co. Antrim, BT37 0QB, UK
*Sulaiman-W@ulster.ac.uk

Abstract: Suitable low global warming potential (GWP) refrigerants that conform to F-gas regulations are needed to extend the operational envelope of high temperature heat pumps (HTHPs) used for industrial processes and waste heat recovery. The thermophysical properties and characteristics of these alternative working fluids need to be assessed to provide a comprehensive understanding of operational effectiveness in HTHP applications. This paper presents the results of a theoretical simulation to investigate a range of low-GWP refrigerants and their suitability to supersede refrigerants HFC-245fa and HFC-365mfc. A steady-state thermodynamic model of a single stage HTHP with internal heat exchanger (IHX) was developed to assess system cycle characteristics at temperature ranges between 60 to 80 °C heat source and 90 to 140 °C heat sink. A practical approach to maximise the operational efficiency was examined to determine the effects of regulating minimum superheat within the process and subsequent influence on energetic and exergetic efficiencies. A comprehensive map of minimum superheat across the HTHP operating variables was used to assess specific tipping points in performance at 30 and 70 K temperature lifts. Based on initial results the refrigerants HCFO-1233zd(E) and HFO-1336mzz(Z) were found to be closely aligned matches to replace refrigerants HFC-245fa and HFC-365mfc. The overall results show effective performance for HCFO-1233zd(E) occurs between 5-7 K minimum superheat, and HFO-1336mzz(Z) between 18-21 K dependant on temperature lift. This work provides a method to optimise refrigerant selection based on operational indicators to maximise overall HTHPs system performance.

1. INTRODUCTION

High temperature heat pumps (HTHPs) could offer a practical solution in many sectors to improve energy efficiency and decarbonise energy intensive industrial processes (Arpagaus, *et al.*, 2018). This technology can integrate within many industrial applications to reprocess low temperature waste heat and upgrade to useful heat up to 165°C. Increasing the operational envelope of this technology to achieve higher sink temperatures up to 200°C would greatly increase the potential suitability in a wider range of industrial processes (Arpagaus, *et al.*, 2020). The development of HTHPs to achieve high sink temperatures is greatly dependent on working fluid selected and the cycle configuration. In many research studies predominantly single stage cycles incorporating an internal heat exchanger (IHX) are used to test and assess system performance with low GWP refrigerant types *(Arpagaus, et al.*, 2018). Most HTHPs experimental studies have investigated HFO refrigerant types HCFO-1224yd(Z), HCFO-1234ze(Z), HCFO-1233zd(E), and HFO-1336mzz(Z) (Mateu-Royo, *et al.*, 2019) and natural refrigerant HC-600 (Bamigbetan, *et al.*, 2019). Alongside energetic evaluation, exergetic analysis is crucial to analyse the HTHP quality of process and determine the losses for each component. Some experimental studies have completed energetic and exergetic analysis to assess the technology's overall performance (Mateu-Royo, *et al.*, 2019) (Nilsson, *et al.*, 2017).

Theoretical simulation of different HTHP cycle configurations provides a method to model many different refrigerant types to assess performance. Arpagaus *et al.* (2018) investigated HFOs HFO-1336mzz(Z), HFO-1234ze(Z), HCFO-1233zd(E) and HCFO-1224yd(Z) comparing COP and VHC with HFC-245fa and HFC-365mfc. Bamigbetan *et al.* (2018) used theoretical modelling to assess natural, HCs, HFCs, HFO and HCFOs, identifying HC-600 and HCFO-1233zd(E) as potential candidates in HTHPs. Mikielewicz & Wajs (2019) evaluated the theoretical exergetic efficiency and exergy destruction of a single stage and cascade type of HTHP using low GWP refrigerants. They revealed that the single-stage HTHP system employing Ethanol and n-pentane showed the best exergetic efficiency and lowest exergetic destruction. Mateu-Royo *et al.* (2019) experimentally analysed the exergetic efficiency in a single cycle HTHP system using the exergy balances for each component, identifying the compressor and expansion valve with the highest potential for improvement. This paper investigated a range of various HFOs, HCFOs and HCs to determine the most suitable candidates to replace HFC-245fa and HFC-365mfc in HTHP applications. Theoretical simulation was developed to assess cycle performance based on energy and exergy analysis to evaluate the effects of minimum superheat within the cycle. Based on the theoretical simulations a practical method to estimate refrigerant operational performance was developed that may be useful to further advancement the development of HTHP systems.

1.1. Nomenclatures

Abbreviations

comp	compressor		VCC	vapour compression cycle
evap	evaporator		VHC	volumetric heat capacity
cond	condenser		**Greek symbols**	
COP	Coefficient of performance		ε	effectiveness
exp	electronic expansion valve		η	efficiency
HP	heat pump		*f*	function
HTHP	high-temperature heat pump		0	reference
IHX	internal heat exchanger		**Subscript**	
GWP	global warming potential		sink	heat sink
HCFO	hydrochlorofluoroolefin		source	heat source
HFC	hydrofluorocarbons		lift	temperature lift
HFO	Hydrofluoroolefins		Ex	exergy
PR	pressure ratio		P_{comp}	compressor power
theo	theoretical		P	pressure
suc	suction		SH	superheat
vol	volumetric		T	Temperature
min	minimum		s	entropy
			h	enthalpy

1.2. Refrigerant screening

The introduction of F-gas regulations and planned phase down of high GWP refrigerants requires the development, testing and availability of suitable commercial replacement working fluids (ASHRAE, 2019). In HTHPs, refrigerants are core to optimum cycle design, predicting the level of discharge temperature, mapping the energetic and exergetic efficiency, and selecting components (Arpagaus, *et al.*, 2018). In Table and Figure a range of potential working fluids with suitable thermophysical and environmental properties (GWP<150) are presented for HTHPs. These refrigerants currently represent the most promising replacements for HFC-245fa and HFC-365mfc that will be phased out under Fgas legislation in the EU and other developed countries.

Table 1: Thermophysical and environmental properties of selected refrigerants suitable for HTHP applications (Lemmon, et al., 2013) (UNEP, 2020). Safety group classification (ASHRAE, 2019), GWP100yrs (Myhre, et al., 2013) (AGC Chemicals, 2017).

| Type	Refrigerant	Composition	ODP	GWP$_{100yrs}$	T_c [°C]	P_c[bar]	NBP	SG
HC	R600	C_4H_{10}	0	4	152.01	37.96	0.00	A3
HC	R601	C_5H_{12}	0	5	196.56	33.58	36.10	A3
HCFO	R1224yd(Z)	C_3HF_4Cl	0.00012	1	156.00	33.30	14.00	A1
HCFO	R1233zd(E)	$C_3H_2ClF_3$	0.00034	1	166.50	36.20	18.00	A1
HFC	R245fa	$C_3H_3F_5$	0	1030	154.05	36.40	15.00	B1
HFC	R365mfc	$C_4H_5F_5$	0	794	186.85	32.66	40.00	A2
HFO	R1234ze(Z)	$C_3F_4H_2$	0	<10	150.10	35.30	9.80	A2L
HFO	R1336mzz(Z)	$C_4H_2F_6$	0	2	171.30	29.00	33.40	A1
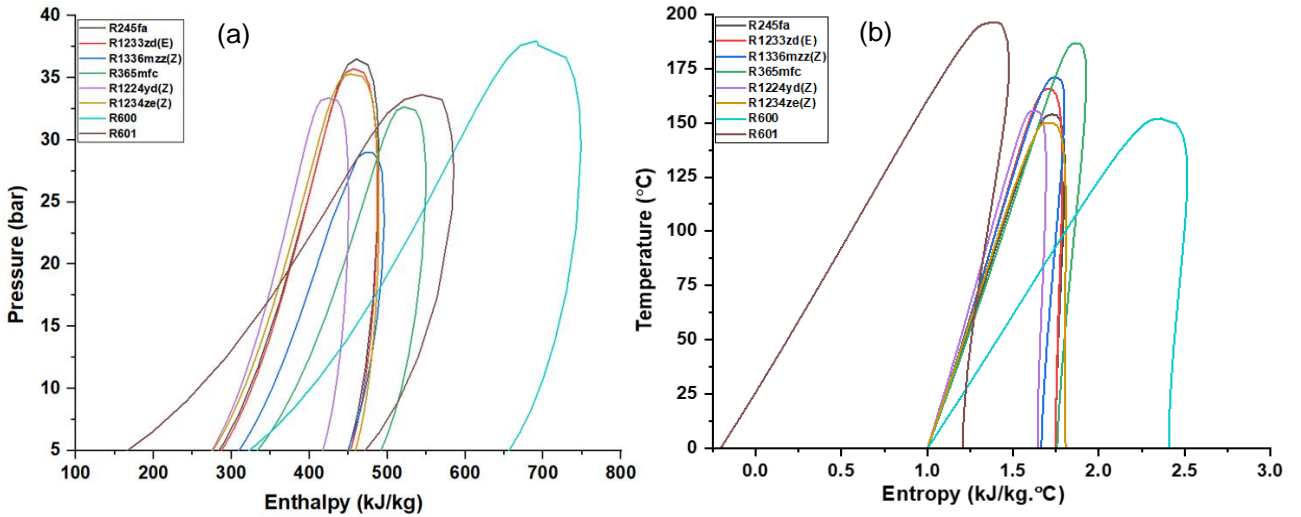
Figure 1: (a) P-h and (b) T-s diagrams for selected low GWP refrigerants that are potential alternatives to HFC-245fa and HFC-365mfc in HTHP applications (Klein, 2017) (Lemmon, et al., 2013).

The refrigerant HFO-1336mzz(Z) is non-flammable and chemically stable at high temperatures compared to other refrigerants, offering a high critical temperature of 171.30°C with a normal boiling point of 33.40°C (Kontomaris, 2014). The eco-friendly refrigerant HCFO-1233zd(E) has a higher critical temperature than HFC-245fa and offers similar thermodynamic properties and boiling heat transfer (Patten & Wuebbles, 2010). HFO-1234ze(Z) has zero ODP and less than 10 GWP value, it has a critical temperature and pressure close to HFC-245fa and has a similar vapour pressure curve, similar thermal conductivities with lower viscosities resulting in better heat transfer (Petr & Raabe, 2015). The HCFO-1224yd(Z) has an ODP value of 0.00012 and a very short molecular lifetime (20 days) resulting in a low GWP value (Eyerer, *et al.*, 2019). The A1, non-flammable HCFO-1224yd(Z) has remarkably similar critical temperature compared to HFC-245fa, with lower vapour pressure and lower critical pressure, it also has a VHC about 8.5% lower than HFC-245 operating at similar volumetric flow rates (Mateu-Royo, *et al.*, 2021). The HC-600 and HC-601 are eco-friendly substances with zero ODP and extremely low GWP, both are flammable and classified in the A3 safety group and thus increased safety measures are required for these substances (Besagni, *et al.*, 2015)

1.3. Cycle configuration

In this work theoretical simulations of the cycle configuration design and a comparison of energy and exergy results for the selected substances was performed in Engineering Equation Solver (EES) (Klein, 2017). Shown in Figure 2 are the transition points related to the different thermodynamic states and a schematic of the single-stage HTHP cycle with internal heat exchanger (IHX).
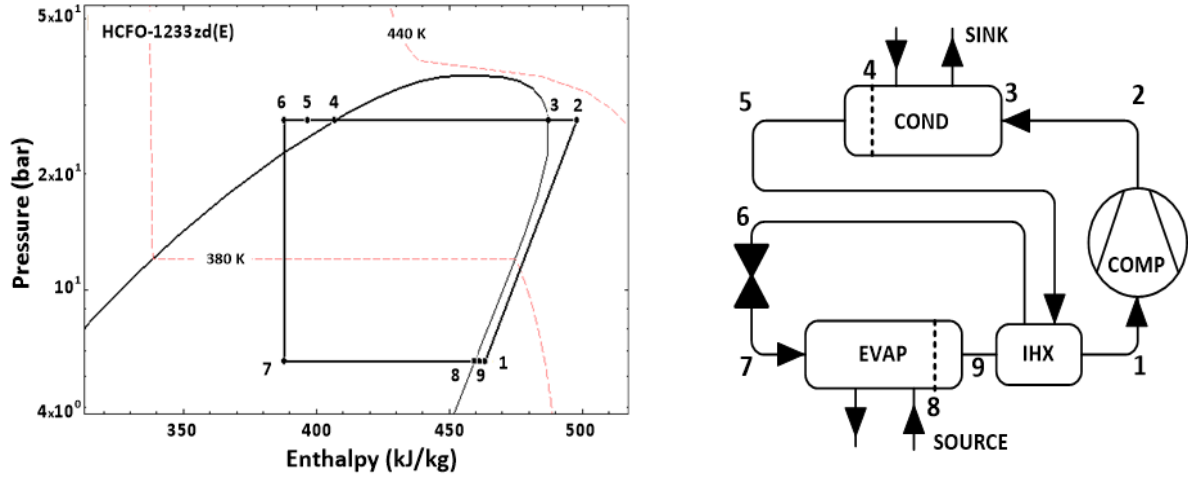
*Figure 2: The P-h diagram and schematic with transition points representing
the heat pump cycle with IHX for HCFO-1233zd(E).*

2. SIMULATION MODEL

The cycle modelling was subjected to the following specific assumptions:

- The cycle was assumed to be at steady-state conditions.

- Discharge and suction temperatures were varied according to the required minimum superheat.

- The potential and kinetic energy were neglected.
- The electromechanical efficiency was assumed to be 0.95 and ambient temperature 295.15 K.
- Pressure drops along the heat exchangers and pipelines was neglected.
- Heat dissipation from the cycle components to the surrounding was neglected.
- The expansion valve process was assumed to be isentropic, therefore, $h_5 = h_4$
- ΔT_{evap} = 3 K and ΔT_{Cond} = 4 K.
- IHX subcooling was set at 5K

The single-stage HTHP thermodynamic cycle was modelled to achieve heat sink temperatures up to 140°C, integrating an IHX to improve energetic and exergetic efficiency and to support dry compression. The model was set-up as a baseline for subsequent experimental activities and optimisation with other Low GWP refrigerants. The refrigerants HFC-245fa and HFC-365mfc were compared with low GWP refrigerants listed in Table to determine outputs for minimum superheat, exergy, and energy. The temperature profiles applied ranged between source temperatures 60 to 80°C and sink temperatures 90 to 140°C, with lift temperatures at 30 and 70 K, Equations 1-5 were used to calculate energy and exergy within the system (Dincer & Rosen, 2015)

$$COP_{theo} = \frac{h_2 - h_5}{h_2 - h_1} \qquad (1)$$

$$VHC = \rho_1 (h_2 - h_5) \qquad (2)$$

$$Ex_{flow} = (h - h_0) - T_0(s - s_0) \qquad (3)$$

$$Ex_{total} = Ex_{comp} + Ex_{cond} + Ex_{exp} + Ex_{evap} + Ex_{IHX} \qquad (4)$$

$$\eta_{ex} = \left(1 - \left(\frac{Ex_{total}}{P_{comp}}\right)\right) * 100 \qquad (5)$$

Pierre's correlations for a reciprocating compressor to theoretically derive the volumetric compressor efficiency Equations 6 based on the provided variable coefficients k_1, k_2, and k_s with constant values of 1.04, -0.07, and 0.15 respectively (Granryd, *et al.*, 1999) The isentropic and compressor efficiencies were calculated using Equations 7 & 8 (McEnaney, *et al.*, 1999) (Byrne, *et al.*, 2012). The IHX effectiveness was computed through Equation 9 rather than assumed and the discharge temperature for all refrigerants was kept below the critical temperature by controlling the degree of superheat.

$$\eta_{vol} = k_1 \left(1 + \frac{t_{suc} - 18}{100} * k_s \right) exp^{PR * k_2} \tag{6}$$

$$\eta_{ise} = 0.9343 - (0.04778 \times PR) \tag{7}$$

$$\eta_{comp} = 0.9962 \times \exp^{(-0.0565 \times PR)} \tag{8}$$

$$\varepsilon_{IHX} = \frac{T_1 - T_9}{T_5 - T_9} \tag{9}$$

2.1. Minimum superheat

Alongside the refrigerant's thermophysical properties the behaviour throughout the isentropic compression process in the HTHP cycle was mainly determined by the working fluid's saturation vapour shape with high values of entropy. Based on the T-s diagram of saturated vapour slope, refrigerants used in the vapour compression cycle (VCC) were categorized into different types: dry, isentropic, or wet (reference). Different methods were employed to identify the working fluid type and were defined as either having a positive slope dT/ds>0 (dry), a negative slope dT/ds< 0 (wet) or infinite slope dT/ds≅0 (isentropic) (Aljundi, 2011) (Bao & Zhao, 2013) (Quoilin, *et al.*, 2013).

The most practical and effective methods to determine the type of refrigerant are to differentiate the slope and determine the angle of vapour slope as shown in Figure. Isentropic refrigerants have an angle of approximately 90 degrees, wet refrigerants have an angle of less than 90 degrees, and dry refrigerants have an angle of more than 90 degrees (Reißner, 2015) and usually described as overhanging or extremely overhanging. In addition, the molecular degree of freedom and molecular weight is another method to determine the type of slope (Su, *et al.*, 2017). According to Tabor & Bronicki (1964), molecules with a small number of atoms are described as wet whereas dry refrigerants have a larger number of atoms and isentropic shape with an atomic number between 5 to 10.
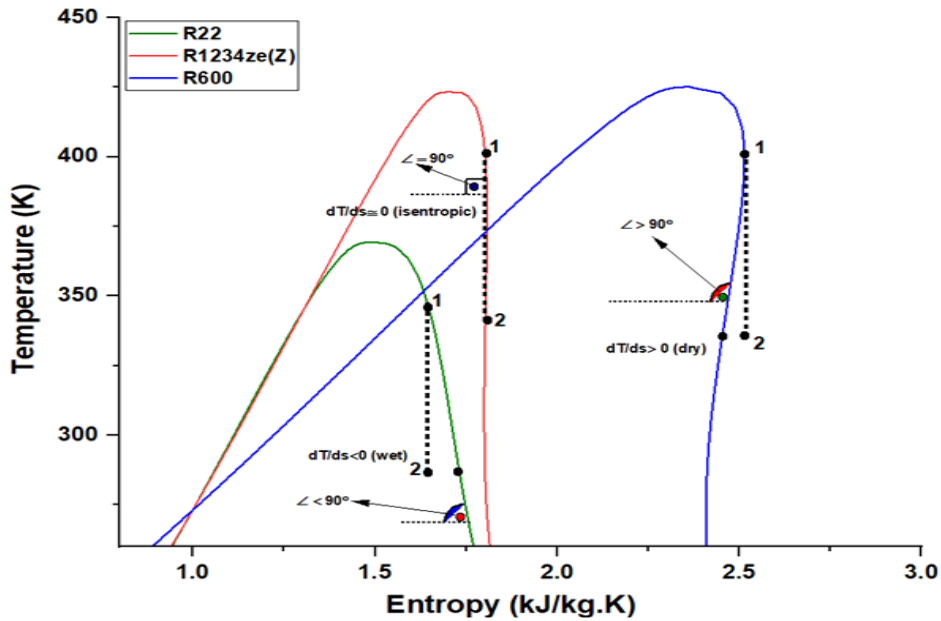
Figure 3: Determination of refrigerant type based on vapour characteristics - wet, isentropic, or dry.

In this work an assessment of the minimum superheat degree required at the compressor for HCFO-1233zd(E), HFC-245fa, HFO-1336mzz(Z), HFC-365mfc, HFO-1224yd(Z), HC-600, and HC-601 refrigerants. The refrigerant HFO-1234ze(Z) was isentropic ≅90° (Figure 2) and it had a negligible superheat requirement (≤5 degrees) for dry compression which occurred inside the evaporator. With these refrigerants the maximum overhanging saturation point was determined at vapour quality (x=1) and T=400 K, at these parameters' entropy remains constant Equation 10 with the suction temperature determined using Equation 11.

$$s_1 = f(T = 400K, x = 1) \tag{10}$$

$$T_1 = f(s_1, P_{evap}) \tag{11}$$

In the case of extremely overhanging refrigerants like HFC-365mfc and HFO-1336mzz(Z) the entropy saturation pressure at the evaporator and condenser were primarily used to calculate the minimum degree of superheat required at the compressor. The suction entropy formula Equation 12 was developed using the T-s diagram and EES software, assuming an isentropic efficiency of ($\eta_{is,ass}$= 0.75) at 70 K temperature lift, with the suction temperature defined as a function of suction entropy and evaporation pressure Equation 13. The minimum degree of superheat required was calculated using Equation 14, which calculated the differential between suction and evaporation temperatures at the maximum point on the vapour curve slope (Figure 4).

$$s_{suc} = \left(\left(s_{cond} - s_{evap}\right)\eta_{is,ass}\right) + s_{evap}\right)) \qquad (12)$$

$$T_{suc} = f(s_{suc}, P_{sat,evap}) \qquad (13)$$

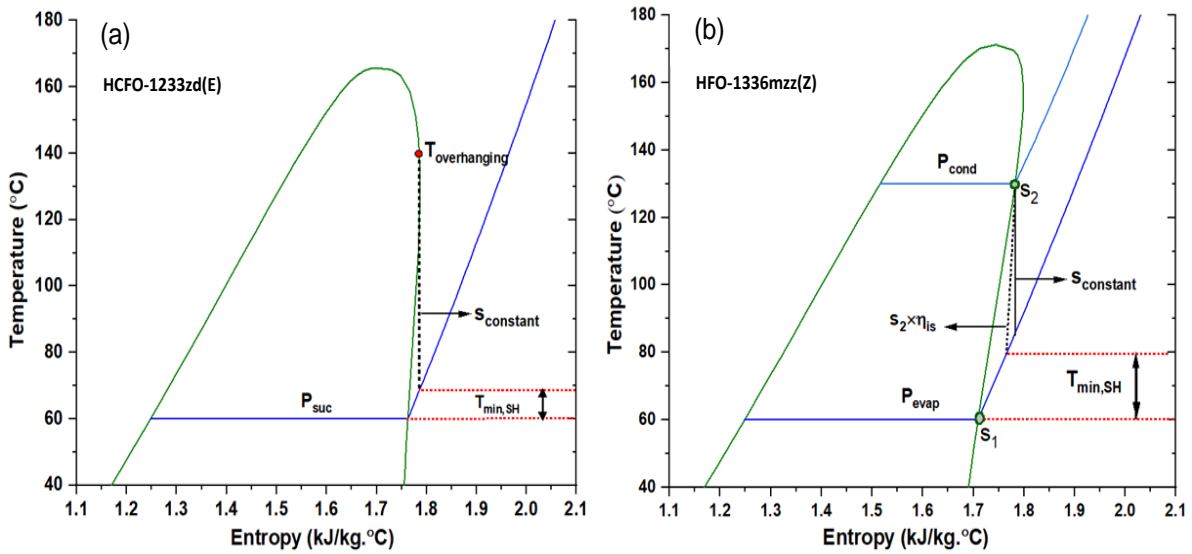$$T_{min,SH} = T_{suc} - T_{evap} \qquad (14)$$

Figure 4: Graphs showing temperature as a function of entropy with minimum superheat; (a) HCFO-1233zd(E) (overhanging) and (b) HFO-1336mzz(Z) (extremely overhanging).

3. RESULTS AND DISCUSSION

The following section discusses and highlights the energetic and exergetic performance of subcritical HTHP units at various heat source and heat sink temperatures as well as a practical method for mapping the minimum superheat.

3.1. Energetic performance

The energetic and exergetic performance results for the refrigerants investigated are presented in Table 2. These results reveal the relationship between the condensation line to the dome of the P-h diagram and COP, as the condensation line moves towards the critical temperature it yields a reduction in COP for all investigated refrigerants. This is because the saturation vapour and liquid line separation distance becomes compressed as the temperature approaches the dome, resulting in a shorter condensation line and smaller enthalpic difference value at the condenser. Furthermore, the decrement in de-superheat area between the discharge point and saturation vapour line occurs due to the characteristic overhanging of each refrigerant. The optimum value of COP was achieved at T$_{cond}$ = 130°C with reduced performance at higher or lower condensation temperatures. Unlike the VHC which is a function of the suction density and the change in enthalpy at the condenser between inlet and outlet points, the VHC increases at higher evaporation and condensation temperatures due to increased suction density. Apart from HFO-1234ze(Z), the discharge temperature was less than 10°C above the condensation temperature for all other candidates based on the input parameters, assumptions, and minimum superheat required by each refrigerant. Compared to HFC-245fa and HFC-365mfc, a trade-off between COP and VHC and exergetic efficiency is necessary to select the most suitable and promising working fluid in HTHP applications.

In Figure (a) a visual overview of the trade-off between COP and VHC for all investigated refrigerants is presented. There is a direct relationship between the temperature lift and the energetic performance of the HTHP system with

lower temperature lift resulting in higher COP and VHC for all refrigerants. At 30 and 70 K temperature lift, HC-600 and HFO-1234ze(Z) showed the highest VHC values, whereas HC-601 showed the lowest. HCFO-245fa showed the lowest COP value at different temperature lifts and HC-601 shows the highest. In Figure(b) the relationship between the pressure ratio and input power of the compressor was evaluated. A higher-pressure ratio results in increased input power to operate the compressor. HFC-245fa provides the highest input power to the system at T_{evap} = 70°C and T_{lift} 30K & 70 K, whereas HC-601 offers the lowest input power to the compressor. Compared to HFC-245fa, refrigerant HCFO-1233zd(E) has a COP 2-3% higher at T_{cond} = 130°C, and 140°C at T_{lift} = 30 K, increasing to 12% at T_{lift} = 70 K at similar heat sink temperatures. This is because HCFO-1233zd(E) possesses a higher critical temperature value and therefore a longer condensation line. As a result of its higher suction density value, HFC-245fa showed a VHC value approximately 15% higher compared to HCFO-1233zd(E) at T_{lift} = 30 K, and this percentage was greatly reduced with increased temperature lift. Due to its favourable thermodynamic features including very high critical temperature, HC-601 provided the highest COP value amongst the candidates, however, as it has a low VHC this would require larger equipment within the system design.

Table 2: HTHP energetic and results at different T_{evap} and T_{cond}.

	$(T_{evap} = 60\ °C\ \&\ T_{cond} = 90\ °C, 130\ °C)$						$(T_{evap} = 70\ °C\ \&\ T_{cond} = 90\ °C, 130\ °C)$					
Refrigerant	T_{dis} °C	COP [-]	VHC $(kJ.m^{-3})$	W_{in} (kW)	Ex_{dest} (kW)	η_{ex} (%)	T_{dis} °C	COP [-]	VHC $(kJ.m^{-3})$	W_{in} (kW)	Ex_{dest} (kW)	η_{ex} (%)
R1233zd(E)	95.97	7.93	3316	1.93	1.03	62.5	104.30	7.82	4110	1.89	1.03	61.81
	137.3	3.08	2633	5.87	3.80	49.59	145.90	3.04	3105	5.81	3.74	47.8
R245fa	95.52	7.76	3925	1.98	1.06	61.1	103.90	7.58	4873	1.95	1.03	60.17
	134.90	2.83	2876	6.47	4.33	45.54	144.00	2.71	3288	6.54	4.40	42.77
R1336mzz(Z)	93.41	7.99	2273	1.95	1.04	62.45	103.50	7.86	2886	1.89	1.01	62.18
	140.90	3.13	1854	6.07	3.91	49.91	148.60	3.09	2203	5.88	3.66	48.75
R365mfc	93.56	8.09	1899	1.95	1.06	62.63	103.10	8.00	2439	1.89	1.01	62.52
	141.70	3.18	1566	6.08	3.96	50.75	149.40	3.14	1948	5.78	3.61	50.37
R1224yd(Z)	95.52	8.14	3602	1.95	1.03	61.71	103.70	8.10	4426	1.92	1.00	60.68
	134.70	2.92	2678	6.23	4.10	46.50	144.00	2.89	3061	6.32	4.18	43.77
R600	95.20	7.62	4633	1.94	1.01	61.66	103.40	7.61	5540	1.92	0.99	60.37
	133.70	2.80	3378	6.00	3.86	46.38	143.50	2.78	3692	6.27	4.13	42.67
R601	93.71	8.28	1935	1.90	1.02	63.70	103.50	8.16	2433	1.85	0.98	63.30
	141.40	3.31	1623	5.54	3.46	53.30	104.01	3.23	1991	5.32	3.20	52.80
R1234ze(Z)	98.24	7.88	3221	1.94	1.08	61.91	107.80	7.75	5177	1.91	1.05	61.02
	142.90	3.02	3174	4.74	4.02	47.88	152.40	3.00	3589	6.12	4.09	45.07

HFO-1234ze(Z) exhibits good COP and a high VHC, however, HFO-1234ze(Z) has a discharge temperature 10 K greater than the condensation temperature which would limit the operating range in industrial applications. HFO-1224yd(Z) has the second highest COP value at T_{lift} = 30 K and this value rapidly falls at T_{lift} = 70 K due to increased input power required at high-temperature lift compared to the other candidates. HFO-1336mzz(Z), which is the most likely replacement for HFC-365mfc, showed a COP value of 3.1 at T_{cond} = 140 °C and T_{lift} = 70 K. Compared to HFC-365mfc, refrigerant HFO-1336mzz(Z) at T_{lift} = 70 K exhibits a 17% higher VHC at T_{cond} = 130°C, and 15% at T_{cond} = 140°C. The refrigerant HCFO-1233zd(E) shows a good trade-off between variables COP, VHC and exergetic efficiency. HCFO-1233zd(E) at T_{evap} = 60 °C and T_{cond} = 130 °C, exhibited a COP value of 3.14, VHC of 2633 kJ/m^3 and exergetic efficiency of 59%. HFO-1336mzz(Z) presented a similar COP value but lower VHC of 1809 kJ/m^3 and lower exergetic efficiency of 52%. At different condensation temperatures, refrigerants HCFO-1233zd(E) and HFC-245fa required a minimum super heat temperature between 5-8 K, whereas HFO-1336mzz(Z) and HFC-365mfc required a value between 19-21 K at T_{lift} = 70 K.
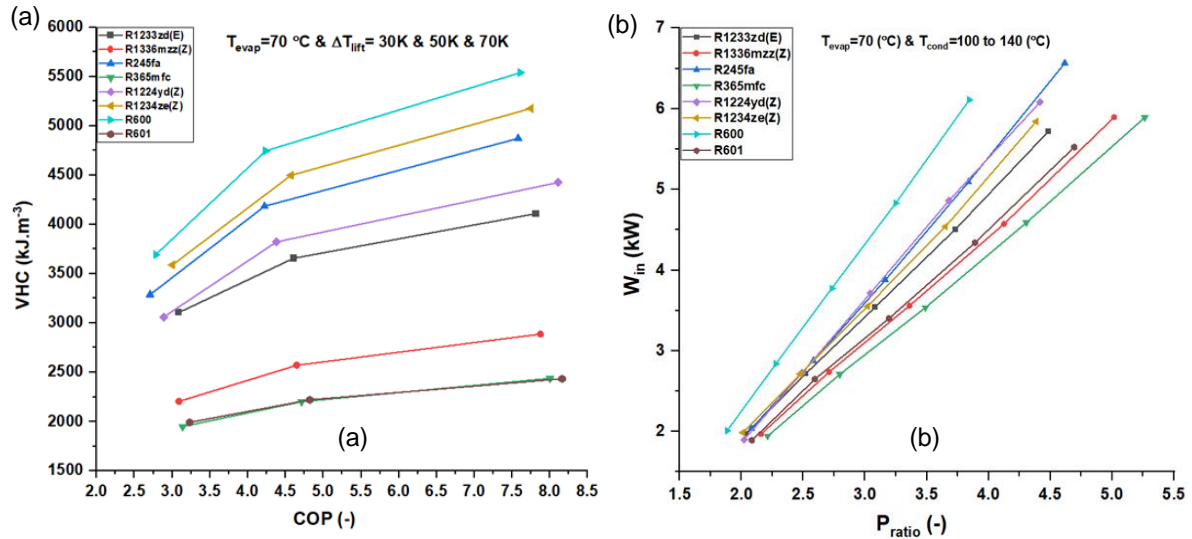
Figure 5: (a) The estimated VHC as a function of COP at temperature lifts 30, 50 and 70K (b) The estimated work done by the compressor as a function of the pressure ratio.

3.2. Mapping minimum superheat

The discharge temperature is a vital factor in achieving increased COP in the HTHP system. The optimum practical method to control discharge temperature involves mapping the minimum superheat required by the compressor for each refrigerant as shown in Figure (a). Alongside the compressor isentropic efficiency, the working fluid isentropic exponent (C_p/C_v) represents a significant factor in predicting the discharge temperature during the compression process. The higher the isentropic value of the system's working fluid, the higher the compressor discharge temperature. According to the theoretical results, as T_{lift} increases T_{min_SH} required by the compressor also increases. The refrigerants HCFO-1233zd(E), HFC-245fa, HC-600 and HFO-1224yd(Z) required T_{min_SH} <10 K above the evaporation temperature to the compressor. Whereas HFO-1336mzz(Z), HC-601 and HFC-365mfc required T_{min_SH} ≥18 K at T_{lift} = 70 K. The results indicate that the minimum degree of superheat required by each refrigerant is influenced by the suction and discharge pressures, as well as the system temperature lift. Increasing the suction pressure reduces the minimum degree of superheat required, as shown in Figure (b) for HCFO-1233zd(E). By mapping the optimal degree of superheat required by the compressor, the energy findings confirmed the theoretical results reported by Arpagaus et al., (2019) with an improvement of up to 0.5%. Overhanging refrigerants will have reduced heat exchange surface area compared to extremely overhanging refrigerants due to higher coefficient values during condensation and evaporation processes.
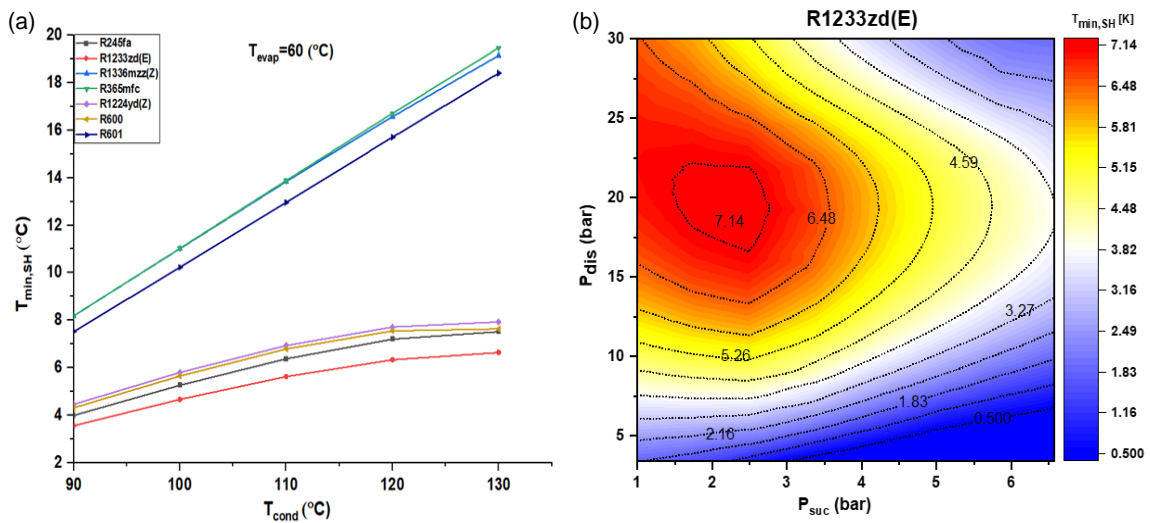

Figure 6: (a) The minimal superheat degree for various refrigerants at a fixed evaporation temperature of 60 °C evaporation and condensation 130 °C temperature ranges up to 70 K temperature lift, (b) Contour plot of discharge pressure as a function of suction pressure for HFO-1233zd(E).

3.3. Exergy results

The exergy analysis is useful to define the quality of mechanical and thermal losses and therefore the potential energetic improvements to conserve energy. The estimated exergy efficiency (η_{ex}) and the total exergy destruction (Ex_d) of each component and refrigerant is presented in Figure. The compressor has the highest exergetic loss compared to other components with the expansion valve second highest at a high-temperature lift. The condenser and evaporator show the lowest exergy destruction as they are not a function of the temperature lift. At low temperature lift the expansion valve exhibits low exergy destruction, which is related to an elevation in dissipative forces because of the high-pressure ratio. At T_{lift} = 70 K the results highlighted HC-601 and HFC-365mfc as the most exergetic refrigerants whereas, HFC-245fa and HC-600 showed the lowest exergetic efficiency. The exergy destruction of HFC-245fa is the highest compared to other candidates and the exergy destruction of the system increases at higher temperature lift. The analysis also shows that increasing the evaporation temperature results in lower exergy efficiency within the system. Based on these results mapping and controlling minimum superheat will enable the system to achieve minimum exergetic efficiency, while also minimising losses from each of the key components.
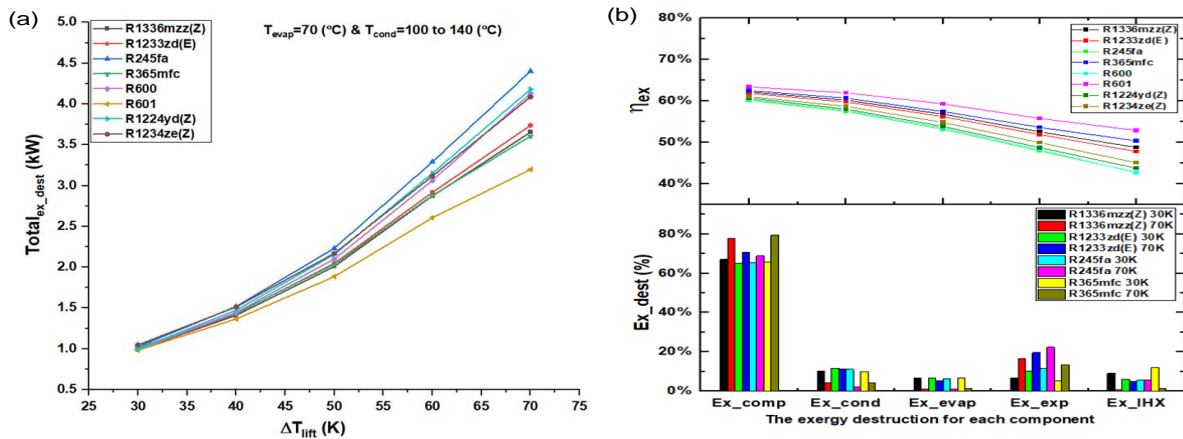

Figure 7: (a) Plots the total exergy destruction as a function of temperature lift. (b) Compares the estimated % exergy destruction for each of the key components in the HTHP system and the % exergy efficiency.

4. CONCLUSIONS

Using theoretical simulation of a HTHP single stage cycle incorporating an IHX, a plausible method to maximise the operational efficiency was investigated to assess the effects controlling minimum superheat has within the overall process. An assessment of suitable low GWP refrigerants was carried out to determine suitable alternatives for HFC-245fa and HFC-365mfc in HTHP applications. The following were the main findings observed from the analysis,

- A review of selected refrigerants thermophysical and environmental properties yields a limited range of potential candidates as successors to HFC-245fa and HFC-365mfc in HTHP applications. Based on the energetic and exergetic performance results for the refrigerants investigated a trade-off between COP and VHC and exergetic efficiency is necessary to select the most suitable and promising working fluid. The findings suggest HCFO-1233zd(E) as the potential replacement for HFC-245fa, and HFO-1336mzz(Z) as a potential replacement for HFC-365mfc.
- Mapping of minimum superheat found T_{min_SH} <10 K for refrigerant HCFO-1233zd(E), HFC-245fa, HC-600, HFO-1224yd(Z), and HFC-245fa, with T_{min_SH} ≥18 K for HFO-1336mzz(Z), HC-601, and HFC-365mfc at T_{lift} = 70 K.
- Exergy analysis shows that there is a considerable improvement in energetic and exergetic efficiency by mapping the minimum superheat for each refrigerant and potentially offer control parameters at heat source and heat sink loops. The exergetic simulations conclude that the compressor and expansion valve are principal areas for future performance improvement due to their considerable losses.

5. ACKNOWLEDGEMENTS

6. REFERENCES

AGC Chemicals, 2017. Technical Information, AMOLEA® 1224yd. [Online] Available at: www.agc-chemicals.com/file/AMOLEAyd_Tech_English_D.PDF [Accessed 09 01 2022].

Aljundi, I. H., 2011. Effect of dry hydrocarbons and critical point temperature on the efficiencies of organic Rankine cycle. Renewable Energy, 36(4), pp. 1196-1202.

Arpagaus, C., Bless, F. & Bertsch, S. S., 2020. Theoretical Analysis of Transcritical HTHP Cycles with Low GWP - Paper ID: 1168. Glasgow, Institute of Refrigeration.

Arpagaus, C. *et al.*, 2018. High temperature heat pump using HFO and HCFO refrigerants - System design, simulation, and first experimental results. Purdue, International Refrigeration and Air Conditioning Conference.

Arpagaus, C. *et al.*, 2018. High temperature heat pumps: Market overview, state of the art, research status, refrigerants, and application potentials. Energy, Volume 152, pp. 985-1010.

ASHRAE, 2019. ANSI/ASHRAE Standard 34-2019- Designation and Safety Classification of Refrigerants. [Online] Available at: https://www.ashrae.org/technical-resources/bookstore/standards-15-34 [Accessed 02 04 2021].

Bamigbetan, O. *et al.*, 2018. Theoretical analysis of suitable fluids for high temperature heat pumps up to 125 °C heat delivery. International Journal of Refrigeration, Volume 92, pp. 185-195.

Bamigbetan, O. *et al.*, 2019. Experimental Investigation of a prototype R-600 Compressor for High Temperature Heat Pump. Energy, Volume 169, pp. 730-738.

Bao, J. & Zhao, L., 2013. A review of workingfluid and expander selections for organic Rankine cycle. Renewable and Sustainable Energy Reviews, Volume 24, pp. 325-342.

Besagni, G., Mereu, R., Di Leo, G. & Inzoli, F., 2015. A study of working fluids for heat driven ejector refrigeration using lumped parameter models. International Journal of Refrigeration, Volume 58, pp. 154-171.

Byrne, P., Miriel, J. & Lénat, Y., 2012. Modelling and simulation of a heat pump for simultaneous heating and cooling. Building Simulation, 5(3), pp. 219-232.

Dincer, I. & Rosen, M. A., 2015. Exergy Analysis of Heating, Refrigerating and Air Conditioning : Methods and Applications. s.l.:Academic Press.

Eyerer, S. *et al.*, 2019. Experimental investigation of modern ORC working fluids R1224yd(Z) and R1233zd(E) as replacements for R245fa. Applied Energy, Volume 240, pp. 946--63.

Granryd, E. *et al.*, 1999. Refrigeration Engineering. K Tek Högskolan: s.n.

Klein, S., 2017. Engineering Equation Solver (EES) V10.268, Madison. USA: Fchart software.

Kontomaris, K., 2014. HFO-1336mzz-Z: High Temperature Chemical Stability and Use as A Working Fluid in Organic Rankine. Purdue, s.n.

Lemmon, E. W., Huber, M. L. & McLinden, M. O., 2013. NIST Standard Reference Database 23: Reference Fluid Thermodynamic and Transport Properties-REFPROP, Version 9.1, Natl Std. Ref. Data Series (NIST NSRDS), National Institute of Standards and Technology, Gaithersburg. [Online] Available at: [online], https://tsapps.nist.gov/publication/get_pdf.cfm?pub_id=912382 [Accessed 09 01 2022].

Mateu-Royo, C., Mota-Babiloni, A. & Navarro-Esbrí, J., 2021. Semi-empirical and environmental assessment of the low GWP refrigerant HCFO-1224yd(Z) to replace HFC-245fa in high temperature heat pumps. International Journal of Refrigeration, Volume 127, pp. 120-127.

Mateu-Royo, C. *et al.*, 2019. Thermodynamic analysis of low GWP alternatives to HFC-245fa in high-temperature heat pumps: HCFO-1224yd(Z), HCFO-1233zd(E) and HFO-1336mzz(Z). Applied Thermal Engineering, Volume 152, pp. 762-777.

Mateu-Royo, C. *et al.*, 2019. Experimental exergy and energy analysis of a novel high-temperature heat pump with scroll compressor for waste heat recovery. Applied Energy, Volume 253, p. 113504.

Mateu-Royo, C. *et al.*, 2019. Experimental exergy and energy analysis of a novel high-temperature heat pump with scroll compressor for waste heat recovery. Applied Energy, Volume 253, p. 113504.

McEnaney, R., Park, Y., Yin, J. & Hrnjak, P., 1999. Performance of the Prototype of a Transcritical R744 Mobile A/C System, SAE Technical Paper 1999-01-0872.

Mikielewicz, D. & Wajs, J., 2019. Performance of the very high-temperature heat pump with low GWP working fluids. Energy, Volume 182, pp. 460-470.

Myhre, G. *et al.*, 2013. Anthropogenic and Natural Radiative Forcing. In: Climate Change 2013: The Physical Science Basis. Contribution of Working Group I to the Fifth Assessment. [Online] Available at: https://www.ipcc.ch/site/assets/uploads/2018/02/WG1AR5_Chapter08_FINAL.pdf [Accessed 09 01 2022].

Nilsson, M., Nes Rislå, H. & Kontomaris, K., 2017. Measured performance of a novel high temperature heat pump with HFO-1336mzz(Z) as the working fluid. s.l., Rotterdam.

Patten, K. O. & Wuebbles, D. J., 2010. Atmospheric lifetimes and Ozone Depletion Potentials of trans-1-chloro-3,3,3-trifluoropropylene and trans-1,2-dichloroethylene in a three-dimensional model. Atmospheric Chemistry and Physics, Volume 10, pp. 10867-10874.

Petr, P. & Raabe, G., 2015. Evaluation of R-1234ze(Z) as drop-in replacement for R-245fa in Organic Rankine Cycles – From thermophysical properties to cycle performance. Energy, Volume 93, Part 1, pp. 266-274.

Quoilin, S. *et al.*, 2013. Techno-economic survey of Organic Rankine Cycle (ORC) systems. Renewable and Sustainable Energy Reviews, Volume 22, pp. 168-786.

Reißner, F., 2015. Development of a Novel High Temperature Heat Pump System, Entwicklung eines neuartigen Hochtemperatur-Wärmepumpensystems. Nürnberg: Friedrich-Alexander Universität Erlangen.

Su, W., Zhao, L., Deng, S. & Zhao, Y., 2017. How to predict the vapor slope of temperature-entropy saturation boundary of working fluids from molecular groups?. Energy, Volume 135, pp. 14-22.

Tabor, H. & Bronicki, L., 1964. Establishing criteria for fluids for small vapor turbines. SAE World Congress & Exhibition, p. 15.

UNEP, 2020. Handbook for the Montreal Protocol on Substances that Deplete the Ozone Layer - Fourteenth edition. [Online] Available at: https://ozone.unep.org/sites/default/files/Handbooks/MP-Handbook-2020-English.pdf [Accessed 09 01 2022].

#52: Design and construction of a mop fan-based photocatalytic air purification device

Emmanuel Tapia-Brito[1], James Riffat[2], Saffa Riffat[3]

[1] Department of Architecture and Built Environment, Faculty of Engineering, University of Nottingham, NG7 2RD University Park, Nottingham, UNITED KINGDOM, b_tapi@hotmail.com
[2] Department of Architecture and Built Environment, Faculty of Engineering, University of Nottingham, NG7 2RD University Park, Nottingham, UNITED KINGDOM, james.riffat@nottingham.ac.uk
[3] Department of Architecture and Built Environment, Faculty of Engineering, University of Nottingham, NG7 2RD University Park, Nottingham, UNITED KINGDOM, saffa.riffat@nottingham.ac.uk

Abstract: SARS-CoV-2, the virus that causes the disease Covid-19, is primarily transmitted through respiratory droplets which linger in enclosed spaces, often exacerbated by HVAC systems. Although research to improve HVAC handling of SARS-CoV-2 is progressing, currently installed HVAC systems cause problems because they recirculate air and use ineffective virus filters. This article details the process of developing a novel method of eliminating air pollutants and suspended pathogens in enclosed spaces using Photocatalytic Oxidation (PCO) technology, previously employed to remove organic contaminants and compounds from air streams using the irradiation of titanium dioxide (TiO2) surfaces with ultraviolet (UV-C) lights causing the disintegration of organic compounds by reactions with oxygen (O) and hydroxyl radicals (OH). The O and OH reactions can also destroy viruses. The result was a functional prototype that demonstrated the operation of PCO-based air purification principle. This prototype mainly comprised a novel TiO2 coated fibre mop system, which could provide the essential very large surface area for UV irradiation. Each component of the prototype is described in depth, along with the criteria by which they were selected and, in some cases, fabricated. A test was conducted that proved the prototype's functionality and its efficiency in lowering VOCs and HCHO. During the next stage of this research, the prototype will be used to conduct more experiments in laboratory and in real-world conditions. The mop, illuminated by a high intensity UV, allowed viruses to be eliminated in an efficient, nearly silent system, adaptable for small or larger applications.

1. INTRODUCTION

As a consequence of the COVID-19 pandemic, people grew more concerned about the air quality in their homes, businesses, and public spaces. Detaining any suspended pollutant that may represent a threat to human health necessitates ongoing study into air purification, not just regarding infectious diseases but also to eliminate any other suspended pollutants that may be hazardous to human health.

SARS-CoV-2, the virus that causes Covid-19, is spread predominantly by respiratory droplets that stay in enclosed places, a condition that is frequently aggravated by HVAC systems. Although research to enhance HVAC handling of SARS-CoV-2 is advancing, currently deployed HVAC systems pose challenges due to their recirculation of air and poor viral filters. Using Photocatalytic Oxidation (PCO) technology, previously used to remove organic contaminants and compounds and viruses (Hoffman, 1995) from air streams, this research study developed a novel method for eliminating SARS-CoV-2 and future viruses in enclosed spaces (OH). Photocatalytic Oxidation irradiates titanium dioxide (TiO_2) surfaces with ultraviolet (UV) light to cause the disintegration of organic compounds by reactions with oxygen (O) and hydroxyl radicals. Additionally, the O and OH reactions can eliminate pathogens. An illustration of this reaction is shown in Figure 1.
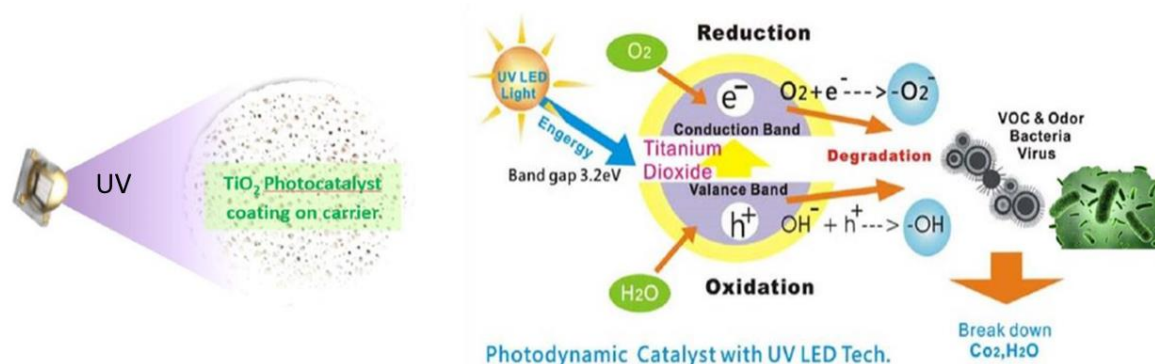

Figure 1: Diagram of the photocatalytic reaction.

Using the known findings from earlier research and development activities, this study aimed to design a unique TiO_2-coated brass mop system, which could function as a fan and offer a desired high surface area for UV irradiation (Wongwatcharapaiboon, 2019). The design required determining UV frequencies, intensity, and setting the best conditions for the photocatalytic oxidation reaction. The revolving fibre fan, lit by a high-intensity UV, enabled viruses to be eradicated in an effective, practically silent system that was suitable for small or big applications. This study presented the first prototype produced to date; a medium-sized air purifier suited for recirculating an average-sized room. These efficient, low-cost technologies could later be presented to the industry to facilitate their quick adoption in buildings and public transportation networks (Kolarik, 2012).

Air filters in conventional HVAC systems cause pressure drops, hence increasing energy costs, and are usually inefficient at preventing the entry and spread of viruses. In the United Kingdom, smaller buildings without HVAC systems, such as care homes, crowded restaurants, pubs, and recreational facilities, utilise natural ventilation, albeit often just during the summer months. During other times, insufficient ventilation is permitted to preserve heat, creating a perfect setting for the spread of SARS-CoV-2 and other viruses. This generates substantial public worries over the safety and future of public transportation, especially considering that increased public transportation use is a vital component of the United Kingdom's decarbonisation objectives. In order to increase the usage of public transportation in the future, people must have confidence in the minimal danger of catching viral infections. There are currently no easy, compact, low-cost, energy-efficient, and readily deployable solutions for removing SARS-CoV-2 and other airborne virus risks from public buildings and transportation. Such solutions are necessary for both a return to normal life and the defeat of SARS-Cov-2, without exacerbating the problem of global warming. As previously mentioned, coupling the UV irradiation of TiO_2, which is already known to destroy viruses and organic contaminants, with an energy-efficient mop fan offered a promising, elegant solution to the problem, either as stand-alone units or as additions to HVAC systems without costly modifications.

2. PROTOTYPE DESIGN

The concept behind the device is described below. Later, the main components selected to manufacture the prototype are illustrated.

2.1. Concept

The system consisted of a flexible fibre mop that resembled a chimney sweep brush but made of flexible bristles coated with TiO2. Unlike conventional filter/mesh UV systems, TiO2-bristles arranged in a mop configuration offers an exceptionally large UV-TiO2 interaction surface area and airflow passage. To hold the brushes, a hub was manufactured which was linked to the motor shaft so that it rotated with the fan blades. In this way, the high-efficiency direct-drive motor could rotate both the fan blades and the mop at the same rotational speed (Figure 2).

When the motor rotates, it moves the blades along with it, which pushes air from the outside upwards and into the mop's bristles, which are also moving with the fan. While contaminated air travels through the purifier's body, UV light would act on the TiO2 and start the photocatalytic reaction. Simultaneously, the mop fan would push the purified air to the air outlet positioned on the top of the device case.

During operation, the air blown by the mop fan travels across the very large TiO2-bristle surface area. The mop is illuminated by UV LEDs of high intensity positioned within the fan housing. The inside surface of the housing is covered with a light-reflective material to maximise the UV-ray's concentration. The result is a fan system that delivers effective airflow and extremely high UV irradiation of the TiO2, producing very large numbers of hydroxyl radicals to remove airborne pollutants such as VOCs, formaldehyde, chloride, benzoin, isobutane, particulates, dust, allergens, etc.

It has been demonstrated that this configuration functions effectively as an air impeller, achieving 97% of the performance of backward-curved centrifugal fans (Riffat, 2001). Since this first study, which established the mop-fan concept, substantial improvements must be made in high intensity UV LED and TiO2 coating techniques.
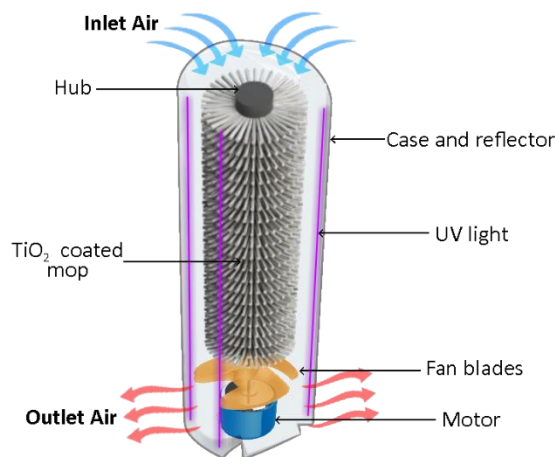
Figure 2: Mop-fan concept diagram.

2.2. Fan motor

In photocatalytic air purification, in addition to light, a displacement of the cleaned air is necessary. To do this, the cylindrical brush is rotated by a motor typically found in tower fans. For this prototype, a 220V 40W AC motor was chosen, with a maximum rotational speed of 1300 RPM that was adjustable through a variable resistor. Attached to this motor were plastic blades with a 200 mm diameter (Figure 3).

Figure 3: 40W AC motor and fan blade.

2.3. UV light

UV light is essential for the system to create the photocatalytic reaction needed to filter the air. The majority of the relevant research publications centres on the use of UV light with wavelengths between 200 and 300 nm. UV LED strips with a pear wavelength of 270~280 nm were selected for this prototype since they are relatively easy to find on the market. Figure 4 depicts the LED strip, which had a density of 30 LEDs per metre, worked at 24 V DC, and used 9.6 W per metre, requiring minimal additional power. A 10-meter LED strip was wrapped around the cylindrical brush on the inner walls of the device casing.

Figure 4: 275nm UV-C LED strip.

2.4. Brushes

The selected brushes were similar to that seen in Figure 5. They were composed of a steel rib that pressed the bristles together with a binding wire. Because it was the most readily accessible material for this sort of brush, 0.4mm crimped brass was chosen. In the future, it is intended to test this prototype with alternative materials. To provide a high number of bristles, ten 400mm long brushes with 50mm long bristles were utilised.

Figure 5: Crimped brass brush strip.

2.5. Hub

The interior of the cylindrical box was covered by ten brushes positioned on a hub. The hub was composed of two sections that retained the ten bristles in a cylindrical shape with their fibres visible. In addition to holding the

26

brushes, the upper portion was equipped with a spindle to assist an aligned rotation. The bottom portion was coupled to the motor, causing the entire hub to revolve. A fundamental feature of its design was that no adhesives were used. Adhesives may emit volatile organic compounds and other contaminants, which may degrade system performance. To hold the brush strips in place, their ribs were triangular. Each groove in the hub was intended to receive a brush strip (Figure 6). To clamp the brushes/blades, the groove grew smaller as it approached the outer surface. By exchanging brushes, it will be possible to test various brushes in the future.
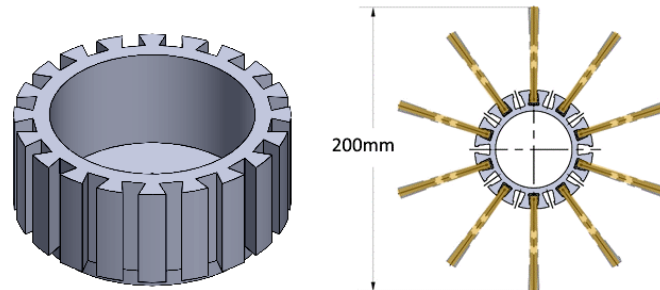
Figure 6: CAD drawing of the hub (left). Cross section of the hub with brushes (right).

2.6. Housing /casing

To maximise UV light dispersion, a 400mm rigid extension and 200mm of diameter sun tunnel, which is a polished sheet metal tube also known as a light pipe, was used to produce high efficiency reflection (Figure 7).

Figure 7: Velux Light tunnel.

2.7. CAD Drawing

The selection of the above-described components was guided by a three-dimensional rendering in which the components were virtually assembled to ensure their proper integration. This design determined the direction of the airflow, which was vertically ascending. From this drawing, design files of the joints and other pieces, such as the base and the lid, were then produced and exported to slicing software for 3D printing (Figure 8(a).

This drawing allowed the authors to determine the length of the cylindrical brush's bristles by adjusting the dimensions of the hub. It also made it feasible to calculate the dimensions and placement of the LED strips so that the light could be dispersed more efficiently. Additionally, space was optimised such that part of the air blown by the fan passed around the brush's perimeter.

This design did not require a complicated assembly. For the most part, this prototype was assembled by hand and without tools, as all the components interlock one on top of the other, allowing for a solid structure with good stability (Figure 8 (b)).
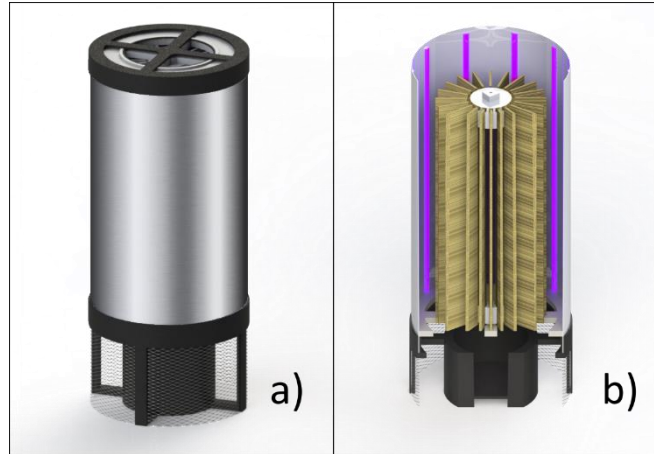
Figure 8: (a) CAD drawing of the prototype assembly. (b) Cross section of the prototype.

3. BRISTLES TREATMENT

Concurrently with defining the physical aspects of the device, the method for coating the brass bristles was investigated. This section describes the pre-treatment administered, the coating, and a microscopic examination of the coat on the bristles.

3.1. Pre-treatment

Because the bristle surface was so smooth, it was difficult for the coating to attach to it. To assist abrasion of the bristles of the brush, a pre-sanding procedure using sandblasting was used. Figure 9 depicts a heavy-duty sand blasting cabinet manufactured by the Clarke brand. The compartment had a capacity of around 140 litres. A 4.5mm ceramic nozzle was utilised with 0.5-1.25mm glass sand and 7 bar of air pressure.

Figure 9: Heavy duty sand blasting chamber (left). Sand blasting of a brush (right).

As can be seen in Figure 10, after being sanded, the fibres of the brushes lost their characteristic gloss; this was to prevent the TiO2 layer from peeling off the brush's surface. If that happened, the prototype would be releasing TiO2 microparticles into the air, which would pollute it instead of purifying it.
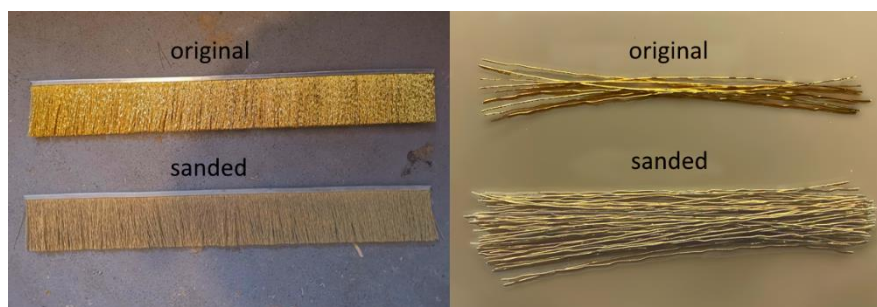
Figure 10: Comparison between the original and sanded brass brush strips (left) and bristles (right).

28

3.2. Coating

First, a concentration of 2% of TiO_2 powder was mixed with 200 mL of water and stirred using a stir bar. Next, 3% sodium alginate (SA) powder was added gently to the solution and stirred well until a uniform consistency was attained. Then, the solution was held at room temperature for eight hours to de-bubble.

Each brush was coated with many layers of the TiO_2 solution using a paintbrush, ensuring that each bristle was coated and that the whole brush was uniformly covered. After being coated, each brush was allowed to air-dry in the open air. After the brushes had dried, they were examined by wiping them with a black cloth and ensuring that no white coating residue was taken from the bristles.

3.3. Microstructure of the coated bristles

To examine and photograph the microscopic structure of the materials, a digital compound microscope KERN OBL 135C825 with a modified camera ODC 825 was utilised.

On the left-hand micrograph of Figure 11, the microscope confirmed that the surface of the brass was remarkably smooth. It also demonstrated, on the central image, that the sanding was successful since the formation of cavities and a reduction in bristle diameter can be observed. On the right-hand picture, it is shown that the TiO_2 solution attached consistently and without flaking off the brass bristle's surface.

Figure 11: Microscopic surface comparison of a brass bristle.

4. ASSEMBLY

With the above-described components, the prototype on which laboratory testing was conducted was built. The motor with the fan blade was mounted to a wooden base, to which the hub was also attached. Figure 12 depicts how the brush strips were inserted into the hub. The capacity of the full roller was ten brushes. The UV light-containing outer shell was installed from above.

Figure 12: Prototype assembly.

5. PERFORMANCE TEST

A purification test was carried out in a real room to further evaluate the effectiveness in real-world settings. The room measured around 45 m². The test conditions were a regulated 20°C temperature and 50 percent relative humidity. A 1 ml stream of methanol was evaporated on a hot plate heated to 80°C placed one metre away. Methanol was utilised to create a polluted environment. For this test in a real room, methanol vapours were utilised as the pollutant source, and a Temptop 1000s+ air quality monitor was used to measure volatile organic compounds (VOCs) and formaldehyde (HCHO) concentrations. The amount of methanol used was sufficient to prevent overloading the monitor sensors and bringing them to their maximum concentration reading without creating a health risk. The prototype was placed next to the hot plate to purify the air in the room. This test recorded the entire process, which can be broken down into three stages: 1) the first stage, during which the methanol evaporated; 2) the stage during which the methanol concentration in the room reached its peak; and 3) the final stage, during which the pollution concentration decreased.

6. RESULTS AND DISCUSSION

The VOC concentration was recorded following the procedure described above. Two different types of tests were conducted: with the device turned off and turned on. The test ran for two hours and data was logged every minute. The result of these experiments can be seen in Figure 13a. As shown by the red line, the concentration of VOCs due to the evaporation of methanol rose sharply in the first five minutes, where it reached the peak of maximum concentration, and then fell gradually, probably because the vapours were distributed throughout the room, and they decant. However, even after two hours had passed, the VOC levels were still high. It was also possible to see that in the case where the device was on, there was a reduction in VOC, which suggested that photocatalysis was taking place. The similarity between the "device off" curve and the other one implied that there was a direct relationship between the concentration of contaminants and the purification from the device. It can also be seen that around minute 70 the concentration of pollutants in the environment near the device was low, so that a smaller number of molecules came into contact with the fibres to carry out the photocatalytic reaction. It was observed that after 2 hours the prototype managed to reduce the VOC concentration below 0.9 mg/m³.

Evaporated methanol, in addition to increasing VOC levels, also increases HCHO concentration so simultaneous VOC and HCHO readings were taken during each test. That is why the concentration curves shown in Figure 13b have a similar profile. It is interesting to note that the purifier was not very effective in high concentrations, but after one hour it managed to reduce the concentration of contaminants. Although a fluctuating behaviour was observed, presumably due to the characteristics of the material, at all times the air purification system managed to reduce the concentration of pollutants. Even the highest peak, in which the HCHO concentration reached close to 0.7 mg/m3, the prototype managed to reduce it to 0.61 mg/m³, which represented a reduction of approximately 13%, which increased throughout of the entire test.
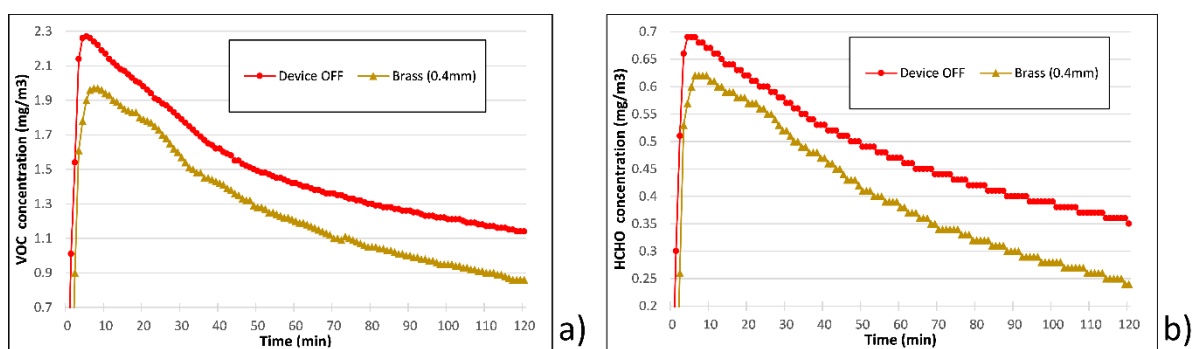
Figure 13: Monitored results of pollutants concentrations: (a)VOCs, (b)HCHO.

The above results show that the photocatalytic reaction was taking place and that some of the contamination was being removed. It was possible that the foundation material, 0.4mm brass, was not the most optimal to promote photocatalytic purification.

Besides, it is probable that the reaction could be enhanced by increasing the relative humidity. For this purpose, possibly a component might be introduced to increase the local humidity.

7. CONCLUSIONS

A prototype MopFan-based device for testing photocatalytic air filtration was successfully manufactured. A test was conducted using the prototype with a brush made of brass wire (0.4mm) bristles. Concentrations of VOCs and

HCHO were measured in order to evaluate the antiviral activity and air purification efficacy of interior environments. According to the collected data, the prototype was capable of lowering VOC and HCHO when UV light was activated and a photocatalytic process took place. Clear reductions in VOC and HCHO concentrations were observed as a result of the MopFan brush system's ability to maximise the TiO2 exposure area while also circulating the air. In addition, it was demonstrated that the purifying capacity of MopFan was proportional to the amount of contaminants. It was proven that incorporating a highly reflective material into the housing eased the reaction. Like similar products on the market, the fan was positioned near to the air outlet, hence it was easier to manage the wind direction and system pressure. This may also affect the system's accumulated dust and pollutants when utilising a longer duration. The device built was as compact as any commercially available fan or air purifier because the UV LED lights can be found in a very compact package that did not increase the demand for space inside.

Metal bristles turned out to be effective in terms of purification. They consistently lowered VOCs and HCHO by 13%. However, they must be sanded prior to being coated with the TiO2 solution. They also showed promising antiviral capabilities, however further study is necessary in this area. An additional advantage of the brass bristles was that being a durable material meant that they would have a long lifespan and hence less detrimental to the environment. In future examinations it would be beneficial to analyse the impact the use of this purification system has on the TiO2 cover in order to determine its degradation rate and anticipate its longevity. Possible future research might involve experimenting with brushes made of other materials, such as plastics or even organic fibres.

In these trials, the decrease of VOCs and HCHO was confirmed, therefore it was reasonable to believe that additional airborne pollutants may also be eliminated. Unfortunately, it was difficult to do the same studies with biological components, such as the SARS-COV2 virus. It is required to conduct biological experiments to see if this device is capable of decreasing this and other pathogenic agents in the air. This project's next step will consist of these biological testing.

In summary, the MopFan-based photocatalytic purification system showed a high potential for purification of chemical and biological pollutants commonly found in homes and workplaces.

8. ACKNOWLEDGEMENTS

9. REFERENCES

Costarramone, N., Kartheuser, B., Pecheyran, C., Pigot, T. and Lacombe, S., 2015. Efficiency and harmfulness of air-purifying photocatalytic commercial devices: From standardized chamber tests to nanoparticles release. *Catalysis Today*, *252*, pp.35-40.

Hoffmann, M.R., Martin, S.T., Choi, W. and Bahnemann, D.W., 1995. Environmental applications of semiconductor photocatalysis. *Chemical reviews*, *95*(1), pp.69-96.

Kolarik, J. and Wargocki, P., 2010. Can a photocatalytic air purifier be used to improve the perceived air quality indoors?. *Indoor Air*, *20*(3), pp.255-262.

Riffat, S.B. and Shehata, H.A., 2001. Development of a novel mop fan. *International journal of energy research*, *25*(7), pp.601-619.

Wongwatcharapaiboon, J., Gan, G. and Riffat, S.B., 2019. A new air PM2. 5 filtrative lamp with a combination of fabric filter and TiO2 coating mop. *International Journal of Low-Carbon Technologies*, *14*(3), pp.394-399.

#54: A clustering-based analysis of heat demand profiles for energy storage and demand flexibility operations

Osaru AGBONAYE[1*], Stefan SMITH[1], Cagri KUTLU[2], Diana S.N.M. NASIR[3], Yuehong SU[2], Ben HUGES[3], Saffa RIFFAT[2],

[1]School of Built Environment, University of Reading, Whiteknights House, Reading. RG6 6UR, UK
[2]Department of Architecture and Built Environment, University of Nottingham, University Park, Nottingham. NG7 2RD, UK
[3]Faculty of Science and Engineering, University of Hull, Hull. UK
[*]Corresponding Author: o.agbonaye@reading.ac.uk

Abstract: Large scale increases in electrification of domestic heat, combined with increasing intermittent renewable supply, are motivating the implementation and exploration of various flexibility approaches (time of use tariffs, direct load control, energy storage etc.) to deal with resulting network constraint issues. Understanding of the dynamics of household demand are important to the operation and design of these flexibility measures. Current understanding of heat demand patterns has been heavily influenced by expected seasonal and aggregated daily profiles. However, these aggregations of heating demand are not necessarily useful for understanding how storage and control technology can enact flexibility at the scale of households and neighbourhoods. Variation in demand matters. Using heat-pump demand data from 418 households, as part of the Renewable Heat Premium Payment trial in the UK, clustering and property classification techniques were combined to explore demand variability in the sample population. Previous studies on clustering of heat demand patterns have offered little explanatory power as to why demand clusters exist. To overcome this limitation, clustering is combined with meta-data on the 418 households as an exploration of the ability of property type, property age, heat pump type, number of bedrooms and emitter type to inform on clustered features of demand. The clustering took 45 different attributes into account, using k-means for exploration of seasonality and agglomerative hierarchical clustering for grouping profiles based on the selected attributes. This paper presents key attribute-based heat demand patterns with interpretations that could help system planners develop better tariff plans, and thermal storage control algorithms.

Keywords: heat demand clustering; demand side response; energy storage operations; cluster interpretation; agglomerative hierarchical clustering

1. INTRODUCTION

Large scale increases in electrification of domestic heat, combined with increasing intermittent renewable supply, are motivating the implementation and exploration of various flexibility approaches (time of use tariffs, direct load control, energy storage, etc.) to deal with resulting network congestion and constraint issues (Agbonaye et al., 2022). It is usual in price models to apply a component of time to tariffs - with cheaper unit pricing set to certain times of day (e.g., overnight) or tariffs that respond dynamically to real-time peaks in demand. The actual timing of these dynamic tariffs will be further influenced by other scales of demand variation, such as weekday vs. weekend and seasonal shifts (summer/winter). Technological measures such as storage and control must, therefore, be able to operate on these variable timescales in order to support the dynamic requirements of demand response: a version of flexibility offering (Chen et al., 2018).

Understanding the variability in demand is important to the operation and design of flexibility measures (lo Piano & Smith, 2022). The capability to use technology for temporal shifts in demand is both a function of the temporal capacity of the technology (e.g., storage capacity, response rates, and energy loss over time) and the consumption profile associated with demand (Agbonaye et al., 2021). Current understanding of heat demand patterns has been heavily influenced by expected seasonal and aggregated daily profiles. However, these aggregations of heating demand are not necessarily useful for understanding how storage and control technology can enact flexibility at the scale of households and neighbourhoods.

Using various machine learning algorithms and a data set of heat pump loads, the temporality of heat and electricity demand of heat pumps in residential properties were explored in this study. Profile signatures such as timing of peak in day, length of peak periods in day, and number of peaks in day (amongst others) were identified as characteristics of demand temporality and used to distinguish daily heat profiles in the data. These temporal features (signatures) were further explored on monthly and annual basis as a means of identifying and characterising seasonality in demand. A description of the data and clustering techniques used is given in the methods before key results are presented and discussed. The paper is presented around two main objectives: to determine seasonal trends and to evaluate whether property characteristics are determinants of the temporal features of heating load.

2. METHODOLOGY

The various methods used to investigate the clustering results are discussed in this section.

2.1. Data collection and processing

Heat pump load profiles were sourced from the datasets of the Renewable Heat Premium Payment (RHPP) trial, which monitored heat pump loads in nearly 700 homes. The time-series data (in watt-hours) for both space heating and domestic hot water were recorded with two-minute resolution. Some filters were applied to the processed sample to remove sites that either had technical issues such as incorrect sensor installations or when a significant amount of consecutive datapoints were missing. The 12-month period with fewest data issues was selected for each site. The results were uploaded as Sample B2, which contained 418 sites (Love et al., 2017). However, Sample B2 also contained lots of missing rows; hence, further cleaning was carried out, as shown in Figure 1.

Figure 7: Processing and selection process for the RHPP dataset

2.2. Metadata (property characteristics) for the RHPP dataset

The dataset includes metadata describing the kind of heat pump, the tenure, and the type of dwelling of each site as shown in Table 1.

Table 1: Metadata description of the RHPP dataset and the associated Code used in this paper.

Meta Data	Code	Values
Heat Pump Type	M_{1A}	Air Source Heat Pump (ASHP)
	M_{1B}	Ground Source Heat Pump (GSHP)
Property Type	M_{2A}	Detached House
	M_{2B}	Semi Detached House
	M_{2C}	Mid Terraced House
	M_{2D}	End Terraced House
Property Age	M_{3A}	Pre 1919
	M_{3B}	1919 – 1944
	M_{3C}	1945 – 1964
	M_{3D}	1965 – 1980
	M_{3E}	1981 – 2000
	M_{3F}	After 2000
No of Bedrooms	M_{4A}	1 Bedroom
	M_{4B}	2 Bedroom
	M_{4C}	3 Bedroom
	M_{4D}	4+ Bedroom
Emitter Type	M_{5A}	Underfloor Heating
	M_{5B}	Radiators
	M_{5C}	Both

2.3. Attributes / feature extraction

Certain attributes were not immediately noticeable from usual average plots. It was important to extract features that expose essential properties of the dataset. To extract the features, the authors decomposed each property's annual time-series profiles to 365 daily profiles and derived the various attributes for the system as shown in Figure 2. Table 2 shows a list of attributes associated with demand minima, maxima and averages that were extracted from the dataset. Attributes were generated for the electrical profile as well as the heat profile. Inspection of the time-series profile showed that many sharp increases may occur which might not be sustained or consistent enough to be classified as peaks in relation to demand-response and flexibility. Therefore a rule was apply for distinguishing between 'peaks' (as relevant to understanding demand-response potential) and more transient 'spikes' in demand. For an increase in demand to be classified as a peak, there must be at least two consecutive increases in demand before the time-step and two consecutive decreases in demand after the time-step and the demand must be greater than the average demand for the day, otherwise it is classified as a spike.
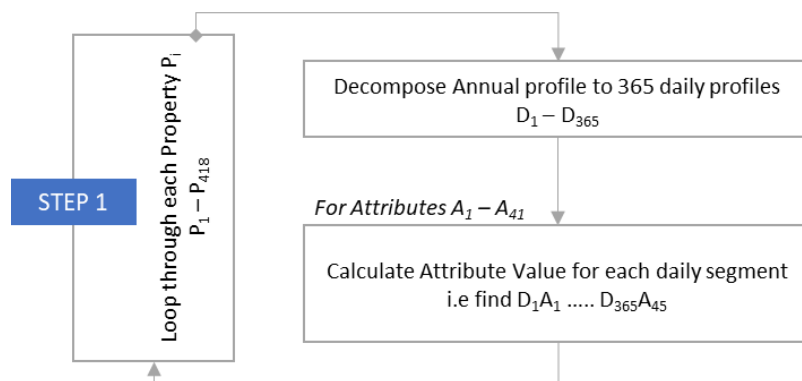

Figure 2: Flowchart for feature extraction process

Table 2: List of all extracted attributes and their definition

Code	Attribute	Description
A_1	Peak Electric Demand (EHp)	Electric demand (kW) at the time of peak electric demand
A_2	Peak Electric Demand (HHp):	Heat demand (kW) at the time of peak electric demand
A_3	Peak Electric Demand (COP)	Coefficient of Performance at the time of peak electric demand
A_4	Peak Electric Demand Time	Time at which peak electric demand occurred
A_5	Peak Heat Demand (EHp)	Electric demand (kW) at the time of peak heat demand
A_6	Peak Heat Demand (HHp):	Heat demand (kW) at the time of peak heat demand
A_7	Peak Heat Demand (COP)	Coefficient of Performance at the time of peak heat demand
A_8	Peak Heat Demand Time	Time at which peak heat demand occurred
A_9	Second Peak Heat Demand (EHp)	Electric demand (kW) at the time of second peak heat demand
A_{10}	Second Peak Heat Demand (HHp)	Heat demand (kW) at the time of second peak heat demand
A_{11}	Second Peak Heat Demand Time	Time of second peak in the heat demand profile
A_{12}	Third Peak Heat Demand (EHp)	Electric demand (kW) at the time of third peak heat demand
A_{13}	Third Peak Heat Demand (HHp)	Heat demand (kW) at the time of third peak heat demand
A_{14}	Third Peak Heat Demand Time	Time of third peak in the heat demand profile
A_{15}	Average Electric Demand	Average electric demand (kW) for the day
A_{16}	Average Heat Demand	Average heat demand (kW) for the day
A_{17}	Average Demand COP	Average COP for the day
A_{18}	Total Electric demand	Sum of the daily electric demand profile (kWh)
A_{19}	Total Heat Demand	Sum of the daily heat demand profile (kWh)
A_{20}	Minimum Electric Demand (EHp)	Electric demand (kW) at the time of minimum electric demand
A_{21}	Minimum Electric Demand (HHp):	Heat Demand (kW) at the time of minimum electric demand
A_{22}	Minimum Electric Demand Time	Time at which minimum electric demand occur
A_{23}	Minimum Heat Demand (EHp)	Electric Demand (kW) at the time of minimum heat demand
A_{24}	Minimum Heat Demand (HHp):	Heat Demand (kW) at the time of minimum heat demand
A_{25}	Minimum Heat Demand Time	Time at which peak heat demand occurred
A_{26}	ON Times	No of Hours in which heating is turned on
A_{27}	OFF Times	No of Hours in which heating is turned off
A_{28}	Min – Max EHp	Difference between the minimum and maximum electric demand
A_{29}	Min – Max HHp	Difference between the minimum and maximum heat demand
A_{30}	Average – Max EHp	Difference between the average and maximum electric demand
A_{31}	Average – Max (HHp)	Difference between the average and maximum heat demand
A_{32}	Minimum – Second Peak EHp	The lowest electric demand between the first and second peak
A_{33}	Minimum – Second Peak HHp	The lowest heat demand between the first and second peak
A_{34}	Minimum – second Peak Time	Time of the lowest heat demand between first and second peak
A_{35}	Minimum to Third Peak EHp	The lowest electric demand between the second and third peak
A_{36}	Minimum to Third Peak HHp	The lowest heat demand between the second and third peak
A_{37}	Minimum to Third Peak Time	Time of the lowest heat demand between second and third peak
A_{38}	Min – Avg EHp	Difference between minimum and average electric demand
A_{39}	Min – Avg HHp	Difference between minimum and average heat demand
A_{40}	Min Demand Duration	Duration of minimum demand (demand less than 20% of average)
A_{41}	Peak Demand Duration	Duration of peak demand (Hours of continuous peak (80% of peak)
A_{42}	EHp No of Peaks	No of Peaks in the electrical demand profile
A_{43}	EHp No of Spikes	No of Spikes in the electrical demand profile
A_{44}	HHp No of Peaks	No of Peaks in the heat demand profile
A_{45}	HHp No of Spikes	No of Spikes in the heat demand profile

2.4. Discovering seasonal trends

Figure 3 provides a breakdown of the process used to determine seasonality. A representative profile was generated for each day of the year for each attribute, by averaging the attribute value across all properties or, in the case of time-based attributes, by modal values (e.g., the most popular time of peak heat demand across all properties for that day).
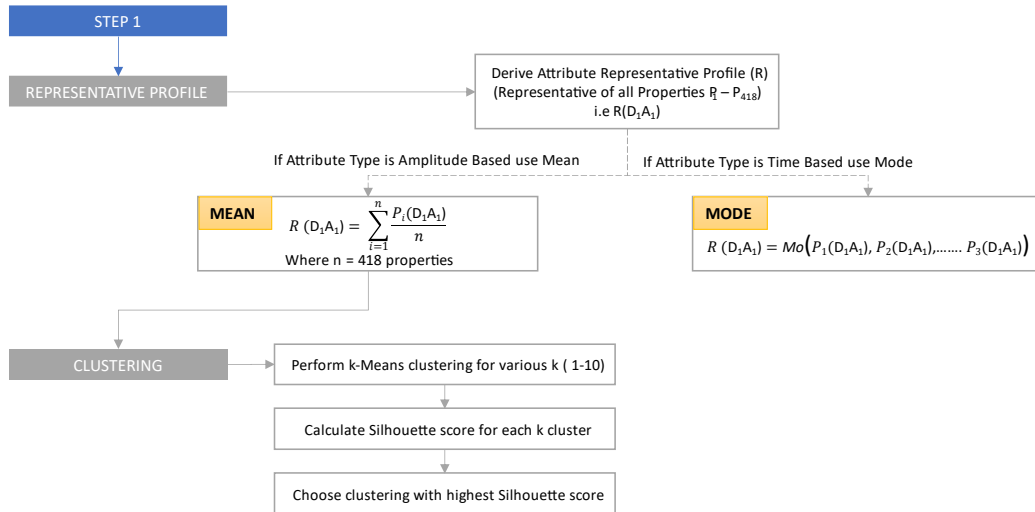
REPRESENTATIVE PROFILE

Derive Attribute Representative Profile (R)
(Representative of all Properties P̲ – P₄₁₈)
i.e R(D₁A₁)

If Attribute Type is Amplitude Based use Mean

If Attribute Type is Time Based use Mode

MEAN

$$R\ (D_1A_1) = \sum_{i=1}^{n} \frac{P_i(D_1A_1)}{n}$$

Where n = 418 properties

MODE

$$R\ (D_1A_1) = Mo\big(P_1(D_1A_1), P_2(D_1A_1),\ldots\ldots P_3(D_1A_1)\big)$$

CLUSTERING

Perform k-Means clustering for various k (1-10)

Calculate Silhouette score for each k cluster

Choose clustering with highest Silhouette score

Figure 3: Flowchart for extrapolating seasonal trends

Using K-Means clustering to determine seasonal trends in the representative profiles, different groupings of similar properties were given. The Silhouette score (Figure 3) was used to determine the number of clusters that best represented the separation of representative profiles in the data. Higher scores (scale of -1 to +1), indicated more dense and well-separated clusters, where -1 indicated invalid clustering. K-means clustering was an unsupervised machine-learning algorithm used to group datasets into different clusters. The clustering with the highest silhouette score was then chosen. K-Means clustering was not performed for time-based attributes since it could skew the results. Hence, the modal values were plotted directly for time-based attributes, and the optimal number of clusters evaluated by visual inspection. The results of the seasonal examination of the various attributes are presented in section 3.1.

2.5. Clustering properties for evaluating impact of various property characteristics

To determine whether property characteristics (metadata) were an influencing factor on the extracted features (attributes of Table 2) of heat demand, agglomerative hierarchical clustering (AHC) was carried out on the load time-series profiles of each attribute. This provided clusters of properties (with their representative profile) for each attribute. As a measure of property characteristic alignment to attribute feature, the standard deviation of ratio of property characteristics in the cluster were used as a determinant of significant heterogeneity between clusters (implying that the cluster formation relates with the metadata). For example, for Metadata M_1, the ratio of M_{1A}, M_{1B} in each cluster was computed and the standard deviation of ratio across the clusters found. A cut-off of standard deviation of 0.3 was set to highlight significant variation in the makeup of each cluster as informed by Deeks et al. (2022). Figure 4 provides a flowchart of the impact assessment methodology. The result of the analysis is presented in Section 3.2.

Loop through each Attribute A_i
$A_1 - A_{45}$

Cluster the 418 Properties using
Agglomerative Hierarchical Clustering

For Metadata $M_{1A} - M_{5C}$

Compute the Standard Deviation of the ratio of properties distribution across the derived clusters

Highlight Attribute/Metadata with significant Standard Deviation (Cut Off: 0.3)
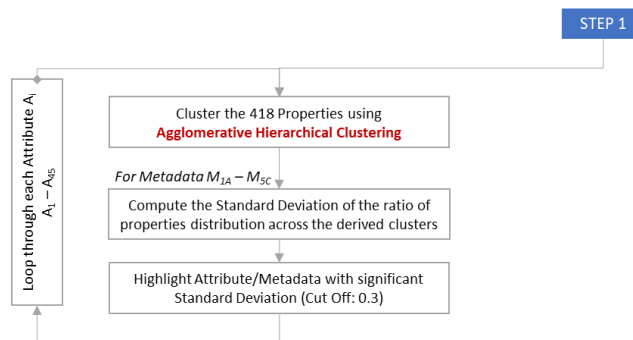
Figure 4: Flowchart for determining influence of property characteristics on extracted attributes.

3. RESULTS

The result of the seasonal clustering (k-means) is presented in Section 3.1 whilst that of the properties clustering (AHC) is presented in section 3.2.

3.1. Clustering annual profiles to evaluate seasonality

Figure 5 shows the summary of the number of clusters identified for each of the 45 defined attributes. 39 out of the 45 attributes investigated exhibited seasonality. The majority of attributes had 2 clusters, while some had 3 or 4 clusters.
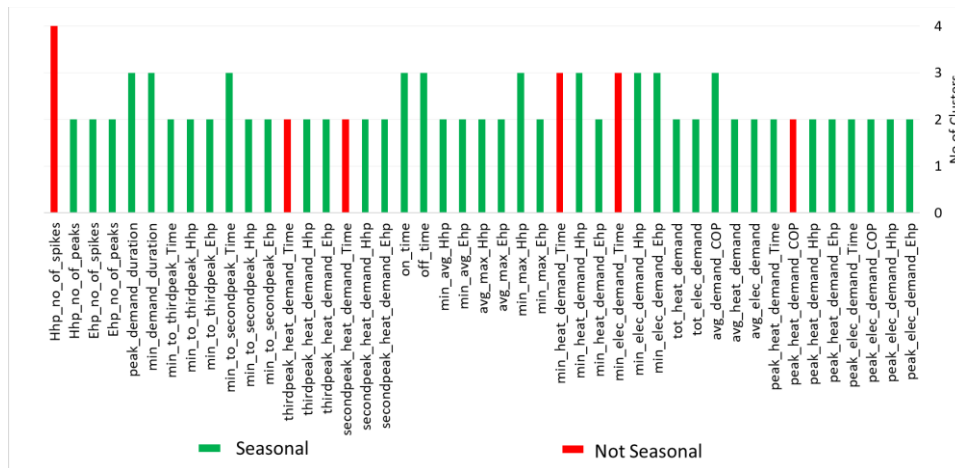

Figure 5: Seasonal cluster distribution summary

Figure 6 shows the clustered mean values for the various attributes classified under amplitude, range, duration, time, peaks and COP. Seasonality was evident in amplitude and duration attributes (Figure 6a and Figure 6c) with heating load and duration reduced between June to October and transition periods evident due to stepping between heating/reduced heating seasons. While there was an early drop in average demand (which also corresponded to total demand and the on and off time or duration) at the end of March, peak demand did not drop until the end of May. Figure 6b shows the seasonality in ranges (min-max, min-avg, min-secondpeak and min-thirdpeak) were consistent with amplitude and duration. However, the avg-max range had a less distinct seasonal difference and only dropped in July/August. This indicated that a similar level of peakiness (difference between peak and average) was maintained for most of the year.

While the timing of peak demand was seasonal (switches from morning during the winter to evening during the summer), the time of additional peaks were not seasonal as shown in Figure 6d. In addition, the time of minimum demand was also not seasonal and mostly started at 11pm at night.
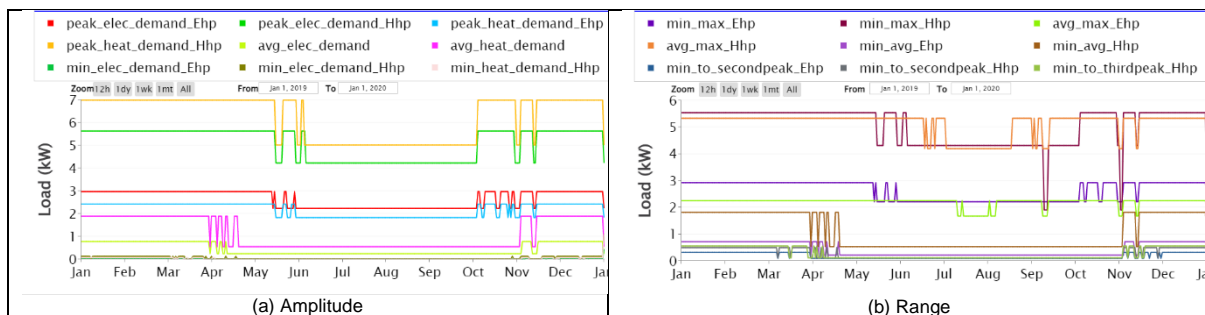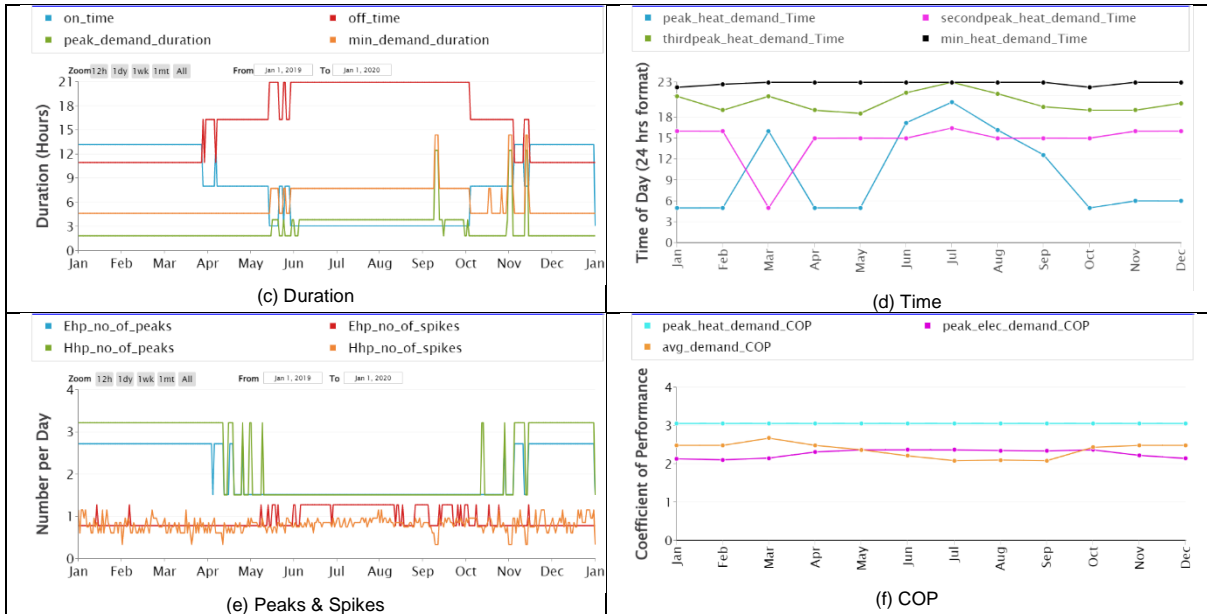

(a) Amplitude

(b) Range

Figure 6: Clustered annual profiles for various attributes (a) Amplitude (b) Range (c) Duration (d) Time (e) Peaks &Spikes (f) COP

Occurrence of peaks was higher from November to April whilst spikes were higher in number from June to September. There was an average of three peaks during the winter, hence it is important to understand the timing and amplitude of these additional peaks. COP was only weakly seasonal for peak electric demand time and daily average COP – increasing slightly from April to September for peak electric demand time and decreasing (contrary to expectation) for daily average COP. Peak heat was generated at maximum COP throughout the year.
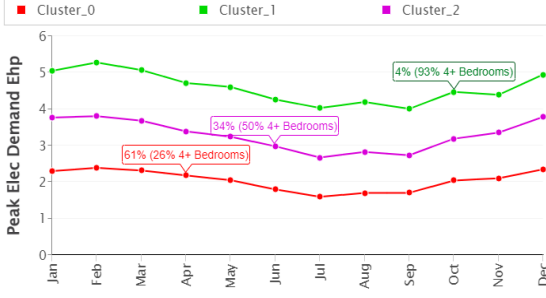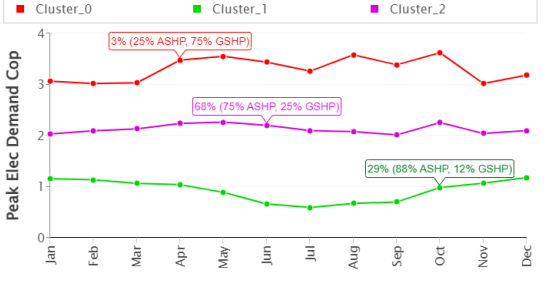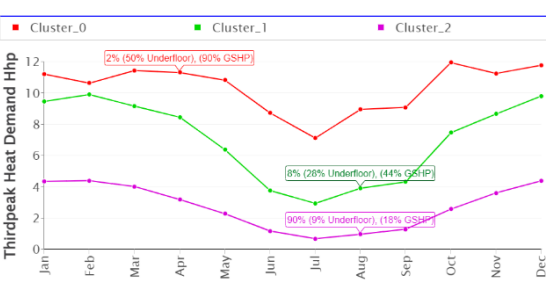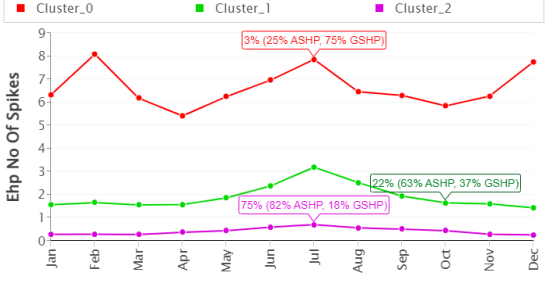
3.2. Clustering properties for evaluating impact of various metadata

The standard deviation of the ratio of properties for each metadata across all attributes is presented in Table 3. Highlighted cells indicate significant standard deviation (> 0.3) in the ratio of properties across clusters, and hence signalling a significant impact of the metadata on the attribute. Each highlighted Attribute/Metadata pair was then examined in detail to understand the impact. Some Metadata were not defined in some properties. Further filtering was done to exclude evaluating cases where a metadata was not defined for greater than 50% of properties (M_2 & M_3 were excluded). Details of the evaluated cases is presented in Table 4.

Table 3: Standard deviation of ratio of properties for each Metadata across all Attributes

Attr	M1A	M1B	M2A	M2B	M2C	M3A	M3B	M3C	M3D	M3E	M3F	M4A	M4B	M4C	M4D	M5A	M5B	M5C
A1	0.1	0.1	0.02	0.02	0	0.18	0.04	0.02	0.01	0.02	0.16	0	0.03	0.23	0.34	0.09	0.25	0.16
A2	0.19	0.19	0.09	0.06	0	0.09	0.11	0.1	0.08	0.01	0.06	0	0.09	0.06	0.17	0.16	0.25	0.11
A3	0.34	0.34	0.11	-	-	0.06	-	-	0.02	-	0.15	-	0.03	0.12	0.11	0.18	0.16	-
A4	0.11	0.11	0.15	-	-	0.09	-	-	-	-	0.2	-	-	0.02	0.07	0.08	0.06	-
A5	0.09	0.09	0.26	0	-	0.05	0.06	0.03	0.06	0.05	0.02	0	0	0.11	0.25	0.04	0.11	0.07
A6	0.23	0.23	0.08	-	-	0.12	0.04	-	-	0.04	0.11	-	-	0.07	0.17	0.19	0.26	0.07
A7	0	-	-	-	-	0	-	-	-	-	-	-	-	-	0	-	0	-
A8	0.06	0.06	0.15	-	-	0.11	-	-	0.02	-	0.05	-	-	0.08	0.03	0.02	0.01	-
A9	0.2	-	0.04	0.03	-	0.05	-	-	0.23	0.04	0.12	-	-	0.1	0.14	0.08	0.21	0.13
A10	0.09	0.09	0.08	0	0	0.09	0.04	0	0.24	0.07	0.04	0	0.07	0.06	0.08	0.11	0.16	0.04
A11	0.09	0.09	0.06	-	-	-	-	-	0.16		0.13	-	-	0.11	0.09	0.05	0.07	0.04
A12	0.19	0.12	0.04	0.06	-	0.09	0.03	0.04	0.12	0.04	0.16	-	0.02	0.15	0.09	0.13	0.17	0.04
A13	0.37	0.37	0.05	0.06	-	0.14	-	-	-	0.02	0.08	-	-	0.09	0.16	0.2	0.34	0.14
A14	0.1	0.02	0.12	-	-	0.04	-	0.09	0.04	-	0.18	-	-	-	0.35	0.08	0.16	0.09
A15	0.19	0.19	0.15	0.15	0	0.22	0.01	0.04	0.01	0.04	0.15	0	0.01	0.05	0.15	0.18	0.2	0.15
A16	0.19	0.19	0.11	-	-	0.11	-	0.08	0.04	-	0.11	-	-	0.12	0.14	0.28	0.27	-
.	.	.	.	.	.	.	.	.	.	.	.	.	.	.	.	.	.	.
.	.	.	.	.	.	.	.	.	.	.	.	.	.	.	.	.	.	.
A30	0.08	0.08	0.11	-	-	0.09	-	0.03	0.04	-	0.08	-	-	0.17	0.25	0.15	0.21	0.06
A31	0.1	0.1	0.09	0.04	0	0.1	0.04	0.03	0.04	0.05	0.1	0	0.06	0.08	0.14	0.12	0.17	0.06
A32	-	0.44	-	-	-	-	-	-	-	-	0.39	-	-	-	0.25	0.51	-	-
A33	0.17	-	-	-	-	-	-	-	-	-	-	-	-	-	-	-	0.12	-
A34	0.2	0.2	0.13	-	-	0.04	-	0.08	0.08	0.14	0.21	-	0.13	0.16	0.03	0.04	0.06	-
A35	-	0.54	-	-	-	-	-	-	-	-	0.48	-	-	-	0.25	0.62	-	-
A36	0.17	-	-	-	-	-	-	-	-	-	-	-	-	-	-	-	0.12	-
A37	0.04	0.04	0.24	0.27						0.52			0.23		0.04	0.05	0.05	
A38	0.1	0.1	0.07	0.09		0.16		0	0.05	0.04	0.1			0.06	0.09	0.16	0.18	0.15
A39	0.15	0.15	0.11	0.01	0	0.08	0.06	0.05	0.07	0.06	0.09	0	0.06	0.09	0.16	0.07	0.12	0.07
A40	0.22	0.22	0.07								0.39				0.31		0.05	0.03
A41	0.11	0.11	0.12			0.14			0.09		0.08		0.16	0.14	0.16	0.07	0.06	0.02
A42	0.09	0.09															0.11	
A43	0.3	0.3	0.06			0.46									0.26	0.03	0.05	0.07
A44	0.08	0.08	0.05			0.11	0.01		0.03		0.39			0.02	0.25	0.20	0.14	0.13
A45	0.32	0.32	0.07			0.49									0.24		0.04	0.07

Attribute	Cluster Presentation	Comments
A_1 - Peak Electric Demand (EHp)		Properties with more than 4 bedrooms were more likely to have a higher peak electric demand (cluster 1). 93% of properties in Cluster 1 had four or more bedrooms, in cluster 2, 50% had 4+ bedrooms while in cluster 1, just 26% had 4+ bedrooms.
A_3 - Peak Electric Demand (COP)		75% of properties in cluster 0 used ground source heat pumps while 88% of properties in cluster 1 and 75% of properties in cluster 2 used air source heat pumps. This showed that properties with ground source heat pumps tended to have better COP values. In addition, the COP values also seemed slightly higher for properties with underfloor heating.
A_{13} - Third Peak Heat Demand (HHp)		Additional peaks for GSHP were as high as 7-12kW; a high percentage of these properties used underfloor heating, while for ASHP, additional peaks were much lower between 0.5kW – 4kW and had radiator heating. However, it was not clear whether the heat distribution system had an impact on the amplitude of additional peaks or if houses installing GSHP were more likely to have underfloor heating installed.
A_{43} – Ehp No of Spikes		Majority of properties in Cluster 0 (the cluster with high number of spikes) used ground source heat pumps.

4. DISCUSSION

4.1. Peak demand and time

Among all metadata considered, only the number of bedrooms significantly influenced peak demand. The peak electric demand was higher for properties with 4 or more bedrooms. Most properties using ground source heat pumps had better COP values. The property type and property age metadata (M_2 & M_3) was undefined for a significant number of properties; hence the effect of property type or property age on peak demand could not be conclusively determined. Figure 7a shows 85% of houses had two to three peaks during the winter and one peak during the summer, whilst the other houses could have 4-6 peaks. Figure 7b shows that most houses had few numbers of spikes, however, there were instances of 12 spikes during the winter.
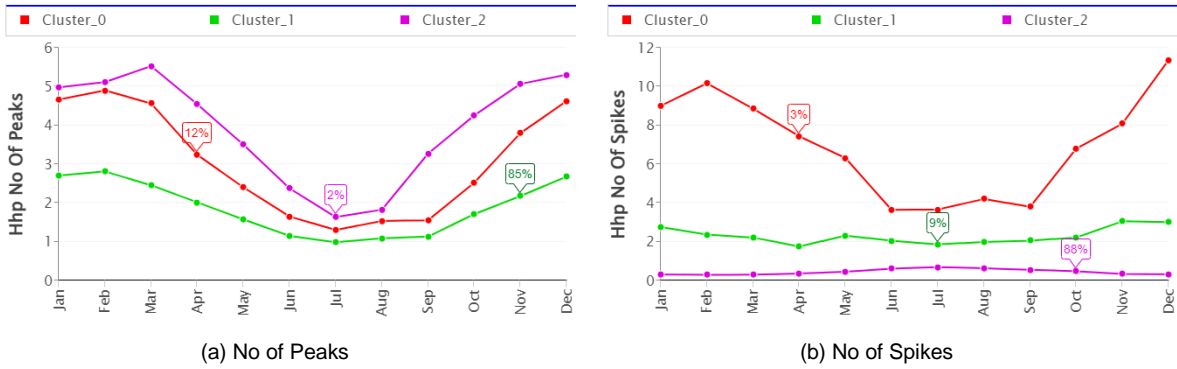
(a) No of Peaks

(b) No of Spikes

Figure 7: No of Peaks vs No of Spikes by cluster

While most properties had 2-3 peaks, about 14% had 4-6 peaks. This may be an indication of households who actively control their heating instead of having fixed periods of heating, and households who stay at home throughout the day. There were three identifiable peak periods in a day across the properties: morning; afternoon/early evening; and late evening peaks, as shown in Figure 8. For 60% of properties, the peak heat demand (Figure 8a) occurred in the morning between 4-7am throughout the year. For 36% of properties, it occurred in the afternoon between 4 – 5:00pm during the winter, but barely kept on during the summer. The second peak demand (Figure 8b) occurred in the afternoon (between 12pm - 3pm) for 61% of properties (Cluster 2), while for 36% of properties (Cluster 1), it occurred in the evening (between 4 - 6pm) during the winter and 9 -11pm in the summer. The timing of peak demand did not show any correlation with any of the property metadata. Clusters based on peak demand time may exist due to other factors such as user behaviours, work patterns, preferences rather than their property types or characteristics.
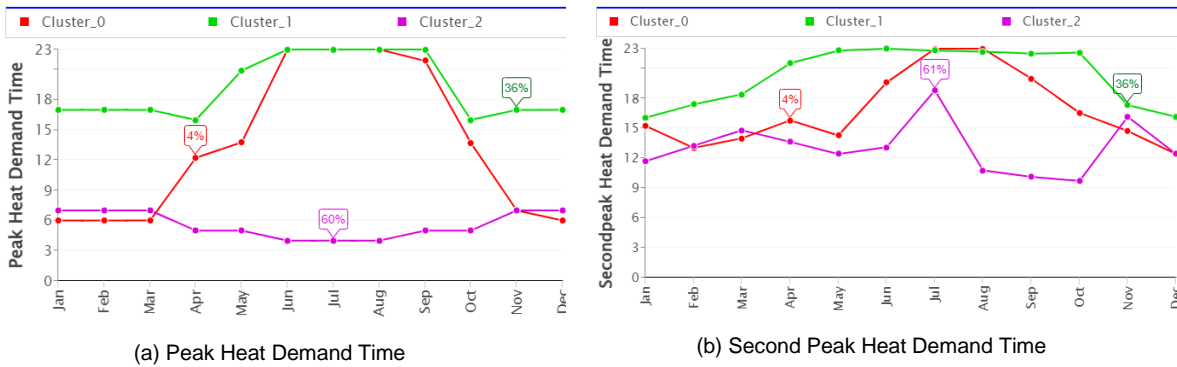

(a) Peak Heat Demand Time

(b) Second Peak Heat Demand Time

Figure 8: Average monthly time of day occurrence for (a) Peak Heat and (b) Second Peak Heat demand by cluster

4.2. Duration of demand, peak demand and minimum demand

Demand duration across various property characteristics were analysed in order to understand how, when and by how much load could be shifted. Three patterns (clusters) were identified for demand duration as shown in Figure 9a. Clusters 0(3%), 1(91%), and 2(6%) differed in daily on-time by as much as ~14 hours (March) and as little as ~4 hours (July) with winter on-time almost all day for cluster 0 and summer on-time of cluster 1 reaching a minimum of ~2 hours. The total demand was higher for properties where heating was turned on for a longer time. This confirmed that the periodical heating of homes is a more energy efficient practice. There was no significant connection between the property characteristics (metadata) and the duration of heating.
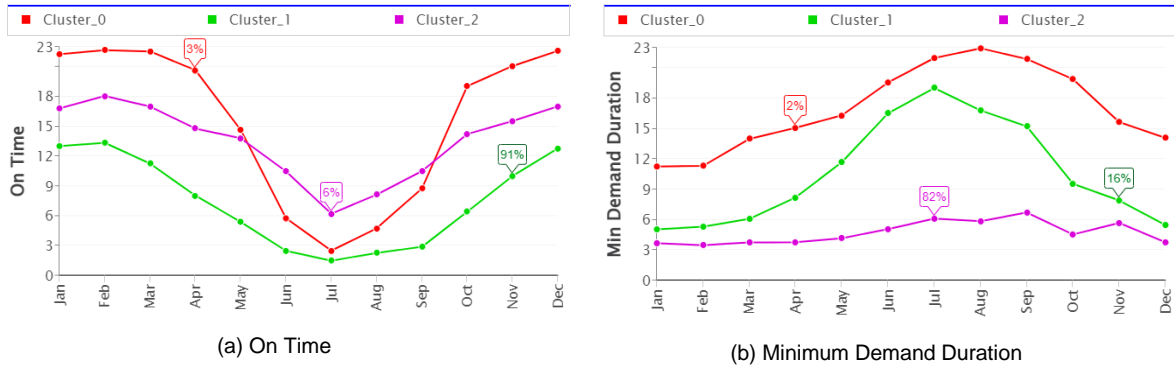
41

(a) On Time
(b) Minimum Demand Duration

Figure 9: Duration of demand and minimum demand by cluster

Peak demand usually lasted for less than 2 hours as shown in Figure 6c, though it could last up to 4 hours. Figure 9b shows the profile for minimum demand duration. For over 80% of properties (Cluster 2), the minimum demand would last for 3.5 hours during the winter and up to 6.5 hours during the summer. The minimum demand lasted longer for clusters 0 and 1, furthermore, during the summer the heat pumps were barely kept on or were operated at minimum demand, hence had a longer minimum demand duration. 92% of properties experienced their minimum demand between 12am – 3am in the winter. The time of minimum demand was spread across the day during the summer period.

4.3. Implications for tariff design and energy storage control strategies

Time of use tariffs are an essential strategy for an efficient and fair electricity system. However, a poorly designed tariff may provide worse outcomes if it signals the wrong incentive to users or is not feasible with the group of properties it was targeted towards. An example of time of use tariff in the UK is TIDE Tariff (Green Energy UK, 2022). TIDE penalizes peak demand between 4pm - 8pm (which reflects the current peak demand time in the UK). However, adoption of heat pumps may change tariff times since many properties experience their peak demand in the morning. Hence, energy suppliers may adjust tariffs to cover morning peaks. By assessing the property type and discerning the peak characteristics within various properties, a better understanding of how tariff strategies could help reshape load may be realised.

With multiple peak periods across the day, an important consideration is distribution of storage to handle the relative timing and duration of peaks. This work shows that peak demand would typically last for less than 2 hours, but on several occasions, it lasted up to 4 hours. If the objective of demand response is peak shaving, then storage capacity, charge and discharge timings and rates need consideration to target multiple peaks. 64% of properties experience their second peak demand in the afternoon between 12-3pm during the winter, hence, afternoon may not be a good time for charging or topping up storage to manage evening peaks. This result aligns with previous research which shows that Economy 10 tariffs (low tariff hours in the afternoon) were not effective in reducing peak demand and resulted in additional peaks created in the afternoon (Sweetnam et al., 2019).

5. CONCLUSION

In this work, we investigated seasonal trends and the influence of various property characteristics (metadata) on clustered features of demand (attributes). The analysis showed that seasonal trends were exhibited by the majority of the considered attributes. Attributes may have had two, three or four clusters within the year. There was a transition period for seasonal attributes marked with values switching between heating and reduced heating periods. The number of bedrooms had an impact on peak demand and properties with ground source heat pumps tended to have better coefficient of performance (COP). Most houses experienced more than two peaks during the winter; during the summer, they experienced greater spiking in demand (irregular and non-consistent peaks). Hence, tariffs and storage control should not be restricted to the already established morning and evening peaks but should consider the occurrence of multiple peaks. Attributes were evaluated for daily cycles only in this work but could also be evaluated for longer consecutive time series (such as weekends) to understand the relation of multiple day attribute variation for possible demand management measures through thermal storage technology and agile price-tariffs.

6. REFERENCES

Agbonaye, O., Keatley, P., Huang, Y., Ademulegun, O. O., & Hewitt, N. (2021). Mapping demand flexibility: A spatio-temporal assessment of flexibility needs, opportunities and response potential. *Applied Energy*, *295*, 117015. https://doi.org/10.1016/j.apenergy.2021.117015

Agbonaye, O., Keatley, P., Huang, Y., Odiase, F. O., & Hewitt, N. (2022). Value of demand flexibility for managing wind energy constraint and curtailment. *Renewable Energy*, *190*, 487–500. https://doi.org/https://doi.org/10.1016/j.renene.2022.03.131

Chen, Y., Xu, P., Gu, J., Schmidt, F., & Li, W. (2018). Measures to improve energy demand flexibility in buildings for demand response (DR): A review. *Energy and Buildings*, *177*, 125–139. https://doi.org/https://doi.org/10.1016/j.enbuild.2018.08.003

Deeks, J. J., Higgins, J. P., & Altman, D. G. (2022). Chapter 10: Analysing data and undertaking meta-analyses. In: Cochrane Handbook for Systematic Reviews of Interventions. In *Cochrane Handbook for Systematic Reviews of Interventions*. www.training.cochrane.org/handbook

Green Energy UK. (2022, June). *TIDE | Time of use tariff | Manage Energy Consumption*. https://www.greenenergyuk.com/tideabout

lo Piano, S., & Smith, S. T. (2022). Energy demand and its temporal flexibility: Approaches, criticalities and ways forward. *Renewable and Sustainable Energy Reviews*, *160*, 112249. https://doi.org/https://doi.org/10.1016/j.rser.2022.112249

Love, J., Summerfield, A., Biddulph, P., Wingfield, J., Martin, C., Gleeson, C., & Lowe, R. (2017). *Investigating Variations in Performance of Heat Pumps Installed via the Renewable Heat Premium Payment (RHPP) Scheme*. *8151*, 2013–2015.

Sweetnam, T., Fell, M., Oikonomou, E., & Oreszczyn, T. (2019). Domestic demand-side response with heat pumps: controls and tariffs. *Building Research and Information*, *47*(4), 344–361. https://doi.org/10.1080/09613218.2018.1442775

#55: How to increase the photocatalytic activity of titanium dioxide for hydrogen production

E. Esra KASAPBAŞI[1], Serap KIRCI[2], Arzu HATIPOĞLU[2]

[1] Haliç University, Faculty of Arts and Sciences, Department of Molecular Biology and Genetics, İstanbul, Turkey
esrakasapbasi@halic.edu.tr
[2] Yıldız Technical University, Chemistry Department, Davutpaşa Campus, İstanbul, Turkey, ahatip@yildiz.edu.tr

Abstract: Photocatalytic hydrogen production by the splitting of water is a sustainable, renewable and promising technology. Being able to meet future energy needs by producing green and clean hydrogen fuel will have a significant impact on the environment. By using a TiO_2 photocatalyst with sunlight, water can be separated into H_2 and O_2 and hydrogen fuel production can be supported. However, TiO_2 has a wide band-gap (~3.2 eV) and is only excited by UV-light: it is inactive under visible light irradiation. Thus, much of the research developed in recent years has been focused on extending the optical absorption of TiO_2 to the visible region of the spectrum in order to substitute UV-light by sunlight to make use of solar energy for practical applications. It has been known that doped cations induce visible-light absorption and influence the photoreactivity of TiO_2. Despite extensive research on cation-doped TiO_2, there is still no unifying result or explanation for the effect of cations on the photocatalytic activity of TiO_2 under solar light. In this study, the non-defective anatase (001) surface was modelled with finite, neutral, stoichiometric cluster models cut from the anatase bulk structure in order to determine the location and the bonding status of the dopant cations. In the doped models, substitutional locations of cations were analyzed. The structures of the doped models were constructed by replacing one titanium atom by one cation. All the calculations were carried out using the Density Functional Theory (DFT) method. The DFT calculations were performed by the hybrid B3LYP functional. 6-31 G(d) basis set was used. The dopant positions were optimized by changing their locations in the clusters to find the lowest energy configuration. All of the investigated cations reduced the band gap energy of TiO_2, thus increasing visible-light activity. In addition, it was calculated that metal doping affected the decomposition of water positively.

Keywords: TiO_2; DFT; photocatalysis; water splitting; doping

1. INTRODUCTION

H_2, which can be used as fuel, is a renewable green energy source and does not emit CO_2 to the environment. H_2, which can be used in fuel cells, can produce higher energy per weight unit (120.7 kj/g) compared to other hydrocarbons (Ehteshami *et al.*, 2014; Da Silva Veras *et al.*, 2017*)* It is also a type of fuel that can be transferred like hydrogen gasoline and stored in gas or liquid phase (Balat, 2007; Shakya, 2005). Hydrogen can be stored by physical and chemical methods, but both methods have many disadvantages (Ismael, 2021).

One of the most preferred and attractive approaches of all conventional hydrogen production techniques is to split water using photocatalyst and renewable solar energy to produce hydrogen. With the help of photocatalyst and sun light, water can be split to produce hydrogen (Chen, 2010).

1.1 TiO$_2$ photocatalyst

Water, the world's most valuable and important natural resource, is at risk of contamination by organic pollutants (Choa *et al.*, 2011). After the discovery of the photocatalytic activity of titanium dioxide (TiO_2) by Honda and Fujishima in 1972, TiO_2 photocatalysis has been used as an advanced oxidation method (Fujishima *et al.*, 1972). TiO_2 has three different crystal structures as shown in Figure 1. These are anatase, rutile and brookite and they have different (TiO_6) structures (Yalçın *et al.*, 2010; Yu *et al.* 2010).
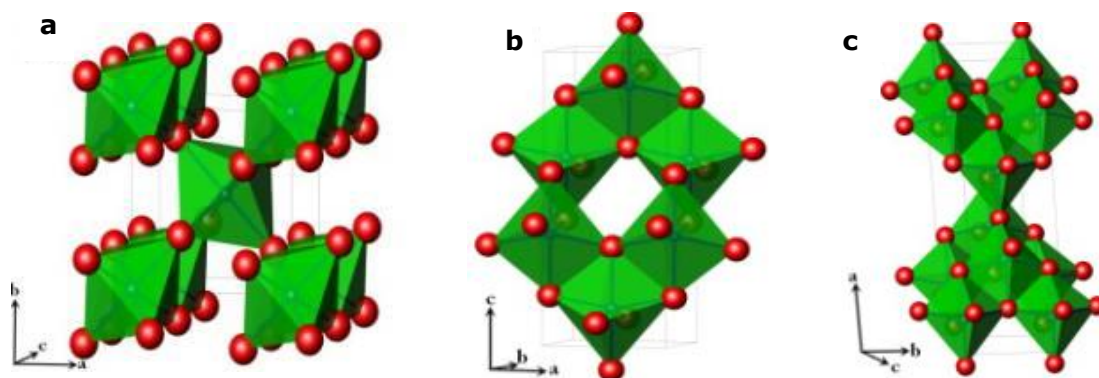

Figure 1: Crystal structure of the three common polymorphs of titania (a) rutile b) anatase, c) brookite) (Kirca, 2022)

Anatase crystal is used as a photocatalyst in the presence of UV light and has a tetragonal structure. The anatase form is preferred because its photocatalytic activities are higher than other crystal structures. TiO_2 is a widely studied photocatalyst due to its potential applications in photocatalysis in the degradation of organic compounds in air and water. In addition to many semiconductor photocatalysts such as WO_3, ZnO, ZnS, Fe_2O_3, CdS and $SrTiO_3$, TiO_2 is a preferred heterogeneous photocatalyst because it is inexpensive, non-toxic, chemically inert, and photo-stable. TiO_2 can only be excited by UV-light due to its wide band gap (~3.2 eV) so not active under visible light. This disadvantage of TiO_2 limits the utilization of solar energy. The fact that TiO_2 can be activated by UV light, which constitutes a very small part of the solar spectrum, limits the use of this material in practical applications. For practical applications, the photoactivity of TiO_2 needs to be improved. For this reason, the development of visible light-active semiconductor photocatalysts will increase the gain associated with the use of sunlight (Birben *et al.*, 2015; Gurkan *et al.*, 2012). One way to increase photoactivity under sunlight is by doping TiO_2 with transition metals or noble metals. As a result of this doping, the absorption band is shifted from the UV region to the visible region.

The first step in photocatalysis is the formation of electron-hole (e^-/h^+) pairs by excitation with light with an energy equal to or higher than the band gap of TiO_2. In the presence of oxygen, these pairs migrate to the interface to give oxidizing species. In liquid suspension systems, electrons are trapped in the cavities (Ti^{3+}) on the surface and react with the adsorbed O_2 to form superoxide anion radicals. The cavities react with surface OH^- groups or water molecules to produce $OH^•$ radicals. In order to increase the activity of TiO_2 under visible light, doping with metals or nonmetals and surface modifications are made (Ho *et al.*, 2016; In *et al.*, 2007).
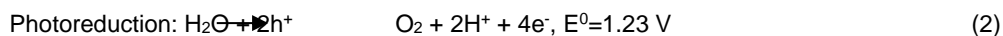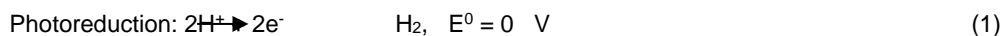
In order to increase the efficiency of TiO_2 photocalibrants under visible light, doping with metals and nonmetals has been done frequently in recent years (Birben *et al.*, 2015; In *et al.*, 2007; Likodimos *et al.*, 2013; Lu *et al.*, 2013; Wu *et al.*, 2006; Wu *et al.*, 2010; Yalçın *et al.*, 2010; Yu *et al.* 2010; Zaleska 2008; Jho *et al.*, 2008; Liu *et al.*, 2011; Moradi *et al.*, 2016). Doping with cations increases the photocatalytic activity due to reducing the recombination of e^-/h^+ pairs and increasing the charge distribution distance.

Karakitsou *et al.* (1993) concluded that doping with valence metals larger than Ti^{4+} increased the photocatalytic activity, while doping with metals equal to Ti^{4+} or low valence metal ions such as 3+, 2+, 1+ did not have much effect on the activity. The same researchers investigated the effects of W^{6+}, Ta^{5+}, Nb^{5+}, In^{3+}, Zn^{2+} and Li^+ cations on the performance of the photocatalytic activity of TiO_2 for the water separation process. They noted that H_2 production increased when W^{6+}, Ta^{5+}, Nb^{5+} cations were doped into TiO_2, whereas doping of TiO_2 with In^{3+}, Zn^{2+} and Li^+ decreased H_2 production.

1.2 Photocatalytic water splitting

Hydrogen is an ideal green fuel because it is produced from reusable energy and is not toxic. It can be obtained as a result of the breakdown of water by sunlight. The presence of ultraviolet (UV) or visible-light irradiation causing incoming photons to semiconductor photocatalysts such as, ZnS, TiO2 and ZnO, results in typical photocatalysis processes.

When sufficient photochemical energy is applied, electrons can be excited from the VB to the CB of the semiconductors, leaving positively charged holes in the VB. After that, electrons and holes should be separated and transferred to the surface of the photocatalyst to initiate the redox reactions to produce H_2 (Equation 1) and O_2 (Equation 2), respectively. As a result of the calculations, it was attempted to determine whether water preferred to bind to the structure in molecular or dissociated form.

$$\text{Photoreduction: } 2H^+ + 2e^- \qquad H_2, \quad E^0 = 0 \quad V \tag{1}$$

$$\text{Photoreduction: } H_2O + 2h^+ \qquad O_2 + 2H^+ + 4e^-, \ E^0 = 1.23 \ V \tag{2}$$

2. MATERIAL AND METHOD

As is known, the anatase phase is the most abundant phase. The surface of anatase particles predominantly consists of (101), (100) and (001) lattice planes. (001) surface has the highest photocatalytic activity (Homann *et al.*, 2004; Wahab *et al.*, 2008). Therefore, to determine the location and binding state of the dopant ion, the non-defective anatase (001) surface was modelled with finite, neutral and stoichiometric cluster models cut from the anatase pile. Each Ti atom coordinates with adjacent six O atoms, and each O atom coordinates with adjacent three Ti atoms, forming a $[TiO_6]$ octahedron structure. The first cluster $Ti_7O_{19}H_{10}$ (Model A) cut from anatase the bulk structure was constructed using the anatase unit cell structure. The unit cell for anatase has a tetragonal structure with aggregate lattice constants a = b = 3.78 Å and c = 9.51 Å. The second cluster is Model B with 75 atoms, $Ti_{19}O_{44}H_{12}$ formula, created by repetition of Model A along 4x1x1 network axes. All calculations were carried out with the Density Functional Theory (DFT) method (Stephens, *et al.*, 1994; Stephens, *et al.*, 1996) within the Gaussian 16 program package (Frisch, *et al.*, 2016). DFT calculations used the B3LYP hybrid functional (Becke, *et al.*, 1993) at the LanL2dz basis set (Hay *et al.*, 1985). The cluster geometry was kept constant during all calculations, but the dopant ion, hydrogen and OH groups were released. In order to find the optimum doping position in the doped models, the position of the doping ion was shifted to the possible positions on the cluster surface and the calculations were repeated and the lowest energy configuration was determined. All the structures were confirmed by frequency analyses at the same level of the theory. As a result, all geometric parameters and thermodynamic energies of the structures were calculated

There are two possible mechanisms for water adsorption: molecular adsorption and dissociative adsorption. Water adsorption on the surface of all models developed was investigated to determine which mechanism was more likely. For molecular adsorption, the oxygen atom of the water molecule was attached to a Ti atom on the surface in each model. Then, the calculation was repeated by shifting the connection position to different titanium. For dissociative adsorption, on the other hand, the OH group was attached to the possible titanium and additive ions on the surface of the models, and the H was attached to the oxygen atom next to it.

While calculating the binding energies of water to TiO_2 structure, basis set superposition error (BSSE) corrected bond energies were used. Errors resulting from the use of different base functions by two or more interacting molecules are called BSSE. In order to correct this error and to ensure that the molecules use the same base functions, the energies of all molecules were calculated in the same system. For this, calculations were made using the keyword B3LYP/LanL2dz counterpoise=2 (Foresman *et al.*, 2015). The adsorption energies of H_2O on TiO_2 surfaces were calculated with using Equation 3.

$$\Delta H_{ads} = \Delta H_{H2O-TiO2} - \Delta H_{TiO2} - \Delta H_{H2O} \tag{3}$$

Where:

- − ΔH_{ads} is the adsorption energy,
- − $\Delta H_{H2O-TiO2}$ is the energy of TiO_2 with adsorbed H_2O,
- − ΔH_{TiO2} is the energy of the TiO_2 cluster and
- − ΔH_{H2O} is the energy of water.

3. RESULTS AND DISCUSSION

Water adsorption on the TiO_2 surface occurs as a result of the electrostatic attraction between the positively charged titanium and the negatively charged oxygen of the water. Water adsorption can occur in two ways: molecular adsorption and dissociative adsorption. In order to find out which mechanism is valid on the doped TiO_2 surface, water adsorption on the surface of the modelled clusters was investigated by both methods. For H_2O adsorption on the Model A surface, molecular H_2O is as in Figure 2a; the OH^- of the H_2O molecule in the dissociated structure was attached to the X atom, and the H^+ to the oxygen atom next to it, as shown in Figure 2b.
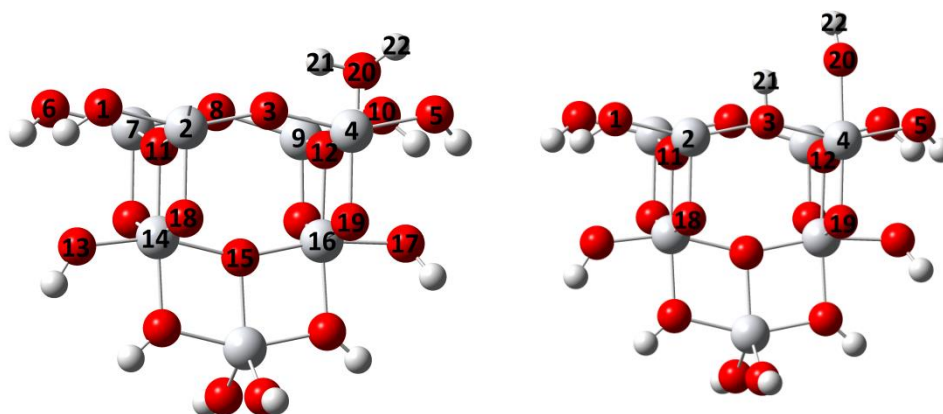

Figure 2: Binding of H2O on the Model A surface a) in molecular form b) dissociative

3.1 Water adsorption on model of surface

The geometric structure of the Model A with water adsorption is given in Figure 2-a. In order to explain the effect of water adsorption on TiO_2 surface, O-Ti, O-H bond lengths, Ti-O-Ti, O-Ti-O and H-O-H angles and Ti-O-Ti-O dihedral angles were measured in doped and undoped structures. The results are given SI 1.

There is a bond length of 2.086 Å between the O of the water attached to the undoped TiO_2 cluster and the titanium in the structure (Ti4-O20). When the water molecule is not attached to any cluster, it has a bond length of 0.96 Å and an angle of 109.5° between its oxygen and hydrogens. There is an angle of 116.1° and a bond length of 0.98 Å between the H21-O20-H22 atoms of the water molecule attached to the unadulterated TiO_2 cluster. According to these values, it can be said that the hydrogens of the water molecule move away from each other by being affected by the O of the cluster. The water molecule is located in the cluster with a dihedral angle of 127.2°.

The angle values between the H21-O20-H22 atoms of the water molecule added to the cluster in Co^{3+}, Ru^{3+}, Os^{3+}, Bi^{3+} doped are higher than the water's own value at the same time, these values are less than the value of the water molecule added to the pure TiO_2 cluster. For this reason, it is observed that the doping cations push the H^+ of the water molecule more than the additive and the angle becomes narrower. Although there is no significant change in bond lengths, there is little increase. It was observed that the geometric parameters in the 4+ valent cation doped clusters were closer to the values in the undoped TiO_2 cluster.

The H21-O20-H22 angle of water in clusters doped with 5+ cations (Sb^{5+}, Nb^{5+}, Ta^{5+}, V^{5+}) was greater than the H-O-H angle value of water itself. In the Sb^{5+} doped cluster, the water molecule moved away from the cluster surface upwards, and therefore the O3-H21 distance was 2.831 Å. In Nb^{5+}, Ta^{5+}, V^{5+} doped structures, the water molecule was positioned similarly in the cluster. Due to the interaction between the hydrogen of the water molecule and the 5+ d-doped metal in the cluster, the bond length between O3-H21 decreased by an average of 0,300 Å. It was

observed that the bond lengths between the O and H of water in 5+ doped clusters increased slightly due to the O in the TiO_2 cluster. While the water was positioned perpendicular to the surface in the Sb^{5+} doped structure in the clusters doped with 5+ valence cations, in the Nb^{5+}, Ta^{5+}, V^{5+} doped structures it deviated towards the horizontal with an average dihedral angle of 20°, in other words, similar to the undoped cluster position. As a result, H_2O tended to shift towards the doped metal in clusters doped with 5+-valent cations.

In clusters doped with 3+, 4+, 5+ valence cations, the water molecule moved away from the cluster, albeit slightly. In the adsorption of water on the Model A surface, the H-O-H angle and O-H bond length of the water molecule generally increased. These values were higher than the H-O-H value when the water molecule was alone, but less than the H-O-H value of the water molecule attached to the pure TiO_2 surface. This showed that the doping cations pushed the hydrogens of the water molecule more than the undoped and the angle became narrower.

The geometric structure of the Model A with water dissociative adsorption is given in Figure 2-b. Its geometric parameters are given SI 2. In the dissociative adsorption of water, water was first separated into H^+ and OH^- ions (Figure 2-b). In the developed model, the OH^- was bonded to the 5-coordinated Ti^{4+}, while the H^+ was bonded to the O atom next to this Ti. It was observed that while the water molecules attached to Model A in dissociated state, remained dissociated in clusters doped with 3+ valence cations, water returned to the molecular state in the undoped TiO_2 cluster. It was observed that in Co^{3+}, Os^{3+}, Bi^{3+} doped clusters, OH^- moved upwards from the cluster surface, that is, away from the Ti atom. In all clusters doped with 5+ valence cations, water remained dissociated. It was observed that the OH^- of water and hydrogen bonded to oxygen in the cluster were similarly positioned in clusters doped with Nb^{5+}, Sb^{5+}, Ta^{5+}, V^{5+}. It was observed that the OH^- of the water was positioned to the left from the end of the cluster and was displaced in the direction of approaching the oxygen of the water. In general, in clusters doped with 3+ cations, the H^+ and OH^- structures approached the cluster the most, while the approximation was less in 5+ valent cations. The least change occurred in the structures doped with 4+ valence cations, as in the adsorption of water.

The energy values of the water adsorption studies carried out with Model A were compared and the relationship between these values and whether the model remained in the "molecular" or "dissociated" state was examined (Table 1).

Table 1: Energy values obtained as a result of adsorption of water on the Model A surface

Metal	ΔE_{ads} molecules (kcal/mol)	ΔE_{ads} dissociated (kcal/mol)
Ti^{+4}	-32.76	-28.97
Co^{+3}	-9.45	-18.78
Ru^{+3}	-19.40	-129.54
Os^{+3}	-21.26	-27.72
Bi^{+3}	+47.44	-14.13
Zr^{+4}	- 29.63	-49.70
Sn^{+4}	-37.64	-141.67
Pd^{+4}	-28.21	-79.16
Cr^{+4}	-3.08	-164.46
Ge^{+4}	-21.56	-115.16
Nb^{+5}	-1.45	-126.50
Sb^{+5}	-34.52	-137.04
Ta^{+5}	-42.02	-133.08
V^{+5}	-35.51	-144.73

When the energy values given in Table 1 are compared, water preferred to bind to the structure in a dissociated state in all doped structures except for pure clusters.

The adsorption order of +3, +4 and +5 cations in doped structures was $Bi^{3+} < Nb^{5+} < Cr^{4+} < Co^{3+} < Ru^{3+} < Os^{3+} < Ge^{4+} < Pd^{4+} < Zr^{4+} < Ti^{4+} < Sb^{5+} < V^{5+} < Sn^{4+} < Ta^{5+}$. The negative adsorption energy values showed that adsorption had taken place in all doped models except Bi^{3+}. According to these results, the water adsorption on the anatase surface of the additive metal increased the most in the Ta^{5+} doped structure. All results showed that it was preferable to bind water in a dissociated state. These results showed that TiO_2 structures supported the degradation of water by the photocatalyst effect. V^{5+} -doped structure gave the best result.

3.2 Water adsorption on model b surface

The geometric structure of the model developed for the molecular water adsorption of the unadulterated Model B is given in Figure 3 and its geometric parameters are given in SI 3.
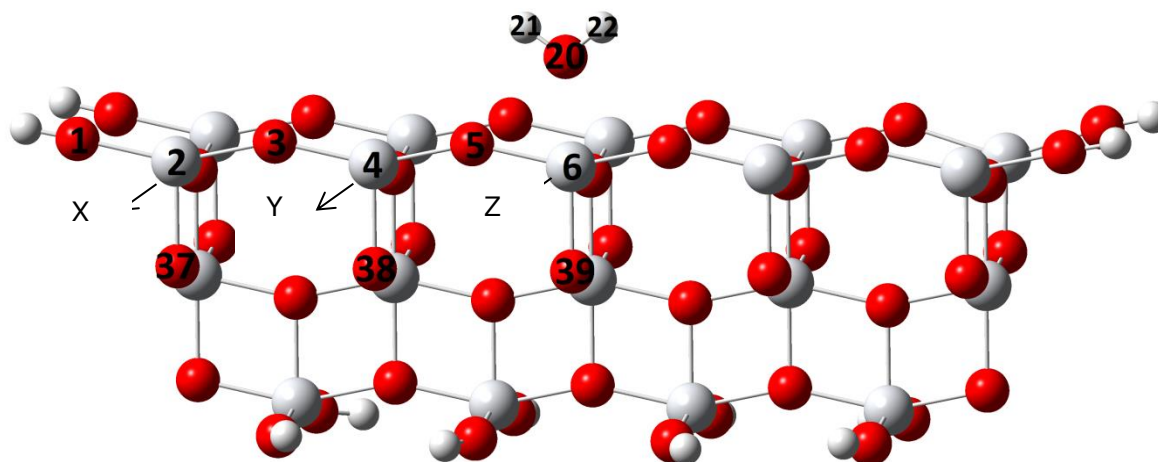

Figure 3: Geometric structure of Model B with molecular H_2O adsorbed on its surface

In the molecular and dissociated water adsorption studies of Model B, calculations were made for the determined (Kirci, 2009) lowest energy states. Adsorption studies of Model B were continued by attaching water molecules to neighbouring Ti atoms where there was no cation in the lowest energy clusters.

Although the water molecules were located in the structure with a similar dihedral angle in both X and Z positions, when they were connected in the Z position, they were further removed from the surface and the angle of the water molecule was less than the value in the X position and closer to its true value. The reason for this can be shown as the fact that the water molecule was less affected by other atoms in the cluster as it moved away from the structure.

When the geometric parameters calculated as a result of the adsorption of water in the 3+, 4+ and 5+ valent cation-doped models were examined, there was a significant change especially in the distance to the oxygen atoms on the right and left sides of Ti^{4+}, to which water was attached, and the angles it made with these atoms. The dihedral angle and the distance of water to the structure differed from the parameters of molecular adsorption of water on Model B.

The doping ion of the calculated lowest energy states of the Co^{3+}, Ru^{3+}, Os^{3+}, Bi^{3+} doped structures was located in the Y position. While there was an dopped ion in the Y position in Model B, the adsorption study was carried out by attaching the water molecules to the X and Z positions. Except for the Ru^{3+} doped structure, the H21-O20-H22 angle increased and the water molecule moved further away from the surface in the clusters doped with other 3+ cations. During the adsorption of water in structures doped with 3+ valent cations, water molecules were generally positioned on the surface with an average dihedral angle of 5°. In the Os^{3+} doped structure, the water molecule was located on the surface by making a dihedral angle of 60°. The reason for this can be seen that the diameter of Os^{3+} was larger than the other 3+ cations that were used as additive cations and that it rotated by affecting the water molecule in the cluster.

In structures doped with 4+ valence cations, the lengths between Ti^{4+} where water was attached, and water's oxygen were closest to the value in the pure structure (2,105 Å). Except for the Zr^{4+} doped cluster, since the most stable structures of Sn^{4+}, Pd^{4+}, Cr^{4+}, Ge^{4+} doped clusters were in the Y position, calculations were made by attaching water molecules to the X and Z positions in water adsorption. In the Zr^{4+} doped structure, water molecules were attached to the X and Y positions. When the angle values between the H_2O atoms of the undoped cluster were compared with the doped structures, there were different increases of between 2° and 12.4° in the doped clusters. This increase was in the Sn^{4+} doped structure with the largest atomic number. In addition, in structures doped with 4+ valence cations, water molecules bent towards the front of the structure with an average dihedral angle of 40° from the surface of the structure.

Since the Z position was the lowest energy state of the Nb^{5+}, Sb^{5+}, Ta^{5+}, V^{5+} doped structures, while there were doping ions in the Z position in Model B, water molecules were attached to the X and Y positions. In structures doped with 5+ valence cations, water molecules moved upwards from the surface while they were displaced horizontally (approximately 100) in a way that made a less dihedral angle towards the front of the surface, unlike clusters doped with 4+ valent cations. It was observed that the angle between H_2O atoms at Y positions was less in Nb^{5+}, Sb^{5+}, Ta^{5+}, V^{5+} doped structures of water molecules. At the same time, the distance between Ti^{4+} to which the water was bound and the oxygen of the water was higher in Y doped structures than in X doped structures. In all 3+, 4+ and 5+ doped clusters, when the water molecule was positioned close to the cluster, the oxygen atoms in the cluster attracted the H^+ of the water towards them, increasing the H21-O20-H22 angle value.

In the 3+, 4+ and 5+ valent cation doped models, the adsorption energies of the clusters with water molecules attached at the X position were higher than the others. For this reason, it preferred the Y and Z positions of the molecular adsorption of water in Model B in clusters.

The geometric structure of the developed model for the water adsorption in the dissociated state of the unadulterated Model B is given in Figure 4, and its geometric parameters are given in SI 4.
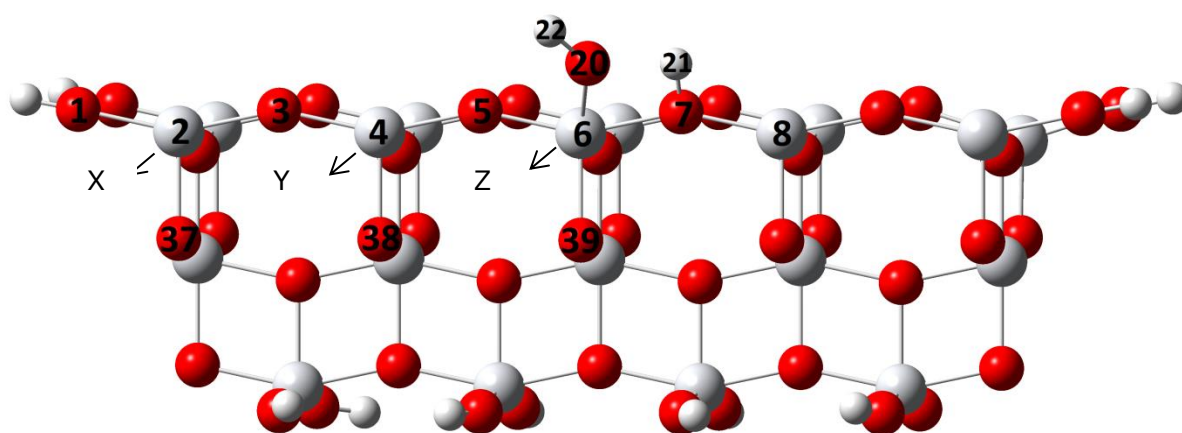

Figure 4: Geometric structure of Model B adsorbed dissociated H_2O on its surface

When water was adsorbed on Model B in the dissociated state, there was an increase of 0.12 Å in the O-H bond length. The bond length between O20-H21 of the water molecule, which was dissociated to the undoped cluster, was 1.547 at the X position and 1.007 at the Z position. These values were the distance between the oxygen of the water in the OH^- ion and the H^+ ion located separately in the cluster. In the X position, the dissociated water was located 0.098 Å further from the surface of the structure than in the Z position. In Y and Z positions, the water molecule stayed closer to the surface and the O20-H22 bond length increased. This was because as the water molecules approached the surface, they were attracted by other atoms in the cluster and caused the bond length (O20-H22) between the hydrogen and oxygen of the water to increase. Similar results were observed in 3+ and 4+ valance metal doped structures. The most striking point in the structures doped with 5+ valence cations was that the OH^- and H^+ ions of the dissociated water in the structure were farther from the surface than the structures doped with 3+ and 4+ valence cations. For this reason, the bond lengths of O20-H21 and O20-H22 in clusters were on average 0.10 Å longer. In the clusters that were connected in molecular form, the water molecules moved away from the surface of the structure. Another important point was that the structures doped with 5+ valence cations were positioned to make an average of 20° dihedral angles from the surface of the cluster to the front, just like the Pd^{4+} doped structure. This situation occurred as an average of 10^0 horizontal displacements of water in structures where water was bound in molecular form.

In Model B clusters that bind water in molecular and dissociated state, the displacement states of water on the cluster were similar. For this reason, the energy values of the doped clusters are given below to clarify in which doping ions. The energy values of the water adsorption studies performed with Model B were compared and its relationship with the "molecular" or "dissociated" state was examined (Table 2).

Table 2: Energy values obtained as a result of adsorption of water on the Model B surface

Metal	ΔE_{ads} molecules(kcal/mol)	ΔE_{ads} dissociated (kcal/mol)
Undopped (TiO_2)	-29.81	-92.49
Co^{+3}-Z	-12.09	+10.05
Ru^{+3}-Z	-37.6	-127.9
Os^{+3}-Z	-25.87	-79.16
Bi^{+3}-Z	-16.4	-36.8
Zr^{+4}-Z	-19.63	-27.90
Sn^{+4}-Y	-12.03	-95.09
Pd^{+4}-Y	-13.81	-120.57
Cr^{+4}-Y	-26.80	-100.52
Ge^{+4}-Y	-25.04	-104.83
Nb^{+5}-Z	-33.87	-128.16
Sb^{+5}-Z	-34.52	-130.55
Ta^{+5}-Z	-72.4	-142.8
V^{+5}-Z	-63.4	-169.2

When the adsorption energies were listed in Model B, $Sn^{4+} < Co^{3+} < Pd^{3+} < Bi^{3+} < Zr^{4+} < Ge^{4+} < Os^{3+} < Cr^{4+} < Ti^{4+} < Nb5^{+} < Sb^{5+} < Ru^{3+} < V^{5+} < Ta^{5+}$. The negative adsorption energy values showed that adsorption had taken place in all doped models. According to these results, in Model B, as in Model A, the water adsorption of the additive metal on the anatase surface increased the most in the structure with Ta^{5+} doped. In the calculations of water adsorption on the Model B surface, the values of water attached to two different atoms were calculated for each additive model. As seen in Table 2, the closer the place to which the water was attached to the doped atom, the lower the energy value. This showed that water preferred to be located close to the doped cation. Just like in Model A, in Model B, water preferred to remain decomposed.

4. CONCLUSIONS

In this study, energy and geometry calculations were performed by DFT method to increase visible light activity with cation contribution to TiO_2. In water adsorption studies, 3+ valence cations doped structured, the water molecule tended to move away from the doped cation. It was observed that while it remained dissociated in clusters doped with 3+ valence cations, water returned to molecular state in the undoped TiO_2 cluster. In the clusters doped with 4+ and 5+ valence cations, water preferred to remain dissociated. Structures doped with 3+, 4+ and 5+ valence cations generally increased the photocatalytic activity. As a result of this effect, water dissociation gave better results in structures doped with metals than in undoped structures. This increased the efficiency of obtaining H_2 fuel by breaking down the water. In future studies, calculations with different metal doped can be made with a higher basis set, and the studies can be continued.

5. REFERENCES

Balat M., 2007. Hydrogen in Fueled Systems and the Significance of Hydrogen in Vehicular Transportation. Energy Sources Part B., 2:49–61.

Becke, A. D. J., 1993. Density-functional thermochemistry. III. The role of exact Exchange. Chem. Phys. 98, 5648.

Birben, N.C. Uyguner-Demirel, C.S. Sen-Kavurmaci, S. Gurkan, Y.Y. Turkten, N. Cinar, Z. ve Bekbolet, M., 2015. Comparative Evaluation of Anion Doped Photocatalysts on the Mineralization and Decolorization of Natural Organic Matter. Catalysis Today, 240, Part A: 125-131.

Chen X, Shen S, Guo L, Mao SS.2010 Semiconductor-based Photocatalytic Hydrogen Generation. Chem. Rev.110(11):6503–70

Choa M. T., Mohammed A. R., 2011. Roles of Titanium dioxide and İon-Doped Titanium Dioxide on Photocatalytic Degradation of Organic Pollutants (Phenolic Compounds and Dyes) in Aqueous Solutions : A Review. Journal of Alloys and Compounds, 509, 1648-1660

Da Silva Veras, T., Mozer, T.S., da Costa Rubim Messeder dos Santos, D. and da Silva Cesar, A., 2017. Hydrogen: Trends, production and characterization of the main process worldwide. Int. J. Hydrogen Energ., 42, (4), 2018-

Ehteshami S. M. M., Chan S.H.,2014. The role of hydrogen and fuel cells to store renewable energy in the future energy network – potentials and challenges. Energy Policy; 73, 103–109.

Foresman J. B., Frisch Æ.,2015. Exploring Chemistry with Electronic Structure Methods, 3rd ed. Gaussian, Inc., Wallingford, CT, 2015). ISBN: 978-1-935522-03-4.

Fujishima, A., Honda, K., 1972. Electrochemical Photolysis of Water at a Semiconductor Electrode. Nature, 238: 37-38.

Gaussian 16, Revision B.01, Frisch, M.J., Trucks, G.W., Schlegel, H.B., Scuseria, G.E., Robb, M.A., Cheeseman, J.R.; Scalmani, G.; Barone, V.; Petersson, G.A.; Nakatsuji, H.; Li, X.; Caricato, M.; Marenich, A.V.; Bloino, J., Janesko, B.G., Gomperts, R., Mennucci, B., Hratchian, H.P., Ortiz, J.V., Izmaylov, A.F., Sonnenberg, J.L., Williams-Young, D., Ding, F., Lipparini, F., Egidi, F., Goings, J., Peng, B., Petrone, A., Henderson, T., Ranasinghe, D., Zakrzewski, V.G., Gao, J., Rega, N., Zheng, G., Liang, W., Hada, M., Ehara, M., Toyota, K., Fukuda, R., Hasegawa, J., Ishida, M., Nakajima, T., Honda, Y., Kitao, O., Nakai, H., Vreven, T., Throssell, K., Montgomery Jr., J.A., Peralta, J.E., Ogliaro, F., Bearpark, M.J., Heyd, J.J., Brothers, E.N., Kudin, K.N., Staroverov, V.N., Keith, T.A., Kobayashi, R., Normand, J., Raghavachari, K., Rendell, A.P., Burant, J.C., Iyengar, S.S., Tomasi, J., Cossi, M., Millam, J.M., Klene, M., Adamo, C., Cammi, R., Ochterski, J.W., Martin, R.L., Morokuma, K., Farkas, O., Foresman, J.B., Fox, D.J. Gaussian, Inc., Wallingford CT (2016) GaussView 5.0. Wallingford, E.U.A.

Gurkan, Y.Y. Turkten, N. Hatipoglu, A. ve Cinar, Z., 2012. Photocatalytic Degradation of Cefazolin over N-doped TiO2 Under UV and Sunlight Irradiation: Prediction of the Reaction Paths via Conceptual DFT. Chemical Engineering Journal, 184: 113-124.

Hay P. J., Wadt W. R.,1985. Ab initio effective core potentials for molecular calculations - potentials for the

Ho, W. ve Yu, J.C., 2006. Sonochemical Synthesis and Visible Light Photocatalytic Behavior of CdSe and CdSe/TiO2 Nanoparticles. Journal of Molecular Catalysis A: Chemical, 247: 268-274.

Homann T., Bredow T., Jug K., 2004. Adsorption of small molecules on the anatase (100) surface, Surf. Sci. 555, 135–144.

In, S. Orlov, A. Berg, R. Garcia, F. Pedrosa-Jimenez, S. Tikhov, M.S. Wright, D.S. ve Lambert, R.M., 2007. Effective visible light-activated B-doped and B,N-codoped TiO2 photocatalysts. J Am Chem Soc, 129: 13790-13791.

Ismael M,2021. Latest progress on the key operating parameters affecting the photocatalytic activity of TiO2-based photocatalysts for hydrogen fuel production: A comprehensive review. Fuel. 303-121207

Jho, J.H. Kim, D.H. Kim, S.-J. ve Lee, K.S., 2008. Synthesis and Photocatalytic Property of a Mixture of Anatase and Rutile TiO2 Doped with Fe by Mechanical Alloying Process. Journal of Alloys and Compounds, 459: 386-389.

Karakitsou, K. E., Verykios, X. E., 1993. Effects of Altervalent Cation Doping of TiO2 on Its Performance as a Photocatalyst for Water Cleavage. J. Phys. Chem. 97, 1184-1189.

Kirca S, 2022, Design and Investigation of Electronic Structures of Quality Light Sensitive New Metal-Added TiO2 Photocatalizers by Quantum Mechanical Methods. Phd Thesis, Yıldız Technical University

Likodimos, V. Han, C. Pelaez, M. Kontos, A.G. Liu, G. Zhu, D. Liao, S. de la Cruz, A.A. O'Shea, K. Dunlop, P.S.M. Byrne, J.A. Dionysiou, D.D. ve Falaras, P.,2013. Anion-Doped TiO2 Nanocatalysts for Water Purification Under Visible Light. Industrial & Engineering Chemistry Research, 52: 13957-13964.

Liu, Y. Wei, J.H. Xiong, R. Pan, C.X. ve Shi, J., 2011. Enhanced Visible Light Photocatalytic Properties of Fe-doped TiO2 Nanorod Clusters and Monodispersed Nanoparticles. Applied Surface Science, 257: 8121-8126.

Lu, J. Su, F. Huang, Z. Zhang, C. Liu, Y. Ma, X. ve Gong, J., 2013. N-doped Ag/TiO2 Hollow Spheres for Highly Efficient Photocatalysis Under Visible-Light Irradiation. RSC Adv., 3: 720-724.

Moradi, H. Eshaghi, A. Hosseini, S.R. ve Ghani, K.,2016. Fabrication of Fe-doped TiO2 Nanoparticles and Investigation of Photocatalytic Decolorization of Reactive Red 198 under Visible Llight Irradiation. Ultrasonics Sonochemistry, 32: 314-319.

Shakya DB, Aye L, Musgrave P., 2005. Technical feasibility and financial analysis of hybrid wind–photovoltaic system with hydrogen storage for Cooma. Int J Hydrogen Energy.30:9–20.

Stephens, P. J., Devlin, F. J., Ashvar, C. S., Bak, K. L., Taylor, P. R., Frisch, M., 1996. Comparison of Local, Nonlocal, and Hybrid Density Functionals Using Vibrational Absorption and Circular Dichroism Spectroscopy. J. ACS Symp. Ser., 629, 105.

Stephens, P. J., Devlin, F. J., Chabalowski, C. F., Frisch, M. J. J., 1994. Ab Initio Calculation of Vibrational Absorption and Circular Dichroism Spectra Using Density Functional Force Fields. Phys. Chem. 98, 11623.

Wahab H.S., Bredow T., Aliwi S.M., 2008. MSINDO quantum chemical modeling study of water molecule adsorption at nano-sized anatase TiO2 surfaces, Chem. Phys. 354- 50–57.

Wu, L. Yu, J.C. ve Fu, X., 2006. Characterization and Photocatalytic Mechanism of Nanosized CdS Coupled TiO2 Nanocrystals Under Visible Light Irradiation. Journal of Molecular Catalysis A: Chemical, 244: 25-32.

Wu, Y. Zhang, J. Xiao, L. ve Chen, F., 2010. "Properties of carbon and iron modified TiO2 photocatalyst synthesized at low temperature and photodegradation of acid orange 7 under visible light. Applied Surface Science, 256: 4260-4268.

Yalçın, Y. Kılıç, M. ve Çınar, Z.,2010. Fe3+-doped TiO2: A Combined Experimental and Computational Approach to the Evaluation of Visible Light Activity. Applied Catalysis B: Environmental, 99: 469-477.

Yalçın, Y. Kılıç, M. ve Çınar, Z.,2010. The Role of Non-Metal Doping in TiO2 Photocatalysis. Journal of Advanced Oxidation Technologies, 13: 281-296.

Yalçın, Y. Kılıç, M., Çınar, Z., 2010. The Role of Non-Metal Doping in TiO2 Photocatalysis. Journal of Advanced Oxidation Technologies, 13: 281-296.

Yu, C. Cai, D. Yang, K. Yu, J.C. Zhou, Y. ve Fan, C., 2010. Sol–Gel Derived S,I-codoped Mesoporous TiO2 Photocatalyst with High Visible-Light Photocatalytic Activity. Journal of Physics and Chemistry of Solids, 71: 1337-1343.

Yu, C. Cai, D. Yang, K. Yu, J.C. Zhou, Y. ve Fan, C.,2010. Sol–Gel Derived S,I-codoped Mesoporous TiO2 Photocatalyst with High Visible-Light Photocatalytic Activity. Journal of Physics and Chemistry of Solids, 71: 1337-1343.

Zaleska, A., 2008. Doped-TiO2: A Review. Recent Patents on Engineering, 2: 157-164.

#58: Theoretical evaluation of a transcritical high temperature heat pump using eco-friendly refrigerants

Adam Y. Sulaiman[*], Donal F. Cotter, Christopher C. Wilson, Nikhilkumar Shah, Neil J. Hewitt

Centre for Sustainable Technologies, Belfast School of Architecture and The Built Environment, Ulster University, Shore Road, Newtownabbey, Co. Antrim, BT37 0QB, UK

Corresponding author: Sulaiman-W@ulster.ac.uk

Abstract: Decarbonisation of the industrial sector in developed countries is an important element in addressing climate change worldwide. Many high temperature industrial heat processes up to 150°C could consider high temperature heat pump (HTHP) technologies as a viable replacement to existing fossil fuel equipment. Higher process temperatures up to 200°C would require a shift from subcritical HTHPs (SC-HTHPs) to transcritical HTHP (TC-HTHPs). These systems operate at much higher pressures and temperatures resulting in several technical and operational challenges to be solved. This paper investigates three different operating configurations for a TC-HTHP cycle to achieve 200°C using suitable low GWP refrigerants. A steady-state theoretically model was developed to compare and assess the energetic, exergetic and environmental performance for the TC-HTHP cycle. Employing the LMTD method, the gas cooler's heat transfer coefficient, overall length, and heat transfer area were calculated Analysis of the gas cooler indicated that compressor discharge pressure, gas cooler pinch points, and the temperature of waste heat supplied to the evaporator all significantly affect cycle performance. The energetic and exergetic results show that a TC-HTHP cycle with two additional IHX proved to be the most efficient cycle across a variety of heat source temperatures ranging from 75 to 90°C. In comparison to other candidates, the refrigerant R514A had the best performance with a high COP, high exergetic efficiency, lowest TEWI and lowest gas cooler pressure demand. Analysis of the gas cooler indicated that the compressor discharge pressure, the pinch point of the gas cooler, and the temperature of waste heat provided to the evaporator all significantly affect the overall cycle performance.

Keywords: transcritical high-temperature heat pump; low GWP refrigerants; gas cooler; energy; exergy

1. INTRODUCTION

According to the scientific assessment prepared by the Intergovernmental Panel on Climate Change (IPCC), rapid reductions in GHG emissions are required to prevent a 1.5°C rise in global temperature (Masson-Delmotte, *et al.*, 2018). Achieving this goal will require the energy industry within the European Union to decrease CO_2 emissions by 50% to 2030 and achieve net-zero emissions by 2050 (Tsiropoulos, *et al.*, 2020). Eurostat data for 2019 shows the industrial sector consumes around 2784.4 Terawatt hours (TWh) of energy every year, accounting for a considerable portion of overall European energy usage (Eurostat, 2022) with five main industrial sectors (Figure

Figure)   accounting for nearly 70% of total industry energy consumption (Odyssee, 2019). Additionally, Industrial activity releases around 2.95% of the planet's primary energy consumption as low-grade waste heat at temperatures below 100°C due to technical and economic constraints (Forman, *et al.,* 2016). Recovering waste heat improves energy efficiency and reduces industrial sector emissions. Drying, boiling, distillation, and pasteurisation require steam or hot air between 100°C and 200°C. These operations account for approximately 15% of total industrial heat usage (Nellissen & Wolf, 2015). Europe's industrial sector is capable of meeting around 28 TWh of its annual heat needs, with significant growth in sustainable technologies to recover low-grade waste heat from industrial processes (Kosmadakis, 2019). While subcritical HTHPs can operate at temperatures up to 150°C (Nilsson, *et al.*, 2017), transcritical HTHPs operating at temperatures up to 200°C may be possible with future research and development (Arpagaus, *et al.*, 2020).
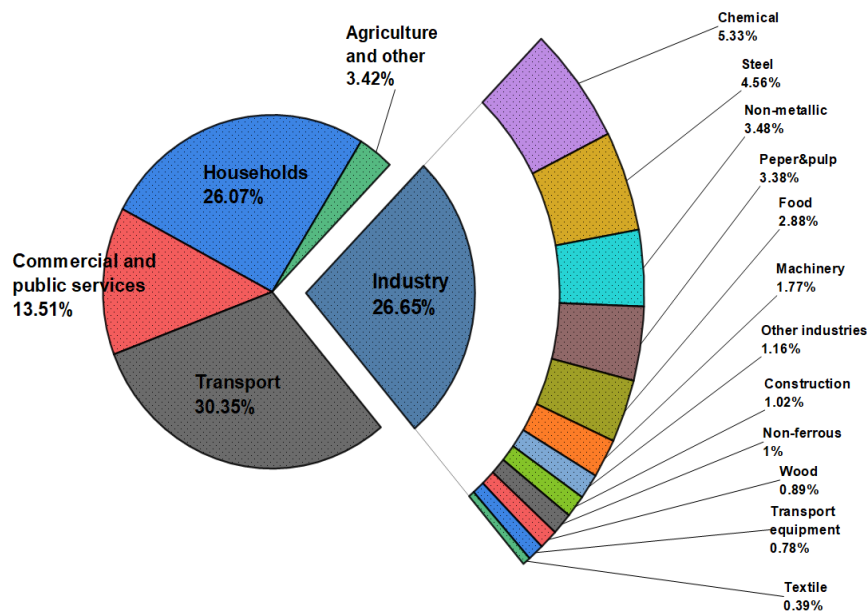

Figure 1: 2019 European energy consumption per sector with energy consumption per industrial area.

Although transcritical CO_2 is well-suited for air conditioning and low temperature heat pump applications, its low critical temperature and high operating pressure makes it unsuitable for HTHP industrial applications (Austin & Sumathy, 2011). The following section provides a summary of theoretical and empirical research activities relating to HTHPs at temperatures over 150°C.

A basic cycle with an additional internal heat exchanger (IHX) using R600 as the working fluid was investigated by Verdnik *et al.* (2019) at 80°C heat source and 170°C heat sink temperature set points. The high-side pressure was critical to boosting the cycle's coefficient of performance, ranging between 2.64 to 3.42. Arpagaus *et al.* (2020) investigated various transcritical cycle configurations using low GWP refrigerants with an 80°C heat source and 200°C heat sink. The analysis revealed that cycles using R514 as the working fluid had the highest COP, while cycles using R600 had the highest VHC. In addition, Kimura *et al.* (2018) examined a basic cycle with IHX by connecting a succession of high-speed oil-free centrifugal compressors with R600 refrigerant. In this investigation, the 300-kW gas cooler delivered thermal oil at a temperature of 180°C. At a sink temperature of 100°C, the cycle exhibited a COP of 3.50. De Carlan (2019) examined the basic cycle with an IHX, using a reciprocating compressor and working fluids R32 and R1234ze(E). Exhaust humid air at 80°C was used as a source for the evaporator, while the gas cooler's secondary fluid was fresh air entering at 90°C. With a COP of 3.32 and a maximum close to 4, the cycle was designed to provide hot air at 150°C. A literature survey of TC-HTHPs revealed a research gap in the analysis of energetic, exergetic, thermodynamic, and environmental impacts. This study's goal is to discuss the

performance characteristics and viability of a TC-HTHP in various configurations with low GWP refrigerants to achieve heat sink temperatures up to 200°C.

1.1. Nomenclatures

comp	*compressor*		*VHC*	*volumetric heat capacity*
COP	*coefficient of performance*		*vol*	*volumetric*
des	*destruction*		**Greek symbols**	
dis	*discharge*		η	*efficiency*
disp	*displacement*		ρ	*density* $(kg.m^{-3})$
em	*electromechanical*		$\bar{T}$	*average temperature*
evap	*evaporator*		Δ	*temperature difference (K)*
exp	*expansion valve*		**Subscript**	
Ex	*exergetic*		*h*	*enthalpy (kJ/kg)*
GC	*Gas cooler*		*0*	*reference state*
GWP	*global warming potential*		*m*	*fluid charge (kg)*
HTHP	*High-temperature heat pump*		*N*	*compressor speed (rpm)*
IHX	*internal heat exchanger*		*n*	*the unit lifetime (years)*
is	*isentropic*		*s*	*entropy (kJ/kg-K)*
LZ	*Lorenze*		*T*	*temperature (K)*
min	*minimum*		α	*heat transfer coefficient* $(W/m^2.K)$
PR	*pressure ratio*		$\dot{W}$	*input work (kW)*
SC	*subcritical*		$\dot{Q}$	*thermal load (kW)*
suc	*suction*		τ	*the annual leakage rate (%)*
TC	*transcritical*		α_{rec}	*recycling factor (-)*
TEWI	*total environmental warming impact*		E_{ann}	*annual energy consumption (kWh p.a)*
UA	*Heat transfer coefficient per unit area*		β	*indirect emission factor (kgCO₂-eq kWh⁻¹)*
V	*volume* (m^3)		$\dot{m}_r$	*refrigerant mass flow rate (kg/s)*

1.2. Refrigerant evaluations

The implementation of F-gas regulations and the phase-out of high-GWP refrigerants will require suitable commercial working fluids for HTHP applications (Calm & Hourahan, 2011). Table and Figure show a range of working fluids that may be suited to TC-HTHP cycles with a comparison of thermophysical and environmental properties.

Table 1: Thermophysical and environmental characteristics of chosen HTHP-compatible refrigerants (Cooperation, 2020), (Stocker, et al., 2014), (UNEP, 2017), (DerjAnecz, 2015).

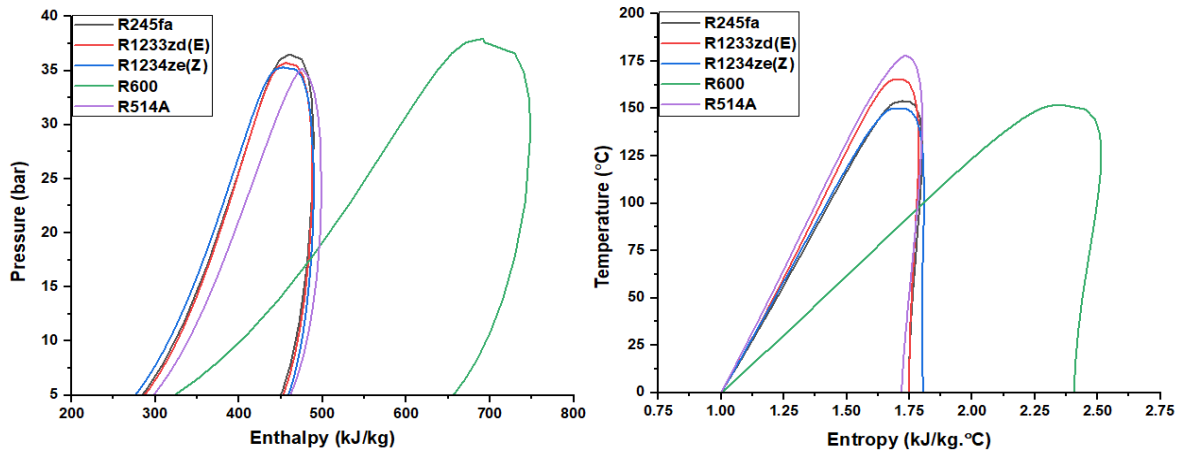| Type	Refrigerant	ODP	GWP₁₀₀yrs	T_{cr} [°C]	P_{cr} [bar]	NBP	SG
HFC	R245fa	0	1030	154.05	36.40	15.00	B1
HCFO	R1233zd(E)	0.00034	1	166.50	36.20	18.00	A1
HFO	R1234ze(Z)	0	<10	150.10	35.30	9.80	A2L
HC	R600	0	4	152.01	37.96	0.00	A3
HFO	R514A	0	2	178.4	34.00	29.3	B1

Figure 2: P-h and T-s diagrams for selected low GWP refrigerants (Lemmon, et al., 2013).

Along with possessing suitable thermophysical characteristics, an appropriate TC-HTHP refrigerant must be free of toxins and flame retardants, non- or low-flammable, entirely stable within the system and environmentally friendly. Although a high critical temperature of the working fluid is essential to achieve the desired heat sink temperature, the refrigerant must also be compatible with lubricants operating at higher temperatures and other materials in the system (Cotter, *et al.*, 2020). In addition, the TC-HTHP working fluid safety classification is particularly crucial due to the cycle's high operating pressure (Cooperation, 2020). The refrigerant R1233zd(E) has equivalent thermodynamic and boiling heat transfer characteristics to the ecologically unfavourable refrigerant R245fa, which has been used in SC-HTHP applications. R1233zd(E) is an eco-friendly refrigerant categorised as an A1 refrigerant with a higher critical temperature than R245fa (Mondéjar, *et al.*, 2015). R514A, a near-azeotropic combination composed of 74.7% of R1336mzz(Z) and 25.3% of R1130 on a mass basis, was recommended as a substitute for R245fa in HTHPs due to its favourable environmental and thermodynamic properties (Kedzierski & Lin, 2021). In comparison to R245fa, the non-toxic, low-flammability R1234ze(Z) exhibited analogous thermophysical properties and better environmental attributes.

2. CYCLE CONFIGURATIONS

This study provides a theoretical analysis of various cycle configurations based on the mass and heat balance of each component, as well as an assessment of the overall cycle performance to determine the feasibility of prospective practical activities in TC-HTHP applications. Various cycle arrangements were developed using a simple single-stage cycle plan as a base model (Figure). To assure dry compression and boost cycle performance, the second cycle configuration uses a basic system with IHX incorporated (Figure). In Figure, dual IHXs at the gas cooler and expansion valve maximise superheat before compression, increasing the cycle efficiency and discharge temperature (Llopis, *et al.*, 2018). To manage the pressure ratio and temperature lift, a compression system with two compressors was applied.
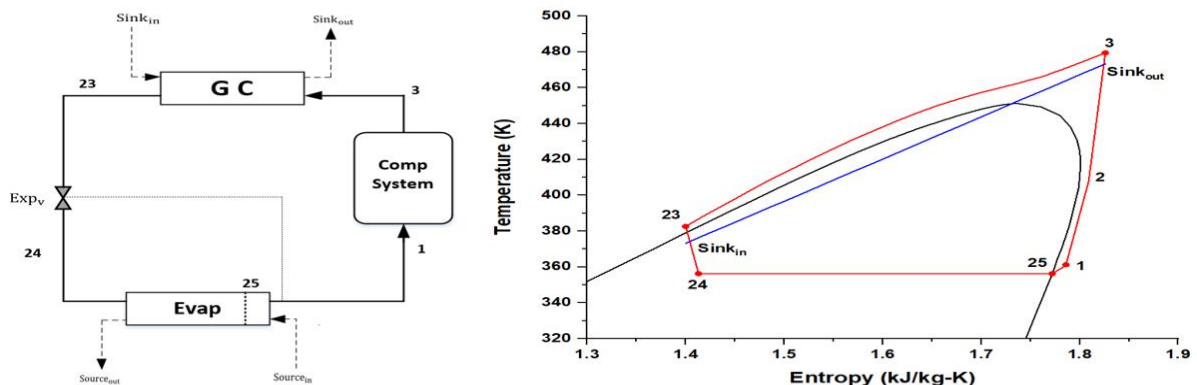

Figure 3: A basic transcritical cycle configuration with a T-S diagram for the cycle component points.
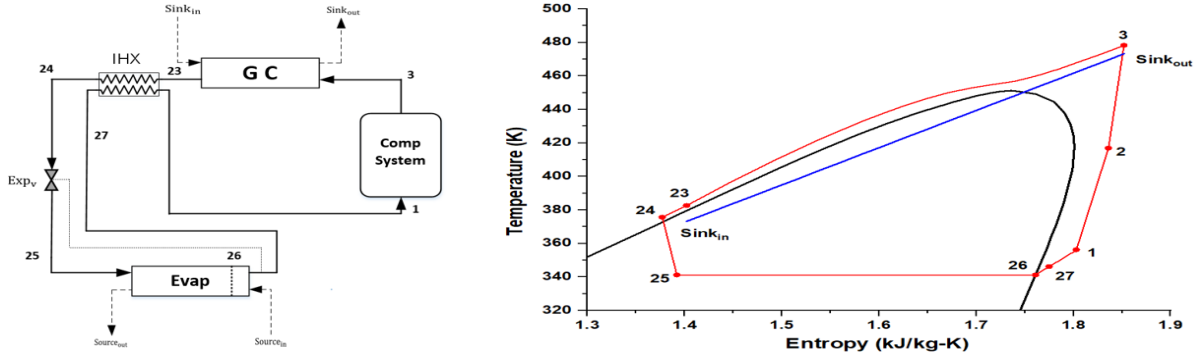
Figure 4: A basic cycle with additional IHX with a T-S diagram for the cycle component points.
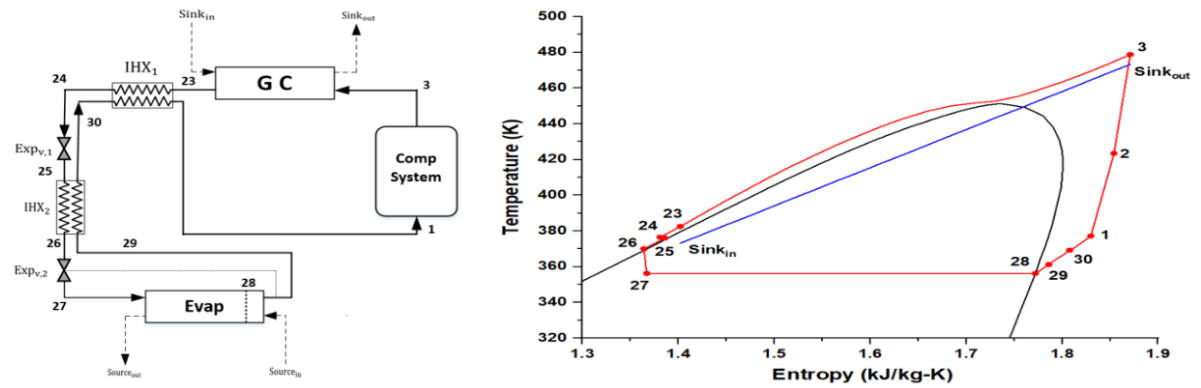

Figure 5: A double IHX cycle with a T-S diagram for the cycle component points.

3. MODELLING APPROACH

The heat source was adjusted to achieve a 6.5kW heat sink for the cycle. In five-degree increments, the evaporation temperature was varied between 75 and 90°C to achieve a heat sink temperature greater than 200°C. Sub-cooling was presumed to be 5K, whereas superheat was 8-15K outside the evaporator, depending on the refrigerant type. The cycle was modelled using the Engineering Equation Solver (EES) platform (Klein, 2019) with the following parameters: the cycle was assumed to be in a steady-state condition, potential and kinetic energy were neglected, each compressor's isentropic (η_{is}) and electromechanical (η_{em}) efficiencies were set to 0.70 and 0.95 respectively, the gas cooler layout was counter-flow, pressure drops along heat exchangers and pipelines were disregarded, and heat losses from pipes and components to the environment were neglected. Figure depicts a simplified schematic of a double-tube heat exchanger for the gas cooler flow direction of both refrigerant and thermal oil.
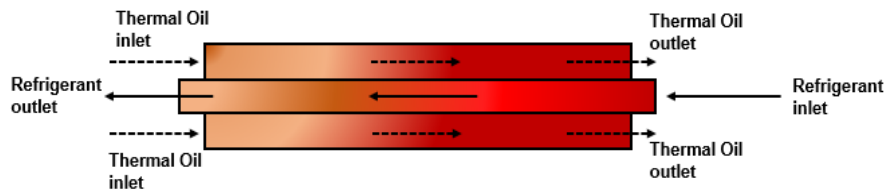

Figure 6: A basic schematic of the flow direction in a double tube heat exchanger with primary and secondary fluids.

The energetic and exergetic balance of each cycle configuration was calculated using the following equations:

$$\dot{m}_r = \rho_{suc}\eta_{vol}V_{disp}\frac{N_{comp}}{60} \qquad\qquad Equation\ (1)$$

$$\dot{W}_{comp} = \frac{\dot{m}_r\Delta h_{is,comp}}{\eta_{is}\eta_{em}} \qquad\qquad Equation\ (2)$$

$$COP = \frac{h_{in,GC}-h_{out,GC}}{h_{out,comp}-h_{in,comp}} \qquad\qquad Equation\ (3)$$

$$VHC = \rho_{in,comp}\left(h_{in,GC} - h_{out,GC}\right) \qquad\qquad Equation\ (4)$$

$$Ex_{flow} = (h - h_0) - T_0(s - s_0)$$ *Equation (5)*

$$COP_{Lz} = \frac{\bar{T}_{GC}}{\bar{T}_{GC} - \bar{T}_{evap}}$$ *Equation (6)*

$$\eta_{LZ} = \frac{COP}{COP_{Lz}}$$ *Equation (6)*

$$\eta_{Ex} = \left(1 - \frac{\sum Ex_{des}}{W_{comp}}\right).100$$ *Equation (7)*

The transcritical gas cooler pinch point analysis is more challenging in comparison to the subcritical condensation process because the refrigerant thermophysical characteristics vary non-linearly. Using LMTD approach, the gas cooler was segmented into twenty elements (number of elements (n) = 20) and supplied into the simulation model, where the ith element (1≤i≤n) (Liang, *et al.*, 2019). The temperature and entropy of the gas cooler segments were computed at each point of the divided control volumes using the following empirical formulae:

$$h_{i,GC} = h_{out,GC} - \frac{i}{n}(h_{in,GC} - h_{out,GC})$$ *Equation (8)*

$$\Delta T_{pinch,min} = min\left(T_{in,r,i} - T_{out,oil,i}, T_{out,r,i} - T_{in,oil,i}\right)$$ *Equation (9)*

$$\dot{Q}^r_{3+i} = (UA)^r_{3+i}\left[\frac{(T^r_{3+i-1} - T^{oil}_{3+i-1}) - (T^r_{3+i} - T^{oil}_{3+i})}{ln\left(\frac{T^r_{3+i-1} - T^{oil}_{3+i-1}}{T^r_{3+i} - T^{oil}_{3+i}}\right)}\right]$$ *(For i=1 to n)* *Equation (10)*

Furthermore, the Total Environmental Warming Impact (TEWI) is an ecological metric extensively used to predict the direct and indirect emissions that affect the environment during the cycle operation. The indirect impact is associated with the CO_2 emissions from the non-renewable energy used to operate the HTHP equipment, whereas the emissions during the lifespan of the equipment are termed direct emissions. The TEWI was computed using the following formula:

$$TEWI = (GWP \cdot \tau \cdot m \cdot n) + \left(GWP \cdot m \cdot (1 - \alpha_{rec})\right) \quad \text{Direct emissions}$$
$$+ \ (E_{ann} \cdot \beta \cdot n) \quad \text{Indirect emissions} \quad \text{Equation (11)}$$

The IPCC estimates a 5% annual leakage rate (Jarraud & Töpfer, 2005). In this study, annual leakage rates from 2.5% to 20% were used to estimate a wide range of leakage scenarios. The unit's estimated refrigerant charge was 5Kg and its expected lifespan set at 20 years. The recycling factor for the HTHP was 0.7 with an indirect emission factor of 0.233 (kgCO_2-eq kWh^(-1)) based on the United Kingdom (Authority, 2018).

4. RESULTS AND DISCUSSION

In the subsequent section, the heat transfer and pinch point analysis of the gas cooler, the energetic and exergetic performance, and the environmental impact of operating three distinct configurations of TC-HTHP are evaluated. The analysis, figures, and discussion all assumed a 200°C constant product temperature, with a compressor discharge temperature greater than 200°C.

4.1. Gas cooler design and pinch point analysis

In comparison to the sub-critical cycle, the heat sink in the transcritical cycle functions in the super-critical domain of the refrigerant, exhibiting a non-linear but rather consistent temperature decline during the gas-cooling process. The non-linear profile of the refrigerants thermophysical properties results from the gas cooler operation in the supercritical region and near the pseudocritical zone of the refrigerant. Consequently, this causes inconsistencies in the dimensionless numbers of Prandtl, Reynolds, Nusselt and the heat transfer coefficient related to each of the gas cooler sections. In Figure (a) the variance in specific heat capacity with temperature, reaches a peak within the pseudocritical region for all refrigerants. In Figure (b) a case study of R514A, illustrates the value of the heat transfer coefficient for each segment of the gas cooler in relation to the bulk temperature. When refrigerant's pseudocritical zone lies between the primary and secondary fluids, high values of specific heat and conductivity resulted in maximum values for heat transfer coefficient. Unlike a subcritical operation where the single-phase forces convection heat transfer of the condenser's de-superheat region, the heat transfer coefficient in the supercritical region fluctuates. This results in an exchange of heat in the direction of the heat flux. According to results, the number and location of pinch points, gas cooler glide temperature between the primary fluid's inlet and outlet, and heat transfer coefficient at each gas cooler segment are vital in determining optimum gas cooler design and size. Temperature differentials between primary and secondary fluids at the gas cooler's inlet and outlet were found to have a direct correlation with the number of pinch points and the length of gas cooler dimensions and heat

transfer area required. Depending on the refrigerant used in the TC-HTHP cycle, pinch points can arise at either the hot or cold end of the gas cooler's primary fluid. Figure (a) illustrates varied pinch points at either end of the unit while maintaining 5K temperature difference at both ends, resulting in a larger size of gas cooler. Increasing the temperature differential at one end decreases the number of pinch points, and as a result it is possible to optimise the length and size of the gas cooler as shown in Figure (b). Conversely, reducing the refrigerant glide temperature in the gas cooler increases the temperature difference between the primary and secondary fluids, resulting in a reduced gas cooler size.
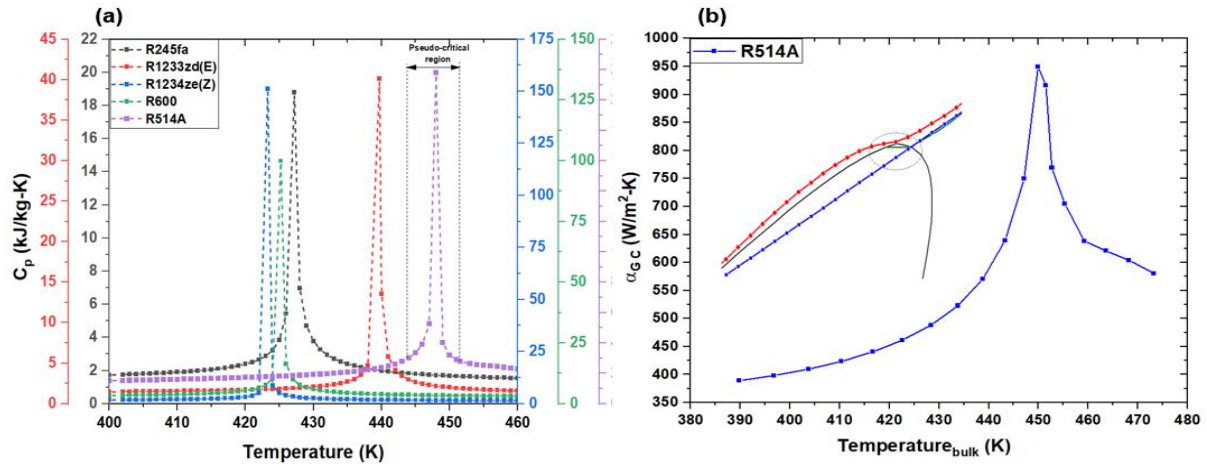

Figure 7: (a) variation of specific heat with temperature (b) heat transfer coefficient variation with average temperature in each gas cooler segment.
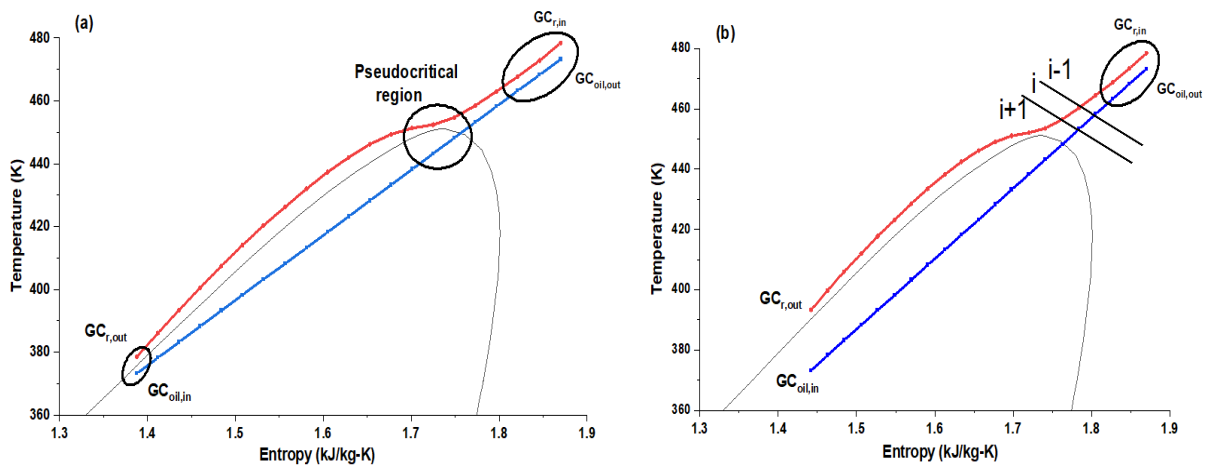

Figure 8: (a) Pinch point locations within the gas cooler; (b) Altering operational conditions to minimise pinch points within the gas cooler.

4.2. Energetic and exergetic analysis

Using three different cycle configurations and five refrigerants this study assesses the potential viability of incorporating a TC-HTHP within an industrial process. Each cycle component's heat, mass balance, performance, and overall cycle efficiency were evaluated by conducting an energetic analysis. On the other hand, the HTHP system's quantified thermodynamic imperfections signify exergy destruction or energy losses. Cycle exergy efficiency provides an assessment of process thermal efficiency and identification of areas for improvement. In

Table the energetic and exergetic findings on the basic cycle configuration served as a baseline for comparing and analysing various cycle configurations and selecting the most efficient cycle configuration.

Table 2: Results of basic cycle at $T_{evap} = 80°C$ and heat sink product of 200°C.

				Basic single-stage cycle				
Refrigerant	P_{dis} (bar)	$\dot{m}$ (kg/s)	COP [-]	VHC (kJ.m^{-3})	W_{in} (kW)	PR [-]	$\sum Ex_{dest}$ (kW)	η_{ex} %
R245fa	83	0.0389	2.93	5961	4.50	12.57	3.23	28.15
R1233zd(E)	55	0.0367	3.04	5036	4.51	9.96	3.25	27.82
R1234ze(Z)	67	0.0349	3.04	6377	4.34	9.25	3.09	28.87
R600	88	0.0199	2.83	6816	4.54	10.14	3.26	28.16
R514A	45	0.0353	3.14	3905	4.22	11.27	2.98	29.45

Initial findings of the basic cycle configuration revealed that R514A has the highest COP and exergetic efficiency among the candidates with a low gas cooler pressure, followed by R1234ze(Z) and R1233zd(E). The refrigerant R600, exhibited the highest VHC value, resulting in the smallest compressor size. According to the findings, R1234ze(Z) combines the advantages of high COP and VHC. In addition, all investigated refrigerants except R1234ze(Z), which has an isentropic shape, require adequate degrees of superheat outside the evaporator and prior to the compressor because of the re-entrant shape type on the T-s diagram. Incorporating an additional IHX ensures dry compression and accurately evaluates the efficacy of the HTHP cycle over a variety of evaporation temperatures. The addition of an IHX improved the COP of R1234ze(Z), R1233zd(E), R514A, and R600 by 3%, 2.9%, 2.6%, and 5.9%, respectively, compared to the basic single-stage cycle. In addition, the high-pressure side of the cycle was significantly reduced, while the cycle's VHC and exergetic efficiency were enhanced.

Figure (a) depicts COP and VHC values for the basic cycle with dual IHX at different evaporation temperatures, while Figure (b) illustrates the exergetic efficiency and total exergetic destruction in the cycle for the refrigerants studied. Increasing the evaporation temperature decreases temperature lift, thereby enhancing the COP and VHC of the cycle for all the refrigerants. Analogously, for exergetic efficiency and total exergetic destruction, reducing the cycle temperature lift increases cycle exergetic destruction and total cycle exergetic efficiency. Using a dual cycle reduces high-side pressure by 16 to 24%, boosts COP by 4 to 8%, improves VHC by 2 to 4%, and increases exergy efficiency from 2 to 5%, according to the results. Figure shows the exergy destruction of each component of a single-stage system with dual IHX at evaporation temperatures of 75°C and 90°C. The simulation revealed that the compression process generated the most exergetic destruction, followed by the expansion process. In a transcritical cycle, the pressure ratio is double that of a subcritical cycle, leading to a significant increase in dissipation force and thermal losses. The considerable rise in compression process is due to the enormous enthalpic difference between the compression inlet point and the compression discharge point during compression. The exergetic destruction of compression and expansion processes was reduced by reducing the cycle temperature lift. As the evaporation temperature increases, the exergetic destruction of IHX also decreases, which corresponds to both IHXs' increasing effectiveness.
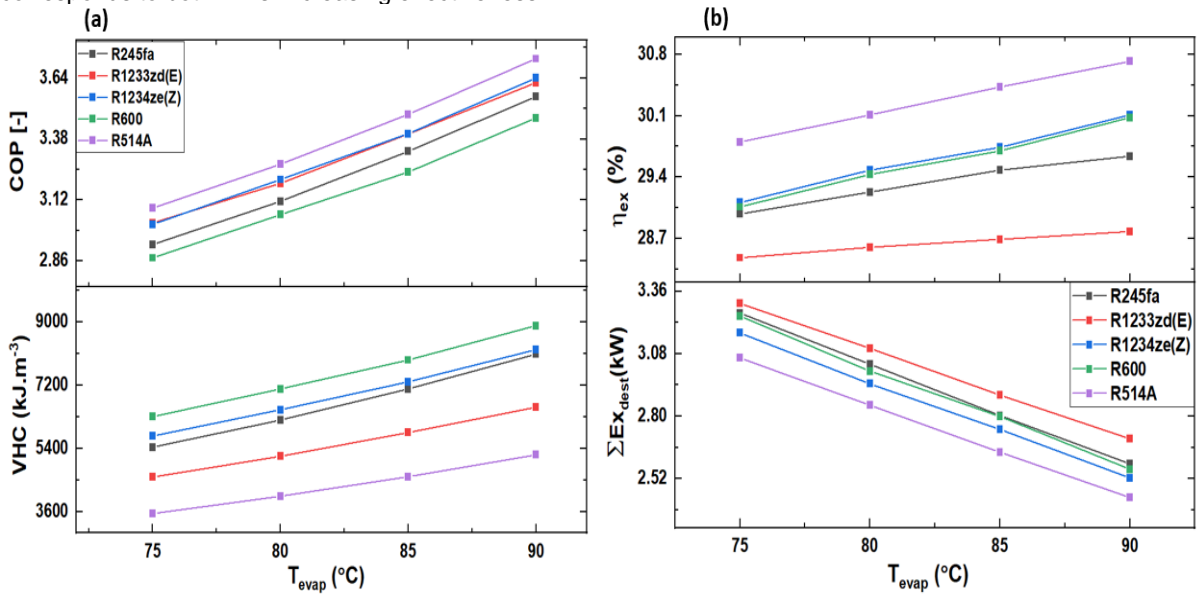

Figure 9: (a) The cycle energetic performance varied with T_{evap}. (b) exergetic performance varied with T_{evap}.
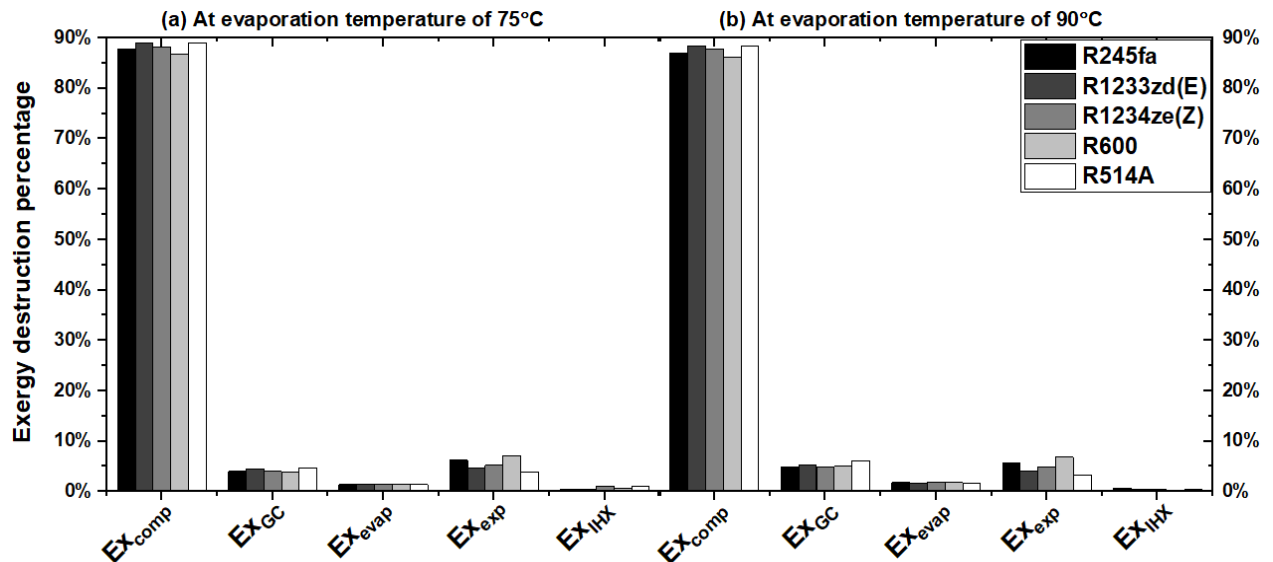
Figure 10: (a) Exergy destruction of each component at T_{evap} = 75°C, (b) T_{evap} = 90°C.

4.3. Environmental analysis results

According to the TEWI estimations, the base line refrigerant R245fa demonstrated the greatest TEWI of 125.94 to 143.97 Ton CO_2-equivalent for the single-stage IHX cycle assuming a leakage rate of 2.5 to 20% per year. In addition, the single-stage with dual IHX cycle revealed values of 123.96 to 141.98 Ton CO_2-equivalent. The refrigerant R514A had the lowest TEWI value, ranging from 114.00 to 114.04 Ton CO_2-equivalent, followed by R1234ze(Z), which had a value ranging from 116.80 to 116.98 Ton CO_2-equivalent. In comparison to the single-stage with IHX cycle configuration, the single-stage with dual IHX cycle configuration exhibited a slight reduction in TEWI due to reduced power demand. Relative to R245fa, R514A showed the greatest decrease in TEWI value, nearly 20%, followed by R1234ze(Z) at 17.5%. The refrigerants R1233zd(E) and R600, show smaller reductions due to their greater indirect effect value, which is a consequence of higher power requirements.

5. CONCLUSIONS

In this article a theoretical investigation of a TC-HTHP cycle using eco-friendly working fluids at a heat sink temperature of 200 °C was conducted. Based on pinch point effect on the gas cooler design, energetic, exergetic, and environmental analysis, the following are the main conclusions:

- The investigation of thermophysical characteristics close to the pseudocritical region is essential for comprehending the pattern of heat transfer during the gas-cooling process and therefore determining the appropriate size of the gas cooler. In addition, reducing the number of pinch points at one end of the gas cooler and adjusting the compressor size to enhance the temperature differential between the two fluids at the gas cooler outlet could be used to overcome the extreme temperature glide in the gas cooler.
- The basic single-stage with dual IHX was found to be the most energy-efficient, least exergy-destructive, and lowest TEWI cycle configuration. Nevertheless, it may be more challenging to regulate this unit during practical activities compared to the other investigated cycle configurations.
- The working fluid R514A exhibited the highest COP, the highest possible exergetic efficiency, the lowest gas cooler pressure demand, and the lowest TEWI value.
- R1234ze(Z) demonstrated a promising trade-off between its high COP and VHC values and its high exergetic efficiency.
- The exergetic analysis confirmed that the compression process, the gas cooler, and the expansion process were identified as the primary process components requiring optimisation.
- Based on this analysis the operation of a TC-HTHP is theoretically viable, with further development and empirical testing needed to validate results.

6. ACKNOWLEDGEMENTS

7. REFERENCES

Arpagaus, C., Bless, F. & Bertsch, S. S., 2020. Theoretical Analysis of Transcritical HTHP Cycles with Low GWP HFO Refrigerants and Hydrocarbons for Process Heat up to 200 °C. Glasgow, IIR International Rankine 2020 Conference – Heating, Cooling and Power Generation.

Austin, B. T. & Sumathy, K., 2011. Transcritical carbon dioxide heat pump systems: A review. Renewable and Sustainable Energy Reviews, 15(8), pp. 4013-4029.

Authority, T. G. L., 2018. Towards low carbon heat Heat pumps in London, London: GLA.

Calm, J. M. & Hourahan, G. C., 2011. Physical, safety, and environmental data for current and alternative refrigerants. Refrigeration for Sustainable Development: Proceedings of the 23rd International Congress of Refrigeration, Issue Paper 915, p. Paper 915.

Cooperation, A. a. U., 2020. Update on New Refrigerants Designations and Safety Classifications, s.l.: ASHRAE.

Cotter, D., Shah, N., Hewitt, N. & Huang, M., 2020. Refrigerant Lubricant Interaction In High-Temperature Heat Pump And Organic Rankine Cycle Systems. Glasgow, IIR Rankine Conference 2020.

De Carlan, F., 2019. Transcritical Heat Pump Solution for industrial dryers. Copenhagen, 2nd Symposium on High-Temperature Heat Pumps.

DerjAnecz, A., 2015. New F-Gas Regulation. Issue 842, pp. 30-32.

Eurostat, 2022. https://ec.europa.eu/eurostat. [Online] Available at: https://ec.europa.eu/eurostat/databrowser/view/TEN00124__custom_2333266/default/table?lang=en.[Accessed 08 April 2022].

Forman, C., Muritala, K. I., Pardemann, R. P. & Meyer TU, B., 2016. Estimating the global waste heat potential. Renewable and Sustainable Energy Reviews, Volume 57, pp. 1568-1579.

Jarraud, M. & Töpfer, K., 2005. Safeguarding the Ozone Layer and the Global Climate System: Issues Related to Hydrofluorocarbons and Perfluorocarbons, Montreal: The United Nations Framework Convention on Climate Change (UNFCCC) and the Montreal Protocol on Substances that Deplete the Ozone Layer.

Kedzierski, M. A. & Lin, L., 2021. Pool Boiling of R514A, R1224 yd(Z), and R1336mzz(E) on a Reentrant Cavity Surface. Journal of Heat Transfer, 143(5).

Kimura, T. et al., 2018. Development of a high temperature heat pump using reusable heat as the heat source. Tokyo, JRAIA INTERNATIONAL SYMPOSIUM 2018.

Klein, S., 2019. Engineering Equation Solver (Version V10. 268): F-Chart Software, s.l.: klein2017engineering.

Kosmadakis, G. M., 2019. Estimating the potential of industrial (high-temperature) heat pumps for exploiting waste heat in EU industries. Applied Thermal Engineering journal, Volume 156, pp. 287-298.

Lemmon, E. W., Huber, M. L. & McLinden, M. O., 2013. NIST Standard Reference Database 23: Reference Fluid Thermodynamic and Transport Properties-REFPROP, Version 9.1, Colorado: Institute of Standards and Technology (NIST).

Liang, X.-Y.et al., 2019. Difference analysis on optimal high pressure of transcritical CO2 cycle in different applications. International Journal of Refrigeration, Volume 106, pp. 384-391.

Llopis, R. et al., 2018. Subcooling methods for CO 2 refrigeration cycles: A review. International Journal of Refrigeration, Volume 93, pp. 85-107.

Masson-Delmotte, V. et al., 2018. Global Warming of 1.5°C.An IPCC Special Report on the impacts of global warming of 1.5°C above pre-industrial levels and related global greenhouse gas emission pathways, in the context of strengthening the global response to the threat of climate change, s.l.: IPCC.

Mondéjar, M. E., McLinden, M. O. & Lemmon, E. W., 2015. Thermodynamic Properties of trans-1-Chloro-3,3,3-trifluoropropene (R1233zd(E)): Vapor Pressure, (p, ρ, T) Behavior, and Speed of Sound Measurements, and Equation of State. Journal of Chemical and Engineering Data, 60(8), pp. 2477-2489.

Nellissen, P. & Wolf, S., 2015. Heat pumps in non-domestic applications in Europe: Potential for an energy revolution, s.l.: EMERSON Climate Technologies.

Nilsson, M., Rislå, H. N. & Kontomaris, K., 2017. Measured performance of a novel high temperature heat pump with HFO-1336mzz(Z) as the working fluid. Rotterdam, 12th IEA Heat Pump Conference (2017).

Odyssee, 2019. https://www.odyssee-mure.eu/. [Online] Available at: https://www.odyssee-mure.eu/publications/efficiency-by-sector/industry/energy-consumption-trend-industrial-branch-eu.html [Accessed 08 April 2022].

Stocker, T. F. et al., 2014. Climate Change 2013: The Physical Science Basis. Contribution of Working Group I to the Fifth Assessment Report of IPCC the Intergovernmental Panel on Climate Change. Cambridge: Cambridge University Press.

Tsiropoulos, I., Nijs, W., Tarvydas, D. & Ruiz, P., 2020. Towards net-zero emissions in the EU energy system by 2050, Petten, The Netherlands: European Commission.

UNEP, 2017. Handbook for the Montreal Protocol on Substances that Deplete the Ozone Layer, Eleventh edition. Eleventh edition ed. Nairobi, Kenya: United Nations Environment Programme.

Verdnik, M., Riberer, R. & Moisi, H., 2019. Trans-critical vapor compression cycle using butane (R600) as refrigerant for industrial waste heat recovery. Refrigeration Science and Technology, Volume 2019-Augus, pp. 4697-4704.

#127: A novel urban heat island calculation workflow: case study and validation

Tianhong ZHENG [1], Ke QU[2], Jo DAKWA[3], John Kaiser CALAUTIT[4]

[1]Department of Architecture and Built Environment, University of Nottingham, Nottingham, UK,
ezxtz4@nottingham.ac.uk (CA)
[2]Department of Architecture and Built Environment, University of Nottingham, Nottingham, UK,
ezxkq@exmail.nottingham.ac.uk
[3]Department of Architecture and Built Environment, University of Nottingham, Nottingham, UK,
lazkd@exmail.nottingham.ac.uk
[4]Department of Architecture and Built Environment, University of Nottingham, Nottingham, UK,
ezzjkc@exmail.nottingham.ac.uk

Abstract: The average degree of global warming is 1.5°C, which means higher levels of warming. If greenhouse gas emissions increase to a high level, the global warming issue will be more serious. In addition, the urban heat island phenomenon positively affects urban energy consumption and greenhouse gas emissions. However, a simple and accurate calculation process is still lacking to analyse the intensity of the urban heat island (UHI). Therefore, this study proposed an innovative urban heat island calculation workflow to exploit the urban heat island change in city centres. This workflow was built by a 3D computer-aided design tool Rhinoceros with Grasshopper, and a visual programming language running within Rhinoceros. Five steps of the workflow are described. A case study in Osaka, Japan city centre, was conducted to assure the operability of the workflow. The results showed the intensity of the average annual UHI in Osaka city centre was around 0.73°C while the average summer UHI was 0.58°C. However, the summer UHI increased quickly in Osaka city centre, and the intensity is expected to increase to 0.71°C by 2040. The results could provide valuable guidance to local authorities, city planners and policy makers for achieving a more sustainable future in city centres.

1. INTRODUCTION

Global net anthropogenic greenhouse gas (GHG) emissions were 59±6.6 GtCO$_2$-eq in 2019, which have continued to increase from 2010 to 2019, about t 12% (6.5 GtCO2-eq) higher than in 2010 and 54% (21 GtCO2-eq) higher than in 1990 (IPCC, 2022). Ideally, global warming should be limited to 1.5°C, depending on GHG emissions, which are low to 430–480 ppm CO$_2$eq. To keep the GHG concentrations at a low and manageable level, low-carbon energy should be increased from 10% to 70% of the global primary energy supply from 2010 to 2050. Cities consume most of the energy in the world, and global carbon dioxide (CO$_2$) emissions have increased by more than 70% in city areas (Churkina, 2016). The increasing populations in cities are responsible for higher energy consumption and GHG emissions (Seto, Güneralp and Hutyra, 2012), therefore, the development of urban energy savings and the reduction of GHG emissions have become global issues.

The urban heat island (UHI) phenomenon occurs in metropolitan centres when an urban area experiences higher temperatures than the surrounding rural areas (Zheng *et al.*, 2022), which usually increases building energy demands (Gonzalez-Trevizo *et al.*, 2021; Tian *et al.*, 2021) and GHG emissions (Hirano and Yoshida, 2016; Roxon, Ulm and Pellenq, 2020). Mitigating the intensity of UHI is an effective method of helping cities and countries achieve their targets of energy-saving and GHG emissions reduction (Roxon, Ulm and Pellenq, 2020). Therefore, urban planners and legislators should analyse the intensity and variation of UHI to develop low-carbon energy systems and control the GHG emissions in the city centre.

Several causes can affect UHI intensity in urban areas, including (i) urbanisation and increasing population in the urban area (Akbari and Kolokotsa, 2016), (ii) fewer green spaces in the urban area (Ambrosini *et al.*, 2014), and (iii) lower albedo artificial construction materials in the urban area (Dong *et al.*, 2020). The intensity of UHI is determined by comparing the average and maximum air temperature between an urban and rural area (ΔT_{u-r}) (Atkinson, 2003).

Four prime methods have been conducted in previous studies to calculate the intensity of UHI:

(i) Field measurement. The stationary network or mobile stations (Mohan *et al.*, 2012) are generally used to measure UHII. However, the parameters at only a limited number of spatial points are simultaneously measured, so it is not possible to demonstrate the three-dimensional spatial distribution of the quantities inside an urban area. Besides, installing the measurement devices on a city scale are costly and time-consuming.

(ii) Numerical studies method. Nonlinear (Olfe and Lee, 1971) or linear (Bottyán and Unger, 2003) calculations were used to estimate the temperature and velocity changes induced in air flowing based on the 2D models. However, numerical studies are based on complex mathematical formulas, which require high research skills.

(iii) Temperature data method. UHI calculation is based on the temperature dataset from the rural and urban weather stations (Yagüe, Zurita and Martinez, 1991; Kim and Baik, 2002). However, the temperature dataset is usually limited in urban weather which is time-consuming.

(iv) Simulation method. With the rapid development of computational techniques, coupling numerical study with simulation models has become an important method. The Weather Research and Forecasting (WRF) model (Giannaros *et al.*, 2013; Wang & Li, 2016; Li *et al.*, 2019) - a meso-scale model - and the computational fluid dynamics (CFD) model (Aghamolaei, Fallahpour and Mirzaei, 2021) - a micro-scale model - are both widely used models to calculate UHII. However, due to the difference of the constant urban parameters and actual variables, inaccuracy maybe occur in the WRF models. Besides, due to the high computational and time costs, the simulation scale is limited in the CFD model.

To track the limitation mentioned above, this research proposed an innovative and simplified workflow for urban heat island calculation (UHI-CW). This workflow combined the local rural meteorological data and accurate city information to simulate UHI change and intensity between the urban built-up areas and rural areas from a micro-scale perspective. The process of UHI-CW should be simple and would not require massive data and information.

2. METHODS

In this study, the UHI-CW was established to analyse the UHI intensity and change on the city scale by calculating urban outdoor air temperatures and evaluating the interactions between buildings and the microclimate. To build the UHI-CW, the rural weather data should be collected, and the data of city objects should be accumulated. Besides, the parametric modelling tool, Grasshopper, is a visual programming interface that runs inside Rhinoceros with two Grasshopper plug-ins (ladybug and dragonfly), and has been adopted to build the urban weather generation engine (UWGE) by dragging the relevant components of Grasshopper onto a canvas. The outputs to these components are connected to the inputs of subsequent components. The UHI-CW was comprised of five steps as shown in Figure 1.
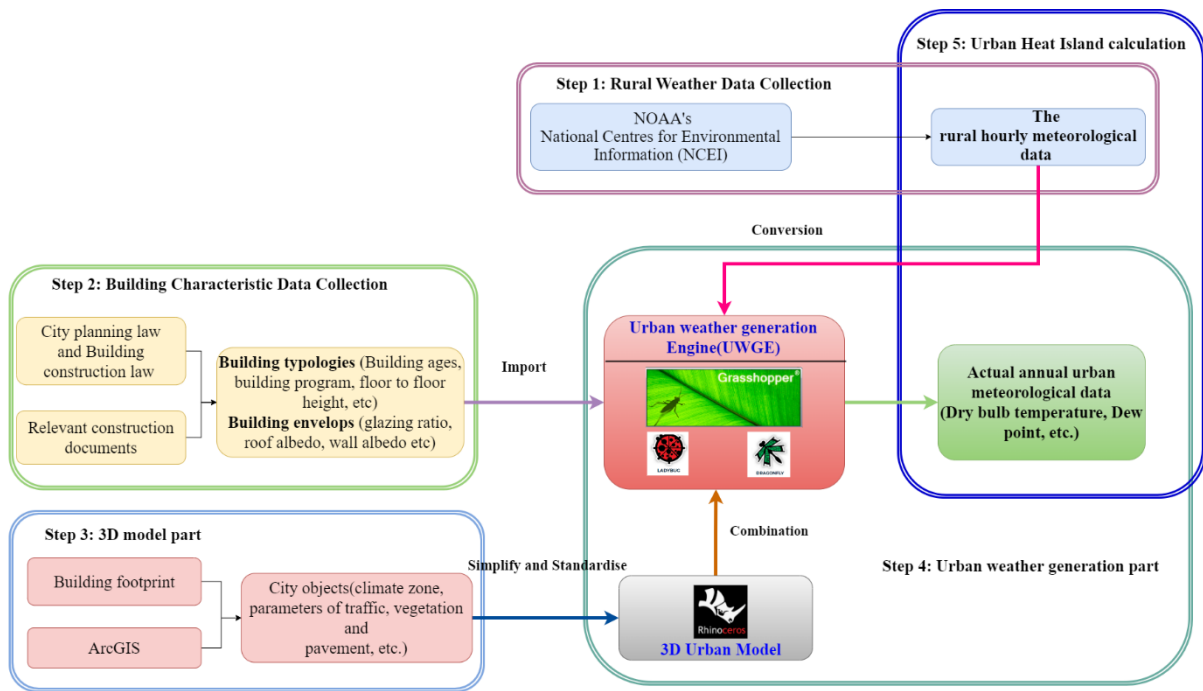
Figure 1: The detailed steps for UHI-CW.

2.1. Step 1: Rural weather data collection

The initial rural meteorological data were collected from National Oceanic and Atmospheric Administration (NOAA) website (https://www.noaa.gov/). That meteorological data included the hourly value of annual weather conditions (e.g., dry bulb temperature, dew point temperature, relative humidity, wind speed and direction, solar radiation, etc.), which was gathered and organised by the local rural weather station. The initial meteorological data was converted to the rural Energy Plus weather file (EPW file) and imported into components of Grasshopper, as shown in Figure 2.
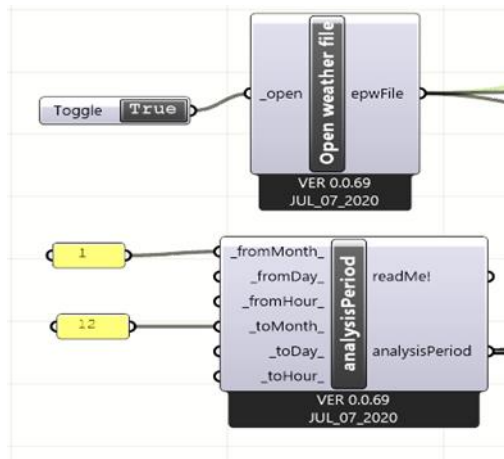

Figure 2: The rural weather components in the Grasshopper

2.2. Step 2: Building characteristic data collection

To define the building characteristic and analyse the interaction between outdoor temperature and buildings, the building characteristics data was collected in step 2, based on information from the local city planning law, building construction law and relevant construction documents. Two detailed sets of data have to be collected as input data of the UWEG. The first part was building typologies data including building age, building program, and floor-to-floor height, which was imported to the building typologies components of the UWGE (see Figure 3).
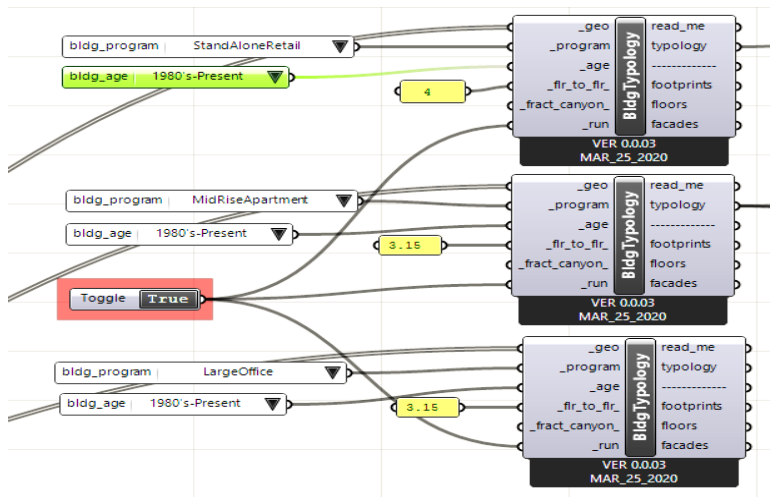
68

Figure 3: Building typologies components in the UWGE

The second part was building envelope data that included glazing ratio, roof albedo, and wall albedo, which was imported into the building envelope component of the UWGE (see Figure 4).
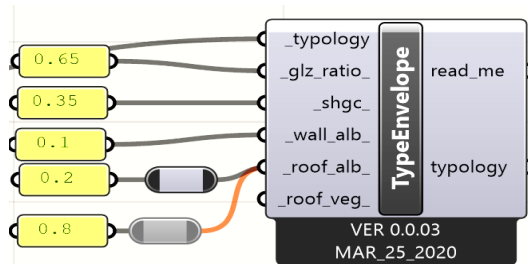
Figure 4: Building envelope component in the UWGE

2.3. Step 3: 3D urban model

Urban geometries have to be connected with weather data. The urban geometrise data included the terrain of the research area, building area, pavement area, and green space (trees and grasses). The footprint or ArcGIS mapping can be used to build the 3D urban canopy model in Rhinoceros to define the city objects data (climate zone, parameters of traffic, vegetation area albedo and pavement albedo, etc.) in the UHI-CW, and was imported into the UWGE (see Figure 5). In this step, the maximum sensible anthropogenic heat flux was considered, which usually originated from vehicle activities and human metabolism.

Figure 5: The city objects components in the UWGE

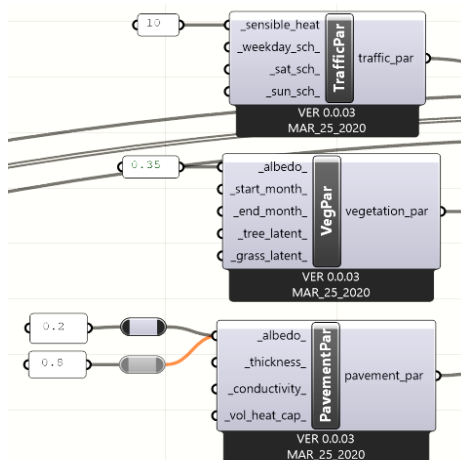## 2.4. Step 4: Urban weather generation engine

The multiple components (Figure 6) were set to link UWGE with the rural weather data collected in step1 and 3D urban model built in step 3. Thus, the hourly urban meteorological data can be generated, such as dry bulb temperature, dew point temperature, relative humidity, wind speed and direction, etc.
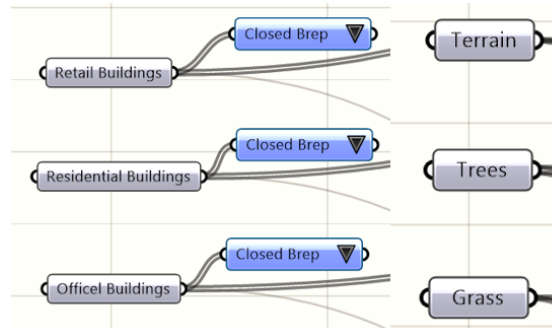

Figure 6: The connection components in the UWGE.

2.5. Step 5: Urban heat island calculation

The intensity of UHI can be calculated in step 5. The hourly values of urban outdoor temperature were obtained by combining the urban patterns with the rural meteorological data collected in step 1. The UHI intensity was determined by comparing the outdoor air temperature between the urban with rural areas (ΔT_{u-r}) in step 5.

In sum, the UHI-CW had the ability to calculate the intensity of urban heat island, which could improve the accuracy for analysing the urban energy consumption and human comfort. There were some advantages of the UHI-CW:

(i) The UHI-CW did not require massive historical meteorological and building data;

(ii) The UHI-CW could calculate UHI intensity through simple processes which were computational and time saving;

(iii) Due to UHI-CW being based on accurate urban parameters and variables, the accuracy of UHI-CW was high.

3. Case study (Osaka, Japan)

A case study was conducted to guarantee the operability of UHI-CW. The 2018 Revision of World Urbanization Prospects (United Nations, 2018) reported that cities are expected to gain all of the growth of the world population in the future. Asia significantly has 54% of the world urban population, therefore, studying the change of subtropical UHI is the key to keeping sustainable development.

The research area selected was a subtropical city centre in Osaka, Japan (34.6937°N, 135.5023°E) and a topical subtropical weather condition city centre. According to the Japan Meteorological Agency (JMA), the annual mean maximum air temperature in Osaka was 20.08°C, and the annual relative humidity of Osaka was 65.3%. The annual average wind speed in Osaka was 4.5m/s (Zheng *et al.*, 2022).

3.1. Rural weather data of Osaka

The rural meteorological parameters were collected from National Oceanic and Atmospheric Administration (NOAA) website (https://www.noaa.gov/), which provide globally annual hourly meteorological parameters collected and managed by the local weather station. To analyse the UHI intensity change, the research period was set from 2000 to 2020, and the rural meteorological parameters were collected from 2000 to 2020.

3.2. Building characteristic data of Osaka

The geography of the research area included three types of buildings (retail buildings, residential buildings, and office buildings), green spaces and pavement areas. The building characteristics data were collected from the

Building Standard Act of Japan (1950), City Planning Law of Japan (1968), and Osaka City Ordinance for Enforcement of the Building Standards Act (Osaka City Ordinance No.62 of 2000). The detailed simulation input parameters are shown in Table 1.

Table 1: The detailed initialisation input parameters of Osaka, source from the Building Standard Act of Japan (1950), City Planning Law of Japan (1968), Osaka City Ordinance for Enforcement of the Building Standards Act (Osaka City Ordinance No.62 of 2000)

Category	User input
Modelling area (L, W, H) (m)	500×500×600
Retail building inputs	
Building ages	1980's-Present
Floor to floor	4m
Average height	29m
Floor area	31816㎡
Footprint area	4538㎡
Façade area	22182㎡
Glazing ration	65%
Mean wall albedo	0.1
Mean roof albedo	0.2
Apartment building inputs	
Building ages	1980's - Present
Floor to floor	3.15m
Average height	24m
Floor area	76587㎡
Footprint area	10679㎡
Façade area	45424
Glazing ration	14%
Mean wall albedo	0.1
Mean roof albedo	0.2
Office building inputs	
Building ages	1980's - Present
Floor to floor	3.15m
Average height	25m
Floor area	99233㎡
Footprint area	13559㎡
Façade area	52831㎡
Glazing ration	38%
Mean wall albedo	0.1
Mean roof albedo	0.2
City inputs	
The sensible heat of traffic	8w/㎡
The albedo of vegetation	0.35
The albedo of pavement	0.2
Site coverage ratio	0.51
Façade-to-site ratio	2.14
Grass coverage ratio	0.02
ASHRAE climate zone	4A

3.3. 3D model for Osaka

The research domain of the city centre covered an area of 2.5km^2 consisting of typical urban land-use types: residential areas, commercial areas, office areas, pavement, green spaces and open spaces. The fraction of urban green coverage (UGC) in Osaka city centre was down to 2%, which is a valuable way to study the relationship between vegetation and UHI. The research area from Google Earth and the 3D model in Rhinoceros is shown in Figure 7.
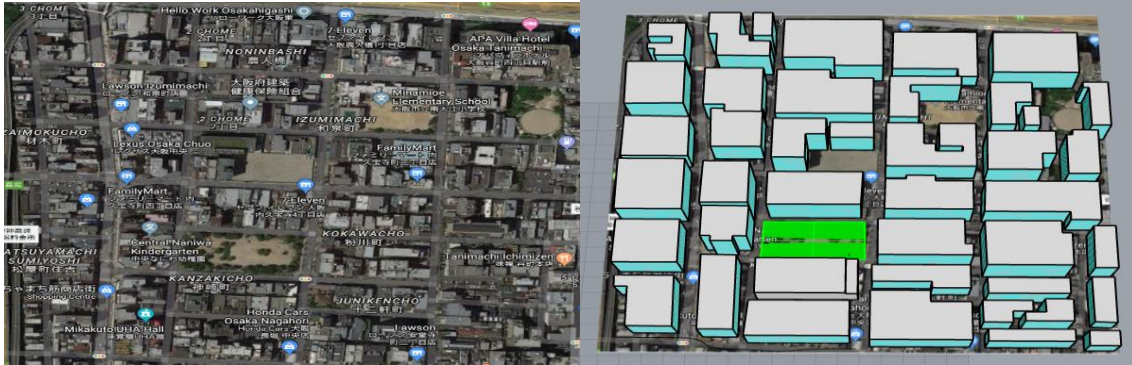

Figure 7: The research area (google earth) and the 3D urban model in Rhinoceros.

4. RESULTS

Dry bulb temperature (T_{db}) is the most critical variable for considering human comfort and energy efficiency (Singh, Reddy and Abushakra, 2014). In this study, the T_{db} was converted and calculated from 2000 to 2020 to indicate the amount of heat in the ambient air. The annual rural dry bulb temperatures (RT_{db}) and annual urban rural dry bulb temperatures (UT_{db}) were compared to evaluate the UHI intensity in Osaka city centre. Besides, due to the extreme heat in June, July, and August (JJA) which can lead to more heat-related illnesses of citizens such as heat syncope, cardiovascular stress, and cardiorespiratory diseases, the summer RT_{db} and the summer UT_{db} in JJA were also collected and contrasted with measuring the summer UHI intensity in Osaka city centre. The proportion of the variation was predictable for the future RT_{db}, UT_{db} and UHI.

4.1. The average dry bulb temperature change

The results showed that the average dry bulb temperature significantly increased in Osaka city centre from 2000 to 2020. The average annual altering of the RT_{db} and the UT_{db} from 2000 to 2020 is shown in Figure 8. For average annual UT_{db}, the minimum annual UT_{db} was 17.2°C, which occurred in 2005, the maximum annual UT_{db} was 18.7°C, which happed in 2004. For average annual RT_{db}, the minimum annual RT_{db} was 15.8°C, which occurred in 2005, the maximum annual RT_{db} was 17.9°C, which happed in 2004. The change of summer RT_{db} and summer UT_{db} in JJA from 2000 to 2020 is shown in Figure 9. For average summer UT_{db}, the minimum summer UT_{db} was 26.4°C, which occurred in 2003, the maximum summer UT_{db} was 28.3°C, which happed in 2004. For average summer RT_{db}, the minimum summer RT_{db} was 25.7°C, which occurred in 2003, the maximum summer RT_{db} was 27.7°C, which happed in 2004.
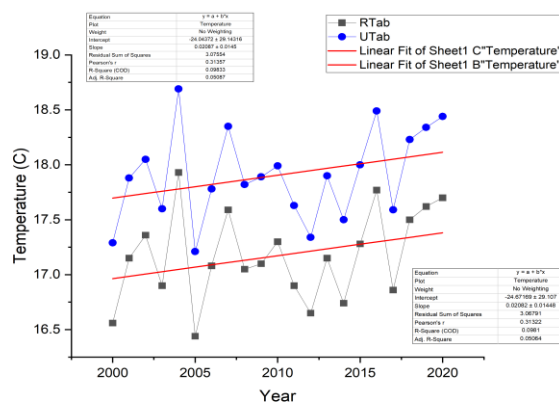

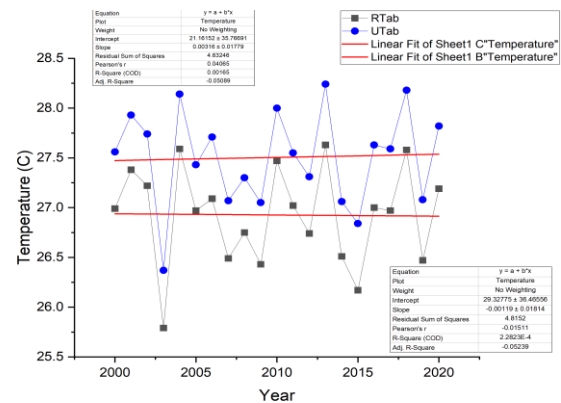*Figure 8: The average annual change of RT_{db} and UT_{db}.*

Figure 9: The average summer change of RT_{db} and UT_{db}.

4.2. Average urban heat island intensity

In this study, the average annual UHI intensity was defined as Equation (1), which was based on the theory of UHI identified by Oke (1982). It is now possible to draw generalisations for the average annual UHI calculation.

$$\text{Average annual UHI} = \frac{1}{Hour_x} \sum_{i=1}^{Hour_x} UT_{db} - RT_{db} \qquad (1)$$

Where:

- $Hour_x$ = hours by a year, which equals 8760 in an ordinary year, 8784 in a leap year;
- UT_{db} = the annual dry bulb temperature in the urban area;
- RT_{db} = the annual dry bulb temperature in the rural area.

The average annual UHI from 2000 to 2020 was calculated by Equation (1). The intensity of annual UHI and summer UHI increased between 2000 to 2020 in Osaka city centre, while the average summer UHI intensity increased quicker than the annual UHI intensity. Figure 10 shows the average annual UHI intensity. The maximum annual UHI intensity was 0.79°C in 2009, and the minimum annual UHI intensity was 0.65°C. Besides, the summer UHI intensity was analysed to predict the future intensity of UHI in JJA, and the average summer UHI was also calculated by the hours of summertime. However, the average summer UHI significantly increased from 2000 to 2020, as shown in Figure 11. The maximum summer UHI intensity was around 0.65°C in 2020, and the minimum summer UHI intensity was 0.47°C in 2005.
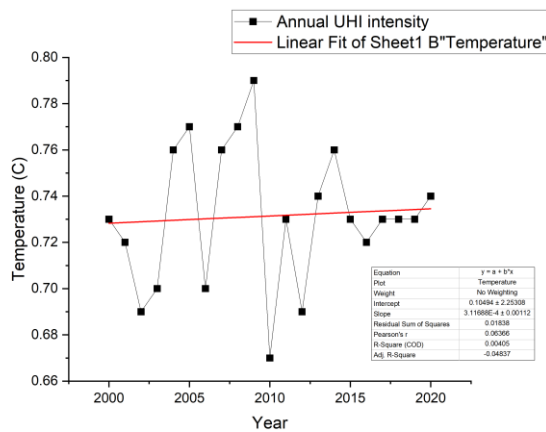
Figure 10: The average annual UHI value.
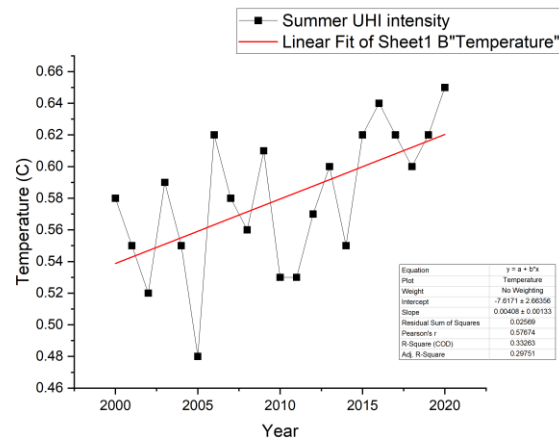
Figure 11: The average summer UHI value.

4.3. Prediction of urban heat island intensity

The average annual UHI and the summer UHI have been predicted for the next 20 years (2040), based on the value of R^2. The prediction showed that the intensity of annual and summer UHI will increase in the future, and that the local outdoor temperature will be higher in Osaka city centre. The average annual UHI intensity prediction from 2020 to 2040, as shown in Figure 12, will increase slowly from 2020 to 2040, and the intensity will be between 0.7°C and 0.8°C in 2040. However, the average summer UHI will significantly increase by 2040, which is shown in Figure 13. The intensity will grow from 0.58°C to 0.71°C in 2040.

73
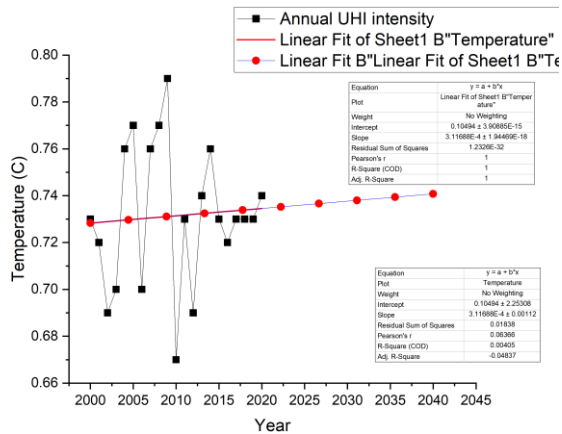
Figure 12: Average annual UHI in 2040.
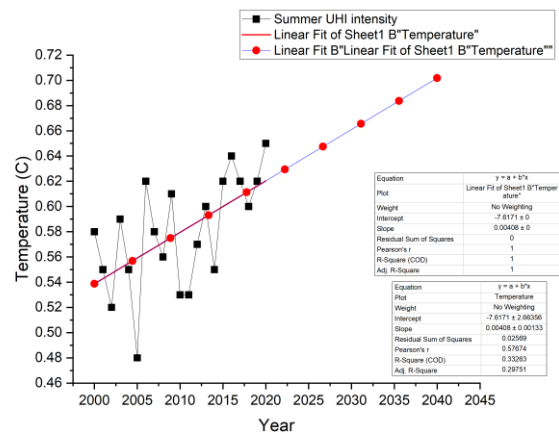
Figure 13: Average summer UHI in 2040.

5. CONCLUSION, LIMITATION AND FURTHER WORK

To encourage urban energy saving and achieve the GHG emissions reduction goal, the UHI intensity has to be assessed for city centres. However, an easy and accurate UHI calculation process was lacking. In this study, to solve this issue, an innovative urban heat island calculation workflow (UHI-CW) was created to evaluate the outdoor air temperature in urban areas by combining rural microclimate information and urban geometry and objects, with the advantages of:

(i) Fewer historical meteorological and building data being required;

(ii) Calculation processes were simple, computational and time-saving;

(iii) The calculation accuracy was high due to accurate urban parameters and variables.

A case study was conducted to guarantee the operability of UHI-CW. The UHI intensity and change from 2000 to 2020 in a subtropical city centre (Osaka, Japan) were analysed. The results showed the intensity of the average annual UHI in Osaka city centre was around 0.73°C and the average summer UHI was 0.58°C. However, the summer UHI increased rapidly in °C saka city centre. The predication for future summer UHI in Osaka city centre is that the intensity will increase to 0.71°C in 2040.

However, some limitations should be considered in further work, as following:

(i) The HACV systems of each building should be considered in further work;

(ii) The visualisation of the intensity of UHI could be achieved in further work;

(iii)The UHI mitigation strategies could be adopted to analyse the UHI intensity change in further work.

Overall, the innovation and operational urban weather generator engine was convenient having the ability to couple the rural weather data and city objects to calculate the intensity of UHI and predicate the future UHI change. The results can provide a functional guide for local authorities, urban planners and policymakers to achieve a more sustainable city centre.

6. REFERENCES

Aghamolaei R, Fallahpour M, Mirzaei PA. Tempo-spatial thermal comfort analysis of urban heat island with coupling of CFD and building energy simulation. Energy and Buildings. 2021;251:111317.

Akbari H, Kolokotsa D. Three decades of urban heat islands and mitigation technologies research. Energy and buildings. 2016;133:834-42.

Ambrosini D, Galli G, Mancini B, Nardi I, Sfarra S. Evaluating mitigation effects of urban heat islands in a historical small center with the ENVI-Met® climate model. Sustainability. 2014;6(10):7013-29.

Atkinson BW. Numerical Modelling of Urban Heat-Island Intensity. Boundary-Layer Meteorology. 2003;109(3):285-310.

Bottyán Z, Unger J. A multiple linear statistical model for estimating the mean maximum urban heat island. Theoretical and Applied Climatology. 2003;75(3):233-43.

Churkina G. The Role of Urbanization in the Global Carbon Cycle. Frontiers in Ecology and Evolution. 2016;3.

Dong J, Lin M, Zuo J, Lin T, Liu J, Sun C, et al. Quantitative study on the cooling effect of green roofs in a high-density urban Area—A case study of Xiamen, China. Journal of Cleaner Production. 2020;255:120152.

Giannaros TM, Melas D, Daglis IA, Keramitsoglou I, Kourtidis K. Numerical study of the urban heat island over Athens (Greece) with the WRF model. Atmospheric Environment. 2013;73:103-11.

Gonzalez-Trevizo ME, Martinez-Torres KE, Armendariz-Lopez JF, Santamouris M, Bojorquez-Morales G, Luna-Leon A. Research trends on environmental, energy and vulnerability impacts of Urban Heat Islands: An overview. Energy and Buildings. 2021;246:111051.

Hirano Y, Yoshida Y. Assessing the effects of CO_2 reduction strategies on heat islands in urban areas. Sustainable Cities and Society. 2016;26:383-92.

IPCC. Climate change 2022 Impacts, Adaptation and Vulnerability. 2022.

Kim Y-H, Baik J-J. Maximum Urban Heat Island Intensity in Seoul. Journal of Applied Meteorology. 2002;41(6):651-9.

Li H, Zhou Y, Wang X, Zhou X, Zhang H, Sodoudi S. Quantifying urban heat island intensity and its physical mechanism using WRF/UCM. Science of The Total Environment. 2019;650:3110-9.

Mohan M, Kikegawa Y, Gurjar BR, Bhati S, Kandya A, Ogawa K. Urban Heat Island Assessment for a Tropical Urban Airshed in India. Atmospheric and Climate Sciences. 2012;Vol.02No.02:12.

Oke TR. The energetic basis of the urban heat island. Quarterly Journal of the Royal Meteorological Society. 1982;108(455):1-24.

Olfe DB, Lee RL. Linearized Calculations of Urban Heat Island Convection Effects. Journal of Atmospheric Sciences. 1971;28(8):1374-88.

Roxon J, Ulm FJ, Pellenq R-M. Urban heat island impact on state residential energy cost and CO_2 emissions in the United States. Urban Climate. 2020;31:100546.

Seto Karen C, Güneralp B, Hutyra Lucy R. Global forecasts of urban expansion to 2030 and direct impacts on biodiversity and carbon pools. Proceedings of the National Academy of Sciences. 2012;109(40):16083-8.

Singh V, Reddy TA, Abushakra B. Predicting annual energy use in buildings using short-term monitoring: the Dry-Bulb Temperature Analysis (DBTA) method. ASHRAE Transactions. 2014;120:397+.

Tian L, Lu J, Li Y, Bu D, Liao Y, Wang J. Temporal characteristics of urban heat island and its response to heat waves and energy consumption in the mountainous Chongqing, China. Sustainable Cities and Society. 2021;75:103260.

United Nations DoEaSA. World Urbanization Prospects: The 2018 Revision (ST/ESA/SER.A/420）. New York: United Nations2019.

Wang X, Li Y. Predicting urban heat island circulation using CFD. Building and Environment. 2016;99:82-97.

Yagüe C, Zurita E, Martinez A. Statistical analysis of the Madrid urban heat island. Atmospheric Environment Part B Urban Atmosphere. 1991;25(3):327-32.

Zheng T, Qu K, Darkwa J, Calautit JK. Evaluating urban heat island mitigation strategies for a subtropical city centre (a case study in Osaka, Japan). Energy. 2022;250:123721.

#166: Current situation of the Turkish organizational field of plastic waste management

Mustafa ŞENYÜCEL

Haliç University, Turkey, mustafasenyucel@halic.edu.tr

Abstract: The plastic waste trade has become a major issue concerning global waste management. Accordingly, the Chinese import ban has received much attention in academic, media and administrative environments. As a result, more bans are expected to affect the plastic waste trade. Furthermore, it may alter sustainability practices of several industries including plastic, cement, and recycling. Thus, it is important for scholars practicing related sustainable technologies to comprehend the inter-organizational dynamic that impacts plastic waste management. From an organizational and managerial perspective, this article demonstrates the current situation in the Turkish context. It reports the study undertaken to observe various organizations such as media, civil society organizations, firms, universities, and governmental agencies. The article aims to help readers forecast the future of waste management in Turkey as a means to shape future sustainable technologies for managing waste. Following the theoretical contributions of prominent scholars Scott (1994), DiMaggio and Powell (1982), and Hoffman (1999), the study utilized an organizational field concept, explaining how plastic waste trade was managed in Turkey and how managerial practices were interpreted by the organizations in question. The study utilized secondary data consisting of various online sources such as academic journals, news articles, non-governmental and governmental organization reports. The data was analysed thematically to understand how field agents interpreted the situation. Thus, research findings demonstrate how the current situation of the plastic waste trade was interpreted among the Turkish organizational field of plastic waste management. The discussions expect to direct future research for management as well as sustainability studies towards global waste trade and management.

Keywords: plastic waste trade; waste management; organizational field; Turkey; circular economy

1. INTRODUCTION

From an organizational field perspective, it can be conceptualized that a Turkish community emerged to manage plastic waste and evolved with discussions about plastic pollution and the plastic waste trade. News portals contributed to the field with critical interpretations of these issues and global civil society organizations carried out field research and furthered political campaigns. They both acted as pressure groups to encourage governmental agencies to institute import restrictions. However, industrial communities were against these restrictions and lobbied with governmental agencies to facilitate the import of wastes. On the other hand, governmental agencies were motivated to maintain regulative authority over industry organizations. Discussions about business and entrepreneurial initiatives towards circular economy became evident. Both universities and research groups contributed to the debate with review papers, survey research, and other scholarly work to examine the impact of plastic pollution as well as the effects of plastic waste trade on social, ecological, or economic processes. However, it is not clear whether it is the academic research and headline news about plastic waste trade that mobilizes organizations towards managing waste. It is not straightforward to deduce whether it is the regulative aspects, political campaigns or technological developments that motivate organizations towards investing in sustainable recycling technologies. This ambiguity is most likely the result of the neglected research about inter-organizational as well as power relations affecting waste management. Therefore, it is beneficial to conceptualize these relations within an organizational field perspective and examine how organizational fields influence the process.

This study followed an exploratory approach with an aim to aid future studies conceptualize how organizational factors affect the implementation and the legitimization of circular economy models and sustainable technologies. It investigated the practices and discussions of individual populations that shaped an organizational field managing plastic wastes. In so doing, it focused on the Turkish context to help readers examine the institutional and competitive forces behind plastic waste trade practices. In sum, this article is an introductory work to encourage scholars and policymakers to observe more about inter-organizational power relations and institutional influences in waste management as well as the developments concerning sustainable recycling technologies.

2. THEORETICAL FRAMEWORK

"Organizational field" is a prominent construct in institutional theory. It facilitates the analysis of inter-organizational relations to answer how organizations act in a field structure. For some time, management and organization studies observed these social relations to explain cause-and-effect relationships between institutional and organizational level changes. Unlike the previous constructs, which emphasized the networks for common technologies, markets, products and services, Hoffman (1999) directed scholarly attention to a central issue that mediated this relationship. The study showed that, not only ongoing business interactions but also frequent debates about a central issue determined the structure of the network. In due course, organizations acquire new insights; new field members contribute to these discussions, decide to leave the field, or motivate others to take action, which eventually changes the structure of the field.

From DiMaggio and Powell's 1983 perspective, understanding the dynamics of rationalisation is the main goal. They argued that organizational attempts towards rationalisation results in structural homogeneity. However, there are external forces that determine the rules of this homogenization. For instance, the struggles to deal with new export regulations on plastic waste, or technological developments in recycling plastic waste, lead organizational behaviour like compliance to new business systems, imitation of social projects emphasizing recycling practices or normative pressures to develop trainings on clean energy technologies. Therefore, institutional forces influence organizations towards developing similar behaviour as a means to minimize the risks of uncertainties such as future regulative requirements or demand changes.

However, Hoffman (1999) debated that the field was a dynamic structure which evolved with "triggering events" that organizations legitimize. For example, a news article or a regulative change may result in an increase in discussions to find solutions to the issue; a lobby with governmental agencies to maintain political relations; or an organization exercising leadership towards the resolution of the issue. Consequently, one inference was that the field consisted of "individual populations" that may present common discourses and practices while the others put forward contradictory views. For instance, we may expect homogeneity in the statements of business media organizations but opposite views from governmental agencies about the same issue. Another inference is that the interactions may alter with a new institutional force. An ecologic practice interpreted as the trend of a period, may not be interpreted as a sustainable solution in a latter period. Eventually this may motivate organizations to change their strategies and course of action. It may also be anticipated that contradictions in interpretations may encourage organizations towards the resolution of a problem, to minimize uncertainties deriving from public backlash, activist campaigns or industrial communities emphasizing economic, social and health concerns.

3. LITERATURE RESEARCH

The literature concerned with global plastic waste trade directed attention to the Turkish context and created a relational space (Wooten and Hoffman, 2016) to observe organizational and managerial dynamics. Mainly, articles interpreted the Chinese import ban as a triggering event. For instance, Zhao *et al.* (2022) argued that new trade links emerged with the Chinese import ban and accordingly, they forecasted an increase in the exports of high-income countries. Moreover, Wang *et al.* (2020) forecasted that high income countries would continue to export their plastic wastes to low-income countries, while low-income countries would not establish complete bans as a means to support this trend.

It was also debated that the structure of the plastic waste trade would negatively impact rural areas with low infrastructure capabilities. In this regard, Mihai *et al.* (2021) reviewed current literature to direct scholars on conceptualizing sustainable technologies towards reducing plastic waste. The study demonstrated the role of entrepreneurs and industrial communities in the development of domestic management systems and discussed that these initiatives may raise awareness about circular economy models and encourage collaborative community work to manage waste. Nevertheless, more research is needed in this area to help engineers, entrepreneurs and policy makers to shape long term action.

Such negligence is also seen in critical work about plastic pollution and plastic waste management. For instance, Dauvergne (2018) discussed why marine pollution was still a major global concern, although there had been significant advancements in international regulations, activism, and business initiatives towards sustainable plastic waste management. Even though the Turkish trade route was heavily debated in media context, only Gundogdu and Walker (2021) discussed the Turkish context in detail and in a critical manner. The article stated that the Turkish government implemented quota restrictions and announced regulations to impose tighter controls. However, it was argued that businesses in plastic and recycling industries still lacked transparency that may present problems in controlling the trade in terms of waste quality, trade illegalities and plastic pollution.

4. METHODOLOGY

This study was exploratory in nature, and a thematic research design was implemented. The data set consisted of online sources published between 2018 and 2022, including news portal websites, non-governmental organization campaign and research reports, governmental policies, and academic journals. Over 130 pages of data units were collected. An abductive approach was utilized for their analysis (Saunders *et al.*, 2019). The study began with deductive analysis. Both in vivo and priori codes were used to code themes. The coding started with a news article of interest. Then, the reports and other news articles that this data cited were read and coded. This coding process was repeated until the main and sub-themes started to reoccur in new data units. The generation of codes for earlier themes was based on the perspectives of organizational field theory and waste trade literature to ensure consistency.

The analysis progressed and concluded with an inductive approach. In the process, each online data was categorised by their publication date to observe changes in the agenda of individual populations. A list of organizational practices was created to facilitate the examination of the relationships between themes. Such approach not only allowed for the content to reveal the organizational field and its discursive orientations, but also facilitated the identification of relationships between institutional level effects and field level practices to be utilized for future research.

5. FINDINGS

Research shows that field interpretations concerning plastic waste trade emerged with news portals and non-governmental organizations monitoring the illegal trade and dumping of plastic waste. Greenpeace has investigated and debated these activities for several years. Their field research, biodiversity projects, signature and political campaigns highlighted the detrimental effects of plastic pollution and plastic waste trade in varying forms. Consequently, the organization exercised normative pressures to remind Basel Convention signatory high-income countries of their legal and financial responsibilities (Greenpeace, 2021). Accordingly, the report of Greenpeace Mediterranean stated that high-income countries that had previously exported their waste to China had changed their strategies after the Chinese import ban and started exporting non-recyclable plastic waste to underdeveloped countries. As more bans were announced, Turkey became a plastic waste trade point with mixed plastic waste which are difficult to recycle (Gundogdu, 2022).

It was not only the ecology news portals that discussed the plastic waste trade, but business news portals also contributed to the field. A Bloomberg article debated the import routine of a large UK-based retailer, which directed media attention to problems emerging from exporting waste overseas (Chellel and Moskwa, 2022). It revealed how

intermediaries, including contractors and waste brokers could exploit the deficit of audit and regulative systems. These reports and news articles resulted in a significant increase in attention to the Turkish context among news portals, non-governmental organizations, academics, and NGO alliances to comprehend the effects of this change (Celik, 2021; Doherty, 2021; Gundogdu and Walker, 2021; Laville, 2021; Marino, 2021; Rethink Plastic, 2021; Wylie 2021).

Several governmental agencies also contributed to the discussions by providing press briefings and reports about waste imports. For instance, the Turkish Court of Accounts interpreted the increase of waste imports due to the increase in the number of licensed waste treatment facilities and the emergence of opportunities to obtain cheap raw materials (Kaşka, 2022). However, news portals also reported that government agencies had not yet announced official information regarding company names, import rates or the quotas used (Ocak, 2022). Indeed, news about the plastic waste trade rocketed around the days of the ban of waste in the ethylene polymer group, and its cancellation (Bia News, 2021; Bildircin, 2021; Erem, 2021; Euronews, 2021; Goebel, 2021; Gundogdu, 2021; Kaska, 2021, 2022; Ocak, 2022; Unal, 2021; Yesil Gazete, 2022; Yigitcan, 2021).

Plastic and recycling industry organizations interpreted the import ban as a hindrance to their economic growth (PAGEV, 2018). It was discussed that the ban resulted in a conflict between plastic industry organizations and petrochemical cartels. Cartels were claimed to reduce the supply and cause raw material prices to rise. Latest news revealed that several Turkish business and non-governmental organizations in the Turkish plastic industry and industry chambers lobbied with governmental organizations to reverse the economic trend. They pressured governmental agencies towards cancelling the import ban (Gundogdu and Walker, 2021; Unal, 2021; Yigitcan, 2021). In return, the government decided to cancel the ban and exercise tighter controls.

6. DISCUSSION

Several inferences can be made when research findings and the theoretical framework are linked. Firstly, it may be suggested that the news articles created the relational spaces when they interviewed academics and civil society organizations who have called for regulative action towards heavier sanctions for illegalities or complete import restrictions. Several press briefings concerning political campaigns and field research mentioned that news articles succeeded in affecting governmental agenda and directed governmental agencies towards import bans (Greenpeace Turkey, 2022; Gundogdu, 2021; McGlone, 2022). Research findings also revealed that there were contradictions in interpretations and practices between individual populations. While most academic environments, news portals and several non-governmental organizations shared negative views about the plastic waste imports and supported the bans, other non-governmental organizations, plastic industry organizations and industry chamber members favoured open import systems and lobbied governmental agencies against import bans.

The outdated recycling habits and norms as well as overproduction seems to have prevailed in the Turkish setting, which impacts recycling practices utilized. This may be due to inadequate infrastructure to recycle or to utilize clean fuel for managing waste. According to Greenpeace, practices such as controlled landfill or composting has not been institutionalized yet (Çelik, 2021).

Secondly, most academic work neglects the profit-seeking behaviour in waste management. Waste entrepreneurs and traders made superior profits from the trade of non-recyclable plastics, which high-income countries have tried to dispose of for many years. (Chellel and Moskwa, 2022; McGlone, 2022; Naayem, 2021). Instead of adapting sustainable recycling and clean fuel practices, utilizing domestic treatment facilities, or implementing circular plastic economy strategies, countries exploited regulative deficits and exported tonnes of waste overseas. For example it has been argued that exporting waste is more profitable due to the fact that domestic recyclers are paid after the material undergoes certain processes, while overseas traders are rewarded for taking the waste, either processed or not (Chellel, and Moskwa, 2022). Nevertheless, it was mainly the news articles that highlighted the weakness of regulative systems in relation with sanctions, auditing of packaging recovery notes, control of the changes made to banned product codes or customs inspections (Bildircin, 2021; Daniels, 2021; McGlone, 2022; Kaşka 2021; Syberg et al., 2021).

Thirdly, it can be expected that the exportation of waste to low-income, underdeveloped countries will increase. However, it was not solely depending on the economic levels of countries, new trade routes or the mismanagement of waste that Zhao et al. deliberated (2022), it was also due to inter-organizational relations. When lobbying attempts by the plastic industry and industrial chambers amplify, when broker facilities become full to overflow, when the cost of trade with cement industry organizations rise, firms will be more inclined to dispose of waste to countries lacking import controls (Brock et al., 2021; Chellel, and Moskwa, 2022). Similar arguments can be made as cement and recycling industries, waste brokers, governments and academicians continue to fail to address transparency issues regarding numbers of wastes traded and recycled, the areas impacted by waste dumping, the ecological outcomes of plastic waste incineration (Brock et al., 2021; Gundogdu and Walker, 2021). In its infancy,

the organizational field may reduce profit seeking behaviour when government agencies impose heavier sanctions for illegal trade activities and support industrial infrastructure for recycling plastic wastes.

Lastly, it is also evident that only a few organizations have discussed the opportunities regarding plastic waste recovery. Even though circular economy models are discussed among academic environments, business and entrepreneurial organizations remain silent. Instead, cement industry organizations and multinational companies have supported the incineration of non-recyclable plastic waste using cement kilns (Brock et al., 2021). However, environmentalists have questioned the sustainability of this energy source, and debated about harmful air emissions as well as its impact on global efforts on waste reducing (Brock et al., 2021; Chellel, and Moskwa, 2022). Furthermore, governmental organizations interpreted the economic opportunities and demonstrated the increase in waste facilities (Kaşka, 2022). Nevertheless, several academics interpreted the situation as an opportunity and directed attention to circular plastic economy (Mihai et al., 2021). On the contrary, news portals and civil society organizations discussed the transparency issues of trade and waste recycling in Turkey as a barrier in the development of sustainable recycling technologies to support the circular economy.

7. CONCLUSION

Most academic work followed quantitative approaches, and they either reviewed existing literature to discuss sustainable solutions or predicted the future of waste management. However, the neglect of a longitudinal qualitative study in the waste trade literature is apparent. Theories of the organizational field have been conceptualized to observe longitudinal changes of field practices, since they are concerned with institutional effects and change. In this sense, the study was limited to the examination of the discussions of Turkish organizational field in the years between 2018 and 2022. So future research may contribute by building their research on organizational field theory and investigating interaction patterns of the waste management field in longer periods, to reveal the institutional and competitive forces that created and evolved the field. The discursive dynamics can be analysed to determine the forces that hinder or encourage the development of sustainable practices in recycling plastic wastes both in global and rural contexts.

Furthermore, the attention theory would also serve as a basis to deliberate organizational and managerial practices of plastic waste management (Ocasio, 1997; Hoffman and Ocasio, 2001). It may be beneficial to comprehend the dynamics affecting issue interpretations. For instance, for the case of plastic waste trade, the patterns from public attention to regulative or industry action or from regulative action to media attention are significant, as several academic articles mentioned (Syberg et al., 2021). Nevertheless, it is still not clear how organizational and field level attention and actions impact each other. The answers to organizational attention may also provide fruitful insights for developing community programs on waste management.

8. REFERENCES

Bia News, (2021, 20 May). Turkey bans import of polymer waste after becoming Europe's top waste importer. https://bianet.org/english/environment/244338-turkey-bans-import-of-polymer-waste-after-becoming-europe-s-top-waste-importer# (Accessed 14.05.2022)

Bildircin, M. (2021, July 12). Ülkeyi Çöplüğe Dönüştürecekler. [They Will Turn the Country into a Dump] https://www.birgun.net/amp/haber/ulkeyi-copluge-donusturecekler-351450 (Accessed 14.05.2022)

Brock, J., Budiman Y. C., Geddie J., and Volcovici V. (2021, Oct 28). Trash And Burn. https://www.reuters.com/investigates/special-report/environment-plastic-cement/ (Accessed 24.05.2022)

Brooks, A. L., Wang, S., & Jambeck, J. R. (2018). The Chinese import ban and its impact on global plastic waste trade. *Science Advances*, 4(6).

Celik, D. (2021, May 29). Greenpeace report highlights extent of European nations' dumping of waste in Turkey. https://globalvoices.org/2021/05/29/greenpeace-report-highlights-extent-of-european-nations-dumping-of-waste-in-turkey/ (Accessed 13.05.2022)

Chellel, K.; and Moskwa, W. (2022, Mar 29). A Plastic Bag's 2,000-Mile Journey Shows the Messy Truth About Recycling. https://www.bloomberg.com/graphics/2022-tesco-recycle-plastic-waste-pledge-falls-short/ (Accessed 17.05.2022)

Daniels, J. P. (2021, Dec 24). Latin America Urges US to Reduce Plastic Waste Exports to Region. https://www.theguardian.com/environment/2021/dec/24/latin-america-urges-us-to-reduce-plastic-waste-exports-to-region (Accessed 29.05.2022)

Dauvergne, P. (2018). Why is the global governance of plastic failing the oceans?. Global Environmental Change, 51, 22-31.

Dimaggio, P. J., & Powell, W. W. (1982). The iron cage revisited: conformity and diversity in organizational fields [working paper]. *Institution for Social and Policy Studies*, Yale University, 52.

Doherty, J. (2021). Greenpeace report sparks plastic export concerns https://www.letsrecycle.com/news/greenpeace-report-sparks-plastic-export-concerns/ (Accessed 13.05.2022)

Erem, O. (2021, May 18). Plastik Atık Ticareti Nedir, Türkiye Nasıl En Çok Atık Alan Ülkelerden Biri Oldu? [What Is Plastic Waste Trade, How Did Turkey Become One of The Countries Importing The Most Waste?] https://www.bbc.com/turkce/haberler-dunya-57142579 (Accessed 14.05.2022)

Euronews. (2021, July 10). Türkiye'de Plastik/Polietilen Ithalatına Getirilen Yasak Kaldırıldı [The Ban on Plastic/Polyethylene Imports in Turkey Has Been Lifted] https://tr.euronews.com/2021/07/10/turkiye-de-plastik-polietilen-ithalat-na-getirilen-yasak-kald-r-ld (Accessed 14.05.2022)

Evode, N.; Qamar, S.A.; Bilal, M.; Barceló, D.; Iqbal, H.M.N. 2021. Plastic waste and its management strategies for environmental sustainability. *Case Stud. Chem. Environ. Eng., 4.*

Goebel, J. (2021, May 07). Türkei Könnte Über 140 Container Mit Plastikmüll Zurück Nach Deutschland Schicken [Turkey Could Send More Than 140 Containers With Plastic Waste Back To Germany] https://www.wiwo.de/unternehmen/handel/abfaelle-tuerkei-koennte-ueber-140-container-mit-plastikmuell-zurueck-nach-deutschland-schicken/27163356.html (Accessed 14.05.2022)

Greenpeace Turkey. (2022, Apr 1). Basın açıklaması: Adana Plastik Atık İthalatı [Press release: Adana Plastic Waste Import] https://www.greenpeace.org/turkey/basin-bultenleri/basin-aciklamasi-adana-plastik-atik-ithalati/ Accessed 05.05.2022

Greenpeace. (2021, May 17). Investigation finds plastic from the UK and Germany illegally dumped in Turkey. https://www.greenpeace.org/international/press-release/47759/investigation-finds-plastic-from-the-uk-and-germany-illegally-dumped-in-turkey/ Accessed 05.05.2022

Greenpeace. (2021) Trashed How the UK Is Still Dumping Plastic Waste on The Rest of The World https://www.greenpeace.org.uk/wp-content/uploads/2021/05/EMBARGOED-GPUK-Trashed-report.pdf

Gundogdu, S. (2022). Atık Oyunları Geri Dönüşümsüz Hayatlar [Waste Games Lives Without Recycling]. https://www.greenpeace.org/turkey/raporlar/rapor-atik-oyunlari-geri-donusumsuz-hayatlar/ Accessed 17.05.2022

Gundogdu, S. (2021). Türkiye Avrupa'nin Plastik Çöplüğü Olma Yolunda: Geri Dönüşüm Miti [Turkey Is on The Path to Be Europe's Plastic Waste: The Myth of Recycling]. https://www.atlasdergisi.com/genel/turkiye-avrupanin-plastik-coplugu-olma-yolunda-geri-donusum-miti.html (Accessed 14.05.2022)

Gundogdu, S. and, Walker T.R. (2021). Why Turkey Should Not Import Plastic Waste Pollution from Developed Countries? *Marine Pollution Bulletin*, 171 (112772).

Hoffman, A. J. (1999). Institutional evolution and change: Environmentalism and the U.S. chemical industry. *Academy of Management Review*, 42(4), 351-371.

Hoffman, A.J. Ocasio, W. (2001). Not All Events Are Attended Equally: Toward a Middle-Range Theory of Industry Attention to External Events. Organization Science 12(4):414-434. https://doi.org/10.1287/orsc.12.4.414.10639

Kaşka, M. K. (2022). İngiltere, Türkiye'ye Plastik Atık İhracatını Yasaklayabilir mi? [Could The UK Ban the Export of Plastic Waste to Turkey?] bbc.com/turkce/haberler-dunya-60846662 Accessed (14.05.2022)

Kaşka, M. K. (2021). Tüm Yönleriyle Türkiye'nin Plastik Atık 'Ithalatı' [All Aspects of Turkey's Plastic Waste 'Import'] https://iklimgazetesi.com/tum-yonleriyle-turkiyenin-plastik-atik-ithalati/ (Accessed 14.05.2022)

Laville, S. (2021, May 17). UK plastics sent for recycling in Turkey dumped and burned, Greenpeace finds. https://www.theguardian.com/environment/2021/may/17/uk-plastics-sent-for-recycling-in-turkey-dumped-and-burned-greenpeace-finds (Accessed 13.05.2022)

Leslie H.A., van Velzen M.J.M., Brandsma S.H., Vethaak D., Garcia-Vallejo J.J., and Lamoree M.H. (2022). Discovery and Quantification of Plastic Particle Pollution in Human Blood. *Environment International*, 10.1016/j.envint.2022.107199

Liu, Z.; Adams, M.; and Walker, T.R. (2008). Are exports of recyclables from developed to developing countries waste pollution transfer or part of the global circular economy? *Resources, Conservation and Recycling*, 136, 22–23.

Marino, G. (2021, May 29). Turkey Like China: Stop to The Import of Plastic Waste. https://www.renewablematter.eu/articles/article/turkey-like-china-stop-to-the-import-of-plastic-waste (Accessed 13.05.2022)

McGlone, C. (2022, Feb 07). UK supermarkets entangled in the murky world of plastic waste. https://eandt.theiet.org/content/articles/2022/02/uk-supermarkets-entangled-in-the-murky-world-of-plastic-waste/ (Accessed 23.05.2022)

Mihai, F.-C.; Gündogdu, S.; Markley, L.A.; Olivelli, A.; Khan, F.R.; Gwinnett, C.; Gutberlet, J.; Reyna-Bensusan, N.; Llanquileo-Melgarejo, P.; Meidiana, C. (2022). Plastic Pollution, Waste Management Issues, and Circular Economy Opportunities in Rural Communities. *Sustainability*, 14,(20). https://doi.org/10.3390/su14010020

Naayem, N. (2021, Apr 12). The Inherent Problem with the Global Plastic Waste Trade. https://rethinkplasticalliance.eu/news/the-inherent-problem-with-the-global-plastic-waste-trade (Accessed 30.05.2022)

Ocak, S. (2022, April 17). Türkiye'nin yeni çevre sorunu: Geri dönüşüm [Turkey's new environmental problem: Recycling]. https://www.dw.com/tr/t%C3%BCrkiyenin-yeni-%C3%A7evre-sorunu-geri-d%C3%B6n%C3%BC%C5%9F%C3%BCm/a-61498695 (Accessed 14.05.2022)

Ocasio, W. (1997). Towards an Attention-Based View of the Firm. *Strategic Management Journal*, 18, 187–206. http://www.jstor.org/stable/3088216

PAGEV. (2021, Jul 10). Polietilen Atık İthalatı Etkin Denetimle Serbest! [Polyethylene Waste Import is Free with Effective Control!]. https://pagev.org/polietilen-atik-ithalati-etkin-denetimle-serbest (Accessed 14.05.2022)

Rethink Plastic. (2021). #WeChooseReuse: Waste Trade and the Importance of Moving From Single-use Plastic to Reuse https://rethinkplasticalliance.eu/news/wechoosereuse-waste-trade-and-the-importance-of-moving-from-single-use-plastic-to-reuse/ (Accessed 13.05.2022)

Saracoglu, G.; and Laville, S. (2018, Oct 18). Turkey's plastic waste imports from the UK are booming – but at what cost?. https://www.theguardian.com/environment/2018/oct/18/uk-plastic-waste-imports-to-turkey-boom-but-at-what-cost (Accessed 17.05.2022)

Saunders, M. N. K., Lewis, P., and Thornhill, A. (2019). Research methods for business students. Harlow: Financial Times/Prentice Hall.

Scott, W. R. (1994). Conceptualizing organizational fields: Linking organizations and societal systems. In H. Derlien, U. Gerhardt, & F. Scharpf (Eds.). *Systems rationality and partial interests* (pp. 203-221). Baden: Nomos.

Syberg, K., Nielsen, M.B., Westergaard Clausen, L.P., van Calster, G., van Wezel, A., Rochman, C., Koelmans, A.A., Cronin, R., Pahl, S.; and Hansen, S.F. (2021). Regulation of plastic from a circular economy perspective. *Current Opinion in Green and Sustainable Chemistry*. https://doi.org/10.1016/j.cogsc.2021.100462

Unal, E. (2021). Plastik Sektörünün Lobi Faaliyeti Sonuç Verdi: Atık İthalat Yasağının Kalkması Için Uzlaşıldı [The Lobbying Activity of The Plastics Industry Yielded Results: It Was Agreed To Lift The Waste Import Ban]. https://yesilgazete.org/plastik-sektorunun-lobi-faaliyeti-sonuc-verdi-atik-ithalat-yasaginin-kalkmasi-icin-uzlasildi/ (Accessed 14.05.2022)

Wang, C., Zhao, L., Lim, M. K., Chen, W. Q., & Sutherland, J. W. (2020). Structure of the global plastic waste trade network and the impact of China's import Ban. *Resources, Conservation and Recycling*, 153, 104591. https://doi.org/10.1016/j.resconrec.2019.104591

Wooten, M.; and Hoffman, A. J. (2016). Organizational Fields Past, Present and Future (2016). R. Greenwood, C. Oliver, K. Sahlin and R. Suddaby (eds.) *The SAGE Handbook of Organizational Institutionalism* (London: Sage Publications): 130-148.

Wylie, C. (2021, May 17). Plastic waste crisis in Turkey. https://theecologist.org/2021/may/17/plastic-waste-crisis-turkey (Accessed 13.05.2022)

Yesil Gazete. (2022, Feb 09). Avrupa'nın plastik çöpü Türkiye'ye zehir oldu. https://yesilgazete.org/avrupanin-plastik-copu-turkiyeye-zehir-oldu/ (Accessed 02.04.2022)

Yigitcan, M. (2021, July 09). Plastik Atık İthalatında Yasak Yerine Denetim! [Control Instead of Ban on Plastic Waste   Imports!]   https://www.dunya.com/sektorler/plastik-atik-ithalatinda-yasak-yerine-denetim-haberi-627510 (Accessed 14.05.2022)

Zhao, C.; Qi, X.;Wang, J.; Du, F.; Shi, X. (2022). Predicting Possible New Links to Future Global Plastic Waste Trade Networks. Sustainability, 14, 4692. https://doi.org/10.3390/su14084692

#169: Exergetic opportunity costs as a sustainability indicator for energy systems

Hossein KHAJEHPOUR

Sharif University of Technology, Tehran, Iran, khajehpour@sharif.edu

Abstract: An integrated sustainability criterion was developed to assess the sustainability of energy systems in a holistic manner. Many analytical methods of sustainability have been developed on the ecosystem-based values subject to the use of production factors, energy carriers, environmental services, and impacts. According to the basic definition of exergy - the maximum theoretical obtainable useful work - in the present research work, a new approach for assessing the exergetic performance of production factors was developed. The novelty of the developed Exergetic Opportunity Cost (EOC) approach was in defining the exergetic performance of the production factors as their capacity to substitute exergy destructions. The EOC was defined to be equivalent to the theoretically achievable reduction in exergy destructions resulted from gaining access to the production factors. The results were then compared with the Extended Exergy Accounting (EEA) developed in the literature. Both of the physical concepts (EEA and EOC) were applied in a case study in Iran to assess the exergetic cost of production factors in an energy system.

1. INTRODUCTION

The energy sector has been responsible for much of the environmental impacts which are key limits to sustainable human growth. Therefore, sustainable and resilient access to affordable energy services has become one of the main concerns of the human being for assuring welfare in the future. These facts have motivated analysts to identify a sustainable energy system in which different pillars of sustainability (social, environmental and economic) are addressed. These efforts could be categorized into the technical development of more efficient and less polluting technologies in the energy supply and demand sectors and development of new conceptual analytical methods and tools to optimize transition of the energy system in order to reduce its effects on the ecosystem (Yi, Hau *et al.,* 2004).

Since sustainability is understood as a constraint to economic development, the economic models have been modified for assessing costs and values of different production factors and ecosystem services. More specific in the energy sector, many energy-economic supply and demand models have been developed to take the ecosystem related costs and constraints into account.(Nakata, 2004) Consequently, in such models, where needed, equivalent economic values (costs) have been assigned to ecosystem services in local or global scales (Sander de Bruyn, 2010; Marzelli, Moning *et al.,* 2017). Indeed, the extension of energy-economic models to account for other sustainability aspects, especially the environmental costs and constraints, has been a fruitful step towards more sustainable decision-making. During the energy crisis in the 1970's, the interest of the governments toward more efficient supply and demand of energy motivated the researchers toward the definition of more meaningful measures for resource consumption (Sciubba and Wall, 2007). Therefore, new methods and corresponding mathematical models have been developed based on the ecosystem-based (physical) evaluation of the production factors, energy carriers, and environmental impacts (Spakovsky and Frangopoulos, 2009; Romero and Linares, 2014). These methods target more comprehensive understanding of the sustainability of the energy systems. Outcomes of these analytical tools have been recognized as complementary to economic methods (Romero and Linares, 2014).

The very basic root of these methods lies in the *energy theory of value* and the idea that thermodynamic concepts could be implemented to assess physical costs or values of production factors, energy, and material streams and ecosystem services (Beaudreau and Pokrovskii, 2010). This concept is based on the presumption that "energy is the only really limited resource on Earth and therefore should be the sole determinant of value" (Glucina and Mayumi, 2010). The applicability of this theory at least for identification of the improvement opportunities in the energy systems has been widely acknowledged (Glucina and Mayumi, 2010). The net energy analysis developed to account for wider spatial and temporal energy requirements in a production chain to internalize external resource destruction. Further development of the concept by Odum in 1971 incorporated more types of resource consumptions and external impacts in the form of a new concept of natural value, *emergy* (Odum, 2007). By definition, the *emergy* carries "the memory of the availability that was used up" and hence considers the resources consumed prior to the main production (Odum, 2007).

Further development of the application of the thermodynamics in the holistic optimization of energy systems has led to the development of *Extended Exergy Accounting* (EEA) method. The EEA method, as the most comprehensive thermodynamic view to the system optimization, takes all production factors (labour, capital, and energy) as well as environmental impacts into exergetic account in a life-cycle span (Sciubba, 2006; Rocco, Colombo *et al.,* 2014). Although, in comparison to energy, the concept of exergy has improved the understanding of the resource consumptions yet it cannot consider all value dimensions of resources and carriers such as life-cycle environmental effects or ease of storage (Herendeen, 2004). As a result, exergy-based cost accounting methods have been gradually developed to consider different aspects of value or cost creations in a more realistic manner. The objective of the present research work is also to contribute to further development of the subject through endogenous evaluation of the value of production factors.

2. METHODOLOGY

In the real world, the exergetic value of a unit of a production factor (labour and capital) is the extra amount of reduction in exergy destruction while keeping the production level constant. This might be available by getting access to the production factor in the geographic, temporal, and specific industrial sector. Also, due to the effect of the economy of scale, structural fluctuations in time or cumulative effects, the productivity of production factors as well as the damages from the environmental emissions are neither constant nor linear. Therefore, the averaged values do not meet the requirements of dynamic optimization. Based on the optimal output rule in neoclassical economics, the perfect price of a production factor or ecosystem service in an assumed system (market) would be equivalent to the marginal productivity of that factor.

A new approach was developed in the present research work to assess the exergetic values of production factors, as an alternative to their extended exergy costs of EEA. Although "exergy", as a thermodynamic concept, can only be used to assess the costs and not the values, here the term "exergetic value", as the exergetic performance of a production factor, is used to highlight the change in the points of view in the EOC from other "exergetic cost" accounting method, e.g. EEA. The opportunity costs were assumed to be equivalent to the marginal exergy productivity (i.e. marginal reduction in exergy destruction) resulted through relaxing the constraints on the production factors. The applicability of the new approach was ensured with the help of defining the exergetic values of the production factors as the opportunity costs of the factors to substitute exergy destructions.

In EEA the assessment of the exergetic cost of the labour and capital production factors are based on national averaged values. In contrast to the method implemented in the EEA, in the proposed EOC approach in the present research work these factors could be specific to the industrial sector under study. The cost factors were equivalent to the marginal rate of technical substitution (MRTS) of exergy destructions (Ex) with the production factors (labour (L) in e.g. work hours (*wh*) or capital (*K*) in monetary units (e.g. €)). By shaping the production function of the sector under study, the MRTS could represent the actual marginal profitability of each unit of labour or capital and its variations through time (**Error! Reference source not found.** and **Error! Reference source not found.**). Assuming the production level (*Y*) as a function of production factors, the MRTS would be equivalent to the relative change in marginal products (*MP*) of production factors.

$$Y_t = f(K.L.Ex)_t \qquad\qquad \text{Equation 1}$$

$$MRTS_{Ex.L} = \left(\frac{\frac{\partial Y}{\partial L}}{\frac{\partial Y}{\partial Ex}}\right)_{t\,(Y.K=cte)} = \frac{\beta_L}{\beta_{Ex}} \times \frac{Ex}{L} \qquad \left[\frac{MJ}{wh}\right] \qquad\qquad \text{Equation 2}$$

$$MRTS_{Ex.K} = \left(\frac{\frac{\partial Y}{\partial K}}{\frac{\partial Y}{\partial Ex}}\right)_{t\,(Y.L=cte)} = \frac{\beta_K}{\beta_{Ex}} \times \frac{Ex}{K} \qquad \left[\frac{MJ}{\$}\right] \qquad\qquad \text{Equation 3}$$

Fundamentally it was expected that due to technical development through time, more capital investments could result in more efficient (less exergy destructive) productions. Also, due to the automation effect, the use of power-driven machinery instead of the workforce in production could result in the substitution of exergy destruction and labour workforce. By definition, the MRTS could be calculated based on the assumption that only two production factors were technically substitutable while keeping the other production factor as well as the production level constant. Also, depending on the type of production function, MRTS was usually a function of the elasticities of substitution as well as the level of production and resource consumptions. The elasticities of substitution were dimensionless measures of the ability to substitute among factors and for typical types of the production functions were assumed to be constant. Therefore, this formulation was only valid for short-term assessments. The extrapolation of this temporal trend of the derived cost factors was valid for the temporal discount rate of the value of the operating factors (which was typically assumed as interest rates in economic analysis).

3. CASE STUDY

The petrochemical industry in the South Pars Special Economic Energy Zone (PSEEZ) was chosen as the case study in the present research work. Gas and condensates are produced offshore from the South Pars/North Dome gas condensate field, located in the Persian Gulf. It is the world's largest natural gas field shared between Iran (38%) and Qatar (62%) (International Energy Agency 2008). Almost 45% of the petrochemical productions of the country (about 32.7 mt/y) are located in the zone (National Iranian Petrochecmial Company 2017). The onshore operating facilities, including 7 gas refineries and 11 petrochemical complexes, are in the Pars 1 region (also known as Assaluyeh) with an area of 140 km^2 (National Iranian Petrochecmial Company 2017). **Error! Reference source not found.** shows a simplified presentation of the region and connections among different subsystems.
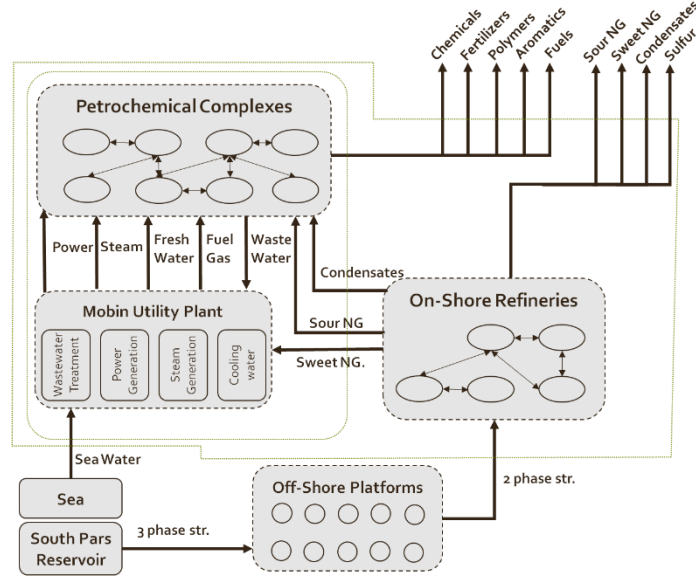
Figure 8: Simplified presentation of the production facilities and interconnections in the PSEEZ. Reproduced from Khajehpour, et al., 2017.

4. RESULTS

4.1. Calculation of EEA factors

The EEA cost factors of labour and capital for the country of Iran were assessed according to the developments of the EEA method in Rocco, Colombo *et al.* (2014). According to the formulations provided in Sciubba (2011), the extended exergy costs of the production factors capital (ee_k) and labour (ee_L) were calculated and reported for Iran by Aghbashlo *et al.,* (Aghbashlo, Tabatabaei *et al.,* 2018). However, in Aghbashlo, Tabatabaei *et al.,* (2018), the input variable *S*, equivalent to the global salaries and wages, in the year 2013 in Iran was assumed to be 43.2b$. while, according to the data provided by the Statistical Center of Iran (Iran, 2018), the true value for S was 321.7 b$. Also the number of the work-hours in a year was assumed to be 54.5 bwh (Aghbashlo, Tabatabaei *et al.,* 2018) while according to the labour report of the Statistical Center of Iran (SCI, 2018), the value was about 84.6 bwh. According to these modifications to the input variables, the EEA coefficients are calculated as Equations 4 and 5 below:

$$ee_L = \frac{365\ HDI\ ex_{sruv}\ N_h}{HDI_0\ N_{wh}} = \frac{365\left(\frac{d}{y}\right)\times 0.749 \times 1.05\times 10^7\left(\frac{J}{Person.d}\right)\times 75{,}706{,}898(persons)}{0.055\times 84.6\times 10^9\left(\frac{wh}{y}\right)} = 46.7\ \left(\frac{MJ}{wh}\right) \qquad \text{Equation 5}$$

$$ee_K = ee_L \times \frac{N_{wh}}{S} = 46.7\ \left(\frac{MJ}{wh}\right) \times \frac{84.6\times 10^9\left(\frac{wh}{y}\right)}{321.7\left(\frac{b\$}{y}\right)} \times 1.28\left(\frac{\$}{€}\right)_{2013} = 15.7\left(\frac{MJ}{€_{2013}}\right) \qquad \text{Equation 5}$$

In the above formula, the *HDI* is the human development index, the ex_{surv} is the minimum exergy required for living, the N_h is the population of the country, the HDI_0 is the minimum recorded HDI, the N_{wh} is the total number of workhours provided by the society under study and finally the S is the global salaries and wages. For further information about the notion behind this formulation and definition of the input factors, see Sciubba, 2006; Sciubba, 2011; Sciubba, 2013; Rocco, Colombo *et al.,* 2014; Aghbashlo, Tabatabaei *et al.,* 2018.

4.2. Calculation of EOC factors

The EOC cost factors were assessed based on the developed method in the present study (Figure 1) for both the labour and capital production factors. The EOC cost factors were calculated based on the exergy included econometric modelling of the petrochemical sector of Iran using the cross-sectional data for 2007. A summary of the output elasticities of production factors (β_K, β_L, and β_{Ex} in Equation 6) for the studied cases are presented in Table 7.

$$Y = a \times e^{\alpha t} \times K^{\beta_K} \times L^{\beta_L} \times Ex^{\beta_{Ex}} \qquad\qquad \text{Equation 6}$$

Table 7: Derived constants and output elasticities of production factors in the studied cases

Case	Type	a	α	β_K	β_L	β_{Ex}
Iranian petrochemical industry	Cross-section for 2007	0.032	--	0.03	1.02	0.32

The EEA and EOC values are presented in Table 2.

Table 8: Cost factors implemented in the model

	EEA cost factors	EOC cost factors
Capital (MJ/ €)	15.7	71.8
Labour (MJ/wh)	46.7	355.6

5. DISCUSSION

The main methodological difference among analytical approaches to sustainable development is in the way of definition and calculation of the cost factors. The cost factors reveal the relative importance of different production factors (capital, labour, energy, and material) and cost components (e.g. environmental costs). Energy theory of values, as well as any other single factor theory of value, has been criticized due to its weakness in the evaluation of other factors and environmental constraints (Glucina and Mayumi, 2010). In the present research work, a new assessment approach was presented in which the marginal *exergetic opportunity costs* (EOC) were assessed as equivalents for exergy cost factors.

Among the developed thermodynamic methods, the EEA approach has been successful in considering different cost factors based on the equivalent exergy destructions for availing the production factors. However, extended exergetic cost factors are based on a top-down analysis of the factor provisions by the society and environmental mitigation costs. Therefore, the cost factors may not consider the real exergetic gain or loss of accessing production factor according to its effectiveness in the sector under study. The EOC approach, which was developed and presented in the present research work, was based on the assumption that the opportunity cost of the production factors could be assessed based on the time-dependent sectoral production functions and the marginal rates of technical substitutions. Therefore, the cost factors revealed the real marginal exergetic costs of the production factors. On the other hand, the exergetic environmental damage costs have been preferred to the exergy costs of the neutralization of the emission streams as the latter could not consider the vulnerability of the environmental assets as the real external costs which the ecosystem is to pay for the regeneration of the damaged assets.

Although, in comparison to the EEA approach, the EOC suffered from the high data requirements and processing for calculation of the exergy cost factors, still the possibility of reflection of the real and sector-specific marginal effectiveness of the production factors in assessing the optimal production system gives the EOC approach the suitability to be considered as a complement to economic and other total energy accounting methods, especially the EEA.

6. REFERENCES

International Energy Agency, (2008). World Energy Outlook 2008.

Aghbashlo, M., M. Tabatabaei, S. S. Hosseini, B. B. Dashti and M. Mojarab Soufiyan (2018). "Performance assessment of a wind power plant using standard exergy and extended exergy accounting (EEA) approaches." Journal of Cleaner Production **171**(Supplement C): 127-136.

Beaudreau, B. C. and V. N. Pokrovskii (2010). "On the energy content of a money unit." Physica A: Statistical Mechanics and its Applications **389**(13): 2597-2606.

National Iranian Petrochemical Company, (2017). NPC Complexes of Petrochemical Industry. Tehran, Iran, NPC, Public Relations Dept.

Glucina, M. D. and K. Mayumi (2010). "Connecting thermodynamics and economics." Annals of the New York Academy of Sciences **1185**(1): 11-29.

Herendeen, R. A. (2004). Net Energy Analysis: Concepts and Methods A2 - Cleveland, Cutler J. Encyclopedia of Energy. New York, Elsevier**:** 283-289.

Iranian Statictical Center, (2018). Averaged annual income of urban and rural families in Iran. Tehran, Iran.

Khajehpour, H., Y. Saboohi and G. Tsatsaronis (2017). "Environmental responsibility accounting in complex energy systems." Journal of Cleaner Production **166**(Supplement C): 998-1009.

Marzelli, S., C. Moning, S. Daube, M. Offenberger, A. Gret-Regamey, S.-E. Rabe, T. Köllner, P. Poppenborg, B. Hansjürgens, I. Ring, C. Schröter-Schlaack, B. Schweppe-Kraft and S. Macke (2017). The value of nature for economy and society: an introduction, Natural Capital Germany – TEEB DE.

Nakata, T. (2004). "Energy-economic models and the environment." Progress in Energy and Combustion Science **30**(4): 417-475.

Odum, H. T. (2007). Environment, Power, and Society for the Twenty-First Century: The Hierarchy of Energy, Columbia University Press.

Rocco, M. V., E. Colombo and E. Sciubba (2014). "Advances in exergy analysis: a novel assessment of the Extended Exergy Accounting method." Applied Energy **113**: 1405-1420.

Romero, J. C. and P. Linares (2014). "Exergy as a global energy sustainability indicator. A review of the state of the art." Renewable and Sustainable Energy Reviews **33**(Supplement C): 427-442.

Sander de Bruyn, M. K., Agnieszka Markowska, Marc Davidson, Femke de Jong, Mart Bles, Maartje Sevenster (2010). shadow prices handbook : valuation and weighting of emissions and environmental impacts. Delft, Netherlands, CE Delft.

Statistical Center of Iran (2018). Abstract of the labour statistics in 2013. P. a. B. O. o. I. Statistical Center of Iran. Tehran, Iran.

Sciubba, E. (2006). Exergy Destruction as an ecological Indicator: merits and limits. ASME 2006 Roma, Italy.

Sciubba, E. (2011). "A revised calculation of the econometric factors α- and β for the Extended Exergy Accounting method." Ecological Modelling **222**(4): 1060-1066.

Sciubba, E. (2013). "Can an Environmental Indicator valid both at the local and global scales be derived on a thermodynamic basis?" Ecological Indicators **29**: 125-137.

Sciubba, E. and G. Wall (2007). "A brief Commented History of Exergy From the Beginnings to 2004." International Journal of Thermodynamics **10**(1).

Spakovsky, M. R. v. and C. A. Frangopoulos (2009). Analysis and Optimization of Energy Systems with Sustainability Considerations. Exergy, Energy System Analysis and Optimization. C. A. Frangopoulos, Encyclopedia of Life Support Systems (EOLSS). **III**.

Yi, H.-s., J. L. Hau, N. U. Ukidwe and B. R. Bakshi (2004). "Hierarchical thermodynamic metrics for evaluating the environmental sustainability of industrial processes." Environmental Progress **23**(4): 302-314.

#171: The effect of reference point selection on dynamics exergy analysis in buildings (Case study: Tehran)

Mohammad Javad FALLAHPOUR[1], Hossein KHAJEHPOUR[2*]

[1] Sharif University of Technology, Tehran, Iran, mohammadjavad.fallahpour@energy.sharif.edu
[2] Sharif University of Technology, Tehran, Iran, khajehpour@sharif.edu

Abstract: One of the necessities for exergy analysis is the correct choice of reference environment. The reference environment is very important in low-temperature exergy analyses because a slight temperature change can greatly affect the calculated values. In this research, a room in Tehran was simulated, and energy analysis performed. Following that, dynamic exergy analysis was performed with two approaches. In one approach, indoor air was defined as the reference environment, while in the other approach, outdoor air temperature was defined as the reference environment for exergy analysis. Conceptually, the outdoor air was an environment that was available for free and unlimited at any time. So, choosing outdoor air temperature as the reference environment for exergy analysis was more accurate, but it had more effort in exergy calculations. Exergy analysis was performed accordingly, and then the two approaches were compared. The comparison showed that in most of the modelling period, when the reference environment was chosen to be indoor, the calculated hourly exergy destruction was less than when the reference environment was outdoor. Results showed that, due to the simplification in choosing the indoor as the reference environment, the error of calculation of the hourly exergy destruction reached a maximum of 60%, high enough to avoid the simplification for dynamic exergy analysis. However, the results showed that calculations' annually-averaged error was limited to 1.5%, an acceptable level for state exergy analysis.

Keywords: energy; exergy; dynamic; building; reference point

1. INTRODUCTION

By the first law of thermodynamics, the quantity of the energy streams in the system can be calculated, but this law cannot provide inefficiencies reasons in a system. By quantifying the quality of the energy streams, the second law of thermodynamics completes energy analysis. It shows the actual thermodynamic value of an energy stream (exergy) and the fundamental thermodynamic inefficiencies reasons in a system (Bejan, 1996).

The building sector accounts for almost 30% of global energy consumption. This large share increases every year due to the increase in the world population and the growing trend towards urbanization and modernization. Most of these energy sources are used to provide comfort inside buildings. Since the difference between room temperature and ambient temperature is very low, the building energy demand is considered low-quality demand. When high-quality energy sources such as electricity or fossil fuels are used for low-quality demand, exergy destruction is much higher than low-quality energy sources such as solar collectors. So, using such high-quality resources is wildly inappropriate and undesirable for processes with low energy quality needs (Sayadi, 2016). In Sayadi's study, a building envelope of an office located in the E.ON Energy Research Center in Aachen, Germany, was used by a dynamic Simulink-based model to carry out a simulation for one year and to calculate the energy demands of the office. Additionally, an approach was developed to calculate dynamic exergy and exergoeconomic analysis.

In Sakulpipatsin (2008), the influence of potential definitions of the quality state of air to determine the exergy of air in buildings was studied. Three different contributions were considered associated with variations in temperature, pressure, and humidity of air inside and outside the building envelope. This study took the natural environment of the buildings as the reference point for air exergy calculations. At first, the study considered all three exergy contributions. It then analyzed the influence of the humidity of air in exergy calculations in order to check the possibility of considering the indoor air and the outdoor air as dry air for exergy analyses.

So far, the exergy conception has been applied to the engineered surroundings in several works (Dovjak, 2012; Kazanci, 2016; Pu, 2010; Sakulpipatsin, 2010; Shukuya, 2009; Wei, 2009) for analyzing buildings and their heating, ventilation, and air-conditioning (HVAC) systems.

In association with exergy analysis, choosing the reference state could be a principal issue. In line with Rosen (2004), once the state of a system was extraordinarily different from the reference state, variations in properties of the reference state do not influence the results of an exergy analysis considerably. On the contrary, once the properties of a system area unit are near the reference state, the results of an exergy analysis endure robust variations counting on the definition of the reference environment (Torio, 2009). This corresponds to the case of applying an exergy analysis to the heating and cooling systems in buildings.

In this study, the authors compared the effect of choosing reference environment on dynamic exergy analysis and also on the annual exergy analysis by simulation of a room in Tehran. First of all, energy analysis was performed, and then dynamic exergy analysis was performed with two approaches. In one approach, indoor air was defined as the reference environment, while in the other approach, outdoor air temperature was defined as the reference environment for exergy analysis.

2. CASE STUDY

For simulations in this study, a similar building and configuration of energy supply system studied in Sayadi (2016) (the E.ON Energy Research Center in the Campus Melaten of RWTH Aachen University of Germany) was assumed to be in Tehran's weather condition. In other words, this building's physical parameters were taken with Tehran's weather parameters for the simulation. Its state-of-the-art building technologies, multi-level usage, and complex HVAC equipment made it an ideal case study for various control and energy-related research (Sayadi, 2016). Detailed information about this building and its energy systems is given in Fütterer (2011 and 2014). Figure 1 shows the layout of the second floor of the E.ON ERC main building and the location of the case study room. Also, Table 1 shows the physical parameter (thermodynamic parameters, sections area of the building & mass flows) of the case study building.

Figure 9: Layout of the second floor of the E.ON ERC main building and location of our case study.

Table 9: physical parameter of the building

Thermal resistance (mK/W)		Thermal capacity (MJ/K)		Surface area (m2)		Other Parameters		
$R_{i,ew}$	13.7	C_{ew}	4.943	A_{win}	2.51	$\dot{m}_{vent}$	45	(kg/hr)
$R_{o,ew}$	6.9	C_{rf}	5.931	A_{ew}	8.60	cp_{air}	1005	(J/kg.K)
R_{ew}	303.7			A_{rf}	18.75	τ_{win}	0.80	
$R_{i,rf}$	7.5					α_{ew}	0.75	
$R_{o,rf}$	2.1					α_{rf}	0.75	
R_{rf}	97.9					ε_{ew}	0.75	
R_{win}	249.4					ε_{rf}	0.75	

3. ENERGY ANALYSIS

First of all, to calculate the energy demand of the room, energy analysis was carried out by the dynamic heat transfer model for thermal elements of the office, which was formulated in Sayadi (2016). This model was developed based on the lumped-capacitance method, which assumed that the walls had uniform temperatures across their volumes. This model was based on the equivalent capacitor and thermal equivalent resistance and considered the following items: (1) conduction through windows and walls, (2) convection due to air movement inside and outside the room, (3) ventilation, (4) solar radiation through windows, (5) absorption of solar radiation to exterior walls and ceiling, (6) internal heat gain, and (7) heat storage capacity of walls.

In this study, we assumed the room temperature was controlled to be constant (21°C in winter and 23°C in summer), and other assumptions were as the model developed by Sayadi (2016).

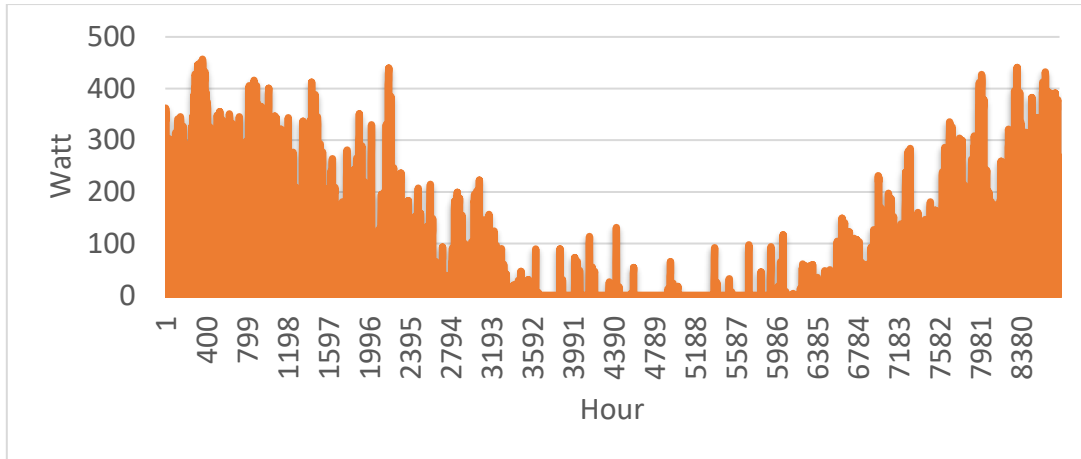Outputs of hourly energy analysis in one year are shown in Figures 2-5.

Figure 10: The thermal load of the room, calculated from energy modelling.
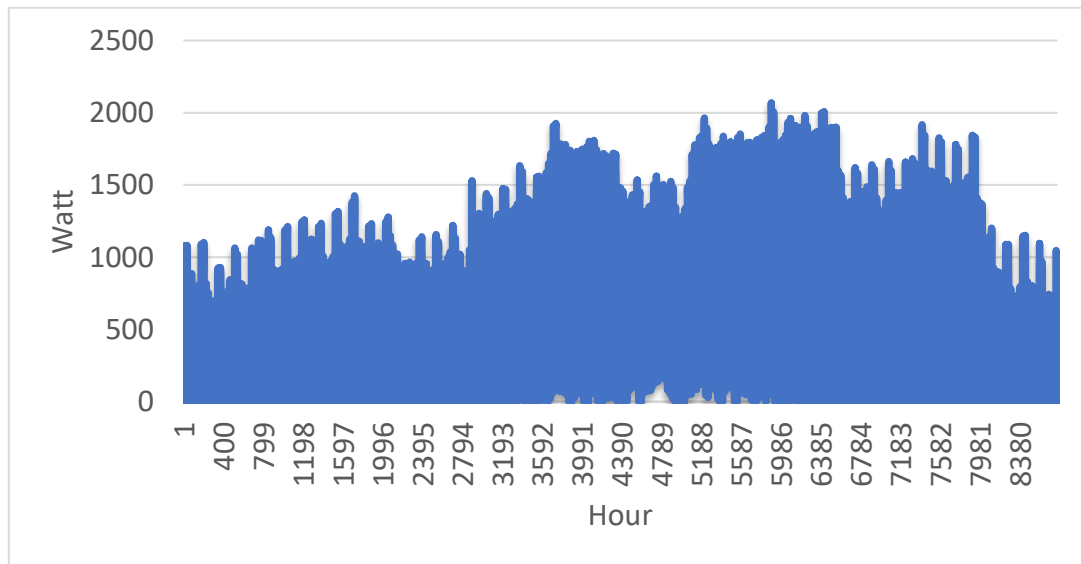

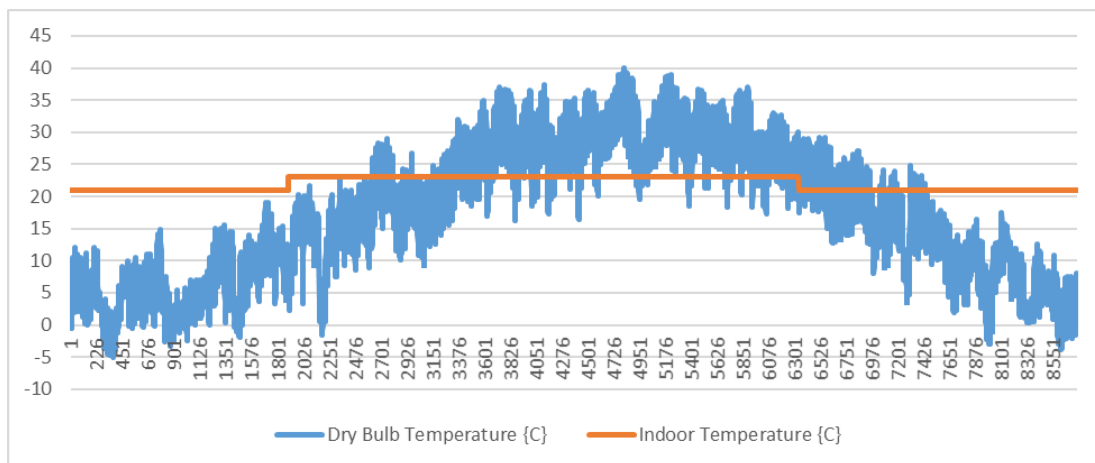*Figure 11: room cooling load, calculated from energy modelling.*

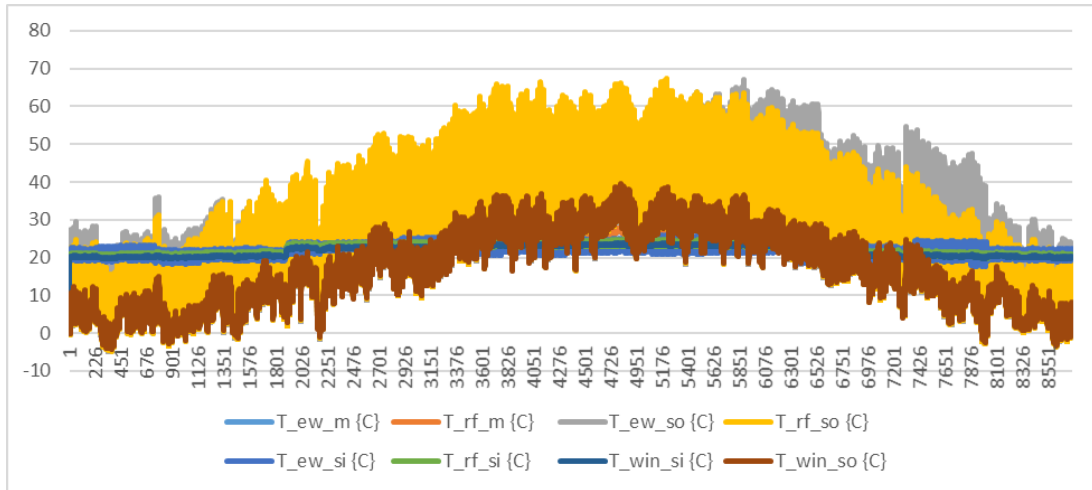*Figure 12: Outdoor and indoor air temperature.*

Figure 13: Temperature of different parts of the room.

4. EXERGY ANALYSIS

According to the calculations stated in the previous section, using the dynamic exergy analysis model developed by Sayadi, the exergy values of each unit can be calculated separately.

To perform the calculations, a computer program code was developed that calculated the exergy values on an hourly basis based on the values calculated in the energy analysis. This operation was performed twice with the assumption of two different reference environments. The amount of exergy destruction was fulfilled with the assumption of indoor temperature (Tr) as the reference point and once with the assumption of outdoor temperature (Ta) as the reference point. Hourly exergy destruction is shown in Figure 6.
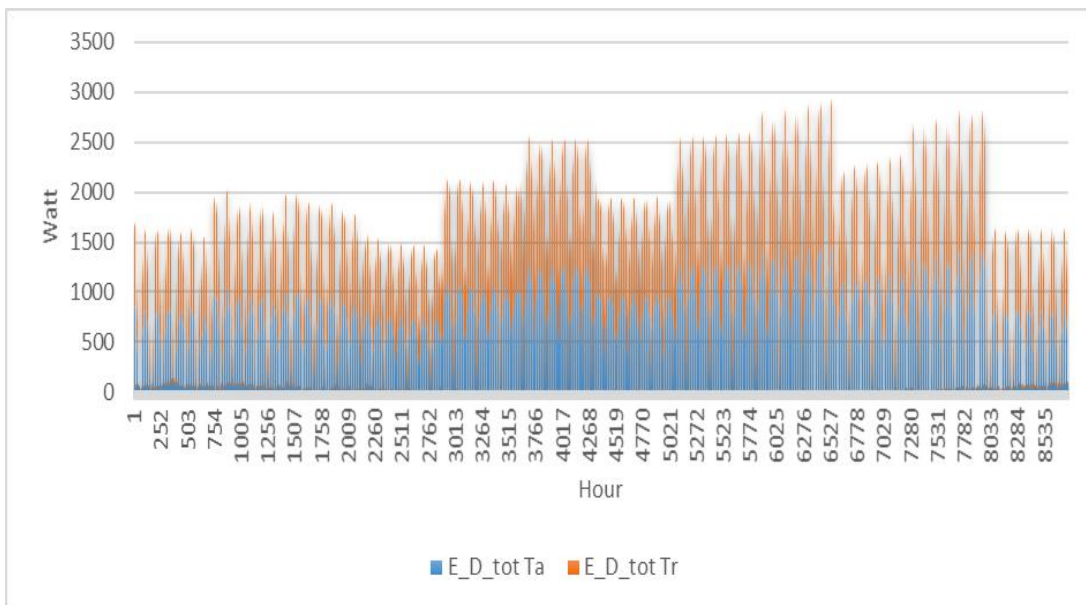

Figure 14: Hourly exergy destruction of the room in the assumption of two different reference points (ambient temperature (Ta) and room temperature (Tr)).

Conceptually, the outdoor environment is available for free and unlimited at any time, so the values calculated in the exergy analysis based on outdoor air temperature as a reference point were more accurate. Accordingly, the amount of error of hourly exergy destruction in the case where the indoor air temperature was selected as a reference compared to the point where the outdoor air temperature was chosen as the reference can be seen as a percentage in Figure 7 based on the outdoor environment being the correct reference environment.
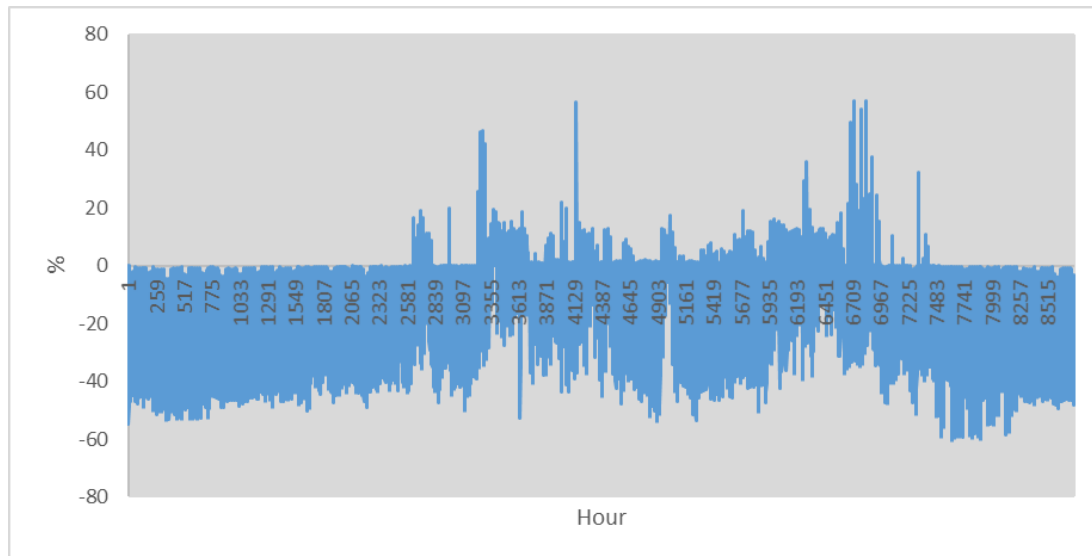

Figure 15: Hourly exergy destruction difference of room in percentage in the assumption of two different reference points based on the outdoor environment is the correct reference environment.

As shown in Figure 7, when the reference environment was assumed to be an indoor environment, the amount of hourly exergy destruction was underestimated compared to the actual value. It could be resolved that because in the calculation of the exergy destruction of the building cover, the inside temperature of the room was often much closer to the temperature of the building boundaries, such as walls and ceilings, which reduced the amount of exergy destruction estimated to be in the range of 0 to 60%.

Also, if we pay attention to Figure 4, which shows the temperature of indoor and outdoor air, it can be seen that at certain times of the year, including summer, the outside temperature was higher than the indoor temperature, which according to the argument caused overestimation in exergy destruction which is also evident in Figure 8.

Overall exergy destruction of the room in one year is the sum of hourly exergy destruction. Overall annual exergy destruction when the reference environment in the case study room was chosen to be indoor was equal to 3.511 MW and when the reference environment in the case study room was determined to be outdoor, it was equal to 3.569 MW. Based on the outdoor environment being the correct reference environment, the overall annual exergy destruction error due to the simplification in choosing the indoor as the reference environment was about 1.5% which was acceptable.

5. CONCLUSION

One of the necessities of exergy analysis is the correct choice of reference environment. The choice of reference environment is critical in low-temperature exergy analyses because the slightest temperature change can have an enormous effect on the calculated values.

For the sake of simplicity and reducing the calculation time, in low-temperature exergy analysis of buildings, the stable (controlled) indoor temperature may be selected as a reference point. Still, as found in this study, this causes significant errors in the hourly exergy calculations. But in the overall exergy analyses during a year, the error was not such that it could be concluded that simplification by choosing indoor environment as the reference point was not acceptable. So based on need, indoor condition may be selected as the reference point for static exergy analysis while for the dynamic exergy analysis which takes more details into account, the simplification may not be acceptable.

6. REFERENCES

Bejan A., Tsatsaronis G., Moran M., 1996. Thermal design and optimization. John Wiley & Sons, Inc.

Dovjak M., Shukuya M., Krainer A., 2012. Exergy Analysis of Conventional and Low Exergy Systems for Heating and Cooling of Near Zero Energy Buildings. Journal of Mechanical Engineering.

Fütterer J., Constantin A., 2014. Energy concept for the E. ON ERC main building. E.ON Energy Research Center Series 4(9).

Fütterer J., Constantin A., Müller D., 2011. An energy concept for multifunctional buildings with geothermal energy and photovoltaic. In: Proceedings of CISBAT International Scientific Conference; Lausanne, Switzerland.

Kazanci O.B., Shukuya M., Olesen B.W., 2016. Exergy performance of different space heating systems: A theoretical study. Building and Environment.

Pu J., Liu G., Feng X., 2010. Application of the cumulative exergy approach to different air conditioning systems. Energy and Buildings.

Rosen M.A., Dincer I., 2004. Effect of varying dead-state properties on energy and exergy analyses of thermal systems. International Journal of Thermal Sciences.

Sakulpipatsin P., Itard L.C.M., van der Kooi H.J., Boelman E.C., Luscuere P.G., 2010. An exergy application for analysis of buildings and HVAC systems. Energy and Buildings.

Sakulpipatsin P., Van Der Kooi H.J., Itard L.C.M., Boelman E.C., 2008. The influence of possible definitions of a reference environment to determine the exergy of air in buildings. International Journal of Exergy.

Sayadi S, Tsatsaronis G, Morosuk T., 2016. A new approach for applying dynamic exergy analysis and exergoeconomics to a building envelope. In: ECOS 2016: proceedings of the 29th international conference on efficiency, cost, optimization, simulation and environmental impact of energy systems; 2016 June 19-23. p. 1e17. Portoroz, Slovenia.

Shukuya M., 2009. Exergy concept and its application to the built environment. Building and Environment.

Torio H., Angelotti A., Schmidt D., 2009. Exergy analysis of renewable energy-based climatisation systems for buildings: A critical view. Energy and Buildings.

Wei Z., Zmeureanu R., 2009. Exergy analysis of variable air volume systems for an office building. Energy Conversion and Management.

#245: An investigation of transparent materials affecting the growing process of greenhouse plants in a tropical climate

Jitiporn WONGWATCHARAPAIBOON

Design, Business and Technology Management Program, Faculty of Architecture and Planning, Thammasat University, Thailand, jjpinx4391@gmail.com, jitiporn@ap.tu.ac.th

Abstract: Greenhouse farming is an alternative agricultural practice implemented in several climatic conditions with different in-use purposes. The general main purpose of greenhouse development tends to optimize energy consumption for climate control and plant productivity by the Internet of Things (IoTs) with few environmental drawbacks. However, in tropical climates, development is focused on pest protection and selective environmental factors to support plant growth by physical materials including net and transparent materials. This research aimed to investigate 1) how transparent materials affect greenhouse air temperature, light intensity, air humidity and plant growth and 2) how those transparent materials impact environments based on the Context, Input, Process and Product (CIPP) framework in tropical climate conditions. The research methodology mainly focused on systematic reviews of in-use transparent materials and their implementation affecting plant growth relying on the CIPP framework. Additionally, Life Cycle Assessment (LCA) and Material, Energy and Toxic (MET) matrix were research tools also used to analyze environmental impacts of those materials. Research findings are critically explained by the CIPP framework: the Context element points to existing weather conditions and greenhouse production and the productivity of Thai case studies, which can be scoped to the melon plant which is a significant proportion of Gross Domestic Product (GDP) in Thailand; Input relates to the transparent materials and other factors affecting the greenhouse ambience and plant growth. Process can be explained based on implementation of technological devices, constructional materials and operation, planting methods and technique. Lastly, Product is the outcome in terms of plant productivity and environmental impacts. Critical analysis of environmental impacts will mean making sure that farmers and developers are additionally aware about the importance of using sustainable materials in greenhouse farms in the future. Consequent contributions to this research will continue as knowledge is gained later in real time by monitoring environmental factors in the melon greenhouses of Thailand.

Keywords: transparent material; greenhouse experiment; greenhouse in tropical climate; LCA of greenhouse material; MET matrix

1. INTRODUCTION

The environment and climate of Thailand is suited to agricultural productivity, which is reflected in it being the main sector contributing to the Gross Domestic Product (GDP). Indeed, over the last 10-year period, agricultural GDP has increased from 68,261 to 168,442 million baths. The main agricultural products are ranked from rice, rubber, field crop and cultivation and perennial plants respectively (Office of Agricultural Economics, 2019). With these five types of agriculture, the cultivation farm covers around 303.65 square kilometres in the middle and north of Thailand. Some cultivation plants can achieve a high financial profit, especially salad vegetables, melons and tomatoes, if grown in a greenhouse.

Agricultural greenhouses in Thailand are employed mainly for pesticide purposes because of suitable existing climate conditions. The greenhouse structure needs to allow flowable ventilation whilst reducing heat transferring materials. The trend of the circular economy has been promoted and has become more important to Thailand's industries over the last the 5-year period. Consequently, the theory of upcycled material could be applied to constructional products, for example, constructional glass and other plastic and wooden wastes (Wongwatcharapaiboon, 2020). Focusing on transparent materials, glass and plastic are considered to be suitable for reuse and recycling thus reducing in-use energy consumption of production. Transparent plastic material provides suitable functions for agricultural greenhouse being lightweight and consuming less energy in the recycling process. However, the type and proportional mixture of plastic needs to be considered for optimizing the function of upcycled plastic.

Polyethylene terephthalate polymer (PET) and low-density polyethylene (LDPE) are generally used as transparent plastics, which are exemplified in terms of drinking water bottles, food containers, fabric fibre, soil and roof covering materials. However, there are some limitations to recycling polymers with non-polymixable types of plastic resulting in the failure of former polymers. For example, PET needs to be recycled alone and is suitable only for the blowing process, while LDPE can be mixed with other types for stronger bonds of polymer. They also have different temperatures of melting point, which results in a fragile structure of the mixture.

This research aimed to investigate how those different transparent covering materials can affect plant growth in terms of light wavelength, intensity, heat transfer and humidity levels. Also, if developed to meet a sustainable goal, materials can be assessed for environmentally friendly properties and performance.

2. LITERATURE REVIEWS

According to the research objectives, a plant's growth and the affected environment need to be reviewed. Also, light and heat transmittance are of concern as being main factors influencing plant growth. To understand the context of research, the theory of melon farming and light impact can be verified by reviews based in Thailand and tropical climate conditions.

2.1. Melon's growth phase

There are 7 phases of melon growth starting from 1) germination, 2) young seedling, 3) older vine, 4) flowering, 5) fruit bearing, 6) harvesting and drying, and 7) postharvest, optimising the 50 x 50 cm space of the planting process (Adeyeye, et al., 2017). Focusing on a plant's productivity, the first 1-5 phases or 'vegetative stages' were researched in terms of chemicals, height, number of nodes and leaves. Phases 4-6 or 'reproductive stages' were concerned with the quality of aroma and sweet taste by which is affected by the proportion of fertilized chemicals (Nascimento, Nascimento & Filho, 2020).

There are 3 types of melon that are popularly planted in central Thailand, which are Cucumis melo L. var reticulata (Persian melon, Japanese melon, Honeydew), Cucumis melo var. Cantalupensis (Cantaloupe), Citrullus lanatus (watermelon). In tropical climate conditions, melons prefer daytime temperatures of 25-30°C and nighttime temperature at 18-20°C, and these temperature conditions are mostly located in the north and central areas of Thailand. Another point to consider is soil preparation; melons are less tolerant to underground flooding. The plant bed should be set 30-40 cm higher than the ground and the pH of the soil should be 6.0-6.4. Watering can be 0.5-1.0 litres per day in the early part of the vegetative stage and up to 2-3 litres per day during the reproductive stage. However, this watering quantity can be adjusted depending on the season. Normally, melons have 3 types of production period, at approximately 60-65 days for honeydew, 70-75 days for the Japanese melon and 80-85 days for the Tibet melon, where the final week's production boosts the sweet taste quality to 14 brix degrees.

2.2. Light and solar radiation

Wavelengths of light are spectrums of electromagnetic radiation, which ranges from X-ray, ultra violet (UV), visible, to infrared (IR), microwave and radio respectively as shown in Figure 16 *Figure 16: The electromagnetic spectrum for wavelengths ranging*(Devrani, 2018; Kern & Ozsoy, 2018). To focus on plants, Photosynthetically Active Radiation (PAR) was proved to have a range of 400-700 nanometres (Levine, 1969), while human visible light ranges from UV light at 200-400 nanometre, and near infrared (NIR) at 700-2500 nanometres. Light wavelengths directly affect plant growth, especially red (648-760 nm), blue (426-492 nm), orange (589-627 nm) and white (380-370 nm) lights. Blue light impacts positively in the germination of seed, while suitable proportions of blue and red light can support the seedling process. Also, orange light affects growth of older vines and the flowering phase of the melon by increasing the photosynthesis effect on plants (Watjanatepin & Boonmee, 2017). There is no guarantee that wavelength can disturb the reproductive stage, however, solar radiation mostly affects the indoor environment of the greenhouse.
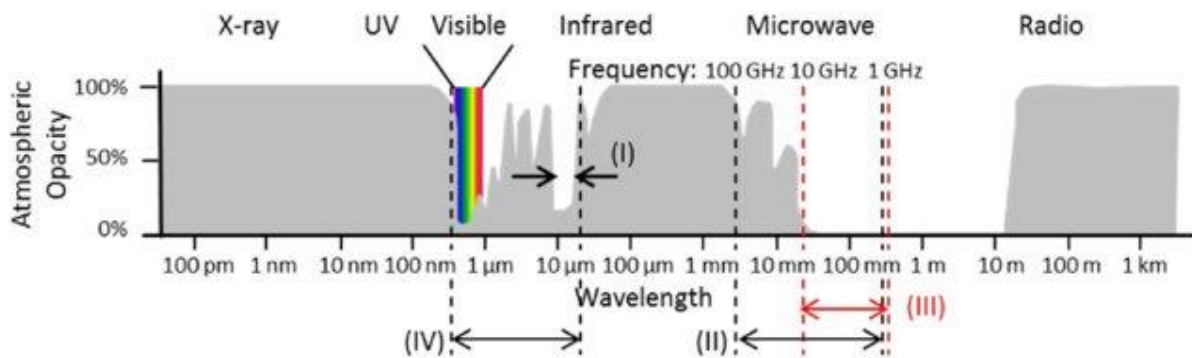

Figure 16: The electromagnetic spectrum for wavelengths ranging (Devrani, 2018; Kern & Ozsoy, 2018)

Solar radiation provides both visibility and thermal conditions for the human experience. In the case of greenhouse farming, heat transfer is mainly from roof and wall materials, which are normally in place for pesticide protection. From the different wavelengths of light, red light has the main impact for increasing heat in the environment, while UV light refraction via transparent material can bring about longer wavelengths and an increase in ambient indoor temperature called Solar Heat Gain (SHG). To explain the reflective, absorbing and transmitting process of transparent material, Shading Coefficient (SC) was used to calculate the material factor as a number between 0 and 1. Being quite similar to Solar Heat Gain Coefficient (SHGC), it is possible to convert the latter to the former using SHGC = SC x 0.87 (Leftheriotis & Yianoulis, 2012; Chan & Chow, 2014). From these radiation and material factors, solar radiation transfers to the inward room via a solid wall and a transparent window, where all heat transfer types were calculated by Overall Thermal Transfer Value (OTTV) as shown in Equation 6*: OTTV calculation.* (Chandra, et al., 2019). However, there are only transparent elements of the roof and curtain wall in the greenhouse structure, so heat transfer can be calculated by looking at window conductivity and transmittivity.

Equation 6: OTTV calculation.

$$OTTV = \alpha\big((1 - WWR) \cdot Uw\big) \cdot TDeq\big) + (WWR \cdot Uf \cdot \Delta T) + (WWR \cdot SC \cdot SF)$$

Where:

- OTTV = Overall Thermal Transfer Value (W/m^2)
- WWR = Window to Wall Ratio
- α = Wall absorptivity (%)
- Uw = Wall heat transfer coefficient (W/m^{2}K)
- TDeq = Temperature different equivalent (K)
- Uf = Window heat transfer coefficient (W/m^{2}K)
- ΔT = Different temperature between indoor and outdoor condition (K)
- SC = Shading Coefficient
- SF = Solar Factor (%)

As a result of heat transfer, the greenhouse ambient temperature can be changed to affect plant growth. Red light directly affects the germination and seedling phase, while it can increase ambient temperature. The ratios of red

and blue light need to be balanced for optimizing the growth rate of plants. Also, heat transfer activities should be calculated for indoor temperature monitoring.

3. METHODOLOGY

According to the research question and objectives, the methodology was conducted based on the Context, Input, Process and Product (CIPP) framework: greenhouse samples were selected from 57 farms in 6 provinces of central Thailand (Likitswat, 2021). The type of farming plant, which was selected based on GDP and greenhouse character, pointed to the melon greenhouses of central Thailand.

3.1. Research framework

Based on the CIPP model (Azari & Kim, 2015; Hasan, Yasin & Yunus, 2015; Poth, et al., 2020; AbdiShahshahani, et al., 2015; Hakan & Seval, 2011), the research framework relied on a rigid structure with different criteria in each stage of research as shown in Figure 17. The criteria content can be scoped into 4 main stages: the first of which can be described through the greenhouse context and environment of location. The input stage focused on selective transparency materials compared to the base material of clear glass. The process focussed on light and heat transfer based on calculations and the review of material's laboratory test, whilst the last stage of the product grasps important points of the plant growth's effect and environmental impact in terms of waste management, Life Cycle Assessment (LCA) and the Material, Environment and Toxic (MET) matrix. Also, the optimization of planting in greenhouses can be assessed in this stage too.
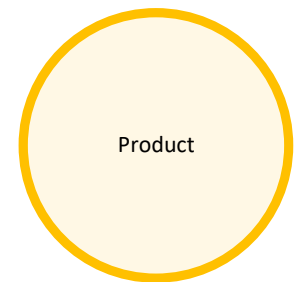

Product

Figure 17: Research framework and criteria based on CIPP model

Each stage of the framework can be conducted by 1) structural review and observation, 2) qualitative interview and 3) material laboratory test. In this research series, reviews and observation were applied in the greenhouse and environmental context and material input, while the interviewing process was used for the farming process, installation and investment. A review of laboratory data and calculation of light and heat transfer can be compared to the average real-time monitoring in the process stage. For the product stage, light and heat transmittance results can affect melon growth and materials can be assessed for the environmental impact in the LiDS Wheel of the LCA and MET matrix. It should be noted that a full experiment of transparent material will be followed up in future work.

Since all elements of the greenhouse were transparent, the Overall Thermal Transfer Value (OTTV) could ignore opaque thermal transfer in the greenhouse calculation shown in Equation 7. Also, Solar Factor (SF) in tropical climate should be considered as Solar Heat Gain Coefficient (SHGC) x Effective Solar Radiation (ESR), which have different results depending on local sun direction (Department of Alternative Energy Development and Efficiency, Ministry of Energy, Thailand. 2010). This equation was applied for thermal transfer based on greenhouse material.

Equation 7: OTTV Calculation for greenhouse
$$OTTV_{GH} = (WWR \cdot Uf \cdot \Delta T) + (WWR \cdot SC \cdot SHGC \cdot ESR)$$

Where:

- OTTV$_{GH}$ = Overall Thermal Transfer Value (W/m^2) for greenhouse
- WWR = Window to Wall Ratio
- Uf = Window heat transfer coefficient (W/m^{2}K)
- ΔT = Different temperature between indoor and outdoor condition (K)
- SC = Shading Coefficient
- SHGC = Solar Heat Gain Coefficient
- ESR = Effective Solar Radiation (W/m^2)

3.2. Research tools for material assessment

According to the last stage of CIPP, product of transparent material can be assessed in 2 areas: plant growth impact and environmental impact of materials. For the impact on the plant's growth, both observations and literature review can be used, while environmental impacts separate into Life Cycle Assessment (LCA) and Material, Energy and Toxic (MET) matrix.

Life Cycle Assessment (LCA) is a systematic calculation approach of production and consumption by analysing input and output of product system as shown in Figure 18. Calculating factors can be material balance and energy consumption. If considering the input stage, there are some concerns of materials, energy, transportation. Also, for the output stage, factorial criteria points to product/service, emission to environment, by-product and disposal activities (Brezet & Hemel 1997; Huulgaard & Remmen, 2012; Wever & Vogtlander, 2014).
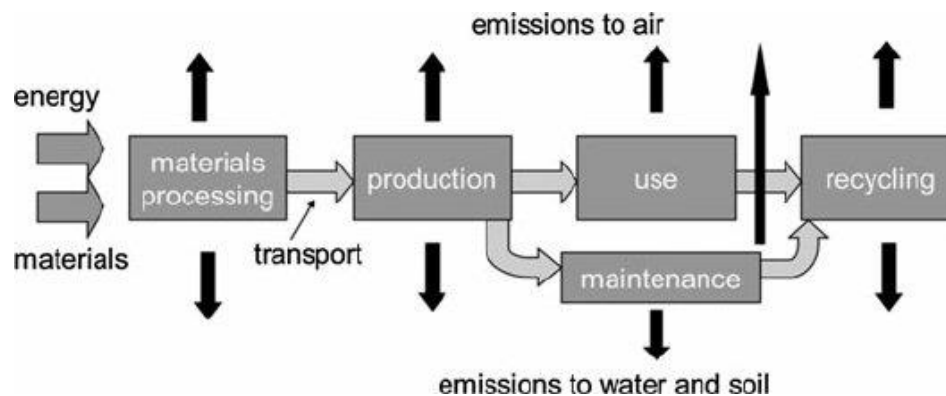

Figure 18: The basic calculation system of LCA (Brezet & Hemel, 1997)

Consequently, LCA calculation results should be demonstrated in the LiDS wheel, which is an EcoDesign strategy to evaluate all stages of production or service (Brezet & Hemel, 1997; Huulgaard & Remmen, 2012; Wever & Vogtlander, 2014). There are 8 stages of product life cycle including 0) new concept development, 1) selection of low-impact materials, 2) reduction of materials, 3) optimisation of production technology, 4) optimisation of distribution systems, 5) reduction of impact during use, 6) optimisation of product life and 7) optimisation of end-of-life system. All activities and criteria of each life cycle stage aim to optimize in-use resources and reduce waste emissions. Another research tool is the Material, Energy and Toxic (MET) matrix (Brezet & Hemel, 1997), which focusses on 3 stages: production, use and disposal based on 3 criteria: material cycle, energy consumption and toxic emissions. This tool can clearly confirm environmental impacts of product usability (Watkins, 2014).

4. RESULTS AND DISCUSSIONS

The climate conditions of central Thailand were identified according to the selected location of Spatra's melon farm. Also, the agricultural context and greenhouse structure with transparent materials, which link directly to the melon farm, can be clarified in this section. Moreover, sampling groups of transparent material inputs were divided into 2 types of plastic and compared to a base case of clear glass of 3mm thickness (Department of Alternative Energy Development and Efficiency, Ministry of Energy, Thailand, 2010). Then the ability to conduct heat and light were compared and analysed based on melon growth impacts. Lastly, the environmental assessment were carried out to prove products of transparent plastic material were suitable for saving energy and managing local waste.

4.1. Greenhouse context

Melon greenhouses in central Thailand were selected by structural dimensions, productivity and land investment size. To scope down the sample group, 57 greenhouse farms were categorized into 3 sizes of 1) small size containing 700-1,600 sq. m., 2) medium size covering 2,000-6,400 sq. m. and 3) large farm covering 8,000-32,000 sq. m. (Likitswat, 2021). A suitable sampling size for a small experiment and insight interview was one small melon farm in Keangkhoi district, Saraburi. There were 4-5 standard greenhouses for rotating crops of melon, quad and grape, with structural dimensions of 6 metre width, 20 metre length and 5 metre height as shown in Figure 4. Transparent materials in Thai greenhouse can be separated into covering roof plastic and curtain wall of plastic net. Transparent roof covering material is generally low-density polyethylene (LDPE) plastic, while nylon net of curtain wall is usually formed of polyethylene terephthalate polymer (PET) or Polyamide (PA) plastic.
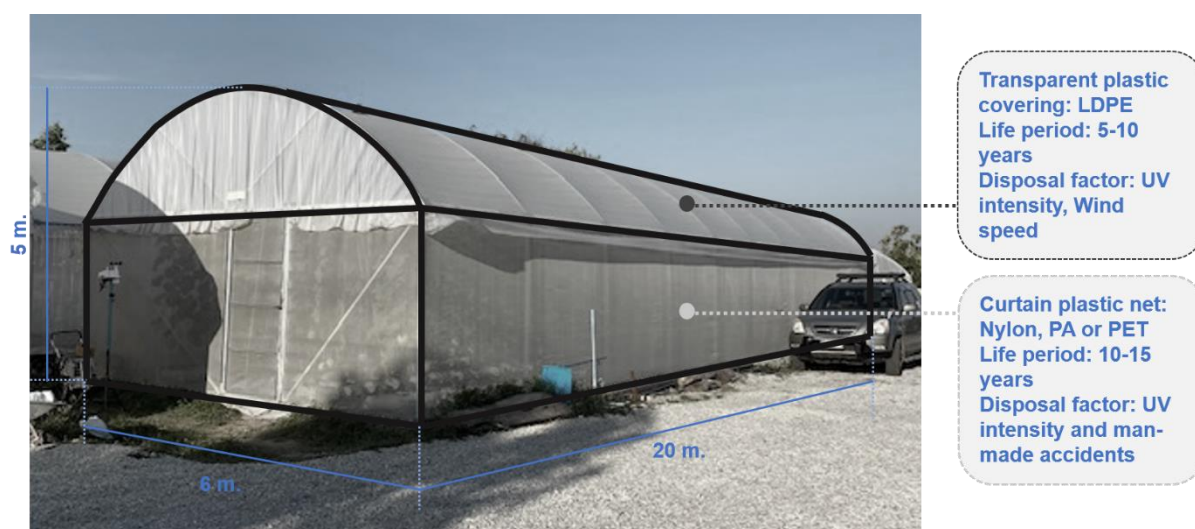

Transparent plastic covering: LDPE
Life period: 5-10 years
Disposal factor: UV intensity, Wind speed

Curtain plastic net: Nylon, PA or PET
Life period: 10-15 years
Disposal factor: UV intensity and man-made accidents

Figure 4: Sampling melon greenhouse, Supatra Melon Farm, Saraburi

According to the main structure of the greenhouse, with planting based on 50 x 50 metres (Adeyeye, et al., 2017), it is possible for each greenhouse to hold 480 trees without allowing for circulation. For 30% of indoor circulation and guest visitor transition, the productivity of a small greenhouse is approximately 300-340 melons per house per planting round. The general process and activities are based on a growing period of melon production, which takes around 3.5-4 months for the preparing and planting processes until harvest. One-month unoccupancy is an important period of greenhouse preparation before planting a new crop of melon. Japanese melon requires 70-75 days for in-house production.

In the environmental context of greenhouses in central Thailand, there were some basic factual data of temperature, light wavelength, light intensity, sun radiation and air humidity. As a result, the review process of statistic data was conducted and compared to a real monitoring experiment carried out in December 2022 as shown in Table 10. Report data identified online statistic data compared to average results during the 3-day real-time monitoring in Keangkhoi District, Saraburi. Full data collection was used for reporting the existing context.

Table 10: Environmental context of Supatra melon farm, Saraburi

Environmental factors	Statistic weather data	Real-time monitor	
		Outdoor	Indoor
Temperature	26 ºC [1]	28.85 ºC	30.25 ºC
Air relative humidity	57% [1]	46 %	47 %
Wind speed	4.17 m/s [2]	0.74 m/s	0 m/s
Solar radiation	Cloud cover 20% [2]	n/a	n/a
Light wavelength	UV index = 7 [2]	Visible white	Visible white
Light intensity	n/a	41,716 Lux	13,502 Lux

Source: [1] Climate-Data.org. (2021).
[2] 2014-2022 Des Clics Nomades SAS. (2022).

The indoor relative humidity and air temperature were both higher than the outdoor conditions, which resulted from watering activities to indoor plants during the monitoring period. There were approximately 60-65 days of melon production during the real-time monitoring session and the reproductive stage of the melon still needed 2-3 litres of water per day.

4.2. Material input and comparison process

This section reports results of material input with property information and comparison processes of various transparent materials and OTTV calculating results within the same place. There were 3 types of transparent materials in the greenhouse structure, particularly low-density polyethylene (LDPE) and polyethylene terephthalate polymer (PET). LDPE film is normally tolerant of the tropical climate and provides 88-90% transmittance of PAR light (Emekli, Büyüktaş, & Başçetinçelik, 2016). Clear glass was used for the base case and comparison purposes, and a review of shading coefficient (SC) and other properties can be used for light transmittance calculation as shown in Table 11. The main information about clear glass was from the handbook for building energy respondent (Department of Alternative Energy Development and Efficiency, Ministry of Energy, Thailand, 2010). There are still more properties of transparent material needing to be clarified for suitable use, especially light diffusion, anti-drip effect, anti-virus, anti-dust effect and thermal effect sun selector.

Table 11: Greenhouse transparent materials' property

Materials Property	Clear glass Base case [1]	Transparent materials		
		LDPE film	PET film	PA (Nylon) net
Thickness	6 mm.	80-220 µm.	200 µm.	n/a
Number of nets per square cm.	n/a	n/a		16, 20, 32, 40 nets
Weight	High density and heavy weight	1.8 mg.	3.2 mg.	n/a
Life cycle years	More than 50 years	2 years	3-5 years	3-5 years
UV tolerance	No chemical action	UV-A, B and C affecting life period		
U value (W/m^{2}K)	5.8	1.8	5.6	1.8
SC	0.96	0.20-0.60	0.85	0.20-0.60
SHGC	0.73-0.81	0.35	0.70	0.35
Thermal conductivity (W/mK)	0.779	0.35	0.24	0.35
Visible light reflectance (%)	7	<25	<25	<25
Visible light transmission (%)	88	37 for blue light, 57 for red light	87 for both blue and red lights	n/a
Solar energy reflection (%)	7			
Solar energy transmission (%)	80	<40	<40	<40
Solar energy absorption (%)	13			
RTTV (W/m^2)	145.96	29.46	122.94	
OTTV (W/m^2)				16.62

Source: [1] Department of Alternative Energy Development and Efficiency, Ministry of Energy, Thailand, 2010.

Light transmittance and heat transfer can be calculated and compared together in Table 11 in terms of OTTV and RTTV values. It can be seen that the base case of glass and PET materials held a high value of RTTV meaning that this type of material allowed for more heat transference to the indoor ambience. LPDE and PA materials allowed less transference of heat to indoor conditions. These results relied on U values of each material and WWR conditions for OTTV calculations. It was also noted that the roof's transparent material had a higher impact to the indoor space than the wall material.

It should be noted that the LDPE material, even though this material provided less transmission compared to other material in visible light transmission, the allowance of longer wavelength transmission can create higher temperatures inside the building. So, it is important to use this roof material while promoting high convection from the wall material to maintain a comfortable climate for the plant.

4.3. Product

As well as considering heat transfer, it is also important to focus on light transmission, which directly affects different stages of melon growth as shown in

Table *12*. The main impacts of material can be separated into 2 types particular in heat and light impacts. Heat transfer and indoor temperature should be controlled for a reasonable climate and to avoid too high a peak in the day or not to exceed 30°C. This peak temperature can be relieved by curtain net wall with PA fibre material. Another focus of plant impact is the light wavelength with the red and blue proportions important for the germination and seedling process. LDPE can provide a suitable ratio of 4R:1B light proportion with high transmission of red light and lower transmission of blue light. This result is based on condition of LDPE transferring directly light from natural radiation.

Table 12: Impact of transparent material on melon growth

Materials Criteria	Clear glass Base case [1]	Transparent materials		
		LDPE film	PET film	PA (Nylon) net
Strength	Suitable for reused and hygiene process	Higher stretching bond and flexible for installation	Crystal clear for transparent material	Strong bond for stretching
Weakness	High embodied energy including recycling process	Various mixture of plastic cannot be recycled for many times.	Preference of purely material for recycling process.	Mixture may lead to failure of bond structure with less UV tolerance. Not proved yet
Wavelength of light transmission	Crystal clear visible light wavelength	Light transmission relies on wavelength and higher transmission for red light	Nearest to clear glass and high transmittance in both red and blue light	
Impact to melon	Visible white light affects all photosynthesis process	Red light is suitable for germination and seedling process	Red and blue mixed proportion is suitable for germination and seedling process	

This section emphasised the environmental impacts of plastic materials too, for the life cycle period, disposal management and agricultural waste can lead to sustainable problems at the end of use. Agricultural waste somehow links to air pollution depending on the burning activities of farmers. To avoid a linear economy of melon farms, this part points to related problems and suggestions for sustainable management. From tools mentioning in the Methodology, transparent materials are divided into 2 assessment results, especially LiDS Wheel from Life Cycle Assessment (LCA) and Material, Energy and Toxic (MET) Matrix.
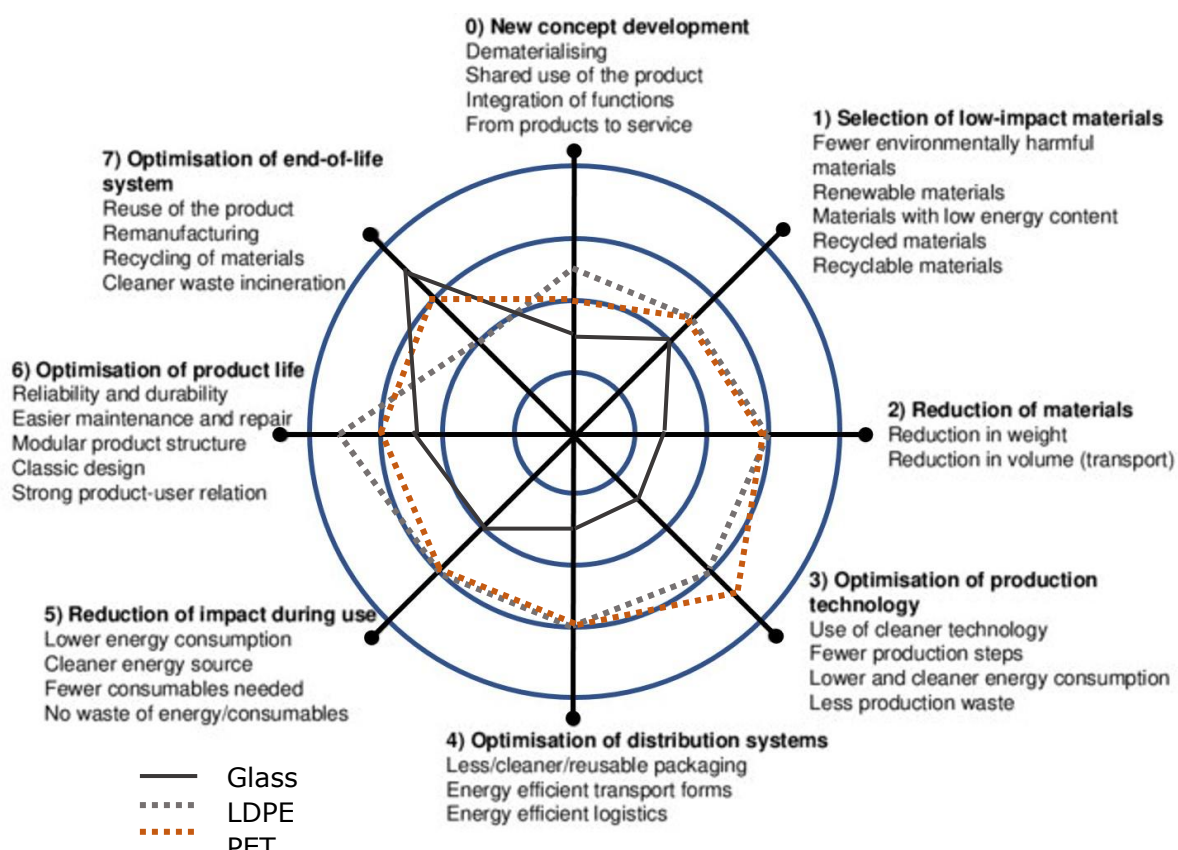

Figure 5: The eco-design strategy (LiDS) wheel of transparent materials

From Life Cycle Assessment (LCA) and LiDs wheel strategy (Brezet & Hemel 1997; Huulgaard & Remmen, 2012), Figure 5 demonstrates the evaluation of three transparent materials generally used in Thailand greenhouses including glass (comparison base case), LDPE and PET. All in-use materials were not new innovations for greenhouses, but LDPE and PET technology and the manufacturing processes are more suitable for innovating production. Glass is well known to be recycled with high energy of transformation, while plastics can still be harmful to wildlife and the environment. For example, plastic burning from agricultural processes emit high concentrations of Volatile Organic Compounds (VOCs) and Particulate Matter (PM2.5) to the air environment.

For the purpose of weight and volume reduction, all plastic types were from petroleum and some manufacturing technology can now optimise in-use material for production processes especially the blowing method of PET recycling processes. For the optimisation of the life cycle, LDPE has a shorter life span than PET, however, LDPE can be blended with other types of plastic to form new property of materials and circulate to new functional product. Also, at the end-of-life stage, glass is normally reused as long as the ceramic bond remains, while recycling glass can have a lower energy consumption in case of Seoul Upcycling Plaza's suggestion.

According to all assessment of environmental impacts, 2 types of polymer materials had quite similar results with the same field of manufacturing process and similar structure of polymer bond. Consequently, in the next step of MET matrix assessment, there will be only 2 types of materials of glass and plastic comparison in Table 13. After assessing MET matrix, there were several concerns of natural resources and the amount of energy consumption for glass material. Plastic consumes fewer natural resources by the mostly recycling manufacturing process. In the use and disposal stages, transportation was the main activity to consume energy. Then, if all material waste can be recycled, it would be possible to carry out recycling activities on-site to save time and energy consumption.

On the toxic emissions point, both glass and plastic production normally release air pollution to the manufacturing environment by burning a mixture of chemicals, for example, NaOH, Volatile Organic Compounds (VOCs) and colour mixture. At the end-of-life process, small pieces of plastic glitter have been found by UK researchers.

Table 13: Qualitative MET matrix for transparent material of greenhouse (Brezet & Hemel, 1997)

		Material cycle	Energy consumption	Toxic emissions
Production	Glass	Depletion of raw materials (natural resources of sand) Recycling of production wastes (same or clear colour only)	High energy consumption for material productions Medium energy consumption for adjusting product	NaOH during production Carbon emission during production
	Plastic	Various types of depletion and renewable materials Recycling	Energy consumption of blowing process	VOCs during production UV reductant
Use	Glass	Consumption of wooden lag and metal container	Energy during transportation	Coating colour and lead
	Plastic	Mixture aggregate of plastic	Transportation	Small piece of glitter
Disposal	Glass	Reused as far as stable structure Recycled by manufacturing	Transportation	NaOH for recycling process Colour mixture
	Plastic	Reused in limited times Recycled by new technological process	Incinerator energy	VOCs and carbon emission Small piece of glitter in sea life Colour mixture

To discuss findings and results with a clearer view of environmental impacts from greenhouse transparent materials, researchers and farmers need to be kept up to date with assessed information and be made aware of in-use materials. Also, for further suitable design product, energy consumption for transforming waste based on innovative knowhow and knowledge is possibly less than general manufacturing process. Another obstacle to promoting the circular economy in Thailand is the mind-set of existing business owners, who are reluctant to change, preferring to do familiar activities to guarantee their own profit.

5. CONCLUSIONS AND RECOMMENDATIONS

Agricultural production is the main activity contributing to the GDP of Thailand, with farmers now creating more value for farming products by using greenhouses for pesticide protection purpose. Melon is one crop for adding product value to the greenhouse investment. From the observation of melon farms in central Thailand, one small farm in Keangkhoi district was selected to be monitored for existing environmental factors. This research aimed to investigate the benefits of transparent materials compared to the base case of clear glass. The environmental impacts were observed using the CIPP model strategy. Starting with the context of a melon farm and general greenhouse, the selected structure was 6 m. wide, 20 m. long and 5 m. high covered by transparent LDPE plastic. A curtain wall of PA net was using, being suitable for natural air flow and promoting convection for controlling thermal comfort conditions for plant. The study relates heat transfer results in terms of OTTV and RTTV, noticing that most heat transfer was from the transparent roof. LDPE materials were suitable as the roof covering as it promoted red and blue lights for germination and seedling process of melon growth, whereas the property of PET was quite similar to clear glass and allowed red and blue light transmission equally.

In the LiDs wheel assessment, the plastics gained higher marks in various dimensions of innovative technology for production and recycling processes, reduction of raw material except with a limitation of the reused concept. In the

MET matrix, there were more focussed points for high energy consumption of production, transportation and recycling processes. Toxins along the life cycle process were NaOH released from glass material, VOCs emission from plastic material and mixture and coating colours in both glass and plastic conditions.

Following on from this research, there are some suggestions for further research. In the case of transparent plastic, it is possible to complete material property for directory and for further calculations of heat transfer in Thailand. Also, the detail of wavelength impact and real time monitoring can be demonstrated in the next research article series.

6. ACKNOWLEDGEMENT

7. REFERENCES

2014-2022 Des Clics Nomades SAS. (2022). Weather in Saraburi in december 2021. Retrieved 10 January, 2022 https://www.whereandwhen.net/when/southeast-asia/thailand/saraburi/december/

AbdiShahshahani, M., Ehsanpour, S., Yamani, N., Kohan, S., & Hamidfar, B. (2015). The Evaluation of Reproductive Health PhD Program in Iran: A CIPP Model Approach. *Procedia - Social and Behavioral Sciences*, 197, 88-97. doi:https://doi.org/10.1016/j.sbspro.2015.07.059

Adeyeye, A. S., Akanbi, W. B., Olalekan, K. K., Lamidi, W. A., Othman, H. J., & Ishaku, M. A. (2017). The Growth and Yield Performance of Sweet Melon as Affected by Planning Spacing in North East Nigeria. *International Journal of Research in Agriculture and Forestry, 4*(8), 17-21.

Azari, R., & Kim, Y-W. (2015). Integration Evaluation Framework for Integrated Design Teams of Green Buildings: Development and Validation. *Journal of Management in Engineering*. doi: 10.1061/(ASCE)ME.1943-5479.0000416.

Brezet, H., & Hemel, C. G. v. (1997). *Ecodesign : a promising approach to sustainable production and consumption*.

Chan, A. L. S., & Chow, T. T. (2014). Calculation of overall thermal transfer value (OTTV) for commercial buildings constructed with naturally ventilated double skin façade in subtropical Hong Kong. *Energy and Buildings, 69*, 14-21. doi: https://doi.org/10.1016/j.enbuild.2013.09.049

Chandra, B., Trisno, R., Gunanta, S., Widayati, N., Susetyarto, M., & Lianto, F. (2019). The Application of Passive Design Chart on the Analysis of Natural Ventilation of Low and Middle Income Flats Case Study Sky View Apartment and 'Rusunawa' Manis Jaya, Tangerang. *Journal of Physics Conference Series, 1179*, 1-9. doi: 10.1088/1742-6596/1179/1/012105

Climate-Data.org. (2021). Saraburi province's temperature and weather forecast in December 2021. Retrieved 10 January, 2022 https://en.climate-data.org/asia/thailand/saraburi-province/saraburi-4205/t/december-12/#weather-forecast

Department of Alternative Energy Development and Efficiency, Ministry of Energy, Thailand. (2010). *Handbook for Building Energy Respondent (Translated from Thais)*. Bangkok: Ministry of Energy Retrieved from http://www2.dede.go.th/bhrd/old/Download/file_handbook/Pre_Build/Build_13.pdf.

Devrani, T. (2018). *Development of automated mapping methods for birch woodlands in the Norðurhraun lava field, Hekla.*

Emekli, N. Y., Büyüktaş, K., & Başçetinçelik, A. (2016). Changes of the light transmittance of the LDPE films during the service life for greenhouse application. *Journal of Building Engineering, 6*, 126-132. doi: https://doi.org/10.1016/j.jobe.2016.02.013

Hakan, K., & Seval, F. (2011). CIPP evaluation model scale: development, reliability and validity. *Procedia - Social and Behavioral Sciences*, 15, 592-599. doi:https://doi.org/10.1016/j.sbspro.2011.03.146

Hasan, A., Yasin, S. N. T. M., & Yunus, M. F. M. (2015). A Conceptual Framework for Mechatronics Curriculum Using Stufflebeam CIPP Evaluation Model. *Procedia - Social and Behavioral Sciences,* 195, 844-849. doi:https://doi.org/10.1016/j.sbspro.2015.06.324

Huulgaard, R., & Remmen, A. (2012). *Eco-design Requirements for Televisions: How Ambitious is the Implementation of the Energy-using Product Directive?*

Kern, S., & Ozsoy, B. (2018). Remote Sensing.

Leftheriotis, G., & Yianoulis, P. (2012). 3.10 - Glazings and Coatings. In A. Sayigh (Ed.), *Comprehensive Renewable Energy* (pp. 313-355). Oxford: Elsevier.

Levine, R. P. (1969). The mechanism of photosynthesis. *Sci Am, 221*(6), 58-70. doi: 10.1038/scientificamerican1269-58

Likitswat, F. (2021). Urban Farming: Opportunities and Challenges of Developing Greenhouse Business in Bangkok Metropolitan Region. *Future Cities and Environment*, 7(1), 8. DOI: http://doi.org/10.5334/fce.118

Nascimento, C., Nascimento, C., & Filho, A. (2020). N:K RATIO FOR PHENOLOGICAL GROWTH STAGES OF NET MELON CULTIVATED IN NFT HYDROPONIC SYSTEM1. *Revista Caatinga, 33*, 108-115. doi: 10.1590/1983-21252020v33n112rc

Office of Agricultural Economics (2019). Agricultural Economic Report 2019 and Outlook for 2020.

Poth, C. N., Searle, M., Aquilina, A. M., Ge, J., & Elder, A. (2020). Assessing competency-based evaluation course impacts: A mixed methods case study. *Evaluation and Program Planning*, 79, 101789. doi:https://doi.org/10.1016/j.evalprogplan.2020.101789

Watjanatepin N, Boonmee C. Which Color of Light from the Light Emitting Diodes is Optimal for Plant Cultivation? *Journal of Science and Technology*. 2017;25(1):158-76.

Watkins, M. (2014). *An investigation into effective methods for teaching social sustainability within product design in British and Irish Universities.*

Wever, R., & Vogtlander, J. (2014). Design for the Value of Sustainability.

Wongwatcharapaiboon, J. (2020). *Circular Economy: Case Studies in Upcycled Industrial Waste Glass in Thailand.* Paper presented at the Conference: 6th International Conference "Green ASIA and Sustainability Forum: BCG in Action; the New Sustainable Growth Engine (Bio-Circular-Green Economy)", Bangkok, Thailand.

#255: Energy-based heuristic system optimizer for off-grid photovoltaic system design: HINTEDIS

Humberto RODRÍGUEZ[1], Octavio ECHEVERRÍA[2], Javier AYÚ PRADO[3], Gabriel GRIMALDO[4]

[1] Universidad Tecnológica de Panamá, Campus Víctor Levi, humberto.rodriguez@utp.ac.pa
[2] Universidad Tecnológica de Panamá, Campus Víctor Levi, octavio.echeverria@utp.ac.pa
[3] Universidad Tecnológica de Panamá, Campus Víctor Levi, javier.ayuprado@utp.ac.pa
[4] Universidad Tecnológica de Panamá, Campus Víctor Levi, gabriel.grimaldo@utp.ac.pa

Abstract: HINTEDIS is a decision support tool that aims to provide a methodology to optimize photovoltaic (PV) systems at the project design phase to establish the most suitable solution for a high energy performance toward Zero Energy Building (ZEB). In addition, via a user-friendly web interface, this tool assists architects and engineers with a fast, easy and precise way to gain insight into the photovoltaic potential of their projects. It is presented via a user-friendly web interface. The web stack is written with popular open-source frameworks, React and Django, for the front-end and back-end respectively. In this study, the authors implemented a deterministic, numerical, energy-based economic system optimizer that minimized the cost of off-grid PV systems and guaranteed an arbitrarily small Loss of Load Probability (LLP). This optimizer extended typical numerical approaches by adding a set of heuristics that considerably reduced the search space and, in return, improved its computational efficiency. HINTEDIS also implements NREL's EnergyPlus as a heat-transfer simulation engine for load estimation. Provided with enough information about a project, the numerical energy model estimates power consumption using historical local data. By estimating the power generation of each PV module with weather data and an improved solar radiation estimation model for Panama, the program could assess whether the system was supplying the load, charging the batteries, dropping the excess energy, or losing the load. This was simulated hourly for a period of a year and the data gathered was used to calculate the LLP, which accepted or rejected candidates. The list of viable candidates was then evaluated by the economic model. Each candidate was ranked by the total estimated capital cost of the system and the first one was selected and presented to the user. The economic model referenced a database of typical costs for modules, inverters, batteries, installation, and other expenses. Given a user-selected configuration, the model scaled each cost by the system size, added all expenses, and returned the expected cost for the candidate system.

1. INTRODUCTION

In recent years, as the installation and maintenance costs have reduced significantly, off-grid or stand-alone photovoltaic (PV) systems have gained more attention in Panama. PV systems are considered to be one of the most important renewable energy sources for the sustainability of residences and commercial buildings. However, the reliability and total costs highly depend on the optimal arrangement and selection of their subsystems, as well as the orientation of the house or building (Khatib, 2013). With this premise, the authors set a goal of developing a computational tool and methodology to assist designers, engineers and architects in decision-making for the design and integration of photovoltaic and thermal hybrid systems during the Initial stage of a project. Applying such a tool was expected to influence the building's design outcomes, particularly the Zero Energy Building (ZEB) and the Building Life Cycle Cost (BLCC). We have named this tool with the acronym "HINTEDIS", which stands for "Smart Tool for the Design of Energy Sustainable Buildings"

For stand-alone photovoltaic system, a design is usually considered optimal if it minimizes both the probability of losing load (LLP) and the overall capital cost of the system. Proposed approaches are regularly categorized into intuitive, numerical, and analytical (Sidrach, 1998; Gordon, 1987; Egido,1992; Khatib, 2016). The intuitive methods use simplified equations that eliminate many important variables causing an inevitable loss in accuracy and are usually compensated by over-designing with a safety factor (Sharma, 1995). Since intuitive methods fail to incorporate variations in load and solar radiation, they have an undetermined LLP and cannot guarantee security for an off-grid system. Although impractical and imprecise, the intuitive methods are fast to execute and often used as a first approximation for more sophisticated approaches.

More precise and popular approaches are the numerical methods. These simulate a PV system throughout a period with time-steps dependent on available data (Klein, 1987; Sidrach, 1999). It is common to have time-steps as coarse as a day or as fine as an hour or less. Approaches that consider uncertainty in data are categorized as stochastic and approaches that do not are categorized as deterministic. While stochastic approaches are considered more accurate, deterministic approaches are still more popular because of the unavailability of stochastic data. The computations of the numerical methods are extensive as they require an evaluation of all mathematical models of the system per time step per proposed design. Depending on the complexity of the mathematical models, the total computation time can become unwieldy.

Analytical methods implement mathematical equations that can describe and size a PV system as a function of its reliability (LLP). The result is a method of very high simplicity and accuracy. However, the equations generated by these methods are highly specific for a given area and the coefficients required are not simple to find (Bartoli, 1984; Sidrach, 1998; Gordon, 1987).

2. HINTEDIS IMPLEMENTATION

In the schematic of Figure 1, the authors show the different modules implemented in HINTEDIS, and the flow of information between them. All started with the user's architectural design of the house/building and the specification of materials, which were imported to the program from Autodesk REVIT. In addition, the user specified which parts of the house would have air conditioning units. Employing the user interface, the designer also introduced the simulation parameters, such as the building location, number of family members, their approximated income, and the type of solar panels, batteries, solar heater, and load controllers to be used. Afterward, the inputs from the different databases were loaded to simulate the incident global radiation, the house/building heat transfer dynamics, and to estimate energy consumption and the requirements for the design of the solar thermal system. These databases include a list of PV panels and solar thermal systems available in Panama and their technical specifications; energy consumption statistical information depending on the city area and income; solar and meteorological data sets from NASA's website.

As a result, the heat transfer dynamical simulation of the house, using Energy Plus, allowed the estimation of the electrical power consumption due to cooling and added to the estimated consumption calculated due to appliances. Also, using the resulting simulation of the global radiation that reached the PV panels and ambient temperature, the daily electrical power generation was obtained.
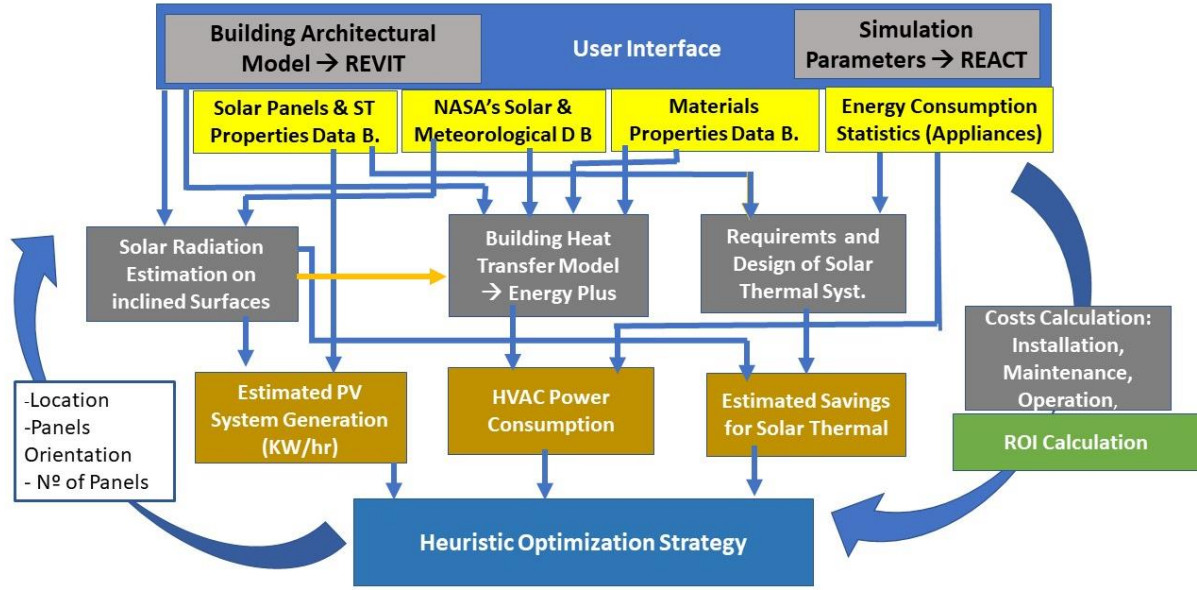
Figure 19: Schematic of HINTEDIS components.

2.1. PV cell and energy storage system models

The PV cell model implemented for HINTEDIS was the one-diode model, which consisted of a current source in parallel with a diode, a series resistance , R_s, and a parallel resistance, R_p, whose value was so high that usually it was assumed to be infinity (Tamrakar, 2015). For this type of model, most of the necessary parameters were known and readily available on a database for the user. The user only needed to select the PV module from the list provided by HINTEDIS. The one-diode model was an accurate and well-known model that took into consideration the cell-temperature which was relevant given the elevated year-round temperatures in Panama. The equation for the one-diode model is as follows:

$$I = I_{ph} - I_0 \left(e^{\frac{q(V+IR_S)}{nkT}-1} \right) - \frac{V+IR_S}{R_p} ,$$

(1)

Where:

- I_{ph}= Photocurrent (A)
- I_0= Diode saturation current (A)
- q = Electron charge, 1.6021x10^{-19} C
- k = Boltzmann constant, 1.3865x10^{-23} J/K
- T = Operating Temperature (Kelvin)
- R_s = Series Resistance (Ω)
- R_p = Parallel Resistance (Ω)

In this equation, the photocurrent (I_{ph}) is a temperature-dependent parameter that can be calculated as:

$$I_{ph} = \left(I_{ph}\right)_{T_1} + K_o(T - T_1),$$

(2)

where, T_1 is a reference standard temperature and $\left(I_{ph}\right)_{T_1}$ and K_o are calculated as:

$$\left(I_{ph}\right)_{T_1} = (I_{sc})_{T_1} \frac{H}{H_{nom}},$$

(3)

$$K_o = \frac{(I_{sc})_{T_2}-(I_{sc})_{T_1}}{T_2-T_1},$$

(4)

112

Where:

- I_{sc} = short circuit current of the PV cell,
- T_2 = second reference temperature,
- H = actual global solar radiation
- H_{nom} = global solar radiation at the reference test.

For the energy storage subsystem, HINTEDIS used a simple lead-acid battery model (Copetti, 1993). A discharging state was set whenever the load surpassed the generation, and the state-of-charge (SOC) was above its minimum value. The difference between load and generation was supplied by the battery system and its efficiency was assumed to be the inverter's nominal efficiency. A charge condition was set whenever the generation surpassed the load, and the SOC was below its maximum allowed value. The difference between generation and load was supplied to the battery system. The electrical to chemical energy conversion is defined by:

$$\eta_c = 1 - \exp\left[\frac{a}{\frac{I}{I_{10}}+b}(SOC - 1)\right] \quad \text{and} \tag{5}$$

$$SOC = (1 - \frac{Q}{C}) \quad , \tag{6}$$

Where:

- η_c = Charging efficiency.
- I = Instantaneous current (A)
- I_{10} = 10h current manufacturer rating (A)
- a, b = Recharge constants
- SOC = State of charge
- Q = Charge in the battery (Ah)
- C = Battery capacity (Ah)

The values a and b were obtained experimentally. For HINTEDIS we used a = 20.73 and b = 0.55 as suggested by Copetti et al. (Copetti, 1993).

2.2. Solar radiation estimation for Panama

The development of a computational model for renewable energy estimation over the coordinates of a specific construction project was crucial for HINTEDIS, especially the analysis of the available solar energy source upon the earth's surface for cities in Panama. The solar energy estimation would in turn be used to estimate photovoltaic (PV) panel's conversion and the stand-alone PV system generation.

The input solar energy is distributed in three main solar radiation components: 3% of the input is reflected back to space, 7% continues downward as a diffuse component and 70% of the initial input becomes direct solar energy until it reaches the earth surface in a sunny day (Lorenzo, 1994). In turn, the solar radiation that gets through to the surface is a summation of the direct and diffused solar energy during solar hours, called global radiation.

A common approach to estimating the total global radiation on a horizontal surface at sea level, H_g, is to use linear regression models, such as the Angström-Page model (Equation 1), which expresses the relative solar radiation (H_g/H_0) as a function of the sunshine ratio (S/S_0):

$$\frac{H_g}{H_0} = a + b\left(\frac{S}{S_0}\right) \tag{7}$$

Where H_0 is the monthly average of daily extraterrestrial solar radiation on a horizontal surface, which can be determined by the following equations:

$$H_o = \frac{24}{\pi} Isc \left(1 + 0.033 \cos\frac{360N}{365}\right)\left(\frac{\pi(\omega_s)}{180}\sin\phi\sin\delta + \cos\phi\cos\delta\sin(\omega_s)\right) \tag{8}$$

$$S_0 = \frac{2}{15}\omega_s \tag{9}$$

$$\delta = 23.34 \sin \frac{360}{365}(284 + N) \tag{10}$$

$$\omega_s = \cos^{-1}(-\tan\delta\tan\phi) \tag{11}$$

Where:

- H_o = Extraterrestrial solar radiation (kWh/m^2-dia)
- H_g = Global solar radiation on a horizontal surface (kWh/m^2-dia)
- S_0 = Theoretical day length
- S = Measured or predicted sunshine hours
- N = day number of the year (1-365)
- δ = Declination angle
- ϕ = Latitude
- ω_s = hourly angle
- Isc = solar constant, 1.367 kW/m^2

Of all these parameters, only the sunshine duration (S) needs to be measured or predicted to estimate the future global solar radiation, since the extraterrestrial radiation (H_0) and the theoretical day length (S_0), are calculated from Equations 2 and 3, respectively.

For this work, an artificial neural network (ANN) model was trained by using the sunshine ratio, (S/S_0), the extraterrestrial radiation, (H_0), and the latitude as inputs and the relative solar radiation, $\left(H_g/H_0\right)$, as output of the ANN. A feedforward multi-layer perceptron neural network (FFMLP) with one hidden layer was implemented. The ANN was trained with data from NASA's satellite meteorological dataset using 132 different locations in Panama and showed a significant improvement in the global solar radiation estimation. The results were evaluated by comparing the correlation coefficient against values estimated using the Angström-Page model, with the same meteorological dataset for linear regression. The prediction using Angström-Page, with samples from the test location in Panama, showed a correlation coefficient of R=0.912 (R^2=0.832), while our model reached a correlation coefficient of R=0.939 (R^2=0.883).

In addition to estimating the global solar radiation on horizontal surfaces, it was also necessary to estimate the incident solar radiation on the PV panels considering their actual angle of orientation. For this calculation the Liu Jordan Model (Liu, 1960) was used. In this model, the diffuse, $H_{T,d}$, and direct, $H_{T,b}$ components of solar radiation on the inclined surface are given by Equations 12 and 13, respectively. The diffuse component was obtained assuming that the diffuse was totally isotropic and the circumsolar and horizon were almost zero,

$$H_{T,d} = H_d \frac{1+\cos\beta}{2} \tag{12}$$

$$H_{T,b} = H_b \frac{\cos(\phi-\beta)\cos\delta\sin\omega_s + \omega_s\sin(\phi-\beta)\sin\delta}{\cos\phi\cos\delta\sin\omega_s + \omega_s\sin\phi\sin\delta} \tag{13}$$

Where:

- β = inclination angle of the PV panel
- H_d and H_b = diffuse and direct components of the global solar radiation on a horizontal surface.

3. THE OPTIMIZER

Before explaining the heuristic optimization strategy used in HINTEDIS, the loss of load probability (LLP) needs to be addressed. LLP is a measure that gauges how likely a load's demand can exceed a system's capacity during a period of time, typically a year, "losing the load" and causing a failure. For off-grid systems, this value is of utmost importance; a high LLP can result in systems reverting to possibly costly auxiliary power (Sidrach, 1998; Gordon, 1987; Klein, 1987). For systems without auxiliary power but with energy storage, e.g. battery back-up, this measure is even more important as a high LLP will correlate with more frequent and prolonged blackouts. This value is often approximated as the time the load surpassed generation over a period (Equation 14).

$$LLP = \frac{\sum_{t=1}^{T} \varphi t}{T} \tag{14}$$

$$\varphi t = \begin{cases} 0, & P_{load}(t) \leq P_{hes}(t) \\ 1, & P_{load}(t) > P_{hes}(t) \end{cases}$$

Where:

- $P_{load}(t)$ = Energy system load at time t (W)
- $P_{hes}(t)$ = Generating resources capacity (W)

The LLP tends to zero for PV systems with a large generation and energy storage capacity. Trying to minimize the LLP without accounting for this can lead to designs with unnecessarily large energy storage, as Equation 14 does not penalize this. To circumvent this, the authors optimized for an arbitrarily small range of LLP (Equation 15).

$$LLP_l < LLP < LLP_u \qquad\qquad (15)$$

Where:

- LLP_l = Loss of Load probability lower bound
- LLP_u = Loss of Load probability upper bound

Please note that Equation 15 allowed for some undesirable Loss of Load. To counter this, the energy storage capacity was continuously increased by 5% until LLP was 0. This effectively set an overdesigned bound to 5%.

The Optimizer: The numerical system optimizer leveraged the computational simplicity of the PV model with a fast and precise initial guess, and a set of heuristics that dramatically reduced the search space and time. An overview of the method is shown in Figure 2.
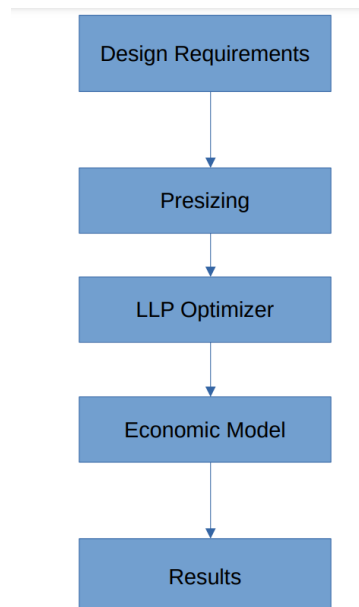

Figure 2: Overview of the Optimization Method.

The first step was known as pre-sizing where relevant information was collected and generated an approximate initial guess for the system optimizer. The relevant information was solar radiation, temperature, and the estimated hourly load. The precision of the initial guess was unimportant as the optimizer could generally compensate for a bad initial guess. An intuitive method like Sidrach (1998) or Sharma (1992) was implemented for this initial

approximation. Equation 16 defines an approximate number of PV modules required to satisfy the load, N_{PV}, and Equation 17 defines C_{batt} as the approximate size of the battery in watt-hour.

$$N_{pv} = \frac{E_l}{\eta_s \eta_{inv} * PSH * P_{mod}} S_f \tag{17}$$

$$C_{batt} = \frac{E_l * D_{Autonomous}}{DOD * \eta_b} \quad , \tag{18}$$

Where:

- E_l = Daily energy consumption (Wh)
- η_s = Solar module efficiency
- η_{inv} = Inverter efficiency
- PSH = Peak Sun Hours (h)
- P_{mod} = Nominal PV module power (W)
- S_f = Safety factor
- $D_{Autonomous}$ = Days of autonomy
- DOD = Depth of discharge
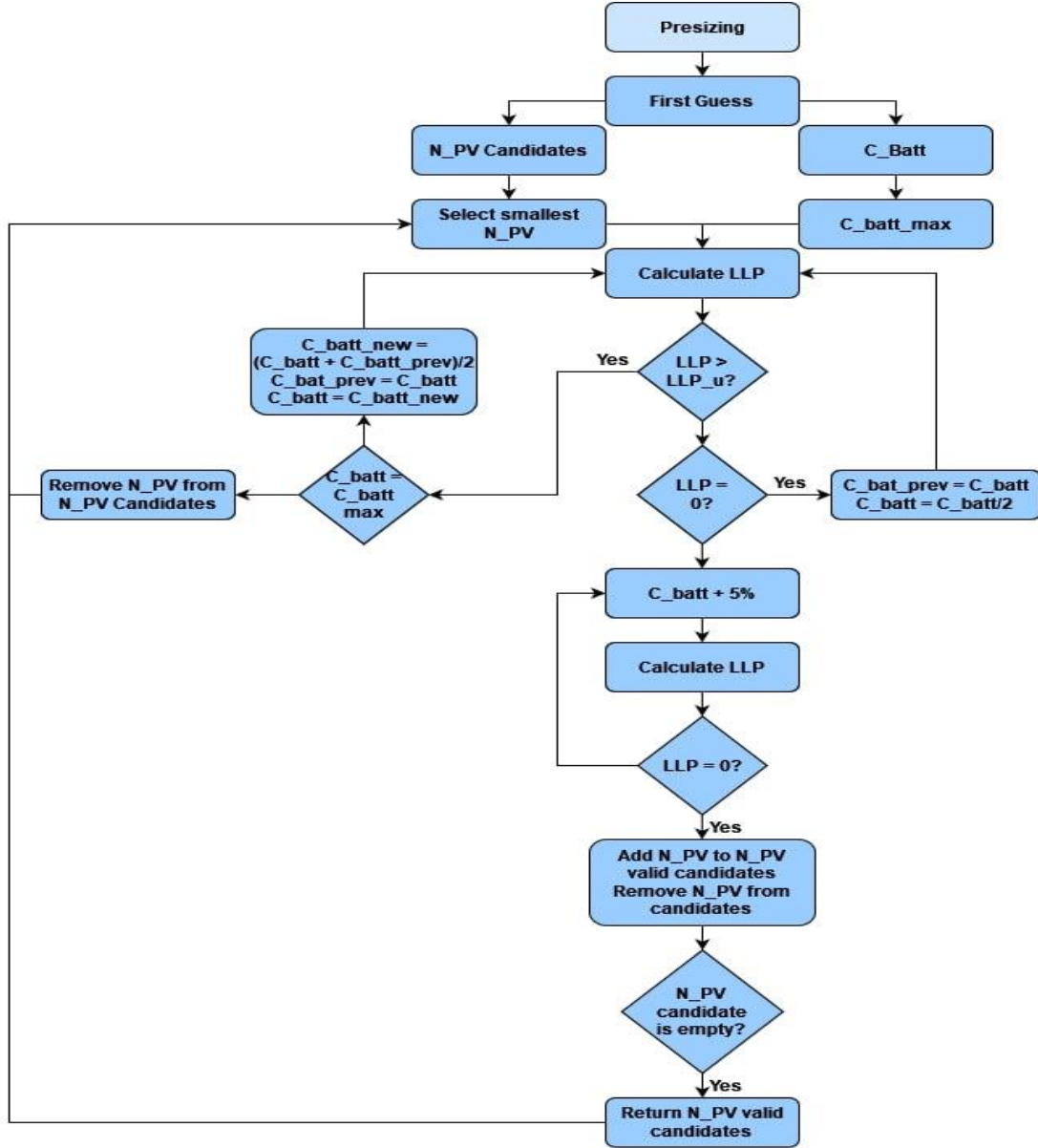- η_b = Battery efficiency

Figure 3: Detailed steps of the Optimization algorithm.

The set of candidates to be tested was created by implementing a set of heuristics that considerably reduced the search space. Using the guess of the intuitive method, a range of N_{PV} was defined by Equation 19 and a maximum battery capacity was calculated by Equation 20. The LLP range was defined by Equation 21 where LLP_u was the upper bound of the LLP and LLP_l was the lower bound.

$$N_{PV} * X < N_{PV} < N_{PV} * Y \tag{19}$$

$$C_{batt} < C_{battmax} \tag{20}$$

$$LLP_l < LLP < LLP_u \tag{21}$$

From the N_{PV} range, a set of discrete values was selected. X and Y must be carefully chosen because they would determine the granularity of the search space. The smallest N_{PV} was paired with the maximum value of C_{batt} ($C_{battmax}$) and their LLP was calculated. If this value was above 0, this candidate was rejected instantly, and the optimizer continued with the next smallest N_{PV}. If LLP was 0, C_{batt} was halved and LLP was evaluated again. If LLP was below LLP_u but above 0, C_{batt} was repeatedly increased by 5% until LLP became 0. The candidate was accepted and the next smallest N_{PV} evaluated with $C_{batt} = C_{battmax}$. This method was done until all N_{PV} candidates

were evaluated. This returned a list of valid candidates (a pair of N_{PV} and C_{batt}). Figure 3 shows in detail the steps of the optimization process.

The last step was to evaluate all valid candidates with the Economic Model. This step considered the capital cost of every component, their maintenance, cost of replacement and cost of energy and took into consideration inflation and interest. This was done for every valid candidate and the candidate with the least capital cost was considered to be the optimal off-grid photovoltaic system.

4. DISCUSSION

The following block diagram (Figure 4) shows the subprograms that constitute HINTEDIS. The frontend and backend were developed in "React" and "Django" deployment environments, respectively. The frontend reads the model files (which the user creates from REVIT) and the meteorological variables database (temperature, humidity, solar radiation). In addition, the frontend is where the user registers and the project is created and configured with the addition of the location and orientation of the house, as well as the number of family members and their income, among other data.

The open software ENERGY PLUS was used to implement the simulation of the heat transfer processes from the atmosphere to the house, considering the climate statistics. This software is widely used and proven by the research community, and it was used in conjunction with OpenStudio, an open-source interface that allows simulations to be configured based on the information provided by the user and the material files exported from the model.

On the other hand, the optimization program was developed entirely in Python and included the power generation models for the solar panels, the operating models of the inverter and the batteries, as well as the optimizer and the econometric module.

In order to validate if the final configuration of solar panels was optimal or sub optimal, the LLP was evaluated, the final total costs and the return of Investment of other configurations close to the selected one (with one less or one more panel and with a battery set of larger or smaller capacity). it was verified that the optimizer's outcome represented the best compromise between LLP and costs. In addition, the heuristic strategy was 4 times faster than the intuitive optimizer previously tested, which was based on a progressive partition of the search space.
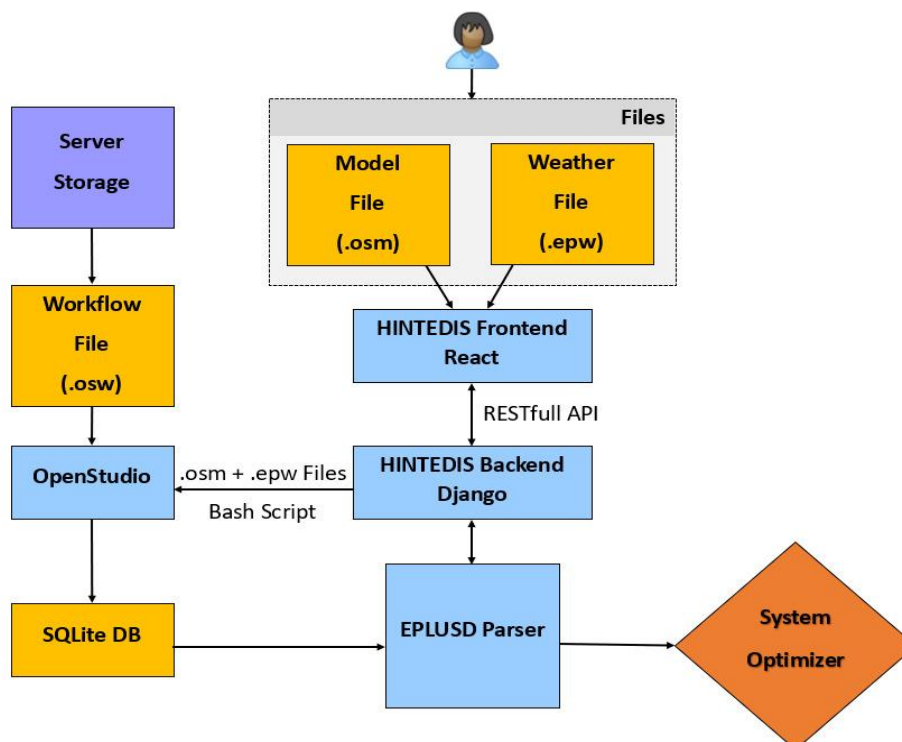

Figure 4: HINTEDIS subprograms: frontend and backend.

5. CONCLUSIONS AND FUTURE WORK

A very useful tool was developed which could help architects and engineers to test how different parameters of a house' initial design could affect the optimal number of solar panels, the total cost and the return of investment. Among these parameters, the orientation of the house, the construction materials, the PV panels specifications and its inclination and position are crucial. In addition, the solar radiation estimation models were tailored for the Panama latitude and meteorological characteristics using an ANN, so that the PV system power generation could be accurately predicted during the project's life. Finally, even though the proposed heuristic optimization strategy performance has not been compared with other AI-based methodologies, it has already shown promising results, since the execution time of the algorithm was significantly faster than other common intuitive methods and the generated configurations represented a good compromise between the optimization criteria (LLP and Costs).

With regard to the future lines of research, the authors are interested, firstly, on the improvement of the optimization method by incorporating the uncertainty of the variables that affect the LLP estimation. In addition, it would be very useful to have an algorithm to find the best solution for the placement and orientation of the PV panels on the building's envelope and for this purpose Genetic Algorithms are being considered.

6. ACKNOWLEDGEMENT

7. REFERENCES

Bartoli, B., et al. 1984. The design of photovoltaic plants: An optimization procedure. *Applied Energy*, 18(1), 37-47.

Bucciarelli, L., 1984. Estimating loss-of-power probabilities of stand-alone photovoltaic solar energy systems. *Solar Energy*, 32(2), 205-209.

Copetti, J., et al.1993. A general battery model for PV system simulation. *Progress in Photovoltaics: research and applications* 1.4, 283-292.

Egido, M., Lorenzo, E., 1992. The sizing of a standalone PV-system: A review and a proposed new method. *Solar Energy Materials and Solar Cells*, 26 (1-2), 51-69.

García, M.C., Balenzategui, J.L., 2004. Estimation of photovoltaic module yearly temperature and performance based on Nominal Operation Cell Temperature calculations. *Renewable Energy*, 29(12), 1997-2010.

Gordon, J.M., 1987. Optimal sizing of stand-alone photovoltaic solar power systems. *Solar Cells*, 20(4), 295-313.

Hansen A.D., et al. 2001. Models for a stand-alone PV system. Roskilde: Risø National Laboratory.

Khatib, T., Ibrahim, I., Mohamed, A., 2016. A review on sizing methodologies of photovoltaic array and storage battery in a standalone photovoltaic system. *Energy Conversion and Management*, 120, 430-448.

Khatib, T., Ibrahim, I., Mohamed, A., 2017. Optimal sizing of a standalone photovoltaic system for remote housing electrification using numerical algorithm and improved system models. *Energy*, 126, 392-403.

Khatib, T., Mohamed, A., Sopian, K., 2013. A review of photovoltaic systems size optimization techniques. *Renewable and Sustainable Energy Reviews*, 22, 454-465.

Klein, S.A, Beckman, W.A, 1987. Loss-of-load probabilities for stand-alone photovoltaic systems. *Solar Energy*, 39(6), 499-512.

Liu, B.Y.H., Jordan, R.C., 1960. The interrelationship and characteristic distribution of direct, diffuse and total solar radiation. *Solar Energy*, 4(3), 1-9.

Lorenzo, E., 1994. Solar electricity: engineering of photovoltaic systems. Earthscan/James & James.

Nishioka, K., et al. 2003. Field-test analysis of PV system output characteristics focusing on module temperature. *Solar Energy Materials and Solar Cells*, 75 (3-4), 665-671.

Sharma, V., Colangelo A., Spagna G., 1995. Photovoltaic technology: basic concepts, sizing of a stand alone photovoltaic system for domestic applications and preliminary economic analysis. *Energy Conversion Management*, 36(3),161–74.

Sidrach-de-Cardona, M., Lopez, L., 1998. A simple model for sizing stand alone photovoltaic systems. Solar Energy Materials and Solar Cells, 55(3),199–214.

Sidrach-de-Cardona, M., López, L., 1999. A general multivariate qualitative model for sizing stand-alone photovoltaic systems. *Solar Energy Materials and Solar Cells*, 59(3), 185-197.

Tamrakar, V., Gupta, S.C., Sawle, Y., 2015. Single-Diode Pv Cell Modeling And Study Of Characteristics Of Single And Two-Diode Equivalent Circuit. *Electrical and Electronics Engineering: An International Journal (ELELIJ)*, 4.

#287: Comparative evaluation of microalgae cultivation systems for biofuel application

Mohit Singh RANA[1], Sanjeev Kumar PRAJAPATI[1]

[1] Environment and Biofuel Research Laboratory, Hydro and Renewable Energy Department, Indian Institute of Technology Roorkee, Uttarakhand, 247667, India, mohit_r@ah.iitr.ac.in; mohitrn90@gmail.com
[1] Environment and Biofuel Research Laboratory, Hydro and Renewable Energy Department, Indian Institute of Technology Roorkee, Uttarakhand, 247667, India, sanjukec@hre.iitr.ac.in; sanjukec@gmail.com

Abstract: Microalgae have been envisioned as a key resource for use as a transportation biofuel. However, microalgae cultivation on a mass scale is associated with several challenges, including production cost and desired quality. In the quest for high-density microalgae cultivation having desired traits applicable to biofuel quality, the present work aimed to evaluate microalgae cultivation systems systematically. Column photobioreactor (PBR) and microalgal-biofilm reactor (MBR) were selected for microalgae cultivation as a suspended culture and as a biofilm, respectively. Microalgae Chlorella pyrenoidosa was grown under mixotrophic mode in laboratory-controlled conditions at an illumination of 15,000-20,000 Lux, a temperature of 25±2°C, and a light/dark cycle of 16/8 hours. The selected microalgae was cultivated in domestic wastewater supplemented with glycerol. The cultivation systems were evaluated in terms of biomass growth, biochemical composition, and quality of biofuels. As a result, MBR was observed to achieve the maximum biomass productivity of 10 g m^{-2} d^{-1}. In contrast, in PBR, biomass productivity of 3 g m^{-2} d^{-1} was attained. The MBR-grown biomass had a higher carbohydrate fraction than PBR-grown biomass. On the other hand, the lipid content for PBR grown biomass was slightly higher than the MBR-grown biomass. Further, the biodiesel based on PBR-grown biomass showed quality in agreement with international standards (ASTM D6751-02, EN14214). In contrast, the case was not the same for microalgae cultivated in MBR. The results showed microalgae cultivation as a suspended culture in PBR was appropriate for biodiesel production. Similarly, the MBR-grown biomass can be directed for biogas or bioethanol production. Therefore, during the selection and scale-up of the microalgae cultivation system, a thorough investigation of biofuel quality along with biomass productivity and biochemical composition is suggested.

Keywords: microalgae; biofuel; photobioreactor; biofilm; renewable energy

1. INTRODUCTION

It has been noted that Microalgal-biofuel has immense potential to meet future renewable energy demand. Higher areal productivity, higher oil content, shorter growth cycle than terrestrial oil-crops, and the opportunity to cultivate throughout the year make microalgae an attractive candidate for biofuel production (Kokkinos et al., 2021; Ratha et al., 2013). In fact, wasteland can be utilized to set up a microalgae cultivation facility, and wastewater and saline water can be used as a growth media (Gao et al., 2022; Tripathi et al., 2019). Considering the high oil content, microalgae were firstly considered for biodiesel production. Noteworthy, microalgae itself is a well-known biofactory, which further provides an opportunity to use a fraction of or whole cellular biomass for bioethanol production (Gao et al., 2022). Even biogas production using the whole biomass has been established; for years microalgae have been harnessed for biodiesel production. Biodiesel obtained from microalgae is characterised with higher calorific value, higher hydrogen to carbon ratio, and lower oxygen content in comparison to the terrestrial oil-crops based biodiesel (Costa and Morais, 2011). In addition, a biorefinery framework is being envisioned to recover maximum of the biofuel precursors or bioenergy from microalgae (Davis et al., 2011; Kim et al., 2020; Wiatrowski et al., 2022).

However, microalgal biomass production, a foremost step in the microalgal biofuel system, is one of the major bottlenecks that contribute to more than 50% of the overall cost and questions on economic viability (Koyande et al., 2019; Markou and Georgakakis, 2011). Mixotrophic cultivation of microalgae by augmenting the media with additional carbon, such as glycerol, is projected to provide an economical solution, yielding higher biomass concentration (Cabanelas et al., 2013; Octavio Perez-Garcia and Bashan, 2015). In a recent study, up to a 300% increase in microalgal biomass production was recorded by adding glycerol to growth media (Chakravarty, 2022). Similarly, Gupta et al. (2016) observed an increase in biomass growth from 0.1 g L^{-1} to 0.8 g L^{-1} under glycerol supplementation in wastewater.

In addition, various kinds of microalgae cultivation systems have been established to obtain adequate biomass with expected metabolites. However, the biomass yield and quality vary with microalgae cultivation systems. For instance, microalgae cultivation as a biofilm in algal turf scrubbers was reported to achieve a higher biomass yield (Davis et al., 2011). However, lower lipid content was reported. Therefore, appropriate selection of microalgae cultivation mode, growth nutrients and harvesting period is crucial considering the desired quality or vice versa based on the applications. Nonetheless, a detailed study on biomass cultivation, harvesting, and appropriate usage are not available.

In line with the above-discussed opportunities and challenges, in this present work, we systematically evaluated the microalgae cultivation systems targeting biofuel production. Column photobioreactor (PBR) and microalgal-biofilm reactor (MBR) were selected for microalgae cultivation as a suspended culture and as a biofilm, respectively. In addition, considering the real-scale economic applicability, wastewater was chosen as a growth media. Furthermore, approaching the high-density cultivation of microalgae enriched with biofuel precursors, the growth media was aided with glycerol. The cultivation systems were evaluated in terms of biomass growth, biochemical composition, and biofuels quality.

2. METHODS

Chlorella pyrenoidosa was selected for the present study based on its properties for biofuels application. Domestic wastewater supplemented with waste glycerol was used as a microalgae growth media. The selected strain was grown under a mixotrophic mode in laboratory-controlled conditions at an illumination of 15,000-20,000 Lux, a temperature of 25±2 °C, and light: dark cycle of 16: 8 hours. *C. pyrenoidosa* was cultivated in a suspended mode in a PBR and as a biofilm in an MBR for 15 days. An aliquot of microalgae culture was intermittently withdrawn from PBR to analyse the biofuel and biofuel precursors. Similarly, the microalgal biomass was manually scraped off from MBR.

The biomass concentration (g L^{-1}) for PBR grown culture was estimated using the corresponding absorbance by following the Equation (1), adopted from Rana et al. (2020).

$$\text{Biomass concentration} = 0.4469 \times A_{680} + 0.003 \qquad \text{Eq. (1)}$$

The daily areal productivity (g m^{-2} d^{-1}) for PBR grown biomass was calculated using the Equation (2)

$$Biomass\ productivity = \frac{Biomass\ conentration \times Net\ volume}{Net\ surface\ area \times Cultivation\ time\ period} \qquad \text{Eq. (2)}$$

The total biomass production and daily areal biomass productivity for MBR were computed using Equation (3) and Equation (4), respectively.

$$Biomass\ production = \frac{Dried\ Biomass\ (g)}{Net\ surface\ area\ (m^2)}$$ Eq. (3)

$$Biomass\ productivity = \frac{Dried\ Biomass}{Net\ surface\ area \times Cultivation\ time\ period}$$ Eq. (4)

The harvested biomass was dried and powdered for further studies. The carbohydrate and lipid content was determined using the phenol-sulfuric acid method (Dubois et al., 1956) and the Bligh and Dyer method, as reported previously by Lee et al. (2010), respectively. Further, the dried lipids were transesterified following the procedure, as provided by Breuer et al. (2013), and the fatty acid methyl ester (FAME) composition was determined. Subsequently, based on the fatty acids profile the biodiesel properties were computed (Arguelles and Martinez-Goss, 2021). Elemental analyses of the microalgal biomass were carried out using an elemental analyzer, and the protein content was determined using the conversion factor of 6.25 (Zhong et al., 2012). The methane potential was computed based on the biochemical composition (2009).

3. RESULTS AND DISCUSSION

Microalgae cultivated in PBR showed a biomass concentration of up to 1.34 g L^{-1}. However, the growth slightly declined to 1.28 g L^{-1} on the 15th day (Figure 1a). Corresponding to biomass concentration, for 6-, 9-, 12-, and 15-day growth periods, the obtained biomass productivities were 5.8, 4.7, 3.5, and 2.7 g m^{-2} d^{-1}, respectively (Figure 1c). On the other hand, a continuous rise in biomass yield was observed throughout the growth period for microalgae cultivated in MBR. Up to 64, 70, 78, and 90 g m^{-2} biomass yield was observed after the 6th, 9th, 12th, and 15th day of cultivation, respectively (Figure 1b). Further, the biomass productivities for microalgae cultivated in MBR were noted as 10, 7, 6, and 5.8 g m^{-2} d^{-1} for 6-, 9-, 12-, and 15-day growth periods, respectively (Figure 1c).

It is worth noting that substantially higher biomass productivity was achieved in the MBR. Moreover, the biomass productivity for MBR-grown microalgae was comparable to the previously reported values. For example, Roostai et al. (2018) recorded maximum biomass productivity of 12 g m^{-2} d^{-1}. Similarly, in a recent study, a biomass productivity of 7.5 g m^{-2} d^{-1} was expressed for *C. pyrenoidosa* cultivated in an MBR (Zhang et al., 2022). Variations in biomass productivities were observed subjected to the microalgae strains, growth media, and growth support material. Furthermore, the enhanced biomass production could be attributed to the cell attachment over the growth support material and continuous nutrient availability to the microalgal cells.
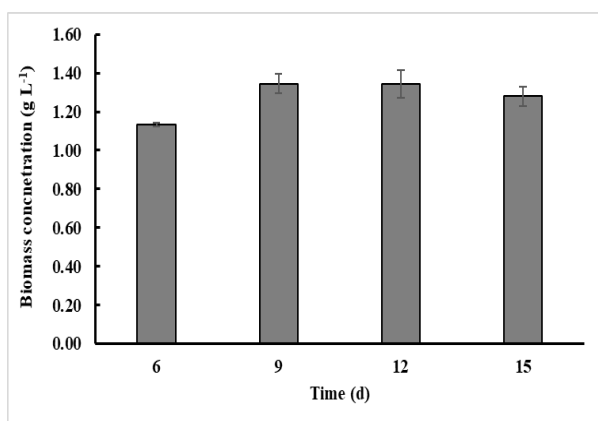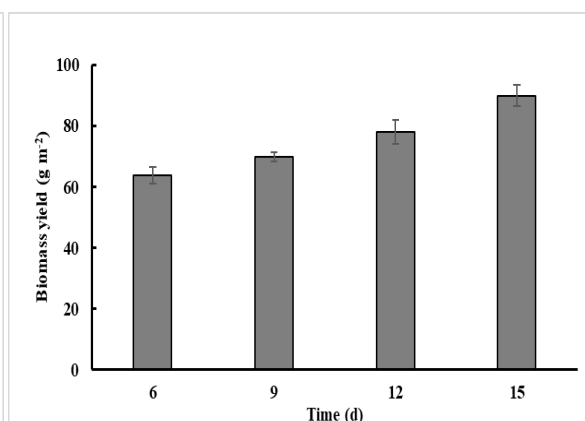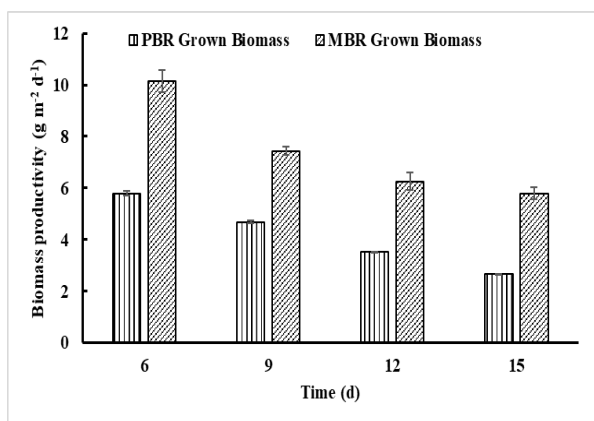

Figure 1a

Figure 1b

Figure 1c

Figure 1: Biomass production for microalgae cultivated in (a) photobioreactor, (b) microalgal biofilm reactor (b), and (c) corresponding biomass productivities.

The biochemical composition for microalgal biomass cultivated in PBR and MBR is presented in Figure 2. For PBR-grown biomass, continuous accumulation of lipid content was observed throughout the growth period. In contrast, the protein content decreased slightly after the exponential phase of the growth. However, substantial variation in carbohydrate content was not observed. After the 15th day of microalgae cultivation period, the harvested biomass was observed with up to 17, 28, and 18% dry cell weight basis, lipid, carbohydrate, and protein content, respectively. Likewise, for MBR-grown biomass, a significant rise in lipid accumulation was observed till the 9th day of cultivation. Further, the lipid accumulation increased gradually. On the other hand, from 7th day onward, the protein content started declining. Similar to the PBR-grown biomass, no significant variation in carbohydrate content was observed throughout the growth period for MBR-grown biomass. MBR was observed to yield microalgal biomass with a maximum of 15, 41, and 16% dry cell weight basis, lipid, carbohydrate, and protein content, respectively.

The elevated accumulation of lipid and decline in protein content during the late phase of the microalgae cultivation period could be attributed to the metabolic shift from protein to lipid synthesis (Levitan et al., 2015). Considering the biomass productivity, the MBR was noted to attain higher productivities for biofuel precursors, i.e., carbohydrates and lipids within 6 day of the cultivation period. Furthermore, the lipid accumulation was observed subjected to the glycerol dose, facilitating mixotrophic conditions for microalgal growth. In another study, for microalgae cultivated in 2, and 5 g L^{-1} glycerol augmented media, 13 and 23 % dry cell weight basis, respectively lipid accumulation was expressed (Rincon et al., 2017). Similarly, up to 15 % dry cell weight basis lipid accumulation was noted for microalgae cultivated in glycerol aided wastewater (2016).
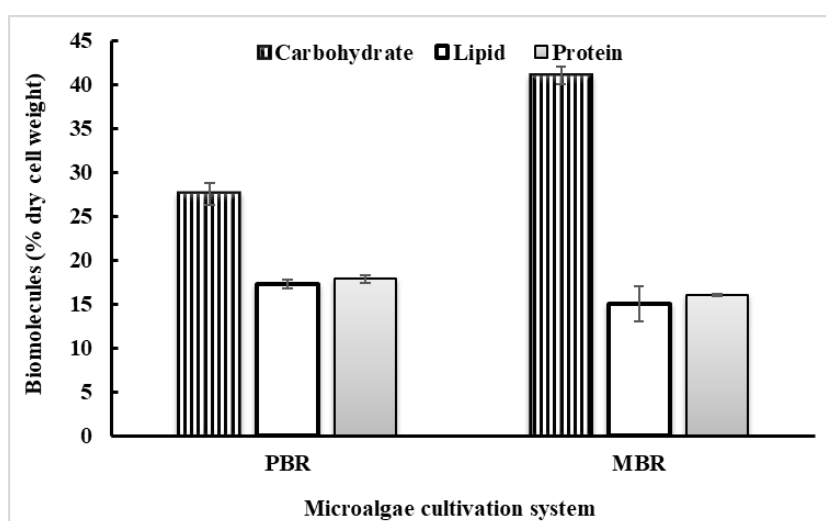

Figure 2: Biochemical composition of column photobioreactor (PBR) and microalgal-biofilm reactor (MBR) grown biomass

124

The biofuel potential of the PBR- and MBR-grown biomass was evaluated in terms of its suitability to use the lipid fraction for biodiesel production, carbohydrates for bioethanol production, and the whole-cell biomass for biogas production. The suitability towards biodiesel was estimated through the FAME profile. The PBR-grown biomass was found to be enriched with oleic acid (a monounsaturated fatty acid desired for biodiesel). Overall, highest fraction of monounsaturated fatty acids was observed, followed by saturated fatty acids and polyunsaturated fatty acids (Figure 3). Furthermore, for the PBR-grown biomass, the biodiesel properties were found in agreement with international standards, ASTM D6751-02 and EN14214. On the other hand, the MBR-grown biomass had the highest fraction of saturated fatty acids. Both monounsaturated and polyunsaturated fatty acids were present. It is worth mentioning when the selected microalgae strain was cultivated in MBR, the fraction of oleic acid was drastically reduced, and the stearic acid increased. The lipid obtained from MBR-grown biomass was not found suitable for biodiesel production. In particular, a high fraction of stearic acid, a saturated fatty acid, was observed to elevate the value for the cold filter plugging point. Similarly, other properties, like the share of a-linolenic acid, density, and oxidative stability, were found out of the range. On the other hand, with higher carbohydrate content, the MBR-grown biomass was observed to yield bioethanol up to 20% dry cell weight basis and biogas up to 0.433 $m^3 kg^{-1} VS_{fed}$. Henceforth, the PBR was noted to be suitable for microalgae cultivation, primarily to obtain biodiesel. Further, the residual biomass obtained after lipid extraction could be utilized for biogas production, as recently demonstrated by Srivastava et al. (2020). On the other hand, the MBR-grown biomass was observed to be appropriate for bioethanol production using carbohydrates or biogas production using whole biomass.
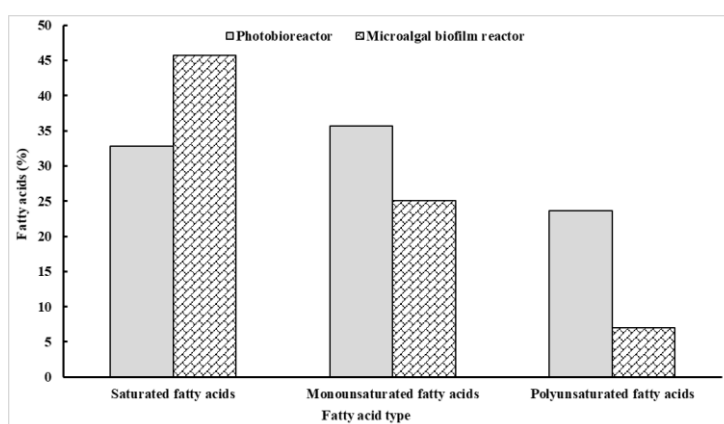

Figure 3. Fatty acids profile for the lipids obtained from microalgae cultivated in column photobioreactor, and microalgal-biofilm reactor

CONCLUSIONS

In this present work, the authors attempted to evaluate the microalgae cultivation systems for adequate biomass production. The microalgal biofilm reactor was observed for higher biomass yield. An optimum harvesting period of 6 days with the highest biomass productivity having substantial biofuel precursors was observed for the microalgal biofilm reactor. On the other hand, biomass harvesting at a cycle of 15 days was suggested for column photobioreactor. Further, the potential of the produced microalgal biomass was investigated for various biofuel applications. Column photobioreactor-grown biomass was observed to be suitable for biodiesel production. Further, bioethanol or biogas production was suggested using microalgal-biofilm reactor-grown biomass.

REFERENCES

Arguelles, E.D., Martinez-Goss, M.R., 2021. Lipid accumulation and profiling in microalgae Chlorolobion sp. (BIOTECH 4031) and Chlorella sp. (BIOTECH 4026) during nitrogen starvation for biodiesel production. J. Appl. Phycol. 33, 1–11. https://doi.org/10.1007/s10811-020-02126-z

Breuer, G., Evers, W.A.C., de Vree, J.H., Kleinegris, D.M.M., Martens, D.E., Wijffels, R.H., Lamers, P.P., 2013. Analysis of fatty acid content and composition in microalgae. J. Vis. Exp. 5, 1–9. https://doi.org/10.3791/50628

Cabanelas, I.T.D., Arbib, Z., Chinalia, F.A., Souza, C.O., Perales, J.A., Almeida, P.F., Druzian, J.I., Nascimento, I.A., 2013. From waste to energy: Microalgae production in wastewater and glycerol. Appl. Energy 109, 283–290. https://doi.org/10.1016/j.apenergy.2013.04.023

Chakravarty, S., Mallick, N., 2022. Carbon dioxide mitigation and biodiesel production by a marine microalga under mixotrophic mode by using transesterification by-product crude glycerol: A synergy of biofuels and waste valorization. Environ. Technol. Innov. 27, 102441. https://doi.org/10.1016/j.eti.2022.102441

Costa, J.A.V., Morais, M.G. de, 2011. The role of biochemical engineering in the production of biofuels from microalgae. Bioresour. Technol. 102, 2–9. https://doi.org/10.1016/j.biortech.2010.06.014

Davis, R., Aden, A., Pienkos, P.T., 2011. Techno-economic analysis of autotrophic microalgae for fuel production. Appl. Energy 88, 3524–3531. https://doi.org/10.1016/j.apenergy.2011.04.018

Dubois, M., Gilles, K.A., Hamilton, J.K., Rebers, P.A., Smith, F., 1956. Colorimetric Method for Determination of Sugars and Related Substances. Anal. Chem. 28, 350–356. https://doi.org/10.1021/ac60111a017

Gao, F., Zhang, X.-L., Zhu, C.-J., Huang, K.-H., Liu, Q., 2022. High-efficiency biofuel production by mixing seawater and domestic sewage to culture freshwater microalgae. Chem. Eng. J. 136361. https://doi.org/10.1016/j.cej.2022.136361

Gupta, P.L., Choi, H.J., Lee, S.M., 2016. Enhanced nutrient removal from municipal wastewater assisted by mixotrophic microalgal cultivation using glycerol. Environ. Sci. Pollut. Res. 23, 10114–10123. https://doi.org/10.1007/s11356-016-6224-1

Kim, E.J., Kim, S., Choi, H.G., Han, S.J., 2020. Co-production of biodiesel and bioethanol using psychrophilic microalga Chlamydomonas sp. KNM0029C isolated from Arctic sea ice. Biotechnol. Biofuels 13, 1–13. https://doi.org/10.1186/s13068-020-1660-z

Kokkinos, K., Karayannis, V., Moustakas, K., 2021. Optimizing Microalgal Biomass Feedstock Selection for Nanocatalytic Conversion Into Biofuel Clean Energy, Using Fuzzy Multi-Criteria Decision Making Processes. Front. Energy Res. 8, 1–20. https://doi.org/10.3389/fenrg.2020.622210

Koyande, A.K., Show, P.L., Guo, R., Tang, B., Ogino, C., Chang, J.S., 2019. Bio-processing of algal bio-refinery: a review on current advances and future perspectives. Bioengineered 10, 574–592. https://doi.org/10.1080/21655979.2019.1679697

Lee, J.Y., Yoo, C., Jun, S.Y., Ahn, C.Y., Oh, H.M., 2010. Comparison of several methods for effective lipid extraction from microalgae. Bioresour. Technol. 101, S75-7. https://doi.org/10.1016/j.biortech.2009.03.058

Levitan, O., Dinamarca, J., Zelzion, E., Lun, D.S., Guerra, L.T., Kyung, M., Kim, J., 2015. Remodeling of intermediate metabolism in the diatom Phaeodactylum tricornutum under nitrogen stress. Proc. Natl. Acad. Sci. 112. https://doi.org/10.1073/pnas.1419818112

Markou, G., Georgakakis, D., 2011. Cultivation of filamentous cyanobacteria (blue-green algae) in agro-industrial wastes and wastewaters: A review. Appl. Energy 88, 3389–3401. https://doi.org/10.1016/j.apenergy.2010.12.042

Octavio Perez-Garcia, Bashan, Y., 2015. Microalgal Heterotrophic and Mixotrophic Culturing for Bio-refi ning: From Metabolic Routes to Techno-economics, in: Prokop, A., Bajpai, R.K., Zappi, M.E. (Eds.), Algal Biorefineries: Volume 2: Products and Refinery Design. Springer, pp. 61–131. https://doi.org/10.1007/978-3-319-20200-6_3

Rana, M.S., Bhushan, S., Sudhakar, D.R., Prajapati, S.K., 2020. Effect of iron oxide nanoparticles on growth and biofuel potential of Chlorella spp. Algal Res. 49, 101942. https://doi.org/10.1016/j.algal.2020.101942

Ratha, S.K., Babu, S., Renuka, N., Prasanna, R., Prasad, R.B.N., Saxena, A.K., 2013. Exploring nutritional modes of cultivation for enhancing lipid accumulation in microalgae. J. Basic Microbiol. 53, 440–450. https://doi.org/10.1002/jobm.201200001

Rincon, S.M., Romero, H.M., Aframehr, W.M., Beyenal, H., 2017. Biomass production in Chlorella vulgaris biofilm cultivated under mixotrophic growth conditions. Algal Res. 26, 153–160. https://doi.org/10.1016/j.algal.2017.07.014

Roostaei, J., Zhang, Y., Gopalakrishnan, K., Ochocki, A.J., 2018. Mixotrophic microalgae biofilm: a novel algae cultivation strategy for improved productivity and cost-efficiency of biofuel feedstock production. Sci. Rep. 8, 1–10. https://doi.org/10.1038/s41598-018-31016-1

Sialve, B., Bernet, N., Bernard, O., 2009. Anaerobic digestion of microalgae as a necessary step to make microalgal biodiesel sustainable. Biotechnol. Adv. 27, 409–416. https://doi.org/10.1016/j.biotechadv.2009.03.001

Srivastava, G., Kumar, V., Tiwari, R., Patil, R., Kalamdhad, A., Goud, V., 2020. Anaerobic co-digestion of defatted microalgae residue and rice straw as an emerging trend for waste utilization and sustainable biorefinery development. Biomass Convers. Biorefinery. https://doi.org/10.1007/s13399-020-00736-8

Tripathi, R., Gupta, A., Thakur, I.S., 2019. An integrated approach for phycoremediation of wastewater and sustainable biodiesel production by green microalgae, Scenedesmus sp. ISTGA1. Renew. Energy 135, 617–625. https://doi.org/10.1016/j.renene.2018.12.056

Wiatrowski, M., Klein, B.C., Davis, R.W., Quiroz-Arita, C., Tan, E.C.D., Hunt, R.W., Davis, R.E., 2022. Techno-economic assessment for the production of algal fuels and value-added products: opportunities for high-protein microalgae conversion. Biotechnol. Biofuels Bioprod. 15, 1–14. https://doi.org/10.1186/s13068-021-02098-3

Zhang, Yonggang, Ma, R., Chu, H., Zhou, X., Yao, T., Zhang, Yalei, 2022. Evaluation of the performance of different membrane materials for microalgae cultivation on attached biofilm reactors. RSC Adv. 12, 1451–1459. https://doi.org/10.1039/d1ra07335d

Zhong, W., Zhang, Z., Luo, Y., Qiao, W., Xiao, M., Zhang, M., 2012. Biogas productivity by co-digesting Taihu blue algae with corn straw as an external carbon source. Bioresour. Technol. 114, 281–286. https://doi.org/10.1016/j.biortech.2012.02.111

#317: AI-enabled waste prevention for a circular economy: challenges and opportunities

Fatemeh GOLPAYEGANI[1], Jack O'SULLIVAN[2], Fionnuala MURPHY[3]

1 School of Computer Science, University College Dublin, Fatemeh.golpayegani@ucd.ie
2 Zero Waste Ireland, jack@zerowasteireland.com
3 School of Biosystems and Food Engineering, University College Dublin Fionnuala.Murphy@ucd.ie

Abstract: Unlike the traditional "Take, Make, Waste" model of the linear economy, the circular economy is a closed loop or regenerative model that eliminates waste and pollution, keeps products and materials in use, and regenerates natural systems. In the circular economy, systems are considered organisms that process nutrients that can be fed back into the cycle. Minimising waste and resource use, maintaining the value of products and materials through good design, durability and repair, reusing a product that has reached its end of life by creating other valuable products are primary efforts in a circular economy. Artificial Intelligence (AI) with the use of the Internet of Things (IoT), big data, and blockchain can accelerate circularity and the dematerialisation of our economy and make us less dependent on primary materials. These technologies can be used to track the journeys of products, components and materials and provide insights to decision-makers and policymakers at different levels.

1. INTRODUCTION

We have only one planet to live on, and yet by 2050, we will be consuming as if there are three. Global consumption of biomass, fossil fuels, metals and minerals is expected to double in the next forty years, and annual waste generation is projected to increase by 70% by 2050. The European Green Deal launched a strategy for a climate-neutral, resource-efficient and competitive economy. Establishing a circular economy contributes to achieving climate neutrality by 2050 and decoupling economic growth from resource use and ensures the long-term competitiveness of the EU (European Commission, 2020).

The circular economy can contribute to a number of the United Nations Sustainable Development Goals (SDGs) such as SDG7 (Affordable and Clean Energy), SDG8 (Decent Work and Economic Growth), SDG9 (Industry, Innovation and Infrastructure), SDG11 (Sustainable Cities and Communities), SDG12 (Responsible Consumption and Production), SDG13 (Climate Action), SDG14 (Life below Water), and SDG15 (Life on Land). The European Circular Economy Action Plan (DECC, 2020) provides a future-oriented agenda for achieving a cleaner and more competitive Europe in co-creation with economic actors, consumers, citizens and civil society organisations. The plan is focused on presenting a product policy framework that will make sustainable products, services and business models the norm and transform consumption patterns so that no waste is produced in the first place. The sustainable product policy framework has three main pillars; designing sustainable products, empowering consumers and public buyers, and circularity in production processes.

An integral part of the sustainable product policy framework is the sustainability challenge posed by key value chains. Electronics and ICT continue to be one of the fastest-growing waste streams in the EU; batteries and vehicles; packaging waste that has reached 173 kg per inhabitant; plastics whose consumption is expected to double in the coming 20 years; textiles, where less than 1% of all textiles worldwide is estimated to be recycled into new textiles; construction and building which is responsible for over 35% of the EU's total waste generation; food, water and nutrients: it is estimated 20% of the total food produced is lost or wasted in the EU.

To make products fit for a climate-neutral, resource-efficient and circular economy, it is crucial to take steps at the time of design, as up to 80% of products' environmental impacts are determined at the design phase. Improving products' durability, reusability, upgradeability and reparability, and increasing recycled content in products are some of the principles set to impact product design positively. In addition, providing consumers with cost-saving opportunities such as the right to repair and green public procurement is a crucial building block of the sustainable product policy framework. Circularity in production processes can deliver substantial material savings throughout value chains and production processes, generate extra value and unlock economic opportunities. This includes promoting the use of digital technologies to track, trace, and map resources and support the sustainable and circular bio-based sector by implementing the Bioeconomy Action Plan (European Commission, 2018).

1.1. Waste prevention in the European Union

In 2018, the EU generated 812 million tonnes of waste (excluding major mineral waste), equivalent to 35 % of the total waste generated; and amounting to an average of 1.8 tonnes of waste per inhabitant. Considering municipal solid waste (MSW), the EU (28 countries) generated 248.65 million tonnes in 2017, equivalent to an average per capita amount of 486 kg, slightly higher than the average of 470 kg per capita in 1995 (Eurostat, 2022).

The re-orientation of the European waste hierarchy towards waste prevention, preparing for reuse, repairing, recycling, and recovery of materials is intended to maximise the value of what we discard as waste, as well as reducing the pressure on the environment, reducing environmental damage and pollution, creating jobs and making the transition to the Circular Economy a reality in the EU (Ghisellini, 2019). The earlier acceptance of burning MSW to extract and use a relatively small proportion of the energy embodied in the materials which we discard has given way to the recognition that waste incineration is a carbon-intensive process which undermines current efforts to decrease carbon emissions and, thus, to reach carbon neutrality on time. Additionally, burning discarded materials or waste harms rather than supports the transition to a circular economy. Since both non-recyclable and recyclable materials can be used as a feedstock for a waste incinerator or for co-fuelling a cement production plant, waste prevention and recycling are thereby discouraged, while tending to lock-in an increasing generation of waste over time (Makavou, 2021).

2. ARTIFICIAL INTELLIGENCE (AI) FOR WASTE PREVENTION AND THE CIRCULAR ECONOMY

Artificial Intelligence consists of a collection of technologies and software that provide models and systems that can reason and learn and make decisions accordingly. Using historical or live data such as text, audio, and video, AI can offer services such as pattern recognition, prediction, recommendation and optimisation. To provide such services, the AI-enabled decision-making power requires data collection, data engineering, algorithm design, development, and refinement. Such data can be multi-modal, unstructured, noisy and collected from various

sources such as sensors, cameras, and IoT devices. Therefore, it is essential to pre-process (e.g. use consistent labelling) and engineer the data (e.g., present in a machine-readable format) before feeding it into any algorithms. During design time, various system and application requirements (e.g., the ability to detect a material pattern in wastewater, visual identification of an object during waste sorting, etc.) are considered in order to design and develop a suitable algorithm. This algorithm is then trained in multiple iterations on available data to be refined and ready for real-world application.

Artificial Intelligence (AI) with the use of the Internet of Things (IoT), big data and blockchain can accelerate circularity and the dematerialisation of our economy, making Europe and Ireland less dependent on primary materials. These technologies can be used to track the journeys of products, components and materials and provide insights to decision-makers and policymakers at different levels.

Globally, it is estimated that the application of AI could double economic growth by 2035. PWC has forecasted that AI will boost Ireland's GDP by 11.6% or €48 billion in 2030 (Purdy, 2016). "AI: Here for Good" is the newly launched Irish government strategy (Department of the Taoiseach, 2021) to highlight the transformative potential of AI for addressing many societal, environmental and economic challenges. AI for societal good and sustainability is the first strand of this strategy, while having a particular focus on waste management and prevention in its AI sectoral opportunities, highlighting the importance and impact of AI in policies and strategies.

AI can accelerate the shift towards a circular economy in three main ways: designing circular products providing rapid prototyping and testing through simulations, digital twinning and algorithms such as learning; operating circular business models using smart inventory techniques, pricing and prediction-based demand response models; optimising circular infrastructure to improve sorting, disassembling products, remanufacturing, and recycling. In an Industry 4.0 example, the product design stage can be enhanced using digital twinning and learning from big data. The Internet of Things, blockchain, cryptography and big data can enhance the main loop of use, re-use, share, and repair by offering service-based models and value assessment tools. They can also provide services such as collection and reverse logistics optimisation and value-based return incentives, sourcing and pre-processing processes and learning-based disassembly robots. AI can be used to design new material for a circular economy. For example, Citrine Platform uses the material data to design adaptive AI-based algorithms to develop new chemicals and materials for high performance applications such as finding a 3D printable, aerospace-grade aluminium alloy. In this example, AI has replaced the 'trial and error' process with sequential learning that can improve and optimise the design and innovation process for materials. AI can also enable dynamic pricing of goods and services for circular business models in various sectors such as retail and energy (Yildizbasi, 2021). Farmers also use AI for precision farming, tracking crop humidity, soil composition, and temperature in growing areas, allowing them to take better care of their crops by informing them of the optimal amount of water or fertilizer to use (Ivanov, 2015). AI and IoT are already being considered for their use in waste management, especially waste sorting and waste handling (O'Sullivan, 2019). For example, determining the most efficient routes for waste collection vehicles, thereby improving fuel efficiency and reducing collection time; using deep learning technology and robotic arms guided by AI to make municipal recycling facilities run more efficiently; and the disassembly of discarded electronic equipment (WEEE). Apple Inc. stated it has started using teams of robots, each with 29 arms, to take apart iPhone 6s in California and the Netherlands, which has proven to be more efficient at recovering materials than traditional methods such as shredding. AI can also help regulatory authorities or agencies to monitor, improve detection rates and assess the risk of irregularities in waste management, e.g., illegal dumping, hidden dumps of waste, etc. Intelligent design by machine is common in the electronics industry where the design of a complex circuit is undertaken by specialised computer software. By applying this approach to the design of new items of equipment, and by including a requirement that the item should be easy to assemble, repair and dismantle at the end of its life, the use of AI can greatly assist the design of products for the Circular Economy.

2.1. Challenges and opportunities

Digitalisation has been proposed as the driving force of the new circular economy where data and Artificial Intelligence play an important role in learning processes faster, and understanding and managing complex systems and models. AI-enabled circular economy is implemented in various European cities offering varying services. Circular Berlin introduced an urban metabolism model which extensively explores the flow of input resources (e.g., water, energy, material, and information) and flow of output (e.g., emission and waste) in various sectors such as household, industry, offices and retail within the city. To understand such a flow, mapping of various layers of information including spatial boundaries, biophysical data, urban energy metabolism data, role of utilities and services, and policy frameworks were identified as an important big data and AI related challenge. Pensumo is a so-called pocket technology developed and in use in Spain as a mobile App focusing on local actors (i.e., citizens) behaviour analysis, sharing data and use of personal data. It focuses on creating more awareness for various stakeholders in the city by analysing the consumers' behaviour and offers incentives to improve positive actions towards recycling. Datafication of the Circular Economy is a KU Leuven research project focusing on developing a conceptual framework for data governance and for the establishment of a data exchange platform, based on the concept of "materials passport", with focus on buildings and road mobility as use cases. SludgeAdvanced, is a

digital service developed in France that provides material passports for the sludge that is recovered from wastewater for agriculture use to understand where it is coming from, what are the constituents and where does it go. This passport will include all the data on the material and will be shared by all the stakeholders to have a transparent material flow. From these cases and many more in use and on-going projects it is clear that there are a number of prominent challenges that must be discussed and addressed in the context of developing AI for waste prevention and the circular economy (Figure 1).

Challenge 1

Identifying the various actors and stakeholder and their interdependencies, and how AI, big data and other digital technologies can enhance their performance in various sectors. For example, public institutions can use AI and such disruptive technologies to monitor the circular economy and the development of its indicator, and enhance the Circular Economy through the opening up of new markets. Companies can use it to create CE-based business models, improve their design and production, fruitful interaction with other actors, and comply with self-monitoring obligations. Consumers/citizens can use AI and big data to make informed societal and economic decisions. Furthermore, the collaboration of business owners, customers and stakeholders is of high importance in providing feedback since AI has the main role in prediction, and feedback can be used to shape the output. Producers can use AI to estimate their yields and characterise their products and waste and identify ways to rebrand their waste as co-products and keep them in the circular economy.

Challenge 2

A digital maturity hierarchy of an organisation starts with data acquisition, storage and validation at the bottom of the hierarchy, continued by data visualisation, events detections and alerts, predictions and simulation, and optimised and automated operations at its apex. In this hierarchy, we can only claim that AI is implemented when predictions are made and optimised, autonomous decision-making is offered. However, AI would not function if the other levels of the hierarchy are not implemented well. Therefore, data availability and accessibility, standard data representations to provide open data platforms, data structures and architectures to allow data sharing within and across organisations are important issues.

Challenge 3

To understand and identify the material and goods flow in a circular economy, we require data sharing platforms, cross sectoral data generation and curation mechanisms, which may also include personal data, and therefore it is essential to know how to regulate and govern data.

Challenge 4

Raising citizens' awareness of how the circular economy works and how AI can enable them to make better decisions is a key factor in CE's success.
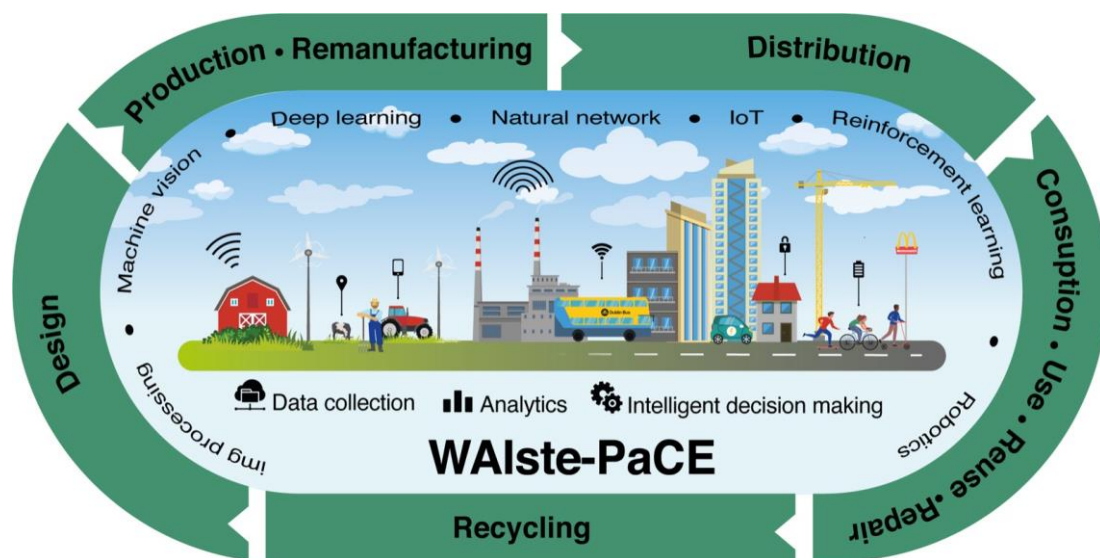

Figure 20: AI-enabled circular economy: what and where AI can be applied.

3. CONCLUSION

Although there have been some digital roadmaps for a circular economy and extensive literature reviews on waste management, and despite the spotlight on the role of AI and advanced digital technology in sustainable waste management, there has not yet been a comprehensive literature review or guidelines on the current state of AI use in practice, identifying and discussing challenges and obstacles and highlighting its prerequisite and potentials (Ranjbari, 2021; Bartl, 2014). This paper highlights a number of activities that must be carried out to address the specified challenges when designing an AI-based solution.

I. Identify the stakeholders and actors, understand their interdependencies and how material and goods flow in and within sectors;

II. Identify the prerequisite. It is not possible to have a successful AI-based system deployed without having the proper policies and regulations in place. Such policies and regulations directly impact the development, availability and accessibility of infrastructures essential for AI development (e.g., data sharing, open data framework);

III. The culture built around using such AI-based products must be examined to identify any educational elements required to raise awareness of people/end-users using AI products.

4. REFERENCES

Bartl, Andreas, 2014 "Moving from recycling to waste prevention: A review of barriers and enablers." Waste Management & Research 32.9_suppl (2014): 3-18.

DECC, 2020 Department of the Environment, Climate and Communications. The Waste Action Plan for a Circular Economy https://www.gov.ie/en/publication/4221c-waste-action-plan-for-a-circular-economy/

Department of the Taoiseach 2021. https://www.gov.ie/en/press-release/f4895-taoiseach-and-minister-troy-launch-government-roadmap-for-ai-in-ireland/

European Commission (2018), Bioeconomy: the European way to use our natural resources https://europanels.org/wp-content/uploads/2021/02/COM-Bioeconomy-Action-Plan-2018.pdf

European Commission, 2020. https://ec.europa.eu/environment/pdf/circular-economy/new_circular_economy_action_plan.pdf

Eurostat, 2022, https://ec.europa.eu/eurostat/statistics-explained/index.php?title=Waste_statistics

Ghisellini, Patrizia, et al. 2019. "Circular patterns of waste prevention and recovery." *E3S Web of Conferences*. Vol. 119. EDP Sciences.

Ivanov, Stepan, Kriti Bhargava, and William Donnelly, 2015. "Precision farming: Sensor analytics." IEEE Intelligent systems 30.4, 76-80.

O'Sullivan, Jack, 2019. The Role of Artificial Intelligence (AI) and the Internet of Things (IoT) in Sustainable Waste Management. EnviroCities eMagazine, Issue 22, pp 27-37.

Ranjbari, Meisam, et al., 2021, "Two decades of research on waste management in the circular economy: Insights from bibliometric, text mining, and content analyses." Journal of Cleaner Production (2021): 128009.

Makavou, 2021), https://zerowasteeurope.eu/2021/05/wte-incineration-no-place-sustainability-agenda/

Purdy, M. & Daughery, D. 2016, Why Artificial Intelligence is the Future of Growth, Worldwide: Accenture.

Yildizbasi, Abdullah, 2021. "Blockchain and renewable energy: Integration challenges in circular economy era." Renewable Energy 176, 183-197.

#342: COP26 and renewable energy representation in Twitter: the case of Turkey, Italy and Norway

Xheni SIMAKU

Haliç University, Istanbul, Turkey. xhenisimaku@halic.edu.tr

Abstract: Comparative studies on climate change communication are fundamental to understanding how societies undertake and react to this global topic (Kohn, 1987). Social media in this context helps to sensitize and spread the already known importance of the phenomenon by trying to minimize the distance between the nation's policies and societal consciousness. This research aimed to analyze three official Twitter accounts of Ministries focusing on COP26, a global event of fundamental importance concerning renewable energy, the policies of which must be followed to combat the crisis. The research was divided into 3 parts: pre-COP26, which analyzed the Twitter accounts 1 week before the event; during COP26 from October 30th to November 13th, 2021; and after COP26 until November 20th to see the change that this global event had on the three countries. As a result, it was noted that Italy and Turkey used Twitter ineffectively, while Norway, being more active, managed to reach a greater audience. This research illustrated the fact that, although the crisis is global, states work nationally.

Keywords: comparative research; Twitter; renewable energy; COP26.

1. INTRODUCTION

The unstoppable climate crisis has drastically increased in recent decades and has shaken public consciousness, making the various countries around the world question which policies to follow and how to inform and raise awareness about this delicate issue. In recent decades climate change has been discussed in different meetings and summits where various nations have tried to find a common path to follow; one of these can be identified as COP26, held in Glasgow in November 2021. The importance of such a big summit was the recognition and the admission of a global issue which touches all countries, and which has to be solved globally with the collaboration of every single nation.

Many tools have been used to try to spread as much information as possible about the climate crisis debates and policies, and one of those tools is the media, which has played an important role in shaping public opinion. COP26 was a pivotal point at which to take global decisions, and media coverage was able to increase societal awareness and knowledge of the issues, ideally cultivating and developing informed individual and collective actions. Media, such as social media, can construct a decisive forum and consensus regarding the formation and legitimation of a particular issue. In this context, media, and particularly social media in the last two decades, has played a crucial role in spreading knowledge whilst also being supportive, by being a digital participatory platform allowing citizens to actively take part in democratic public life through discussions, feeling part of the debate (Potter, 2016). Digital participation has become even more decisive, in particular when the issue debated is not purely about local issues, but when it can have global consequences, such as can be seen with the climate crisis.

2. METHODS

Media have had a preponderant effect both nationally and internationally, but with the globalization policies and the development of ICT (Information and Communication Technology), media effects has spread globally, and in different areas such economic, political, societal and so on (Castells, 2009; Giddens,2000; Simaku,2022). It is precisely under the globalization framework that this research was focused, by comparing a global phenomenon in three countries, two of which, Italy and Turkey, can be gathered under the Mediterranean framework, while the third, Norway, was the farthest case from the previous two. These comparisons are fundamental for examining the differences, similarities, and points of view of countries that have as a common objective the fight of a global emergency. As Esser and Hanitzsch (2012) would affirm, comparisons are crucial for estimating how universal true findings are, and for revealing relationships between social phenomena, therefore to understand also how they have developed in the various nations.

The research, through the comparative method, intended to analyze three official Twitter accounts of the afore mentioned country ministries by focusing on COP26, a global event of fundamental importance concerning renewable energy, and scrutinizing which policies must be followed to combat the crises. The Twitter accounts took in consideration were as following: @MISE_GOV Ministry of Economic Development in the Italian case, @TCenergy Republic of Turkiye Ministry of Energy and Natural Resources for the Turkish case, and @oeddep Norwegian Ministry of Petroleum and Energy regarding the Norwegian case.

The research was divided into 3 parts, the pre COP26, which analyzed the Twitter accounts 1 week before the event, from the 24th to 30th of October, the second during COP26, from the 31st of October until the 13th of November, and the third after COP26 until November the 20th, to see the change that this global event had on the three countries analyzed, but also to investigate the before and after effect of COP26.

In the table (Table 1) below is described the European situation, about Renewable Energy, positioning Norway at the 2nd position after Iceland, while Turkey was 10th and Italy 12th.
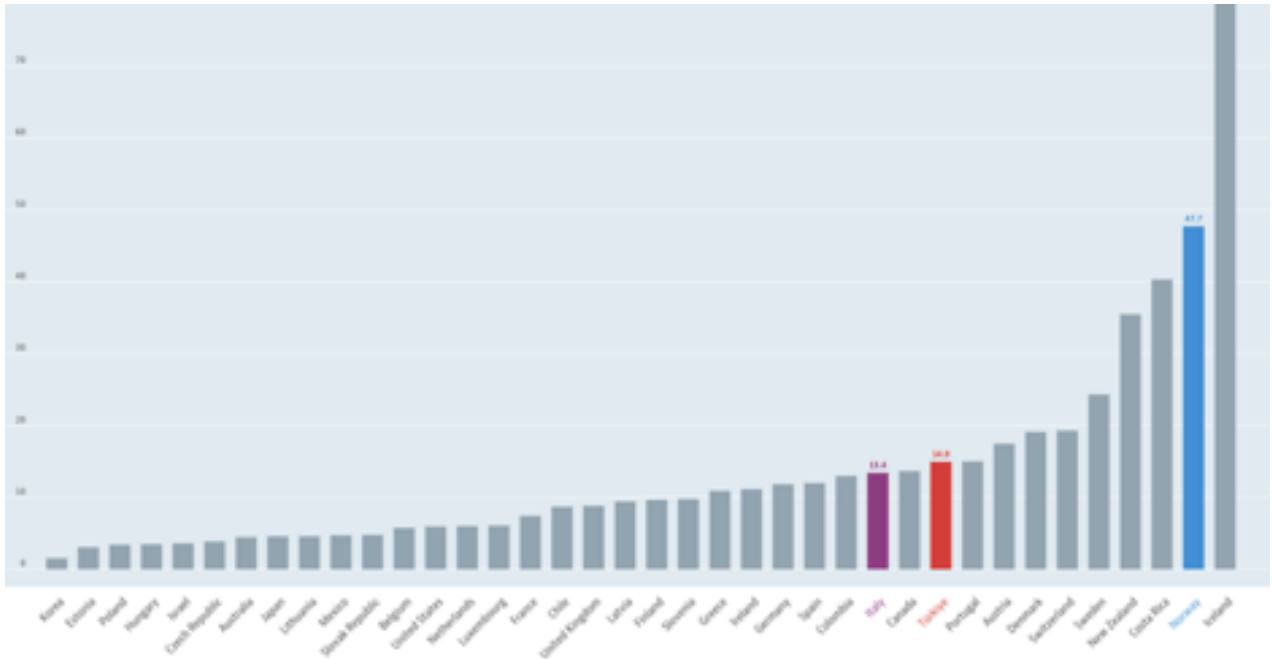
Table 1: Source: OECD data

3. RESULTS

The aim of this research as mentioned before was to compare the representation of COP26 through Twitter and the use of this social media tool by studying the official Twitter accounts and from the results, it was noted that Italy and Turkey used Twitter ineffectively, while Norway, being more active, managed to reach a greater audience. In Table 2, as can be observed, the Tweets, were not as expected, and except for Turkey there was not such a big increase during COP26, as had been seen for example in the Schmidt, Ivanova, & Schafer (2013) work (OECD, 2022), where the authors found an increasing amount of news and media coverage during the previous COP meetings.

Table 2: Tweets

Country	No. of Tweets from 24.10.2021 to 30.10.2021	No. of Tweets from 31.10.2021 to 13.11.2021	No. of Tweets from 14.11.2021 to 20.11.2021	Content and Topics
Italy	10	19	7	NPRR
Turkey	6	29	11	Video post
Norway	5	14	3	COP26, Conferences, Bilateral Agreements

It was noticed that the three accounts used Twitter in different ways; in the Italian case, the account was under the Ministry of Economic Development, and was much more focused on the NNRP (National Recovery and Resilience Plan), by focusing on enterprise incentives. Although Italy had an important role within COP26, the Italian ministry official account did not tweet or retweet any kind of content regarding COP26 during the period analyzed. In the Turkish case there was a high increase of tweets during COP26, but the tweets were not inherent to the event, being much closer to the political aspect of Turkey. In relation to the other two countries, the Turkish account showed much more video than still images. The Norwegian account was the only case that retweeted COP26; in the account the tweets were all concerning energy, and often retweeted other Norwegian ministries official accounts with which they have collaborations, by enhancing the image of common consensus between the ministries. Finally, the Norwegian Ministry of Petroleum and Energy seemed to be very careful to tweet constantly about the renewable energy and climate change conferences.

4. CONCLUSION

Through the study of three cases, this research investigated the Twitter representation of COP26 with the aim of underlining similarities between the cases, since the phenomenon taken into consideration was of global significance, but it appeared that the national Twitter representation of COP26 were manifestly national, and that the differences between these cases were greater than the similarities. The Norwegian case was seen to be more

successful than the other two, because they tweeted and had a strategic plan which addressed issues pertinent to renewable energy and its policies.

5. REFERENCES

Castells, M. (2009). *Comunicazione e Potere.* EGEA.

Esser, F., & Hanitzsch, T. (2012). *Handbook of comparative communication research.* Routledge.

Giddens, A. (2000). *Runaway World How Globalization is .* Routledge.

Kohn, M. L. (1987). Cross-NationaResearch as an Analytic Strategy: American Sociological Association, 1987 Presidential Address. *American Sociological Review*, 713-731.

OECD. (2022, 04 22). *OECD.* OECD data: https://data.oecd.org/energy/renewable-energy.htm adresinden alındı

Potter, W. J. (2016). *Media Literacy.* SAGE.

Schmidt, A., Ivanova, A., & Schafer, M. S. (2013). Media attention for climate change around the world: A comparative. *Global Environmental Change*, 1233–1248.

Simaku, X. (2022). Netflix and Chill: An Analysis of Turkish Generation Z Viewers on the . *İletişim Kuram ve Araştırma Dergisi*, 171-184.

#346: Sustainable and novel closed loop approach to convert black and grey water from multi-storey residential buildings into reusable water and biogas

Venkata Sai POLICHERLA[1], Sharon H[2], Srinivas REDDY K[3]

[1] Heat Transfer and Thermal Power Laboratory, Department of Mechanical Engineering, Indian Institute of Technology Madras, Chennai 600036, India, pvsai1995@gmail.com
2 Department of Mechanical Engineering, Indian Institute of Petroleum and Energy (IIPE), Visakhapatnam – 530 003, India, sharon.mec@iipe.ac.in
[3] Heat Transfer and Thermal Power Laboratory, Department of Mechanical Engineering, Indian Institute of Technology Madras, Chennai 600036, India, ksreddy@iitm.ac.in (Corresponding Author)

Abstract: Domestic blackwater treatment is one of the challenging issues in developing countries. The present study focused on the management of liquid and solid waste generated from human activities using eco-friendly technologies powered by renewable solar energy. This treatment was performed close to the source of waste generation to overcome issues of transportation. The reduction in required water demand for human activities (mainly in water stressed regions of the world) by the recirculation of greywater and reuse of blackwater upon treatment is discussed in this study. The proposed system was designed for a community of 100 families with 3 people (2 adults and 1 children) per family. On average, the total discharge from the considered population was 3,900 litres of wastewater and 160kg of faeces per day. The treatment of wastewater was performed using a multi-effect distillation (MED) system powered by solar evacuated tube collector field with an area of 205 m^2. When the MED operated for 5 hours/day with an average solar irradiation of 864.45 W/m^2 in the month of April, it was found to deliver a recovery rate of 49.25% at the test location of Chennai, India. When operating the MED unit for 300 days in a year, around 13.22 tons of distillate yield was produced. The semi-solid waste separated from the wastewater was supplied to a biogas digester for production of biogas and organic fertilizer. The methane output from the system was found to be around 1875.37 kg along with 55.27 tons of organic fertilizer per annum. The performance analysis of the proposed system was carried out by simulating the developed mathematical model using Matlab R2020a.

1. INTRODUCTION

In view of depleting freshwater resources and an increase in water demand, there has been a rapid development in sustainable water treatment technologies. From the day-to-day human activities, greywater and blackwater discharge from households is inevitable. As the human waste present in blackwater is considered as bio-waste, its proper treatment before disposing to the environment is necessary. The treatment of blackwater can be mainly performed by the separation of wastewater from semi-solid waste (Tilley, 2014). Sai and Reddy (2022) have designed and carried out an investigation of small-scale treatment of wastewater using the distillation of faeces using active solar dryer. Wastewater treatment can be carried out using various technologies but the solar thermal based distillation process was one of the most sustainable and efficient single step treatment process (Sharon and Reddy, 2015). The concept of the solar distillation process has also been experimentally proved as an effective option to treat sewage water (Reddy et al., 2018). For treatment in medium or large scale, multi-effect and multi-stage flash distillation processes are preferred. In multi-stage flash distillation process, hot feed water is supplied from first stage to last where flashing occurs in each stage. The vapours formed in these stages are condensed by preheating feed water (Morin, 1993). In the multi-effect distillation (MED) process, heat is supplied in the initial effect (or stage) where feed water is sprayed and the vapours formed act as heat input for the next effects with brine recirculation to next effects (Morin, 1993). Multi-effect distillation technology presents many advantages over traditional multi-stage flash distillation (Catrini et al., 2018). There are various studies presented by researchers on these technologies out of which Moradi et al., (2019) has integrated the 4 effect distillation unit with power generation cycle to utilize low grade heat energy which generated 143.64 kg/h of distilled water.

The treatment of semisolid waste can be done by unplanted or planted drying beds, co-composting and using a biogas reactor (Tilley, 2014). For the present scale and purpose of treating human waste near to source, it is viable to opt for the biogas digester. There are various studies presenting the biogas generation from livestock waste. Andriani et al., (2015) has reviewed the use of human excreta in biogas digesters and its potential for energy generation in populated regions.

2. SYSTEM DESCRIPTION

In the proposed approach, the water lines/circuit of residential buildings were modified to reduce freshwater consumption significantly. The greywater from one floor was circulated to meet the non-contact water requirements of lower floors. Upon considering 100 families with 3 people (2 adults and 1 children) per family, the average total discharge from the considered population was 3,900 litres of wastewater and 160kg faeces per day. The final blackwater and greywater discharged from the building was supplied to a liquid-solid separator for separation of wastewater from semi-solid faeces. This semi-solid waste was sent to a biogas digester for anaerobic digestion. The wastewater from the liquid-solid separator was mixed with greywater discharged from the ground floor of the building and was pumped to a multi-effect distillation unit for treatment. The energy requirement of the present MED unit is met by solar evacuated tube collector field with distilled water as heat transfer fluid. The whole MED unit along with a solar collector field was installed at rooftop level for effective utilization of available space. The MED unit was designed to have 3 effects and a condenser with a recovery rate of 15% from effect 1 alone when operated in April. The other effects were designed to completely condense the vapours formed in the previous effects. The operating pressures of these effects were maintained higher to lower from effect 1 towards condenser (0.31 bar, 0.2 bar, 0.12 bar and 0.12 bar) using a vacuum pump. This helped in achieving different boiling point temperatures in each effect. The wastewater was initially preheated in the condenser and fed to nozzle inlets of effect 1. This nozzle sprayed wastewater over the evaporator tubes to receive heat from distilled water recirculating between the solar field and evaporator tubes. The hot water outlet from the solar evacuated tube collector field was maintained at a temperature of 90ºC and the cold water returning from the MED was at a temperature of 80ºC with mass flow rate of 8062 L/h. The vapours formed from effect 1 were sent to the evaporator of effect 2 whereas the left-over wastewater or brine was pumped to the nozzle inlet of effect 2. In effect 2, the latent heat of condensation of vapours from effect 1 was utilised to evaporate wastewater sprayed over evaporator tubes This process continued and ended with a condenser unit in which the vapours formed in effect 3 were condensed using wastewater and cold water from the cooling tower. This MED unit releases concentrated brine from the 3rd effect and distillate was collected from effect 2, effect 3 and the condenser. At the same time, the semi-solid waste supplied to the biogas digester underwent the anaerobic digestion process. Upon digestion of organic matter, biogas and organic fertilizer were generated. The complete system description of the proposed processes is shown in *Figure 21*.
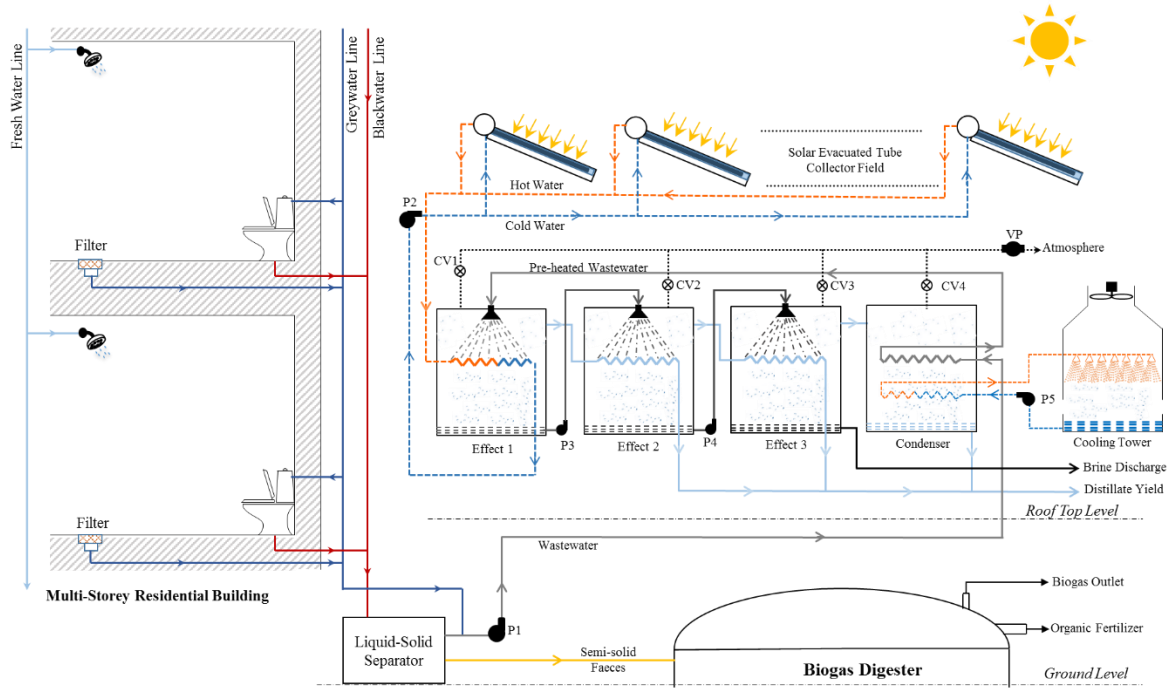
Figure 21: System description of sustainable and novel closed loop approach for multi-storey residential buildings.

3. MATHEMATICAL MODELLING

The present system analysis was carried out by developing a mathematical model using the following relations in Matlab R2020a. With the specifications of solar evacuated tube collector field mentioned in *Table 14*, the amount of useful energy supplied to MED unit can be calculated using Equation 1:

$$\text{ETC Field} \rightarrow \dot{Q}_{\text{useful}} = \dot{m}_c C_{p,c}(T_{co} - T_{ci}) \tag{1}$$

Where:

- $\dot{m}_c$ = mass flowrate of heat transfer fluid in collector field (kg/s)
- $C_{p,c}$ = specific heat capacity of collector heat transfer fluid (kJ/kg-K)
- T_{ci}, T_{co} = temperature in and out of collector field (K)

The mass balance across the effects of Multi-effect distillation unit is given as

$$\dot{m}_{ww} = \dot{m}_{d2} + \dot{m}_{d3} + \dot{m}_{dc} + \dot{m}_{b3} \tag{2}$$

Where:

- $\dot{m}_{ww}$ = mass flowrate of wastewater (kg/s)
- $\dot{m}_{d2}, \dot{m}_{d3}, \dot{m}_{dc}$ = mass flowrate of distillate from effect 2, 3 and condenser (kg/s)
- $\dot{m}_{b3}$ = mass flowrate of brine from effect 3 (kg/s)

The energy balance across the various effects of the MED unit and the condenser is given as

$$\text{Effect 1} \rightarrow \dot{Q}_{\text{req,E1}} = \dot{m}_{ww} C_{p,ww}(T_1 - T_{ww,o}) + \dot{m}_{v1} h_{fg@T_1} \tag{3}$$

$$\text{Effect 2} \rightarrow \dot{m}_{v1} h_{fg@T_2} + \dot{m}_{v1} C_{p,ww}(T_1 - T_2) = \dot{m}_{v2} h_{fg@T_2} \tag{4}$$

$$\text{Effect 3} \rightarrow \dot{m}_{v2} h_{fg@T_3} + \dot{m}_{v2} C_{p,ww}(T_2 - T_3) = \dot{m}_{v3} h_{fg@T_3} \tag{5}$$
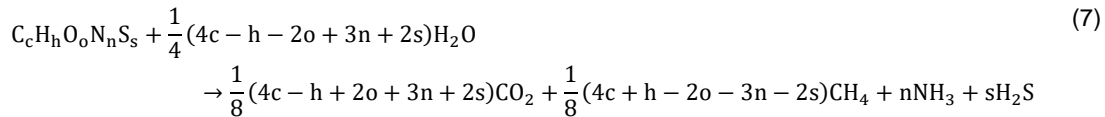
$$\text{Condenser} \rightarrow \dot{m}_{v3} h_{fg@T_c} = \dot{m}_{ww} C_{p,ww}(T_{ww,o} - T_{ww,i}) + \dot{m}_{fw} C_{p,fw}(T_{fw,o} - T_{fw,i}) \tag{6}$$

Where:

- $\dot{m}_{v1}, \dot{m}_{v2}, \dot{m}_{v3}$ = rate of water vapour formation in effects 1, 2 and 3 (kg/s)
- $C_{p,ww}, C_{p,fw}$ = specific heat capacity of wastewater, feed water recirculating from cooling tower (kJ/kg-K)

139

- T_1, T_2, T_3= operating/ boiling point temperatures of effects 1, 2 and 3 (K)
- $T_{ww,i}, T_{ww,o}$= temperature of wastewater in and out of condenser (K)
- $T_{fw,i}, T_{fw,o}$= temperature of feed water in and out of condenser recirculating from cooling tower (K)
- $h_{fg@T}$= latent heat of evaporation/ condensation of water at temperature T (kJ/kg)

To estimate the products of anaerobic breakdown of organic matter ($C_cH_hO_oN_nS_s$) in biogas digester, Buswell proposed an equation as follows (Abarghaz et al., 2011)

$$C_cH_hO_oN_nS_s + \frac{1}{4}(4c - h - 2o + 3n + 2s)H_2O \qquad (7)$$

$$\rightarrow \frac{1}{8}(4c - h + 2o + 3n + 2s)CO_2 + \frac{1}{8}(4c + h - 2o - 3n - 2s)CH_4 + nNH_3 + sH_2S$$

Where:

- c, h, o, n, s = molar proportion of mass fraction of carbon, hydrogen, oxygen, nitrogen and sulphur

Table 14: Design parameters of present system

Parameter	Value	Parameter	Value
Duration of operation	5 h	Length of each collector	1.76 m
No. of effects	3	Space between modules of each collector	0.035 m
Wastewater inlet temperature to condenser	30 °C	Diameter of absorber tube and outer glass tube	0.051m & 0.069 m
Wastewater salinity	2000 ppm	Temperature of water in to collector field	80 °C
Area of each evacuated tube collector	2.27 m^2	Temperature of water out of collector field	90 °C
Number of tubes in each collector	12		

4. RESULTS & DISCUSSION

In this system, for the designed recovery rate of 15% from effect 1, the preheated wastewater at 0.217 kg/s and 50ºC should be heated to T_1 of effect 1 (~70ºC) and supply heat required for latent heat of vaporization. This total amount of heat required by evaporator of effect 1 was found to be 94 kW. For the proposed plant location of Chennai (13.0827 ºN, 80.2707 ºE), India, the average global solar radiation and ambient temperature around the year is presented in *Figure 22*. In the month of April, by maintaining the temperature drop of collector fluid inside evaporator as 10ºC, the required heat load can be met by the solar ETC field of 205 m^2 with a fluid flowrate of 2.239 kg/s. This led to the formation of 0.033 kg/s of pure water vapour and 0.184 kg/s of leftover wastewater in effect 1 which was supplied to effect 2. In effect 2, the latent heat of condensation of vapours and sensible heat drop to reach the operating conditions was used to evaporate wastewater recirculated from previous effect. As the process continued, the complete mass balancing of all the effects and condenser are represented in Figure 24. In the condenser, the vapour entering at 0.038 kg/s and 50ºC from effect 3 needed to be condensed by removing 90.18 kW using low temperature water flowing through condenser tubes. The wastewater entering the condenser at 0.217 kg/s and T_{amb} (37ºC) received sensible heat and raised to a maximum of 50ºC which could only remove 11.65 kW from the vapour. The remaining 78.53 kW energy could be removed by circulating feed water from the cooling tower at 2.381 kg/s and 42ºC. A small fraction of flashing occurred in effect 2 and effect 3 due to a sudden drop in operating pressure and temperature which was 0.0034 kg/s in effect 2 and 0.0026 kg/s in effect 3. The distillate recovery rate and daily distillate yield from the MED unit when operated in various months around the year is presented in Figure 23. The annual distillate yield from the system when operated for 300 days was found to be 13.22 tons.

When it came to semi-solid waste treatment, from the proximity analysis (wt. %), the average composition of human faeces was 77% moisture and 33% dry matter. From the ultimate analysis (% dry basis), the composition of carbon was 50.83%, hydrogen was 6.8%, nitrogen was 4.09%, oxygen was 20.91% and ash was 17.37%. Based on the ultimate analysis, the chemical composition of human faeces can be written as $C_{0.042}H_{0.068}O_{0.013}N_{0.003}S_0$. The percentage of carbon in the dry matter was calculated as 33.3% whereas the percentage of CH_4 (reduced carbon, which contains energy value) and CO_2 (oxidised carbon, which does not contain energy value) in the biogas were calculated as 59.9% and 40.09%. Among the daily waste generation, the dry matter present in the 160kg faeces was 36.8 kg. The amount of carbon (33.3%) present in dry matter was 12.25 kg. Considering 70% biodegradation of carbon, the amount of carbon converted to biogas was 8.59 kg. Of this, only 59.9% carbon was converted to

methane which is 5.14 kg. Considering the typical calorific value of methane as 50 MJ/kg, the energy available in biogas produced per day was 256.9 MJ. When operating the system around the year, the amount of methane generated per annum (365 days' operation) was 1875.37 kg along with 55.26 tons of organic fertilizer. The mass balance across all the components of the system is represented in Figure 25.
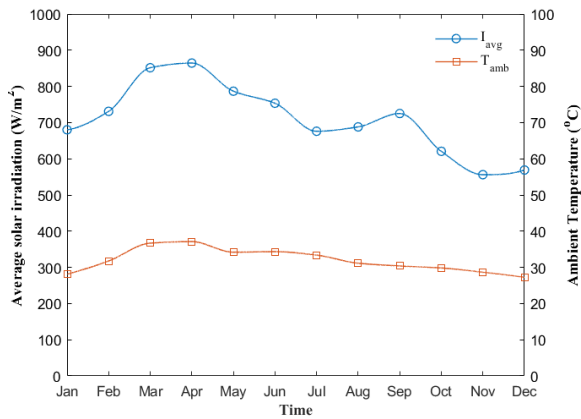

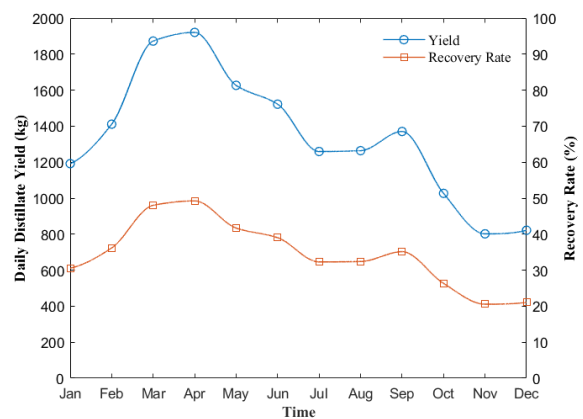*Figure 22: Variation of average solar irradiation and ambient temperature around year*

Figure 23: Variation of daily distillate yield and recovery rate around year
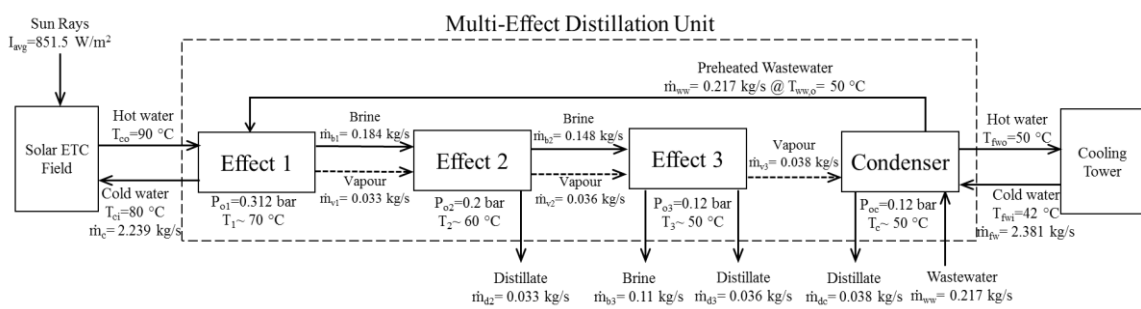

Figure 24: Flow diagram and mass balance across effects of multi-effect distillation unit
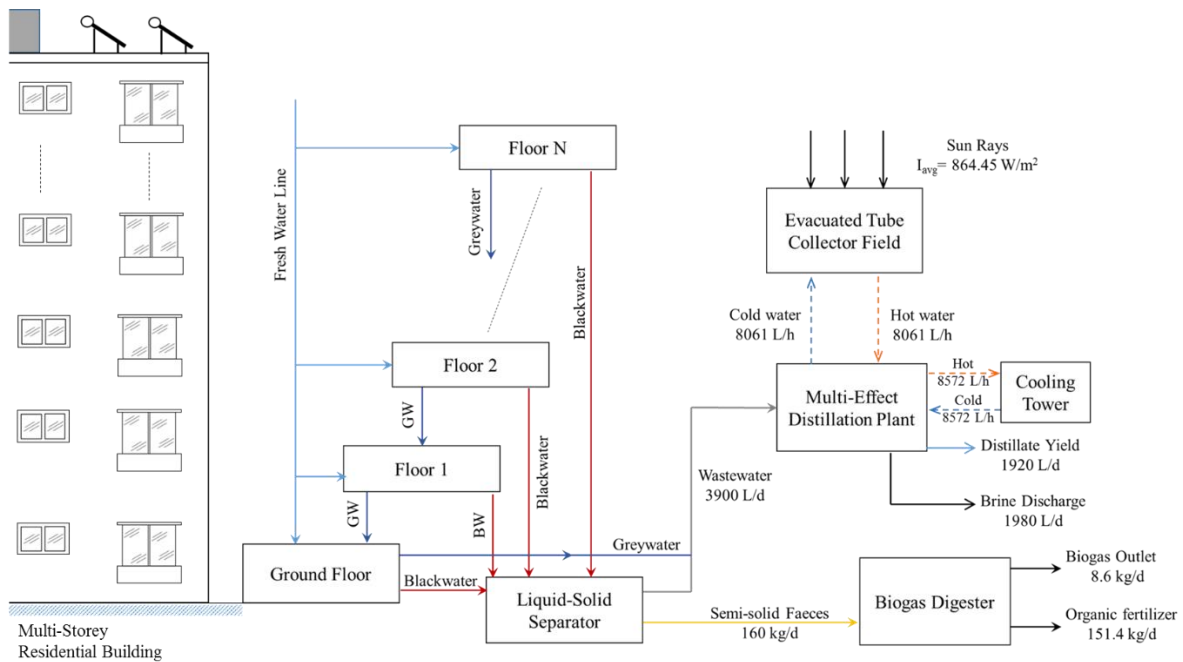
Figure 25: Flow diagram of the system representing mass balance across components.

5. CONCLUSIONS

In the present work, the viability of blackwater treatment using solar thermal and biogas sustainable technologies was studied by using a developed mathematical model. When the MED unit was supplied with 3,900 litres of wastewater, the unit delivered a maximum distillate yield of 1920.8 L with a recovery rate of 49.24% in the month of April. This distillate could be further treated and reused for human activities in the same residential building thereby reducing demand. With constant waste loading, the biogas digester was found to generate 5.14 kg methane which was significant and could be used for cooking and other energy requirements of the building.

6. REFERENCES

Abarghaz, Y., Mali, M., Werner, C., Bendaou, N. and Fekhaoui, M., 2011. Evaluation of formulas to calculate biogas production under Moroccan conditions. Sustainable Sanitation Practice, 9, pp.18-23.

Andriani, D., Wresta, A., Saepudin, A. and Prawara, B., 2015. A review of recycling of human excreta to energy through biogas generation: Indonesia case. Energy Procedia, 68, pp.219-225.

Catrini, P., Cipollina, A., Giacalone, F., Micale, G., Piacentino, A. and Tamburini, A., 2018. Thermodynamic, exergy, and thermoeconomic analysis of multiple effect distillation processes. In Renewable Energy Powered Desalination Handbook (pp. 445-489). Butterworth-Heinemann.

Moradi, M., Ghorbani, B., Shirmohammadi, R., Mehrpooya, M. and Hamedi, M.H., 2019. Developing of an integrated hybrid power generation system combined with a multi-effect desalination unit. Sustainable Energy Technologies and Assessments, 32, pp.71-82.

Morin, O.J., 1993. Design and operating comparison of MSF and MED systems. Desalination, 93(1-3), pp.69-109.

Reddy, K.S., Sharon, H., Krithika, D., & Ligy, P., 2018. Performance, water quality and enviro-economic investigations on solar distillation treatment of reverse osmosis reject and sewage water. Solar Energy, 173, pp. 160-172.

Sai, P.V. and Reddy, K.S., 2022. Techno-enviro-economic investigations on self-sustainable solar powered blackwater treatment system. Solar Energy, 231, pp.297-316.

Sharon, H. & Reddy, K.S., 2015. A review of solar energy driven desalination technologies. Renewable and Sustainable Energy Reviews, 41, pp.1080-1118.

Tilley, E., 2014. Compendium of sanitation systems and technologies. EAWAG.

#348: Evolution of the solar-home-system (SHS) in rural Bangladesh via empowering an underprivileged school – a pilot project

Fahad HAIDER[1], Shah HAIDER[2]

[1] Engineering, Management and Infrastructure (EMI) Consultant, Sydney, Australia, fahad@emi-consultant.com
[2] Engineering, Management and Infrastructure (EMI) Consultant, Dhaka, Bangladesh, szhaider@emi-consultant.com

Abstract: There has been a very common scenario in almost every rural state of Bangladesh regarding aspects of electrification, empowerment and digitisation. Prior to the Covid-19 pandemic, the population growth rate in Bangladesh was up to approximately 8% and is one of the most densely populated countries in the world, but with insufficient electricity production capacity. Over 6 million, mainly DC-Solar Home Systems (SHS) have been deployed since 2003, which was the largest national program in the world for off-grid electrification. However, as a "modern developing country", as of 2022 under a different program, the Bangladesh National Grid swiftly reached 100% of the country, rendering most of these DC-SHS redundant. A solution has been designed to help the rural areas connect to electricity and digital platforms at a very economical and sustainable way, whilst upgrading the design to AC to cater to grid integration. A pilot low-capacity (750Wp) hybrid SHS was designed and setup in a rural, underprivileged school. The practical outputs of this project were evaluated in terms of technical, environmental, social, financial, and educational dimensions, while also providing essential insights into the adoption of such a system. The results have been overwhelmingly positive, with the solar fraction, i.e., the effectiveness of the SHS, found to be 97.3% in the first month, amongst other socioeconomic benefits. With a majority of the DC-SHS ranging from 50-150W, an effective solution could be to combine the PV panels from those existing and unused systems to make up at least 300W. At this wattage, they could be converted to AC via accessible solar inverters with acceptable conversion efficiency and hence be grid connected. The Sustainable Development Goals (SDG), SDG7: Affordable and Clean Energy and SDG4: Quality Education have also been inherently achieved. Finally, this solution can cater to any rural area in any country that is expanding its national grid, which can subsequently impact millions of households and institutions.

1. INTRODUCTION

The energy transition is explicably regarded as a promising opportunity for the economic development of rural areas, particularly in developing countries. This is made possible with the siting of decentralized and small-scale renewable energy (RE) facilities. However, instead of cultivating further the productive link between energy transition and rural development, they seem to have been taken for granted, thus leading to a lack of effective utilisation. Hence, although rural development through the implementation of renewable energy had exceedingly high expectations, its potential has remained largely unfulfilled (ECA, 2018, p.10; OECD, 2012, p.3). Thus, catalysing projects need to be established in the Global South, particularly in rural and remote areas that accelerate the energy transition whilst also using renewable energy to contribute to marked development. At the overall policy level, the development of RE in rural areas has received explicit acknowledgement. However, although on paper it may appear straightforward, the reality has not been as easy, with various evaluations underlining the need for an approach that is well adapted to local conditions and focuses on the competitiveness of rural areas in order to maximize the benefits (Clausen and Rudolph, 2020, p.1).

According to the Global Climate Risk Index 2021, Bangladesh is one of most vulnerable countries in the world to suffer from the impacts of anthropogenic climate change (Germanwatch, 2021, p.13). With the country's recent growth rate of up to approximately 8% before the Covid-19 pandemic (World Bank, 2022a), it can also be regarded as a "modern developing country". Particularly in the energy sector, although the country has been 100%, entirely electrified as of 2022, there is plenty of load-shedding/blackouts, with many rural areas without power for as long as 10 hours a day. Another major concern is that Bangladesh also had the largest national program in the world for off-grid electrification (Cabraal *et al,* 2021, p. xviii): over 6 million, Solar Home Systems (SHS) have been deployed since 2003. This cumulatively has a total capacity of over 789 MW (The Daily Star, 2022), and since they are off-grid and mostly low capacity, they use direct current (DC). Unfortunately, upon the arrival of the National Grid, almost all of these DC-SHS have been rendered redundant. This is because the consumers prefer to use alternating current (AC) grid electricity as it does not have any capacity restraint and the average load uses AC as well, thus forgoing the need to purchase DC specific items. On the basis of the above structures and scenarios, a solution was implemented by the authors for the rural development of Bangladesh using solar energy to generate electricity to enhance the quality of education by means of technology. The design was technically uncomplicated to install, economical and at the same time was upgraded to AC to cater for the grid integration.

A pilot, low-capacity (750Wp) AC Hybrid SHS was designed and setup in a rural, underprivileged school with 110 students. A low-powered, low-cost computer (Raspberry Pi 4) was also setup to enhance the education experience (Nuñez-Unda *et al,* 2018) that ran with the solar. The school was located in Netrokona, Mymensingh, north of Bangladesh. It is one of the most poverty-stricken and underdeveloped areas, also prone to floods and storms, but with good solar irradiation, established during the feasibility assessment. The practical outputs of this project were evaluated in terms of technical, environmental, social, financial, and educational dimensions, while also providing essential insights into the adoption of such a system. The results have been overwhelmingly positive, with further projects already in the pipeline. This system produced clean electricity during the day, reduced electricity bills and provided power during blackouts and at night. Sustainable Development Goals (SDG), SDG7: Affordable and Clean Energy and SDG4: Quality Education were also inherently achieved. This system could be implemented in any institution, business and dwelling where the load demand is not expected to shoot up sharply, e.g., for installing expensive air conditioners. It could also be applied to any country that is expanding its national grid. Various countries like Nigeria (African Development Bank, 2019), Uganda (World Bank, 2022b), Viet Nam, Philippines (Black & Veatch, 2021), Chile (Tractebel Engie, 2022), Peru (BNAmericas, 2022) and many other countries all over the world are involved in grid expansion projects. Grid expansion is definitely lucrative for a developing country since it signifies development, provides ease of electricity usage and accommodates good selling-points locally and internationally. Therefore, the design executed in this study could be implemented in the millions of existing DC-SHS systems anywhere in the world to convert it to Grid Connected AC-Systems, with some technical requirements and limitations as further explained.

2. GOAL AND OBJECTIVES

The key goal for this project was to provide a clean and decentralised renewable energy system to empower and modernise a rural, disadvantaged school with technology. The objectives pertaining to the photovoltaic (PV) system (Figure) were providing the school with energy security and sustainability, as well as helping attain SDG7 and SDG4. As a key technical objective, the practicality of such a low-capacity AC output system implemented in real life was tested, to validate a solution for the conversion of the unused DC-SHS. Finally, a low cost, off-the-shelf AC Smart Switch (that was mainly used to remotely switch on and off items), that also had power monitoring features, was discovered locally and tested as a monitoring device. Adding to the PV system, the highly efficient Raspberry Pi 4 computer was also installed to easily run from the electricity generated via solar. Secondary objectives with the computer were to build technological capacity, contribute to SDG4 and cater to digitisation for the students. This paper mainly focuses on the PV system and its corresponding objectives, with emphasis on the technical

design and socioeconomic benefits. Thus, the overarching goal was to significantly improve the school, while also demonstrating the evolution of the SHS in rural Bangladesh from off-grid DC to grid-connected AC.
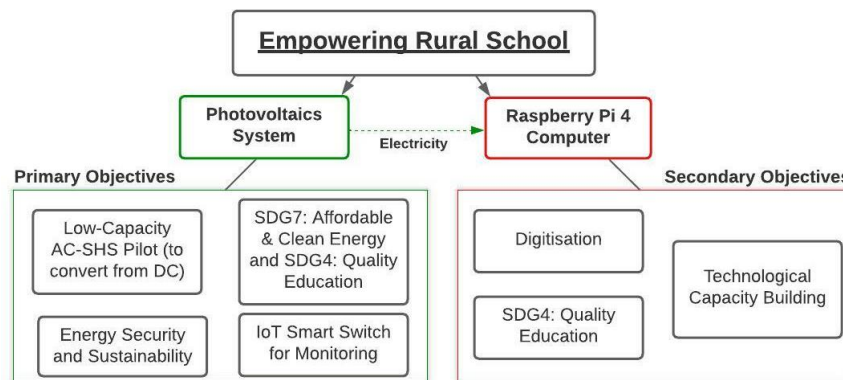

Figure 1: Primary and secondary objectives for project

3. RELATED WORK

Most of the SHS that has been researched can be categorised into two types: the majority were off-grid systems of varying capacity and a few were on-grid. In Sabah, Malaysia, a 20kWp off-grid system was installed with a 27kVA diesel generator (Mahmud, 2011). The Asian Development Bank (ADB) supported the installation of solar panels in a similar project in off-grid schools in Punjab and Khyber Pakhtunkhwa provinces of Pakistan (ADB, 2022). Understandably, there are numerous off-grid solar projects for schools, healthcare units, businesses and so on in developing countries where the local grid is difficult to reach.

For on-grid units however, the results were rather mixed. In Chile, a 6.76kWp on-grid system was installed, sized as per their requirements (Torres *et al.*, 2019). However, it did not cater for blackouts and thus did not have backup batteries. Kumar, Subathra, & Moses, 2018, presented a 95kWp on-grid system, also without batteries, and so it was grid-tied. In Hyderabad, India, solar-powered school pilot projects were initiated and the study evaluated "the various institutional challenges and failure relating to on-grid project models". It also presented the feasibility and implementation of off-grid small scale rooftop solar systems (2-5kWp) (Jain and Horam, 2013). Zhu & Yan, 2018, established two solar PV micro-grid systems to examine and investigate their operation abilities. These were grid-connected, had battery storage and the solar panels were 6.36kWp. Although the capacity was still high as per the requirements of this study, the findings were helpful regarding performance.

The main study where the need for a low-cost, grid-connected system to promote rural electrification for small load applications (such as in primary schools) where the grid was unreliable has been acknowledged in Patil & Todkar, 2019. A 100Wp grid-connected PV system design and model simulation were presented, based on experiences in a school in Anganwadi, rural India. It also, however, did not include batteries, which from a real-world perspective is mandatory due to grid reliability issues in the target sites. Taking information from this paper, a low-capacity AC inverter was sourced with specific characteristics and acceptable efficiency explained in the section Design Framework, which was implemented in an actual school. This was where the originality of this study is highlighted: for a low capacity, grid connected PV system with battery backup, for consumers with less load.

4. DESIGN FRAMEWORK

The following are the vital combination of characteristics which differentiate this project from others and lead it forward in comparison. This has been engineered specifically for the rural setting in a developing country with grid availability. The requirements are as follows:

1. Lowest cost (budget of only US$1200 for full PV System)
2. <1kW Capacity with AC output and battery backup (sizing based on Load Assessment)
3. Priority usage of electricity of PV->Grid->Battery for load (i.e., use PV first, if unavailable then use grid, and if grid is unavailable as well, use batteries)
4. Use PV to run load directly (not charge battery first and then discharge batteries to load)
5. Remote Monitoring
6. Electricity not sent to grid (Uni-directional system)
7. Protection focused with appropriate MCB/Fuses placements
8. Anti-Theft Mechanisms

Local companies have not been found to practise this combination of requirements in Bangladesh, which is why there are rampant complaints among consumers that PV systems break in a very short span of time, i.e. within 1.5 years. Rural areas, from a technological standpoint, along with standard practices, are rather neglected.

A low-income household or institution (which is the target market) will have a load of around 1kW. The system output is in AC. For this study, the selected school only had one large room. The system was designed (and rather oversized to provide leeway for growing demand) at 750Wp but predicting the load pattern in the future accurately was challenging. In the near future, if the amount of load shedding in that area decreases, the system will still be effective in terms of operation using green energy as well as a decentralised generation source to reduce electricity bills. This is in stark contrast to the DC-SHS that have been installed previously, with their uses tremendously minimised after the consumer acquired grid electricity.

A lot of time and resources were spent finding the ideal inverter for the budget, as the inverter is the brain of the system. Most reputed companies mainly provided for higher capacity (3kW+) inverters. A Solar Instant Power Supply (IPS) Inverter called UTL Gamma+ was finally used, at only US$125, and which also catered to all the requirements mentioned. It had Maximum Power Point Tracking (MPPT) solar charging. The AC Output was the more efficient Pure Sine Wave and not Pulse Width Modulation (PWM). The priority setting of the inverter was at PV->Grid->Battery. Thus, the output for load properly utilised PV, reduced electricity bills and also increased battery longevity. This setting can also be changed to PV->Battery->Grid to reduce the grid electricity usage further, but that can lead to faster battery degradation. Finally, the battery low-cut voltage (i.e., the battery voltage at which it stops discharging) was set to 11.5V, which was the maximum that could be set, that entailed a Depth of Discharge (DoD) of 70%, although desired was 50%.

For backup, 2x 100Ah batteries were connected in parallel, and at 12V, the total energy was 2400Wh. Assuming the DoD at 70% as mentioned, the total usable energy was at (2400Wh*70%) = 1680Wh. There were three LED lights at 10W each, two fans at 80W each and the computer and accessories were at around 100W. This meant the maximum load was at (10W*3 + 80W*2 + 100W) = 290W. At that load, the battery could provide backup for (1680Wh/290W) = 5.8 hours by itself. However, most of the time, only one light and one fan would be switched on (on average days during school hours), entailing a load of 90W. Thus, at that load the battery could last for up to 18.7 hours. The computer was used around one hour per day to provide adequate training to the students.

Extra emphasis was put on including remote monitoring in order to routinely check performance and identify any issues early. For low capacity, cheap inverters, this was not available preinstalled as was common with the more expensive ones. Thus, two AC Smart Switches with data logging called Sonoff POW R2 were installed, at a total cost of only US$35. Their Power Rating was 3.5kW maximum resistive load. The first "switch" measured the grid electricity used and the second measured the total output from the inverter (i.e. from the PV, batteries and grid). The difference gave the electricity generation via PV/batteries. Wi-Fi was mandatory with this as it was an Internet of Things (IoT) device. Figure illustrates how the smart switch worked and given the low cost and reliable performance as shown later in 7 and 8, this should be used further for these types of applications.
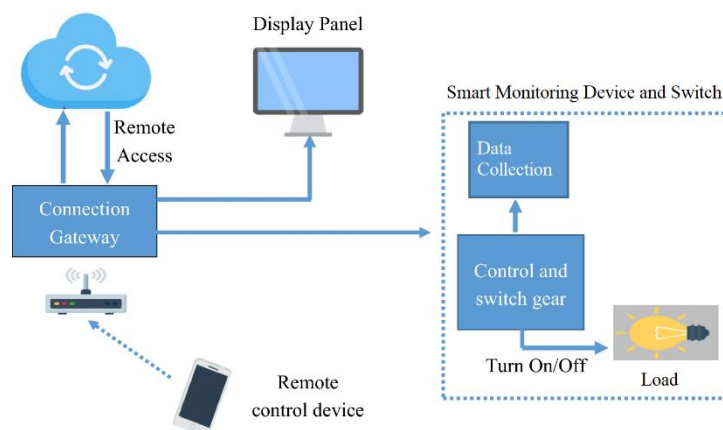

Figure 2: Flowchart of Smart Monitoring Device and Switch (Kumar, Tiwari & Zymbler, 2019)

As PV systems are expected to last for decades, some internal components might eventually breakdown. This is why specifically positioned protection Miniature Circuit Breakers (MCBs) and fuses were placed to ensure the system working as efficiently as possible, whilst also minimising any potential damage to the inverter and battery. Anti-theft steps had also been prompted due to increased risk in the particular area, manifested through online monitoring and triggers, and "Danger- do not touch" signs.

For net-metering, due to the oscillating nature of PV output, grid integration requires stable and steady power injection with good Power Quality (PQ) (Babu *et al.*, 2019). Low-capacity PV systems are unable to provide this stability. They are also single-phase. This is why it was mandatory that the system did not send any electricity back to the grid, as it is incapable of maintaining the voltage, harmonics and so on, which may lead to imbalance. Anti-islanding protection also had to be implemented in that case. Hence, the output from the inverter chosen was only uni-directional, as opposed to being bi-directional, meaning unavailability of net-metering. A diagram of the system is shown in Figure . The DC sources of power were the PV and batteries. These were connected to the inverter, which powered the load in AC. Grid connection was uni-directional, with no electricity flowing back.
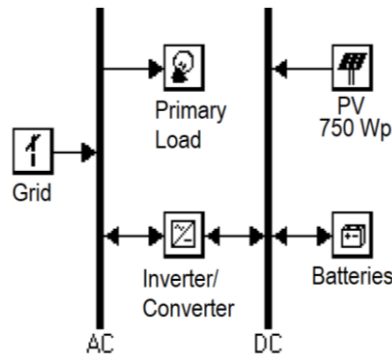

Figure 3: Diagram of Hybrid PV System

The single line diagram (SLD) (Figure) was designed keeping the rural setting in mind. It started with 5x 150Wp PV panels connected in parallel for maximizing the input as mentioned in the datasheet of the inverter (Figure 5:). The system current was additive. The short circuit current (I_{sc}) for each panel was 8.4A. Thus, in case there was a short-circuit in one panel, it could draw all (8.4A*5) 42A towards that short-circuited panel, causing a fire hazard. The roof of the school was made of metal, increasing the risk of shock hazard. As a result, 10A fuses were placed after each module, to break the circuit as soon as the current exceeded 10A. For the MCB that followed them, as per the standard, adding 25% to the total current of 42A bringing the total to 52.5A, and so the nearest available MCB of 63A was placed at the cumulative PV output. The 1kV, 20kA MCB was for lighting protection. A 6A AC MCB was connected to the grid input to stop overdrawing from the grid, for e.g. in case of malfunction and while charging the battery. The battery had a 40A MCB as the inverter charged the battery at a maximum of 40A. Finally, a 3A AC MCB was placed before the load to discourage the consumer from plugging in high-powered appliances like water pumps, etc., which would damage the inverter.
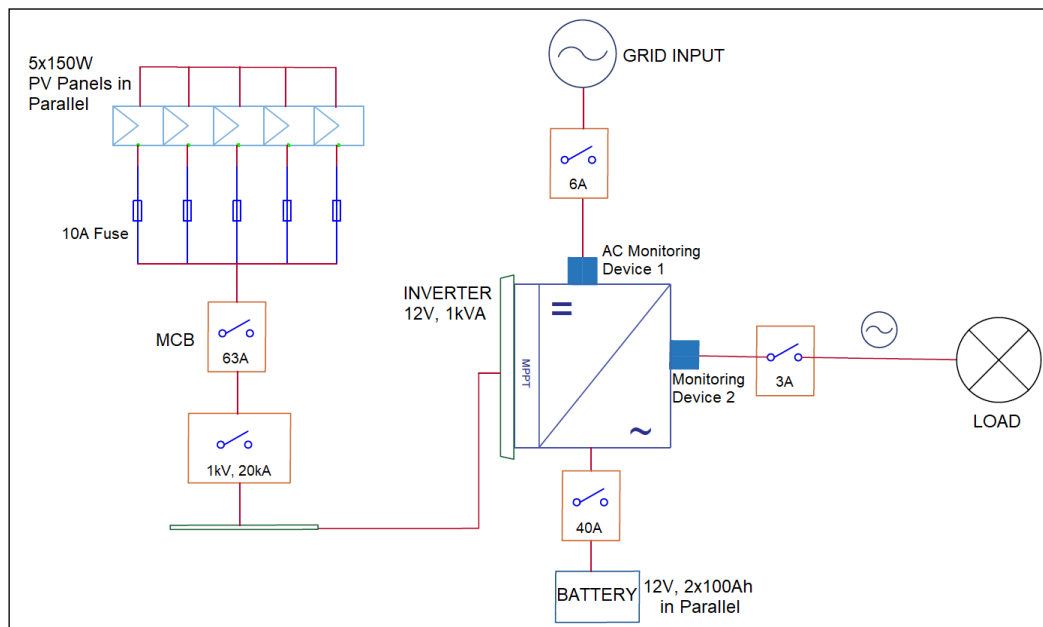

Figure 4: Single Line Diagram (SLD) of Hybrid PV System

Training was also provided to the school management on solar hybrid technology, maintenance for cleaning the panels and instruction to not misuse energy. All loads would only be turned on when required. For example, if during class there was enough sunlight to light the room, LED lights were not to be used.

148

Parameters (Solar)		
Switching Element		Mosfet
Type of Charger		MPPT
SPV Chgarging Voltage (TUB)	Boost	15V ± 0.2V (Each Battery)
	Float	14.2V ± 0.2V (Each Battery)
SPV Charging Voltage (SMF)	Boost	13.7V ± 0.2V (Each Battery)
	Float	13.7V ± 0.2V (Each Battery)
SPV Charging Current		18A ± 2A
Battery Charging Method 3 Stages		Bulk/Absorption/Float
Efficiency		>94%
Input Voltage Range (Min - Max) Voc		15V-45V
Maximum PV Power Recommended (1000W)		(150/160*6)/ (315/320/325*3) Parallel

Figure 5: Datasheet of Inverter with suggested PV configuration (from hard copy)

5. RESULTS AND DISCUSSION

Upon installation, it was necessary to establish how much the system essentially helped the students and school. The 750Wp PV system with 200Ah batteries was set up as elaborated earlier. To run with electricity, a Raspberry Pi 4 computer with all devices (mouse, keyboard, speakers), Wi-Fi, 2x AC monitoring devices, 2x ceiling fans and other smaller items were installed (the school only had LED lights). The project setup is shown in Figure 6. First the technical results of the PV system were verified, especially after all the new load, followed by the socioeconomic impact.

Figure 6: Project setup: Inverter, Batteries, Smart Switches and MCBs

5.1. Technical outcomes

Figure 7 shows the output from the smart switches in real time, displaying the electricity usage. For the example provided, it can be observed that the electricity usage from the grid (top) was 0W, but the output from the inverter (bottom) was 31.67W at that instant, which was provided from the PV or batteries.
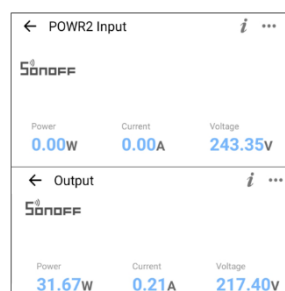
Figure 7: Smart Monitoring: Grid Input (Top) and Inverter Output (bottom)

Figure visualises the daily consumption for the month of April, 2022, which was the first month of operation. The total electricity usage for the month was 9.79kWh, whereas the energy from the grid was only 0.26kWh. Solar fraction is the amount of energy provided by the solar system divided by the total energy required, including from the grid (Mahmud, 2011, p.7). From the data for the month of April, the solar fraction was as high as 97.3% (i.e. (9.79-0.26)/9.79*100%). This signified the success of the project for utilising PV along with battery backup.

Figure 8: Total Electricity Usage (Left) and Grid Electricity Usage (Right) for April '22

5.2. Socioeconomic outcomes

Only via modernising a single school, various socioeconomic outcomes were observed that had an extensive impact throughout the whole community. Some of the notable socioeconomic findings and observations were:

1. *Modernising rural school and the youth:* The system was setup in one of the most poverty-stricken parts of Bangladesh. The students and management readily accepted the new technologies, providing them with instant, 24/7 electricity (and a computer with Wi-Fi). The concept of using said technology increased the enthusiasm of the students and improved the school's environment. As electricity has become secure, digital education (via the computer) is always available, with the students practising whenever they are being allowed. Over time, this will improve the quality of education, making the children adaptable and confident to digitisation as they grow older. In the future, income generation through existing general line methods will decrease and new trends will be more digital (as evident in the developed countries), so this is a mode of preparing the youth. This means, due to the electrification from the solar panels, more residents in this rural village are getting educated and are creating a potential future where they are not obligated to resign to being crop farmers (Figure 9).

Figure 9: Installed solar panels with school children

2. *Ancillary items facilities:* Not just providing electricity, but donating the two ceiling fans were timely, with both already running at almost full speeds for the over 110 occupants. Even after school, it was observed that students were staying back rather than returning home in the sweltering heat, as fans were not available in their homes. An LED light was also installed outside which was switched on at night, thus providing greater security in an otherwise poorly lit area (Figure). All of these have been facilitated due to the availability of electricity. Figure 11 shows students using the computer and fan.

Figure 10: No Lighting at Night in School Area

3. *Teacher Benefits:* All teachers agreed that the technology provided great benefit to the learning environment. The teaching and learning process had also been made easier, as teachers could use interactive teaching methods using the computer.
4. *Financial Savings:* Approximately BDT300 or US$3.2 was saved per month from not having to pay the electricity bills, which accumulated to BDT3600 every year. This money could instead be used for the maintenance of the school and in purchasing stationary such as chalk, pencils, books and so on.

Figure 11: Students using the Computer and Fan

5. *Increased Working Hours:* As observed, children were more encouraged to go to school if there was electricity available along with the corresponding facilities. This meant that both their parents could go to work as they did not have to leave their children at home for a significant period of time. This should lead to more income for the family.
6. *Ownership and Responsibility:* Focusing on the Development Effectiveness Principles (EPRS, 2020, p.2), as this project provided instant, highly positive results, the ownership and responsibility were automatically taken by the school authorities. However, for lasting reliability on a local level, forming inclusive partnerships and building relations were vital - with the school management, students, their parents, the people living nearby, local solar installers, technicians, workers and so on. Acquiring a school with accountable management was key, as with transparent communication, it led to understanding and focusing on the development priorities (SDG4 and SDG7) as well.
7. *Energy Transition and Development*: The success of this project showed that energy transition and development of rural areas via renewable energy can go hand-in-hand with proper preparation and cooperation, despite the challenges in the field level as mentioned in the Introduction. It is also imperative to have a low-level approach – to communicate directly with the beneficiaries to understand their requirements and also for recommendations and adaptation to changes during implementation.
8. *Electricity during Storms and Floods:* PV changes lives via rural electrification and improves networks, with benefits far outweighing the cost. Not just the school but the whole community has been utilising the

services. Netrokona is a storm and flood prone area, which is one of the key reasons for its underdevelopment. In May 2022, there was a severe storm there that damaged the transmission lines of the grid resulting in no electricity for almost 4 days. The school was used as a shelter at that time, where some of the families worst affected spent the nights in a safe environment. The whole village went dark at night due to the complete absence of electricity, but the lights and fans in the school, as well as the light outside were still powered, providing some security and solace to the residents.

9. *Role Model for Regional Development:* This school acted as a role model for the whole region. As the PV system produced green energy, other households or schools can realize that they too can contribute to significant improvements of the ecological situation and reduce carbon emissions. Further awareness-raising can be done by the school and pupils by disseminating more information.

10. *Green Energy Source:* As it is a completely green and renewable source of energy, and silent as well (as opposed to the more common diesel generators), it mitigates air and noise pollution.

11. *Learning from Experience:* An initial challenge was that the school was reluctant to try new technology, and also initiating the capital cost at the beginning was difficult. However, once up and running, the problem was solved. Adding to that, they had been led to understand that electricity was an important element for developing a community and therefore can bridge the development gap between the urban and rural areas in economy, education, lifestyle, communication and so on.

12. *Prospect of Scale:* The ease of installation of this tailored system and comparatively low cost made it highly scalable, provided the load was less than 2kW. The innovative, cost-saving features as per the requirements should also increase the lifetime of the system and optimize the output. This exact design (SLD has been provided in Figure 4) is ideal for schools, shops, medical and other institutions, dwellings/houses and so on with loads that are mostly lights, fans, computer, refrigerator, phone-chargers, etc. It also reduced the electricity bill significantly. Many other rural institutions have already shown a willingness to adopt solar energy or put their existing DC-SHS to use. If possible to implement at a larger scale, various advantages of renewable energy and community development will be even more prominent, potentially reaching a national level. Large scale advantages can lead to less pressure on an already strained electricity grid, improved balance of the Energy Trilemma (of energy security, affordability and sustainability) and reduced burden on the domestic oil/gas and US dollar reserve.

13. *Effective use of over 6 million idle DC-SHS:* This was one of the main underlying objectives of the project, to find a potential solution for the redundant DC-SHS. Most of these SHS in Bangladesh are around 50-150W (i.e., the capacity of the PV panels), and the smallest capacity for an AC Inverter (Solar IPS) with acceptable conversion efficiency available is 300W. A scalable solution could be to combine a few 50-150W PV panels to make 300W and over, and then fit the inverter to make it grid-connected. The price of the Solar IPS has been discussed and is inexpensive. This puts the DC-SHS to effective use, rather than lying idle and eventually being dumped into landfills.

This project used solar energy to modernize the entire school and greatly improve the quality of the students' education in a poverty-stricken community. As the various results of improved education take time to come to fruition, the benefits are eventually expected to increase even further.

6. CONCLUSION

Catering to the low load-profile of a grid-connected dwelling in Bangladesh, a 750Wp PV system was set up in a rural and underprivileged school, along with an energy-efficient computer. The school previously had only LED lights, and thus was modernised overnight and the technologies were warmly welcomed. Previous studies indicated that grid connected, low-capacity systems that efficiently utilise PV are difficult to implement, with generic systems usually starting from 3kW. However, many rural institutions and households do not require this much capacity. Thus, a smaller system was successfully designed and implemented with a Solar IPS inverter, accommodating all the technical requirements in a rural setting. The measurements and monitoring of the system showed the solar hybrid system was generating reliable power to meet the electricity demand of the rural school. The solar fraction was found to be 97.3% in the first month of operation. The availability of PV->Grid->Batteries prioritisation reduced the dependency on the grid, reduced the electricity bill and could also improve battery longevity. This pilot project describes how small-scale solar energy systems in places with grid availability can contribute to clean energy production in rural areas along with methods for mobilizing a sustainable lifestyle. Electricity is a sure way of enriching lives. Enabling continuous electricity through PV in a school for this case study has greatly improved the quality of education, thus also fulfilling SDG7: Affordable and Clean Energy and SDG4: Quality Education. This project is also highly scalable, due to its non-complexity and low cost. In Bangladesh alone, a country that is 100% electrified and has over 6 million off-grid DC-SHS, the provided design can convert the DC-SHS to AC. This puts them to actual use, as currently most of them are redundant. Many other countries are also expanding their grids, and again, millions of households in those countries have also been given access to similar DC-SHS through national or international development programs. Low capacity, grid-connected AC-SHS is a very important topic for developing countries that require more attention and implementation. This solution presented can connect those millions of off-grid systems to the national grid. It is replicable for any household or institution where the grid is available, the load does not exceed 2kW and the PV capacity is starting from only 300W. Importantly, the capital

cost of the conversion or even a new installation is relatively cheap, and the system has been proven to provide excellent results. Thus, through this pilot project, not only was a rural school significantly improved and empowered leading to numerous socioeconomic benefits, it also demonstrated the evolution of the SHS in rural Bangladesh from off-grid DC to grid-connected AC.

7. REFERENCES

ADB (2022). Powering Pakistan's Schools through Solar Energy. [online] Asian Development Bank (ADB). Available at: https://www.adb.org/results/powering-pakistans-schools-through-solar-energy.

African Development Bank. (2019). Nigeria Transmission Expansion Project Phase 1 (NTEP1).

Babu, P. C., Dash, S. S., Bayindir, R., Behera, R. K., & Subramani, C. (2016). Analysis and experimental investigation for grid-connected 10 kW solar PV system in distribution networks. 2016 IEEE International Conference on Renewable Energy Research and Applications (ICRERA). doi:10.1109/icrera.2016.7884441

Black & Veatch (2021). Asia Eyes Transmission Capacity Expansion. [online] Available at: https://www.bv.com/perspectives/asia-eyes-transmission-capacity-expansion [Accessed 28 Jun. 2022].

BNamericas (2022). At a Glance: Peru's 2023-32 Power Transmission Roadmap. [online] Available at: https://www.bnamericas.com/en/news/at-a-glance-perus-2023-32-power-transmission-roadmap.

Cabraal, A., Ward, W. A., Bogach, V. S. & Jain, A. (2021). Living in the Light: The Bangladesh Solar Home Systems Story. World Bank, Washington, DC. © World Bank. https://openknowledge.worldbank.org/handle/10986/35311 License: CC BY 3.0 IGO.

Clausen, L. T., & Rudolph, D. (2020). Renewable energy for sustainable rural development: Synergies and mismatches. Energy Policy, 138. https://doi.org/10.1016/j.enpol.2020.111289

European Court of Auditors (ECA), (2018). Special Report No. 05. Renewable energy for sustainable rural development: significant potential synergies, but mostly unrealized. [online] Available at: https://www.eca.europa.eu/Lists/ECADocuments/SR18_05/SR_Renewable_Energy_EN.pdf.

European Parliamentary Research Service (EPRS). (2020). Understanding Development Effectiveness. [online] Available at: https://www.europarl.europa.eu/RegData/etudes/BRIE/2017/599401/EPRS_BRI(2017)599401_EN.pdf.

Germanwatch, (2021). Global Climate Risk Index 2021. [online] Available at: https://reliefweb.int/attachments/b6a6928e-214a-3398-bc01-1460f32bb3ad/Global%20Climate%20Risk%20Index%202021_1.pdf

Jain, A. & Horam, P. (2013). Solar Powered Schools - a Pilot Project on Awareness for Decentralized Solar Energy Production in India. 10.13140/RG.2.2.22281.85602.

Kumar, N. M., Subathra, M. & Moses, E. (2018). On-Grid Solar Photovoltaic System: Components, Design Considerations, and Case Study. 10.1109/ICEES.2018.8442403.

Kumar, S., Tiwari, P. & Zymbler, M. (2019). Internet of Things is a revolutionary approach for future technology enhancement: a review. J Big Data 6, 111. https://doi.org/10.1186/s40537-019-0268-2

Mahmud, A. M. (2010). Evaluation of the solar hybrid system for rural schools in Sabah, Malaysia. PECon2010 - 2010 IEEE International Conference on Power and Energy, 628–633. https://doi.org/10.1109/PECON.2010.5697657

Moury, S., & Ahshan, R. (2009). A feasibility study of an on-grid solar home system in Bangladesh. Proceedings of 1st International Conference on the Developments in Renewable Energy Technology, ICDRET 2009, 92–95. https://doi.org/10.1109/icdret.2009.5454208

Nuñez-Unda, A., Vera, Á., Haz, L., Pinos-Medrano, V., Zurita, R. & Medina, S. (2018). The Raspberry Pi as a Computer Substitute at Elementary Schools in Developing Countries: A Pilot Experiment in Ecuador. MATEC Web of Conferences. 210. 04023. 10.1051/matecconf/201821004023

Organisation for Economic Co-operation and Development (OECD), (2012). Linking Renewable Energy to Rural Development. OECD Publishing, pp. 18–19. https://doi.org/10.1787/9789264180444-en.

Patil, P. & Todkar, R. (2019). Grid Connected Micro-inverter Based Solar PV System for Rural School Application. 449-453. 10.1109/RTEICT46194.2019.9016954.

The Daily Star (2022). Villagers Selling Solar Power to National Grid. [online] The Daily Star. Available at: https://www.thedailystar.net/news/bangladesh/news/villagers-selling-solar-power-natl-grid-3053376 [Accessed 30 Jun. 2022].

Torres, C. J., Cabrera, M. H., Morales, A. S. & Ramirez, A. G. (2019). Performance Evaluation of an On-Grid PV Installation in the Rural Foothill of Central Chile – Case Study. 2019 IEEE CHILEAN Conference on Electrical, Electronics Engineering, Information and Communication Technologies (CHILECON). doi:10.1109/chilecon47746.2019.8987998

Tractebel Engie (2022). Chile's biggest transmission project to enable transport of energy across 1,500 km. [online] Available at: https://tractebel-engie.com/en/references/chile-s-biggest-transmission-project-to-enable-transport-of-energy-across-1-500-km.

World Bank (2022a). GDP - Bangladesh. [online] Available at: https://data.worldbank.org/indicator/NY.GDP.MKTP.KD.ZG?locations=BD [Accessed 4 Aug. 2022].

World Bank (2022b). Uganda Grid Expansion and Reinforcement Project (GERP) - P133305. [online] Available at: https://projects.worldbank.org/en/projects-operations/project-detail/P133305 [Accessed 28 Jun. 2022].

Zhu, Y. & Yan, J. (2018). Performance of solar PV micro-grid systems: A comparison study. Energy Procedia. 145. 570-575. 10.1016/j.egypro.2018.04.083.

#364: Improvement of load ability in distribution systems using distributed generation

Mahmoud Zadehbagheri[1], Mohammad Javad Kiani[2], Nozar Rahimi[3]

[1] Department of Electrical Engineering, Yasuj Branch, Islamic Azad University, Yasuj, Iran
Ma.zadehbagheri@iau.ac.ir
[2] Department of Electrical Engineering, Yasuj Branch, Islamic Azad University, Yasuj, Iran,
Mj.kiani@iau.ac.ir
[3] Department of Electrical Engineering, Yasuj Branch, Islamic Azad University, Yasuj, Iran,
nozar4706@yahoo.com

Abstract: The traditional approach to delivering electrical power to end-users requires power to be generated by huge power plants where the voltage is increased to a desirable level using transformers. Then, electrical power is delivered via long-distance lines to the destination. After one or two stages of voltage reduction, consumers receive the delivered power. Recently, due to higher demand for electricity and higher outputs of generation units, small power companies are more likely to exploit the mentioned units in their distribution system near the consumers. These small units attached to the distribution systems are called non-concentrated generation or distributed generation. Nowadays, distributed generation plays a vital role in electrical distribution systems because of, for instance, the reliability improvement index, stability improvement and loss reduction. One main aspect of using distributed generation is to displace these resources in distribution networks. Load ability in distribution systems and its promotion are some keys in power systems. Up to now, displacement of distributed generation resources in order to promote the load ability of distribution system has not been discussed. It is obvious that displacement and usage of distributed generation using genetic algorithm improvement maximize the load ability in distribution systems. After the considered flowchart has been extracted, this method is used in IEEE standard 12-bus network. Results have shown the efficiency of the mentioned algorithm.

Keywords: load ability; voltage profile; loss reduction; distributed generation; distribution systems

1. INTRODUCTION

In the interconnected system, power generation is undertaken in a concentrated way via huge power plants. In the early years of interconnected systems evolution, this system had a 6-7% growth rate of electricity consumption per year. In 1970s, issues such as the oil crisis and environmental problems posed new obstacles for the power industry. In 1980s, these factors and economic changes led to load growth reduction of up to 1.6 to 3% annually. At this time, the expense of delivering and distributing electrical power increased significantly. Therefore, central generation by huge plants was impractical due to load growth reduction, higher payments for delivering and distributing electricity, environmental issues, technological changes and various legislations (Bajaj and Singh, 2021; Abbas et al., 2021). Some problems including environmental pollution, new transmission networks, technology development in industrialization of small-scale generation units compared with huge generation units have led to higher usage of small generation units called distributed generation (DG) which are mostly attached to the distribution network and do not need transmission lines. Studies conducted by research institutes such as EPRI have indicated that up to 2012 more than 25% of electricity consumption was generated by distributed generation. Across the United States and Europe distributed generation is considered to be a practical, financial and technical alternative for consumers and generators. (Haider et al., 2021; Xu et al., 2022). It also increases the reliability and creditability of power generation. In most countries, DG constitutes 10% of installed capacity of total generation. This value is above 30-40% for countries such as Netherland and Denmark and it is predicted to be up to 78% in a few countries including Australia by 2012.

1.1. Nomenclature:

VPII	Voltage profile improvement index
LLRI	Line loss reduction improvement index
DG	Distributed Generation
EIRI	Environmental impact reduction index
LTAPII	Line transmission apparent power improvement index
EIRI	Dynamic Programming
DNLP	Dynamic Non-Linear Programming
Eld	Electrical demand
ES	Electrical Storage
ESS	Energy Storage System

2. EVALUATION AND SELECTION OF INDICES TO INSTALL DG

2.1. Voltage profile index-VPII

One main problem in distribution networks is improper voltage profile. The effect of distributed generation units on voltage regulation can be positive or negative depending on the distribution system, characteristics of distributed generation units and the location selected to install distributed generation units (Azeroual et al., 2022). Because voltage is one the most significant factors in the power quality point of view, investigation of the effect of distributed generation units upon voltage has been emphasized. Accordingly, DG increases and retains voltage in an acceptable range in the consumer terminal. Using DG reduces the transmission line current and enhances load ability and finally leads to consumer voltage range boosting (Griffin, 2000).

$$\text{VPII} = \frac{\text{VP}_w/\text{DG}}{\text{VP}_{WO}/\text{DG}} \tag{1}$$

$$VP = \sum_{i=1}^{N} V_i . L_i . K_i \tag{2}$$

2.2. Line loss reduction index-LLRI

Using reduces the power transmission in lines and leads to loss reduction. Line loss is a significant factor in the condition of heavy loads such that the expenditure will be paid by consumers as a higher price for energy (Xu et al., 2022).

$$\text{LLRI} = \frac{\text{LL}_w/\text{DG}}{\text{LL}_{wo}/\text{DG}} \tag{3}$$

$$LL = \sum_{i=1}^{M} I_{Li} . R_i . D_i \tag{4}$$

2.3. Transmission line apparent power improvement index-LTAPII

Another advantage of using DG is aspect power reduction in transmission lines. This leads to higher load ability and prevents the need to install new lines and other equipment including transmission and distribution stations. Therefore, less money is spent although network is fed with higher lead (Kojovic, 2002; Barker and De Mello, 2001).

$$LTAPII = \frac{\frac{LTAP_{WO}}{DG}}{\frac{LTAP_W}{DG}} \qquad (5) \qquad LTAP = \sum_{i=1}^{M} I_i . V_j \qquad (6)$$

3. OBJECTIVE FUNCTION

In this problem, objective is defined in a way where the least voltage loss in network buses leads to higher capacity for the line (Bryant, 2000; Rogers, 2002).

$$BI = (BW_{VPI}).(VPII) + \left(\frac{BW_{LLR}}{LLRI}\right) + (BW_{LTAP}).(LTAPII) \qquad (7)$$

$$BW_{VPI} + BW_{LLR} + BW_{LTAP} = 1 \qquad (8)$$

4. GENETIC ALGORITHM METHOD

The most important optimization methods in order to solve the problems of displacement of distributed generation include sensitivity analysis, dynamic programming method, linear programming method, second order gradient method, Newton Raphson method and genetic algorithm method (Dianati, Song and Treiber, 2002). In order to conduct the genetic algorithm method for displacement of local plants, some points must be considered: objective function, network loss and network voltage. Loss is calculated according to the below equation (Borgrs and Falcao, 2006):

$$P_{Loss} = \sum_{i=1}^{n} P_{Gi} - \sum_{i=1}^{n} P_{Di} \qquad (9)$$

Where:
- n is the number of busses,
- P_{GI} indicates the generated power of the bus i and
- P_{DI} represents consumed power of the bus i.

At last, P_{Loss} is network active loss.

4.1. Using Genetic Algorithm Method

The main obstacles to using the first five methods are approaching local optimized point instead of general optimized point and requiring aid information such as second order gradient, Jacobean matrix and sensitivity matrix. A genetic algorithm was used to resolve the problem of dynamic programming. In the mentioned method, optimization was used according to natural selection and genetic rules (Wang, 2008; Borgrs and Falcao, 2006). Optimization starts with a series of data and follows a chain of numbers. Subsequently, the possibility to reach local optimized point is reduced. A genetic algorithm works with a collection of encoded parameters and begins to research a series point collection instead of one single point. In this condition, there is less possibility of reaching a false optimized point (Padilha and Harrison, 2006). This algorithm uses the main information of objective function and there is no need for aid information such as derivation of objective function. The operational method of genetic algorithm is encoding parameters, creating chains and copying them and finally transforming some parts of these chains. In the operational phase, there are three phases including duplication, splitting of two chains and creation of new chains along with mutation operator. Duplication is a process in which separated chains are copied according to their specific objective function. Objective function shows the appropriateness and optimization of what is to be maximized (Ijumba, Jimoh and Nkabinde, 1999).

5. PROBLEM CONSTRAINTS

Problem constraints are: limitation of power plants' generation power $P_{Gi}min < P_{Gi} < P_{Gi}max$,; limitation of power plants' generation reactive power $Q_{Gi}min < Q_{Gi} < Q_{Gi}max$,; limitation of flow passing of lines $P_{ij}min < P_{Gij} < P_{ij}max$.; and limitation of bus voltage $V_imin < V_i < V_imax$. Objective functions must be solved considering technical conditions and the voltage profile must be maximized. Additionally, the most important conditions of the genetic algorithm are convergence condition and achievement of considered objects. Generally, a maximum is induced on

generation and the generation is blocked when mean value of appropriateness is constant for some sequential population and no condition is breached (Sayed et al., 2022; Ali et al., 2021).

6. THE RESULT OF SIMULATION ON IEEE 12 BUS NETWORK

This network included only one main feeder. The voltage of bus 1 was considered as 1pu. basic voltage is 6.5 KV and basic apparent power equaled 10 MVA. Figure 1 represents a 12-bus network (Al-Ammar et al., 2021; Chakraborty et al., 2021).
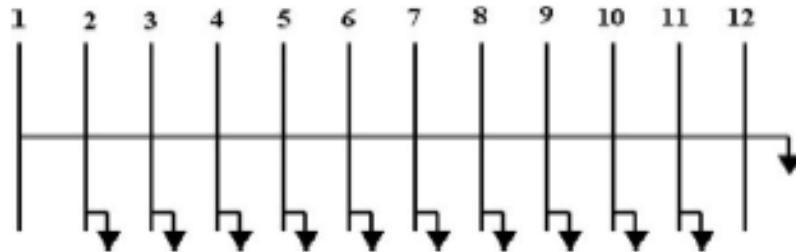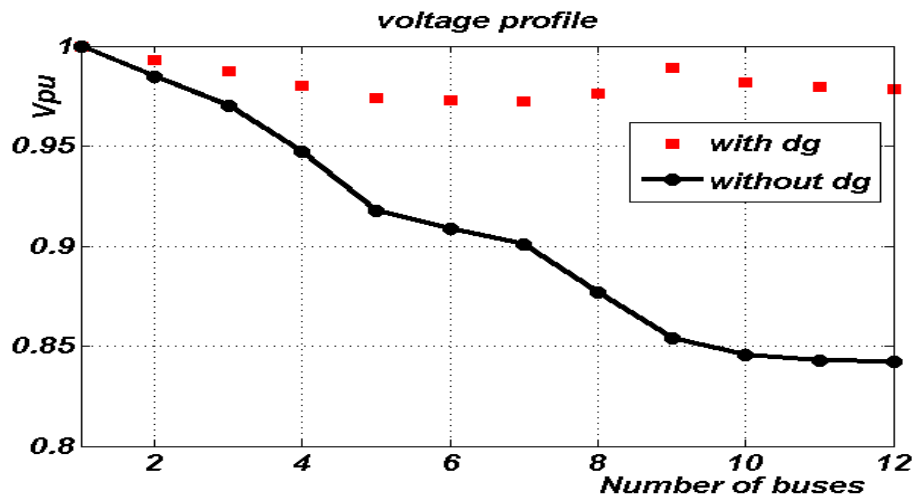

Figure 26: IEEE 12- Bus Network

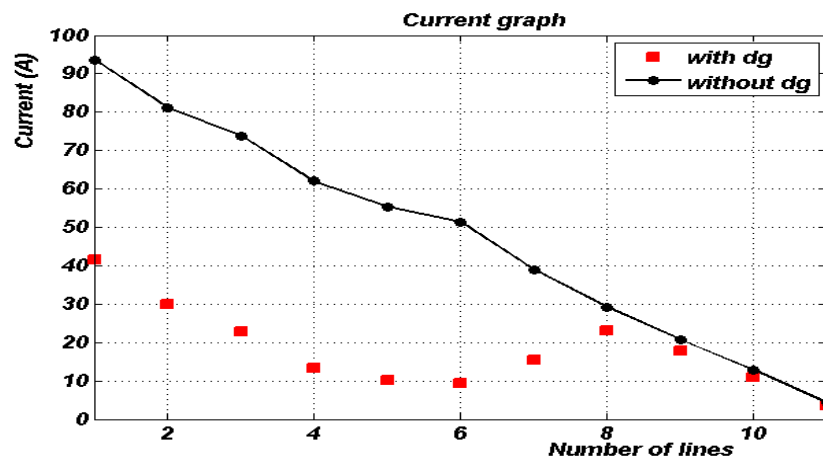Figure 2: Voltage profile for 12 bus network using one DG

Figure 3: Current profile at the main feeder lines (1-11) using one DG

Table 15: The result using one DG

Quantity under study	With DG	Without DG	Percentage reduction
Active Losses (KW)	*18.7*	*60.1*	*68%*
Reactive Losses (KVAR)	*7.6*	*23.3*	*67.38%*
Line current 1(A)	*65.02*	*93.6*	*30.5%*
Line current 2(A)	*52.7*	*81.3*	*35%*
Line current 3(A)	*45.4*	*73.8*	*38.4%*

Table 2: The result using two DG in buses 7 and 10 with the capacity of 0.1 MW and 0.125 MW

Quantity under study	With DG	Without DG	Percentage reduction
Active Losses (KW)	*5.9*	*60.1*	*90.18%*
Reactive Losses (KVAR)	*2.3*	*23.3*	*90.13%*
Line current 1(A)	*41*	*93.6*	*56.2%*
Line current 2(A)	*29.25*	*81.3*	*64%*
Line current 3(A)	*22.2*	*73.8*	*70%*

Table 3: The result using four DG with 25% increase of load

Quantity under study	With DG	Without DG	Percentage reduction
Active Losses (KW)	*4*	*102.8*	*96%*
Reactive Losses (KVAR)	*1.5*	*39.7*	*96%*
Line current 1(A)	*22.27*	*121.11*	*81%*
Line current 2(A)	*16.88*	*105.58*	*84%*
Line current 3(A)	*18.41*	*96.20*	*80%*

Table 4: Comparison between VPII, LLRI, LTAPII indices using one DG and two DG

Indices	Without DG	One DG	Two DG
LLwDG	*0.0020*	*0.0034*	***0.0001***
LLwoDG	*0.0020*	*0.0020*	***0.0020***
LLRI	*1*	*0.3109*	***0.0974***
LTAPwoDG	*0.1140*	*0.1140*	***0.1140***
LTAPwDG	*0.1140*	*0.0616*	***0.0322***
LTAPII	*1*	*0.540*	***0.2822***
VPwDG	*0.0178*	*0.0186*	***0.0190***
VPwoDG	*0.0178*	*0.0178*	***0.0178***
VPII	*1*	*1.045*	***1.071***

Table 5: Comparison between VPII, LLRI, LTAPII indices using three DG and four DG

Indices	Without DG	Three DG	Four DG
LLwDG	0.0034	0.0019	**0.0013**
LLwoDG	0.0034	0.0034	**0.0034**
LLRI	1	0.0564	**0.0385**
LTAPwoDG	0.1464	0.1464	**0.0034**
LTAPwDG	0.1464	0.0291	**0.0257**
LTAPII	1	0.1990	**0.1754**
VPwDG	0.0178	0.024	**0.0243**
0.0178 VPwoDG		0.0216	**0.0216**
VPII	1	1.011	**1.126**

As the numbers in Table 5 show, LLRI and LTAPII indices have decreased significantly, which indicates a reduction in losses and a decrease in apparent power at transmission lines, or in other words, an increase in line capacity. VPII also shows the improvement of the voltage profile in the bus bars.
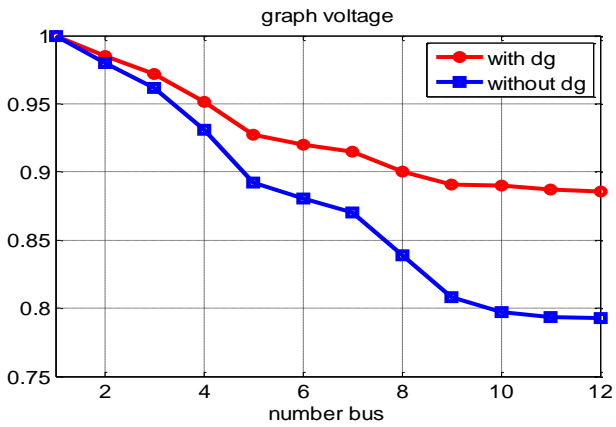

Figure 4: Voltage profile of 12-bus network with 25% increase of load using one DG
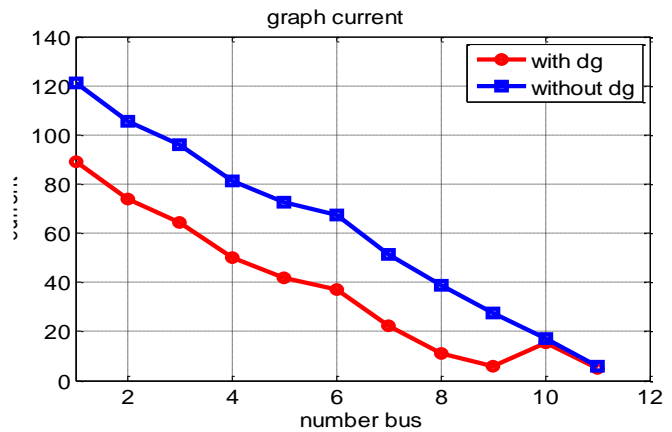

Figure 5: current profile at the main feeder lines (1-11) with25% increase of load using one DG
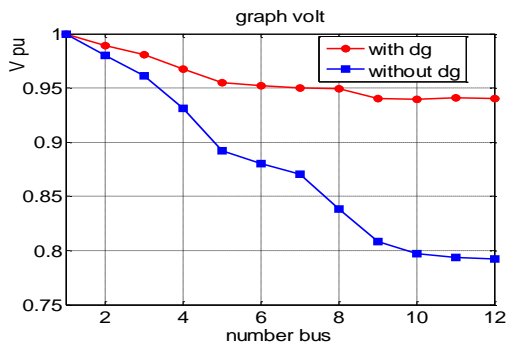

Figure 6: Voltage profile of 12-bus network with 25% increase of load using two DG
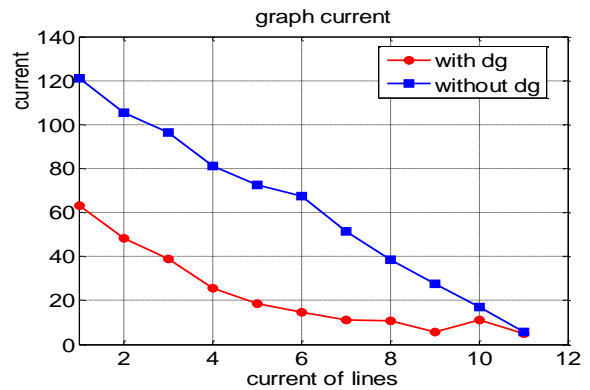

Figure 7: Current profile at the main feeder lines (1-11) with 25% increase of load using two DG
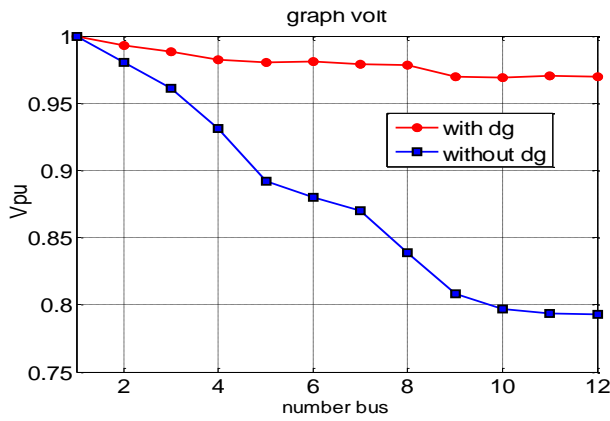
Figure 8: Voltage profile of 12-bus network with 25% increase of load using three DG
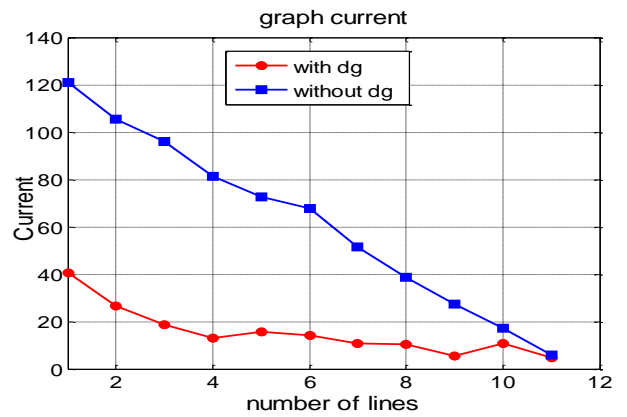

Figure9: Current profile at the main feeder lines (1-11) with 25% increase of load using three DG
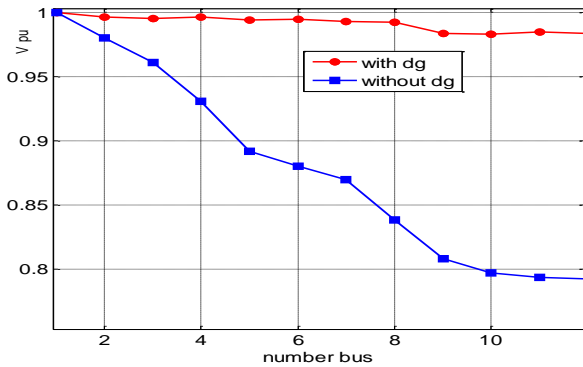

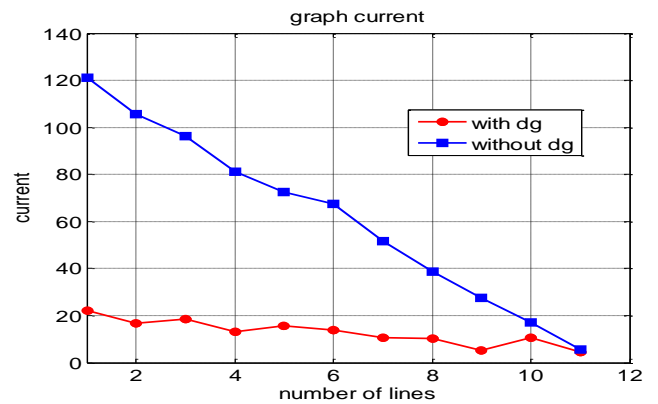*Figure 10: Voltage profile of 12-bus network with 25% increase of load using four DG*

Figure 11: current profile at the main feeder lines (1-11) with25% increase of load using four DG

7. CONCLUSION

In this study, optimized displacement of distributed generation plants in the network was investigated in order to evaluate the effect of displacement on network load ability improvement despite stability in system equipment. Tables have shown clearly that a 25% increase of load led to a lower loss index and aspect capacity while using DG compared to the absence of DG. Additionally, the voltage profile index was higher in the presence of DG. More DGs means a higher growth rate of the mentioned parameters. It also means that the presence of distributed generation systems leads to improved load ability of distribution system. in this situation, there is no need for new equipment. Generally, it is concluded that the presence of distributed systems with optimized displacement reduces lone loss, aspect power and network current. It boosts voltage profile. This enable the enhancement of load ability with no need for new networks or developing the current network. It diminishes expenditures especially in the areas far from concentrated generation resources using distributed generation. Therefore, line capacities are released and load ability is increased. There is no need to have new installation and equipment. The best condition would be with 4 DGs. However, according to the studies, the following can be mentioned as the main indicators for decision-making regarding the use of distributed generation resources in Iran which should be considered in the decision-making process:

- Predicting the existing potential and capacity in the country.
- The technological future of distributed generation resources in the world (in terms of cost).
- Predicting access to technology.
- The type of initial energy required and its future.
- Economic evaluation of distributed generation resources (in the present and future conditions).

- The classification of distributed generation sources is suggested as follows:
- Capacities available in the country's industries.
- Urban applications (micro turbines and gas turbines).
- Applications of scatter points (wind, water and photovoltaics).

It is suggested that distributed generation resources be used in more places instead of in one place, to further reduce losses, reduce the apparent power of the transmission line, and ultimately improve the voltage profile of the buses. Optimization algorithms such as genetic algorithm and fuzzy logic, neural network, OPF, ant colony algorithm, and other algorithms are used to perform the best work.

8. REFERENCES

Abbas, A.S., El-Sehiemy, R.A., Abou El-Ela, A., Ali, E.S., Mahmoud, K., Lehtonen, M. and Darwish, M.M., 2021. Optimal harmonic mitigation in distribution systems with inverter based distributed generation. Applied Sciences, 11(2), p.774

Al-Ammar, E. A., Farzana, K., Waqar, A., Aamir, M., Haq, A. U., Zahid, M., & Batool, M. (2021). ABC algorithm based optimal sizing and placement of DGs in distribution networks considering multiple objectives. Ain Shams Engineering Journal, 12(1), 697-708.

Ali, Z. M., Diaaeldin, I. M., El-Rafei, A., Hasanien, H. M., Aleem, S. H. A., & Abdelaziz, A. Y. (2021). A novel distributed generation planning algorithm via graphically-based network reconfiguration and soft open points placement using Archimedes optimization algorithm. Ain Shams Engineering Journal, 12(2), 1923-1941.

Azeroual, M., Boujoudar, Y., Bhagat, K., El lysaouy, L., Aljarbouh, A., Knyazkov, A., Fayaz, M., Qureshi, M.S., Rabbi, F. and Markhi, H.E., 2022. Fault location and detection techniques in power distribution systems with distributed generation: Kenitra City (Morocco) as a case study. Electric Power Systems Research, 209, p.108026.

Bajaj, M. and Singh, A.K., 2021. Hosting capacity enhancement of renewable-based distributed generation in harmonically polluted distribution systems using passive harmonic filtering. Sustainable Energy Technologies and Assessments, 44, p.101030.

Barker, P.P. and de Mello, R.W. "Determining the Impact of Distributed Generation on Power Systems: Part 1-Radial distribution systems", proc, 2000 IEEE/PES summer Meeting, Vancouver, BC, July 15-19, 2001.

Borges, Carmen L.T. and Falcao Djalma M. "Optimal distributed generation allocation for reliability, losses and voltage improvement" ELSEVER 2006.

Bryant, Kylie, Genetic Algorithm and the Traveling Salesman Problem, Hervey Mudd college , 2000

Chakraborty, S., Das, S., Sidhu, T., & Siva, A. K. (2021). Smart meters for enhancing protection and monitoring functions in emerging distribution systems. International Journal of Electrical Power & Energy Systems, 127, 106626.

Dianati, Mehrdad, Song, Insop and Treiber, Mark, An Introduction to Genetic Algorithms and Evolution Strategies, University of Waterloo, Canada , 2002

Griffin, T., Tomsovic, K., Secrest, D. and Low, A. 2000. "Placement of dispersed generations systems for reduced losses", sys-tem sciences, 2000 IEEE, proceedings of the 33rd Annual Hawaii International conference on 2000 IEEE, pp . 1446-1456

Haider, W., Hassan, S.J.U., Mehdi, A., Hussain, A., Adjayeng, G.O.M. and Kim, C.H., 2021. Voltage profile enhancement and loss minimization using optimal placement and sizing of distributed generation in reconfigured network. Machines, 9(1), p.20.

Ijumba, N.M., Jimoh, A.A., Nkabinde, M., "Influence of distributed generation on distribution network performance" FRICON, 1999, IEEE, Volume: 2, 28 Sept.-1 Oct. 1999, Page(s): 961-964 vol2.

Kojovic, "Impact of DG on Voltage Regulation", Proc. 2002 IEEE/PES summer Meeting Chicago, IL, July 21-25, 2002.

Ochoa, L.F., Padilha, A., Harrison G.P. "Evaluating Distributed Generation Impacts With a Multiobjective Index" IEEE transactions, vol.21, NO. 2006

Rogers, Alex. CM2408, Symbolic AI Lecture 8 – Introduction to Genetic Algorithms, December 2002

Sayed, M.M., Mahdy, M.Y., Abdel Aleem, S.H., Youssef, H.K. and Boghdady, T.A., 2022. Simultaneous Distribution Network Reconfiguration and Optimal Allocation of Renewable-Based Distributed Generators and Shunt Capacitors under Uncertain Conditions. Energies, 15(6), p.2299.

Wang, Caisheng, and Nehrir, M. Ha-shem, "Analytical Approaches for Optimal Placement of Distributed Generation Sources in Power Systems" IEEE Transaction on power systems, Vol. 19, No. 4, November 2008

Xu, Z., Liu, H., Sun, H., Ge, S. and Wang, C., 2022. Power supply capability evaluation of distribution systems with distributed generations under differentiated reliability constraints. International Journal of Electrical Power & Energy Systems, 134, p.107344.

#365: Voltage control improvement in electrical power distribution systems using solar resources

Mahmoud ZADEHBAGHERI[1], Mohammad Javad KIANI[2], Mohammad KARAMI[3]

[1] Department of Electrical Engineering, Yasuj Branch, Islamic Azad University, Yasuj, Iran,
Ma.zadehbagheri@iau.ac.ir
[2] Department of Electrical Engineering, Yasuj Branch, Islamic Azad University, Yasuj, Iran,
Mj.kiani@iau.ac.ir
[3] Department of Electrical Engineering, Yasuj Branch, Islamic Azad University, Yasuj, Iran,
Ketabmark@yahoo.com

Abstract: Usage of distributed generation systems is increasing. One advantage of using distributed generation systems is the stability of distribution network voltage. One distributed generation resource is the photovoltaic system which is used along with an energy storage component and incident angle tracer in order to be able to inject a monotonic flow of power into the network. In this study, the photovoltaic system was used without the above-mentioned equipment to evaluate the effect of this system on network voltage. A sample 33-bus network was introduced and the photovoltaic system was used on bus 18. The results have shown that if the radiation angle tracer was not used, then the voltage of the bus on which the photovoltaic system was installed reached 0.986 by midday. Before sunrise and after sunset, when there were no sun rays, this bus voltage reached 0.948 indicating 4% change in the bus voltage.

Keywords: voltage control; renewable energies; distribution networks; distributed generation; photovoltaic (PV)

1.   INTRODUCTION

Because of environmental pollution caused by fossil fuel resources and the inability of these resources to produce sufficient electricity, countries are looking for new energy resources to meet their energy requirements. One of these renewable energy sources is solar energy. The sun is a major energy resource and acts as the origin of life; it is the mother of other energy resources. According to scientific estimation, the sun was born 6000 million years ago and 4 million tons of the sun's mass is converted into energy every second. This hot globe is considered to be a huge energy resource for 5 billion years. In traditional systems, electricity production is a concentrated process with generated power being transmitted to charge centers via transmission systems and then discharged to consumers by distribution systems. In these systems, new lines, transformers and stations are installed in order to meet customers' needs (Willis, 1997). Due to low levels of voltage, high levels of current in distribution systems and the wideness of the mentioned current, a major part of system loss is related to distribution networks. On the other hand, immediate communication between distribution network and end users leads to greater reliability (Zadehbagheri et al., 2022). This motivates engineers and researchers to optimize and reduce the loss of distribution network. There are multiple ways to mitigate the loss in distribution networks (Khator & Leung, 1997; Movahedpour et al., 2022) and the majority of these methods, including reactive power control using a capacitor, require the installation of new equipment. Another method is to use distributed generation resources in distribution networks. Using distributed generation resources not only reduces the distribution network loss but covers the increasing demand. A replacement method to deal with the mentioned problem is to use local power generation using distributed resources. Distributed generation improves requirements of generation capacity, power transmission and distribution networks. It also eliminates the need for installing new lines and stations (Chalmers et al., 1985; Sarfi, Salama & Chikhani, 1995). Different terms have been used in various papers to name the distributed generation which leads to confusion, whereas all terms have the same meaning. A general definition for distributed generation is as below: distributed generation is a power resource which is connected to the distribution network directly (Papadopoulos, Hatiargriou and Papadakis, 1987; El-Khattam and Salama, 2003). Generally, distributed generation is able to better coordination various applications such as sources of backup or emergency, peak loads, production fractional and overall supply of load demand. Therefore, optimal replacement of distributed generation provides some advantages including loss reduction, reliability improvement of the system, more capacity for distribution and transmission, delaying the need for network reconstruction and a reduction in voltage drop in buses. In this study, the effects of photovoltaic systems as distributed generation resources on voltage stability in buses was examined (Mantawy & Al-Muhaini, 2007).

2.   SOLAR ENERGY

The Sun is a huge natural nuclear reactor in which substances convert into energy due to nuclear fusion. Each day, 350 billion tons of its mass is converted into light. The internal temperature of the sun is 15 million degrees centigrade. The energy is provided for us in the form of visible, infrared and ultraviolet spectra in the amounts of $1kw/m^2$. The sun is similar to a gigantic firing globe 100 times bigger than the earth in magnitude. The mentioned star includes hydrogen and helium, and these gases are combusted and produce rays of light and heat which travel towards the earth. On the way to the earth, one-third of rays are scattered into space and the remaining reach the earth as heat and light. It is known that light speed is 300,000km/s and it takes 8 minutes for solar rays to reach the earth. Therefore, it is possible to calculate the distance between the earth and the sun. Over this long distance, a huge amount of solar heat and energy waste away. But the remaining amount reaching the earth is enough to keep creatures alive and provide them with a suitable habitat. The most important feature of solar energy is that it is endless, it is a clean resource, it does not damage the environment and it is easy to utilise it: it is possible to design devices according to demands (Feng et al., 2003; Ackermann & Knyazkin, 2002).

3.   PHOTOVOLTAIC SYSTEMS

With increasing populations and associated energy demands and consumption, the sun is considered to be a ubiquitous and cheap major energy resource. In this section, solar panels and photovoltaic systems are introduced. When located in suitable positions, these panels, which are composed of silicon cells (Pepermans et al., 2003), absorb solar energy and convert it into electricity. When they are exposed to solar rays, electron movement is caused due to some interactions inside the panels and then DC load flows at the cell outlets. Photovoltaic systems are one of the most used samples of new energy applications. To date, multiple systems with different capacities from 0.5 watt to some megawatts have been introduced and installed worldwide. According to reliability and applicability, the number of these systems is increasing, therefore, various studies on photovoltaic systems have been conducted recently. The word photovoltaic is derived from two Greek words: photo indicating light and voltaic indicating electricity. Accordingly, photovoltaic points to light-based electricity. A phenomenon to produce electricity using incidental light without an actuator mechanism is called photovoltaic phenomenon. Every system using this phenomenon is referred to as a photovoltaic system. The panel converting solar energy into electricity is called the solar panel or battery. Solar panels are composed of silicon. According to increasing population and more energy demand and consumption, the sun is considered to be the only ubiquitous energy resource. Components of photovoltaic system are solar panels, modules, arrays, voltage regulators and controllers, and storage batteries for

electrical energy. To achieve desirable voltage and current, cells with different arrays are attached together as a module, see Figure 1. Modules are installed on to a metal plate or frame (usually aluminum) to make the photovoltaic panel (El-Khattam & Salama, 2004).
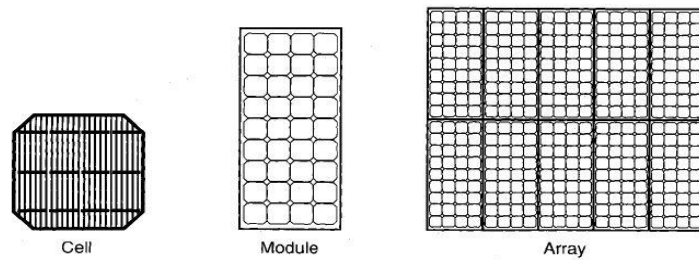

Figure 1: Cell, module and PV array

According to Figure 2, it is possible to obtain desirable voltage and current by making a series or shunt array of cells. Series cells provide higher voltage but the shunt ones are able to produce higher current. Figure 3 shows cells, modules and arrays and how they are placed together (Werven & Scheepers, 2005).

Current = 3 x I_{cell}
Voltage = V_{cell}

Current = I_{cell}
Voltage = 3 x V_{cell}
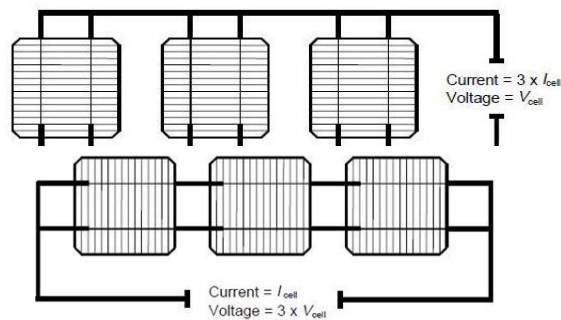
Figure 2: Series and shunt electrical connection of cells
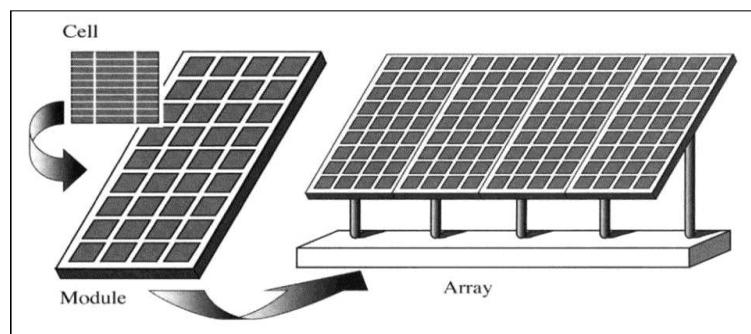
Figure 3: Cells, modules and arrays and how they are placed together

3.1. Voltage regulation and system control

Due to the fact that the electricity generated by PV arrays is of direct current type, it is necessary to convert the output to AC power with voltage, frequency and phase suitable for connection to the mains or local load. This is done by a device called an inverter (Messenger & Ventre, 1999; Saidi, 2022). If the intensity of solar radiation changes at ambient temperature, the output voltage of the PV arrays also changes. Therefore, in systems that have battery storage, it is necessary to adjust the output voltage of the arrays to prevent the battery from overcharging. In this case, a converter is used (Figure 4).

Figure 4: How to connect arrays to the consumer and the battery bank

3.2. Advantages and disadvantages of photovoltaic systems

The most important advantage of photovoltaic systems is the lack of requirement for fossil fuels; environment protection; pollution reduction; long life cycle; great reliabili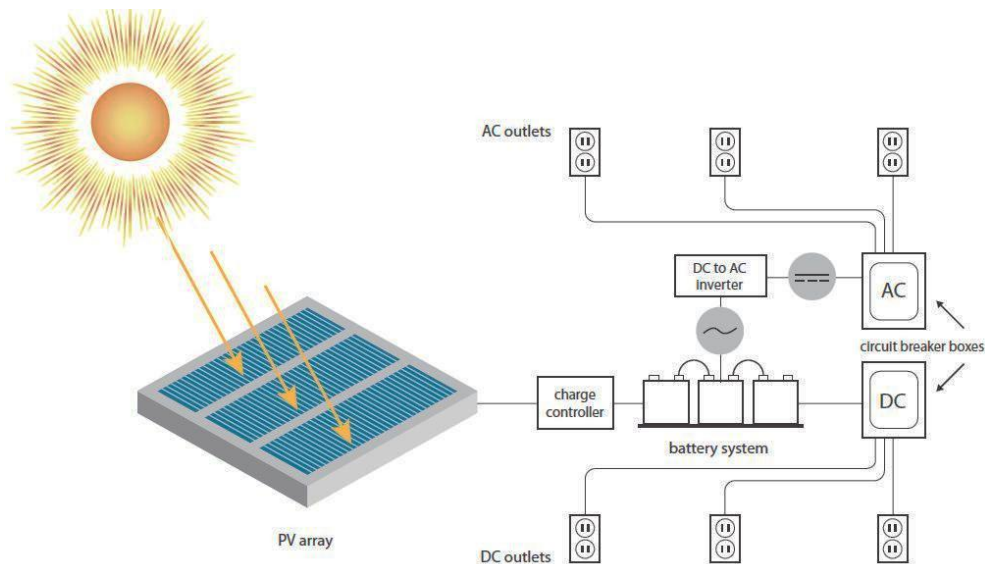ty due to lack of mechanical portable parts; less danger of fire or explosion; ease of installation and operation; no need for complicated equipment and human labour; and the ability to change the power according to increase or decrease of capacity in photovoltaic systems (by increasing or decreasing the number of modules). The primary disadvantage is the astronomical price. Although the price of photovoltaic systems is decreasing due to developing technology, it is necessary to evaluate the economics of resources. Economic studies on renewable systems have shown that, despite the great investment required to produce electricity, the final price of electricity transmitted to places far from basic network is economical. Photovoltaic systems are made up of three types: independent, dependent, and hybrid. Dependent systems inject electrical energy produced by solar panels into the global network directly. These are important systems with multiple megawatts power plants being installed (Hamidan & Borousan, 2022). Voltage dip compensation of transmission line is a main feature of these systems. Regarding the effect on power systems, power coefficient of photovoltaic generation units is about 1. Investigations show that in some cases, the presence of at least 10% of power generation of the mentioned units prevents usage of capacitors in systems in order to correction voltage profiles. Figure 5 shows a diagram of a photovoltaic system connected to the network which feeds AC and DC loads (Jayachandran et al., 2022).
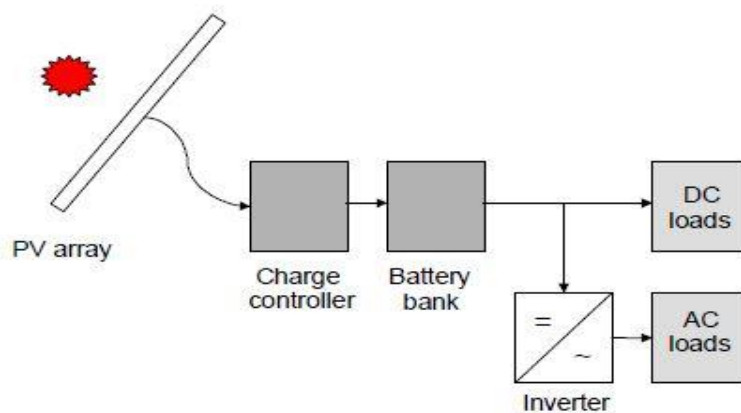
Figure 5: Photovoltaic system connected to the network

3.3. Characteristic power of two moving and fixed arrays during the day

Comparing two photovoltaic arrays, one moving and the other constant, the moving solar array produces more power due to direct sun light on the array, while the constant array is exposed to skewed light. In Figure 6, voltage-current curves of moving and constant photovoltaic arrays are shown.
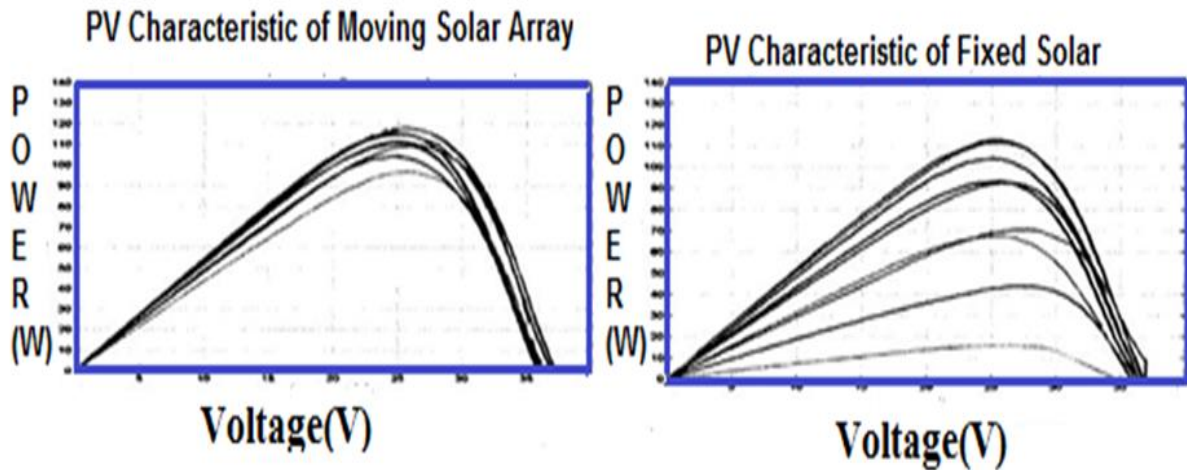
Figure 6: Voltage-current curves of moving and fixed PV arrays during a day

3.4. Hybrid systems

Hybrid systems use multiple power supplies to supply the required electrical energy with the PV system being one of the main power sources. Other energy sources used in this complex include the national grid, diesel generators, wind turbines, and so on. (In this model, based on the situation and the need for load, the use of each of these power supplies is prioritized and controlled). In hybrid systems, multiple power sources are used in case of interruption of any one source. In this model, the possibility of power outage is minimized (Figure 7).
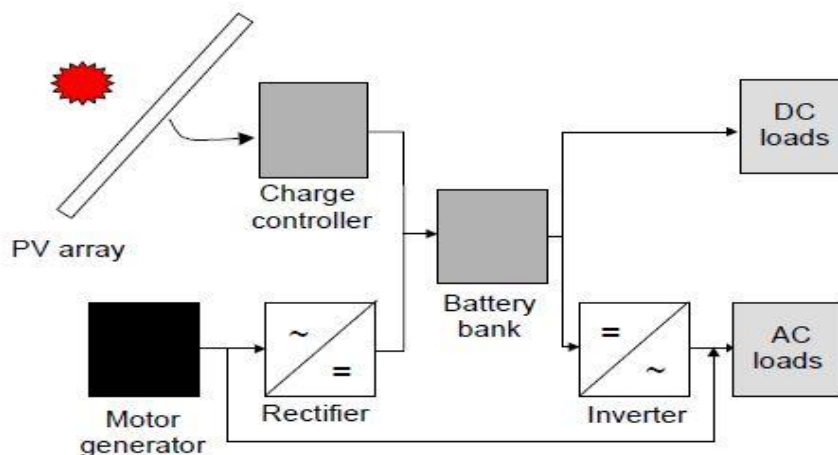
Figure 7: Diagram of a hybrid PV system combined with a diesel generator

4.   REVIEW ON POWER DISTRIBUTION NETWORKS

Power distribution is the last step of the power chain where power received from the generation or transmission stage with a certain voltage is converted into the voltage required of consumers. Delivering electricity to consumers is carried out by using 63kv or 132kv lines in distribution networks. Primary distribution feeders are responsible for delivering electricity power from main stations into distribution transformers via medium voltage lines. Most medium voltage networks are of 20kv in Iran. But 11kv and 33kv networks are also used in limited applications. Distribution transformers are of two kinds: aerial and ground. The mentioned transformers reduce voltage levels up to 380 volts which is related to secondary circuits. Secondary distribution systems include reducing distribution transformers, secondary circuits, branches for meeting electricity demands and certain tools to measure the amount of electricity consumed by consumers. Generally, distribution systems for houses are of single-phase type but for commercial and industrial consumers, three-phase systems are used. Two-phase systems are used rarely. There is direct communication between distribution systems and users. Accordingly, these systems have to become accustomed to variable conditions during various periods of time due to seasonal variances. Sometimes, problems are caused such as technical obstacles, overload of ultra-distribution stations, voltage reduction in distribution stations, extra current in 20kv feeders and imbalance of charge. On the other hand, increasing the number of subscribers leads to multiple problems especially when the newcomers increase the load of network. Due to a change of load in distribution systems, system loss is variable and also changes the voltage level and feeder current (Eskandari et al., 2022).

5.   SIMULATION AND RESULTS

In this paper, to investigate the effect of photovoltaic systems on distribution system voltage stability, IEEE 13-bus and IEEE 33-bus networks are used.
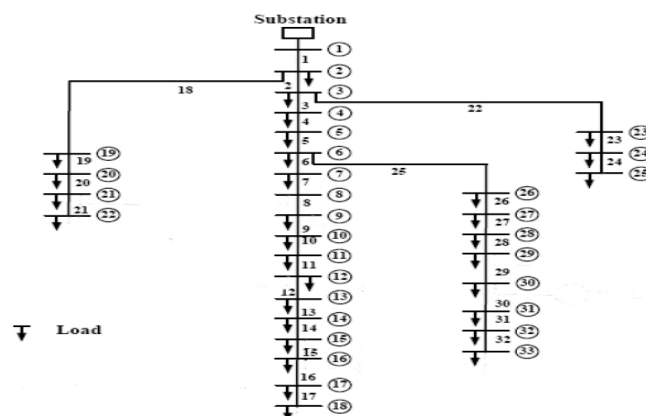
Figure 8: IEEE 33-bus test network

It was assumed that a photovoltaic system with maximum power of 120kv was attached to bus 18. The output of the photovoltaic system during the day is presented in Table 1. Characteristics of this network including load power and impedance of lines are shown in Table 2 and Table 3.

Table 1: Power output of PV systems at different hours

Power output of PV systems(Kw)	Time (S)
73	9:00
94	10:00
106.5	11:00
113	12:00
115.2	13:00
110.3	14:00
95.5	15:00
69.2	16:00
45	17:00
16.2	18:00

Table 2: Network Loads Power

Reactive Power (KVAR)	Active Power (KW)	Bus No.
0	0	1
60	100	2
40	90	3
80	120	4
30	60	5
20	60	6
100	200	7
100	200	8
20	60	9
20	60	10
30	45	11
35	60	12
35	60	13
80	120	14
10	60	15
20	60	16
20	60	17
40	90	18
40	90	19
40	90	20
40	90	21
40	90	22
50	90	23
200	420	24
200	420	25
25	60	26
25	60	27
20	60	28
70	120	29
100	200	30
70	150	31
100	210	32
40	60	33

Table 3: Network Feeders Impedance

Inductive Resistance	Resistance (ohm)	Line No.	To the Bus	From the Bus
0.047	0.0922	1	2	1
0.2512	0.493	2	3	2
0.1864	0.3661	3	4	3
0.1941	0.3811	4	5	4
0.707	0.819	5	6	5
0.6188	0.1872	6	7	6
0.2351	0.7115	7	8	7
0.74	1.0299	8	9	8
0.74	1.044	9	10	9
0.0651	0.1967	10	11	10
0.1298	0.3744	11	12	11
1.1549	1.468	12	13	12
0.7129	0.5416	13	14	13

0.526	0.5909	14	15	14
0.5449	0.7462	15	16	15
1.721	1.2889	16	17	16
0.5739	0.732	17	18	17
0.1569	0.164	18	19	2
1.3555	1.5042	19	20	19
0.4784	0.4095	20	21	20
0.9373	0.7089	21	22	21
0.3084	0.4512	22	23	3
0.7091	0.898	23	24	23
0.7071	0.8959	24	25	24
0.1034	0.2031	25	26	6
0.1447	0.2842	26	27	26
0.9338	1.0589	27	28	27
0.7006	0.8043	28	29	28
0.2585	0.5074	29	30	29
0.9629	0.9745	30	31	30
0.3619	0.3105	31	32	31
0.5302	0.3411	32	33	32

As mentioned before, to increase the efficiency of photovoltaic systems, a radiation angle tracer was installed on the panels used. By changing the angle of the panel, maximum power was obtained from sunrise to sunset. In this study, it was assumed that such a system was not installed on the panel. Changes of the buses on which photovoltaic system was installed are shown in Figure 9. According to the figure, the voltage of bus 18 reached 0.986 at noon. But, before sunrise and after sunset when there was no sunshine, this value was about 0.948 indicating 4% changes in this bus voltage.
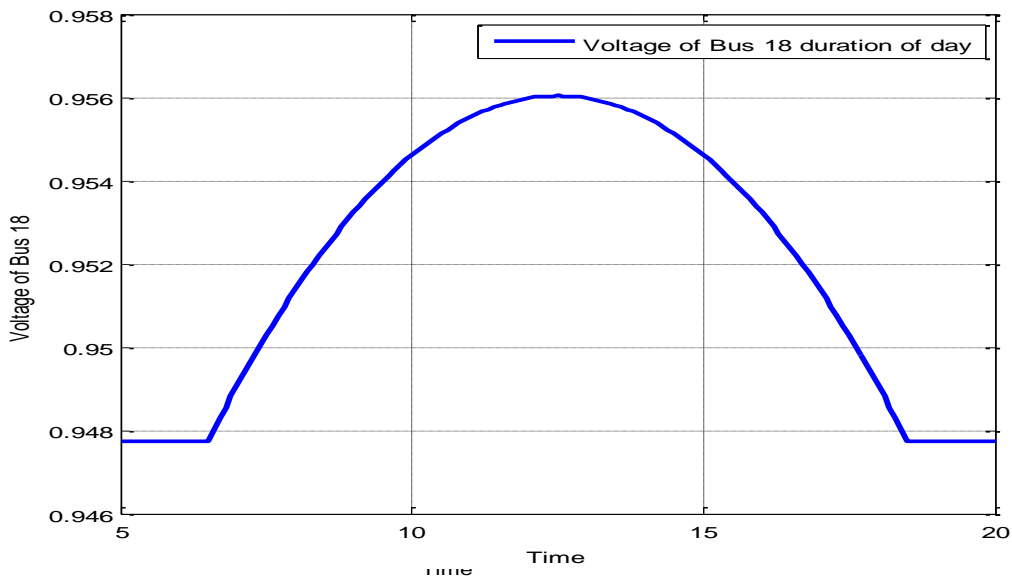

Figure 9: Voltage change of bus 18 during the day

To evaluate the effect of generative power level change of photovoltaic system on voltage of other buses, voltage levels of 33 buses were investigated for two different times: 6 a.m (when there was no sunshine) and 12 noon (maximum amount of sunshine). The related values are represented in Figure 10.
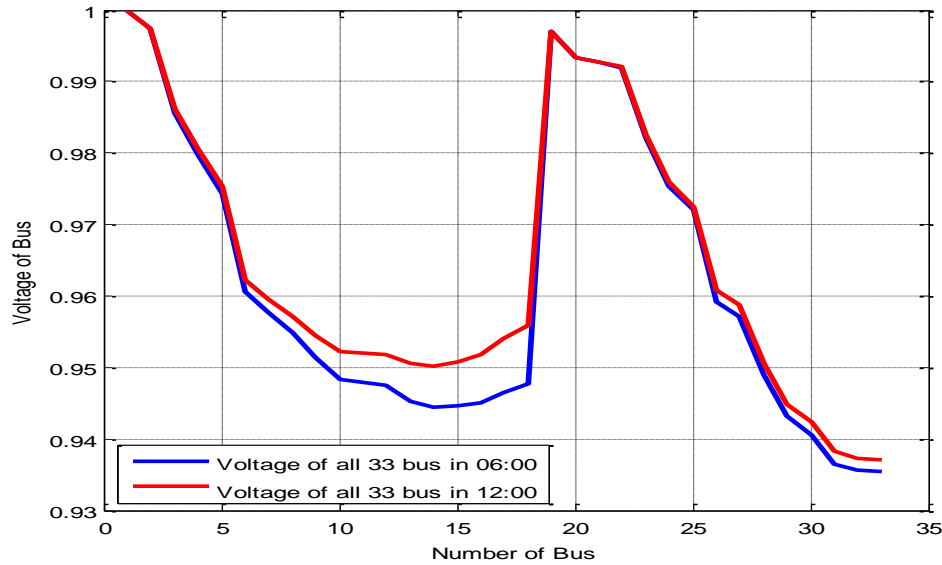
171

Figure 10: Buses voltage of distribution network for two different times during a day

6. CONCLUSION AND RECOMMENDATION

In this paper, photovoltaic systems were studied. Advantages, disadvantages, technology of solar cells, components of photovoltaic systems, various types including independent, dependent and hybrid and also characteristic output of a sample panel during a day were discussed. Finally, IEEE 33-bus network was considered and a photovoltaic system installed on a bus of network. Then, the effect of incident light on bus voltage was examined. The results of the simulation done by MATLAB indicated promotion of voltage control in the considered network. Finally, it was recommended to use FACTS devices in addition to distributed generation systems. Using an algorithm such as PSO, the two mentioned systems were coordinated in order to have both power active and reactive generation. As the last step, the effect of this coordination on the bus voltage and network loss was investigated.

7. REFERENCES

Ackermann, T., and Knyazkin, V., " Interaction between Distributed Generation and the Distribution Network: Operation Aspects ", Transmission and Distribution Conference and Exhibition 2002: Asia Pacific. IEEE/PES, Vol.2, pp. 1357- 1362, 2002.

Chalmers, S.; Hitt, M.; Underhill, J.; Anderson, P.; Vogt, P.; Ingersoll, R. "The Effect of Photovoltaic Power Generation on Utility Operation." IEEE Transactions on Power Apparatus and Systems; PAS-104, 1985, pp. 524–530.

El-Khattam, W., and Salama, M. M. A., "Distribution System Planning Using Distributed Generation", Electrical And Computer Engineering, IEEE CCECE 2003, Canadian Conference, Vol.1, pp. 579- 582, 2003.

El-Khattam, W., and Salama, M. M. A., "Distributed Generation Technologies, Definitions And Benefits", Electric Power Systems Research, Vol. 71, Issue 2, pp. 119-128, Oct. 2004.

Eskandari, H., Kiani, M., Zadehbagheri, M., & Niknam, T. (2022). Optimal scheduling of storage device, renewable resources and hydrogen storage in combined heat and power microgrids in the presence plug-in hybrid electric vehicles and their charging demand. Journal of Energy Storage, 50, 104558.

Feng, X., Liao, Y., Pan, J., and Brown, R., "An Application of Genetic Algorithms to Integrated System Expansion Optimization", IEEE PES General Meeting, Toronto, Canada, July 13 - 17, 2003.

Hamidan, M. A., & Borousan, F. (2022). Optimal planning of distributed generation and battery energy storage systems simultaneously in distribution networks for loss reduction and reliability improvement. Journal of Energy Storage, 46, 103844.

Jayachandran, M., Rao, K. P., Gatla, R. K., Kalaivani, C., Kalaiarasy, C., & Logasabarirajan, C. (2022). Operational concerns and solutions in smart electricity distribution systems. Utilities Policy, 74, 101329.

Khator, S. K., and Leung, L. C., "Power Distribution Planning: A Review Of Models And Issues" IEEE Trans. Power Syst., Vol. 12, No. 3, pp. 1151–1159, Aug. 1997.

Mantawy, A. and Al-Muhaini, M., "a new particle swarm algorithm for distribution system expansion planning including distributed generation", proceedings of the 2nd IASME/WSEAS international conference on energy & environment (EE'07), Portoroz, Slovenia, May 2007, pages 236-241.

Movahedpour, M., Kiani, M. J., Zadehbagheri, M., & Mohammadi, S. (2022). Microgrids Operation by Considering Demand Response and Supply Programs in the Presence of IGDT-Based Reverse Risk. IEEE Access, 10, 48681-48700.

Papadopoulos, M. P., Hatiargriou, N. D. and Papadakis, M. E. (1987). "Graphics aided interactive analysis of radial distribution networks." IEEE Trans on PWRD, Vol. 2, No. 4.

Pepermans, G., Driesen, J., Haeseldonckx, D., D'haeseleer, W., and Belmans, R., "Distributed Generation: Definition, Benefits and Issues", Katholieke Universiteit Leuven, 19 August 2003.

Roger A Messenger & Jerry Ventre (1999): Photovoltaic Systems Engineering. CRC Press ISBN 10: 0849317932

Saidi, A. S. (2022). Impact of grid-tied photovoltaic systems on voltage stability of tunisian distribution networks using dynamic reactive power control. Ain Shams Engineering Journal, 13(2), 101537.

Sarfi, R. J., Salama, M. M. A. and Chikhani, A. Y. (1995). "Practical aspect of performing a distribution system loss reduction study." CCEC, PP.164-167.

Werven, M., and Scheepers, M., "Dispower - The Changing Role Of Energy Suppliers And Distribution System Operators In The Deployment Of Distributed Generation In Liberalised Electricity Markets". Ecn Report Ecn-C--05-048, NL, 2005.

Willis, L.H., "Power Distribution Planning Reference Book" ABB Power T&D Company Inc. Cary, North Carolina, Published by Marcel Dekker, Inc., 1997.

Zadehbagheri, M., Kiani, M. J., Sutikno, T., & Moghadam, R. A. (2022). Design of a new backstepping controller for control of microgrid sources inverter. International Journal of Electrical & Computer Engineering (2088-8708), 12(4).

#367: Sliding mode control of a doubly fed induction generator (DFIG) for a wind energy conversion system

Mahmoud ZADEHBAGHERI

Department of Electrical Engineering, Yasuj Branch, Islamic Azad University, Yasuj, Iran,
Ma.zadehbagheri@iau.ac.ir

Abstract: Wind energy is one of the most important sources of renewable energy globally with economic justification worldwide. Due to the growing needs for electrical energy, increased environmental pollution and limitations in fossil fuel resources, the use of wind energy in the power industry is increasingly necessary and inevitable. The broad use of wind turbines in the power system have caused turbines to have a dominant place in these systems. Because of the better power quality of variable speed wind turbines, they are more appropriate than the constant speed turbines. Advantages such as good quality control, high efficiency, improved power quality, no need for capacitor banks and cost effectiveness in doubly fed induction generator (DFIG) mean that they are increasingly being used. This paper presents a study of speed control of a doubly fed induction generator according to the sliding mode controller using a simulation in the MATLAB/Simulink environment and the simulation presented results that demonstrated the ability of the proposed control strategy.

1. INTRODUCTION

At the present time many countries are using wind energy as a constant energy source. The installed capacity of wind power is more than 25 GW worldwide. The wind turbines systems in use include those with constant speed armed with one induction generator; variable speed armed with one squirrel cage induction generator and/or synchronous, variable speed with multi-pole permanent magnet synchronous generator; and turbines with variable speed armed with a doubly fed induction generator (DFIG). Nowadays the most used type of turbine on wind farms are based on the doubly fed induction generator because they have some outstanding features such as the ability to produce different speeds, the ability to control active and reactive power, improvement of power quality, reduced costs related to inverter, etc. (Harini, Kumari & Raju, 2011; Chen & Hsu, 2006; Poitiers, Bouaouiche & Machmoum, 2009). Variable speeds in these turbines give them the ability to be able to operate in broader areas of wind, working to maximum efficiency. This study used a wound-rotor induction generator where the wound rotor was connected to the network via sliding rings to a converter machine and the stator machine. One of the most important advantages of DFIG is that the electronic equipment carries only a fraction of the total power, around 20 to 30%, meaning a reduction in losses and costs in the electronic power converter. In addition to providing necessary conditions for the electrical network, a wind system control zone has a duty to provide maximum possible transfer of wind energy with the best efficiency. In this regard different controlling methods have been proposed by the researcher (Belgacem, Mezouar, & Massoum, 2013; Utkin, 1977).

In this study, a sliding mode control was used to control the speed of a doubly fed induction generator. Sliding mode control theory was proposed by Utkin in 1977 since when theoretical work and applications of the sliding mode control have been developed. One of the most important benefits of sliding mode control is robustness and this method is a nonlinear control method, so it will be used in the system where there is uncertainty. This uncertainty may be structural (parameters uncertainty) and/or non-structural, for example unmodelled dynamics. In this control method, stability will be gained by holding states of the system on the sliding base (Utkin, 1977; Amimeur et al., 2012; Bekakra & Attous, 2012). This paper offers a control method for an inverter machine to regulate active and reactive power exchanged between the machine and the grid. Control of the active power of the wind speed was adapted in a wind energy inverter system and the control of the reactive power allowed a unity power factor between grid and stator to be reached.

2. OVERVIEW OF DOUBLY FED INDUCTION GENERATOR

Tremendous progress has been made since 1975 in development in the field of wind turbines for power production. The first modern turbine was connected to the grid around 1980. With increased usage of wind energy and wind power production DFIG is used widely nowadays. The reason that this type of generator is known as doubly fed induction generator is that the produced electrical power transfers in two ways, stator as well as rotor. These generators deserve special attention because of their features which allow them to work with variable wind speed. The use of the wind power plants with variable speed has advantages compared to wind power plants with constant speed. Although the wind power plants with constant speed can be connected to the grid directly, a wider energy range can be covered by wind power plants with variable speed. Additionally, they have less mechanical stress and noise. Nowadays, with development of power electronics, control of all speed is possible and cost effective (Gautam, Vittal & Harbour, 2009; Tapia, Tapia, & Ostolaza, 2004). This paper considers DFIG with variable speed which has important features in working with variable wind speed. Figure 1 shows the designs of a wind power plant structure in which the stator's orbit of DFIG was connected directly and rotor's orbit was connected by a back-to-back converter (generator side converter and grid side converter) with slippery rings to the grid. A capacitor known as a DC link was used between two converters as an energy saver and to reduce voltage ripple (Yanhua et al., 2011; Junyent-Ferre & Gomis-Bellmunt, 2010).
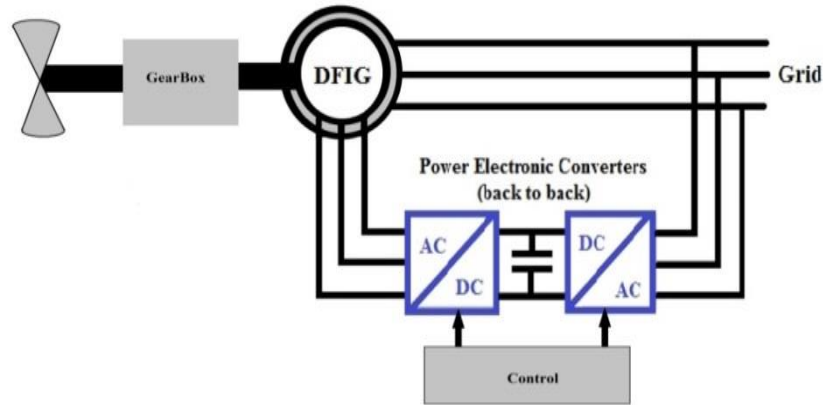
Figure 1: A grid connected doubly fed induction generator and its convertors

At the normal operation mode DFIG can control active and reactive power separately via a grid side converter. Furthermore, the rotor side converter can remove the need for a soft starter at the time of grid connection. Two subsystems known as mechanical and electrical systems were present that show the overall control plane of the DFIG. The control systems were designed for different purposes, but the main goal was to control the power to be injected to the grid (Jadhav & Roy, 2013). The active power released to the grid was controlled by the rotor side converter, while injected reactive power was controlled by both converter (Figure 2).
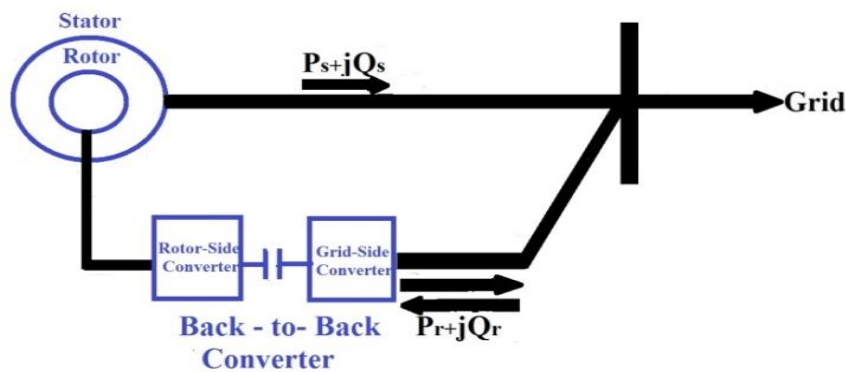
Figure 2: doubly fed induction generator

An electrical system to protect against overloading was also constructed. A mechanical subsystem to control the mechanical power output of the wind turbine by pitch adjustment was designed. Design of a low speed multipolar DFIG is not possible technically because the DFIG based on the wind energy conversion systems gearboxes are still required. Use of the DFIG will make production of good usable energy possible even when the machine speed is out of synchronous speed (Jadhav & Roy, 2013; Huazhang & Chung, 2012).

3. WIND GENERATION SYSTEM MODELLING
3.1. Modelling of the DFIG

For modelling the DFIG system with variable wind speed, the following elements needed to be modelled: DFIG, turbine, the control unit as well as designing a sliding mode controller and this paper will investigate all respectively. The rotating field wound rotor induction machine model is shown in Figure 3 (Hamane, 2012).

Figure 3: Park's transformation model of the DFIG

The equivalent circuit of a doubly fed induction machine with reference to magnetic losses is shown in Figure 4 and the mathematical machine model has been written in order to gain a decoupled system from control at a suitable reference field (d-q) with a fixed stator flux. In this case the flowed active and r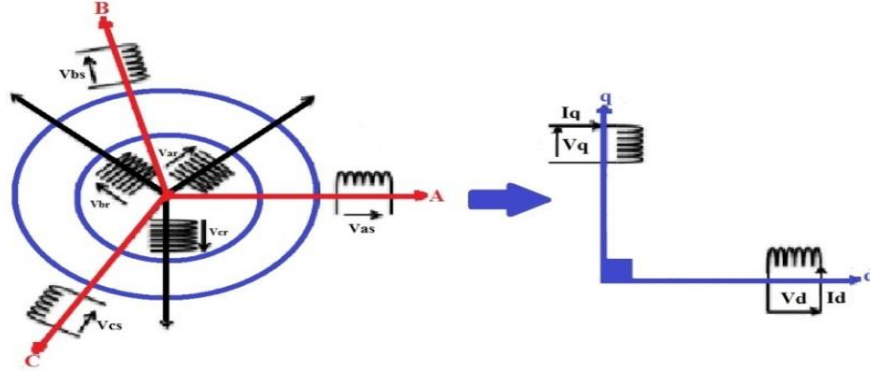eactive power control between DFIG stator and power grid with use of the sliding mode controller will be synthesized (Slottweg et al., 2003; Han, Zhang & Yin, 2008).
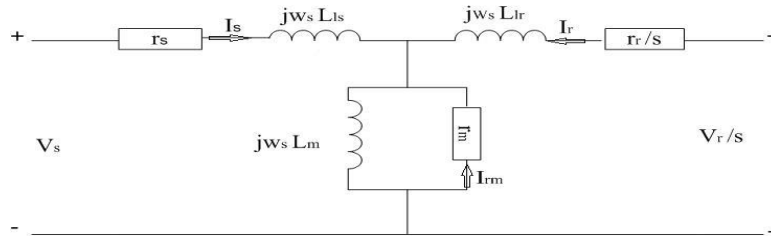
Figure 4: Equivalent circuit of DFIG

DFIG classic electrical equation in the Park field is written as follow (Belgacem, Mezouar & Massoum, 2013; Rao & Laxmi, 2012):

Equation 1, Stator and rotor voltage equations:

$$V_{ds} = \frac{d}{dt}\Phi_{ds} - \omega_s \Phi_{qs} + r_s i_{ds}$$

$$V_{qs} = \frac{d}{dt}\Phi_{qs} + \omega_s \Phi_{ds} + r_s i_{qs} \qquad (1)$$

$$V_{dr} = \frac{d}{dt}\Phi_{dr} - (\omega_s - \omega)\Phi_{qr} + r_r i_{dr}$$

$$V_{qr} = \frac{d}{dt}\Phi_{qr} + (\omega_s - \omega)\Phi_{dr} + r_r i_{qr}$$

The flux equations for stator and rotor are as Equation 2:

$$\Phi_{qs} = (L_{ls} + L_m)i_{qs} + L_m i_{qr}$$

$$\Phi_{ds} = (L_{ls} + L_m)i_{ds} + L_m i_{dr} \qquad (2)$$

$$\Phi_{qr} = (L_{lr} + L_m)i_{qr} + L_m i_{qs}$$

$$\Phi_{dr} = (L_{lr} + L_m)i_{dr} + L_m i_{ds}$$

Torque generated of DFIM based on stator currents and rotor flux is shown in Equation 3:

$$T_e = \frac{3}{2} P \frac{L_m}{L_r}(\Phi_{dr} i_{qs} - \Phi_{qr} i_{ds}) \qquad (3)$$

Where P = number of pairs of the poles.

177

Equation 4, mechanical dynamic equation is expressed as:

$$J\frac{dw_m}{d_t} + Bw_m = T_e - T_L \qquad (4)$$

Where:
- J = Moment of machine inertia
- B = friction coefficient respectively.
- T_L = external load torque and
- ω_m = rotor's mechanical speed.

The total active and reactive power production is as follow:

$$P = V_{ds}i_{ds} + V_{qs}i_{qs} + V_{dr}i_{dr} + V_{qr}i_{qr} \qquad (5)$$

$$Q = V_{qs}i_{ds} - V_{ds}i_{qs} + V_{qr}i_{dr} - V_{dr}i_{qr}$$

3.2. Modeling of the wind turbine and gearbox

Wind Energy Conversion Systems (WECS) are systems used to convert wind energy to mechanical energy. The amount of capacity which is receivable as P_t by the wind turbine has direct proportion with power coefficient C_p and its relationship as follow:

$$P_t = \frac{1}{2}C_p(\lambda,\beta).\rho_{air}.R^2.V^3 \qquad (6)$$

Where:
- ρ_{air} = air density,
- R = Blade radius,
- V = air speed, and
- B = angle of the blade's turbine.

The power coefficient curve $C_p(\lambda,\beta)$ for a given speed will be expressed based on the λ. The turbine torque is the ratio of output power to shaft speed w_t and is equal to:

$$T_t = \frac{P_t}{w_t} \qquad (7)$$

The turbine normally connects to the shaft generator by a gearbox where the ratio of its gear is equal to G. On the other hand the shaft speed of the generator was chosen at a suitable speed area. Regardless of the transfer losses, torque and shaft speed of the wind turbine which is related to the gearbox side is given by Equation 8:

$$T_m = \frac{T_t}{G} \quad And \quad \Omega_{mec} = G.\omega_t \qquad (8)$$

where T_m is torque of the generator and Ω_{mec} is the wind turbine's mechanical speed. The wind turbine was able to produce a certain amount of the power proportional with wind speed. This amount, which is expressed by C_p, is a function of wind speed and also a function of pitch angle blades of the wind turbine (Belgacem, Mezouar & Massoum, 2013; Gaillard et al., 2009). Although this equation looks simple, C_p is dependant on the λ relation that is actually between turbine's angular velocity w_t and wind speed V. This ratio is known as tip speed ratio and is written as Equation 9:

$$\lambda = \frac{\omega_t.R}{V} \qquad (9)$$

The relation between C_p and λ is shown in Figure 5, showing that some of the λ there is a return to C_p that will be maximum and this factor causes maximum power for the given wind speed.

Figure 5: Aerodynamic power coefficient variation C_p against tip speed ratio λ

Figure 6 shows the overall simulated schematic for the wind turbine, gearbox and shaft.

Figure 6: simulated schematic for the wind turbine, gearbox and shaft
.

4. WIND TURBINE CONTROL BY DFIG

Control of the fixed output DFIG was by stator, such as three phase voltage, frequency and output power function that feeds the network via stator current. Control of the machine was by converter; moreover, output active power can be controlled by the slope of the turbine blades which it adjusts on the β angle blade. In other words, coefficient of aerodynamic efficiency changes the rotor's blade angle. If the wind speed exceeds the rated value, this angle control is used for output power fixation. The wind turbine with doubly fed induction generator included two main controls: back-to-back converter and vane angle control, both of which will be investigated (Yin, Li & Zhou, 2006; Lei et al., 2006).

4.1. Back-to-back converter control

The back-to-back converter consists of four main parts: two inverters which each have, as well as a switching control another control as well. The rotor side converter is responsible for voltage control or reactive power and extraction of the optimal power from the wind, while the network side converter is responsible for control of the DC bus voltage amount; DC is the interface of the two converters and transformers or series reactors which connects the converter to the network.

Rotor side converter (RSC) control

The main task of this converter is output power control and terminal voltage of the DFIG. In this method, the rotor side converter is similar to common methods used in the doubly fed induction generator. Converter controls will be modelled based on the rotor-controlled voltage source, so in the space of two axial d and q the amount of the rotor's d and q axial voltage should be clear.

Grid side converter (GSC) control

Since DFIG based on the wind system is sensitive to voltage changes, disturbed grid voltage conditions should be considered in the quality design of GSC. As noted, the most important task of the grid side converter is to regulate bus voltage regardless of the rotor power flow side, so V_{dc} should be compared with its reference amount and applied to a PI controller to take the amount of the flow at the grid side converter. Control of the GSC by use of the merged sliding mode controller (SMC) and PI controller under grid disturbances for the dynamical control performance evaluation of DFIG were carried out in this study.

4.2. Vane angle control

According to the C_p- λ curve shown in Figure 5, in order to maximise power extraction of the wind, zero helix angles should always be considered unless the rotor speed is greater than that allowed. So, for the control of vane angles, only the velocity difference between the maximum speeds should apply to a PI controller and areas of change can be limited between zero and the maximum angle. Also, it should be noted, speed changes of the vane angle should not be more than a clear amount.

5. DESIGN OF SLIDING MODE CONTROL ALGORITHM

The sliding mode control is a nonlinear control method which guarantees the control strategy in the face of uncertainty. In this case the system stability was obtained by keeping the system's states on the sliding surface. The sliding mode controller is a variable structure controller which switches with high-frequency between several control rules. Basically, the variable structure controller includes several different continuous environs that can map plant state to a control surface, while switching between different environs by shown plant state is determined by a function switching controller implements a nonlinear control rule in order to drive and keep the state of the system on a favourable hyper surface. A special issue about the control plan is that it defines a sliding surface with property guaranteed to be stable and attractive. The sliding mode method has high flexibility, also it is an effective and very strong method (quite robust), whilst on the other hand it needs relatively little information about the system and is also insensitive to the parametrical changes of the system. The sliding mode controller does not need to follow mathematical models accurately like classical controllers but needs to know the range of parameter changes for ensuring sustainability and satisfactory conditions. The block diagram of the SMC in a variable speed wind turbine application studied in this paper is shown in Figure 7. The parameters are shown in Table 1.
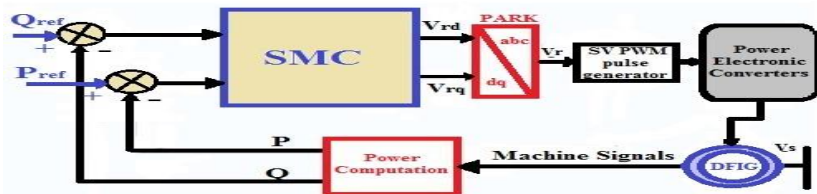

Figure 7: Block diagram of a sliding mode control of a DFIG.

Table 1: Parameters

Rated Power(DFIG)	1.5MW
V_s (Stator Voltage) (DFIG)	300/690V
B (Coefficient of viscous friction) (DFIG=+Turbine)	0.071 / .N. m .s/ rd
r_s (Stator Resistance) (DFIG)	0.012 ohm
r_r (Rotor Resistance) (DFIG)	0.021ohm
R(Blade radius)(Turbine)	2m
L_s (Stator Inductance) (DFIG)	13.732mH

L_m (Mutual Inductance) (DFIG)	13.528mH
L_r (Rotor Inductance) (DFIG)	13.703mH
J (Moment of inertia) (DFIG=+Turbine)	50kg.m2
P (Poles Pairs) (DFIG)	2
Rated Speed(DFIG)	100rad/s
F (Nominal frequency) (DFIG)	50Hz

The sliding mode control method includes the calculation of equivalent and discontinuous variable control from a favourable surface of the selected sliding mode.

$$S(\phi_{dr}) = \overset{*}{\phi}_{dr} - \phi_{dr}, S(\phi_{qr}) = \overset{*}{\phi}_{qr} - \phi_{qr} \qquad (10)$$

Reference fluxes ϕ_{qr}, ϕ_{dr} will be defined in accordance with the objectives control of stator current. In the sliding mode regimen of the system dynamic, the sliding mode is subjecting to the following conditions: $S(\phi) = 0$ and we have for the ideal sliding mode: $\dot{S}(\phi) = 0$. Reference stator voltage components for sliding mode conditions are defined as follow:

$$V_{dreq} = \overset{*}{\phi}_{dr} + \frac{1}{Tr} \phi^*_{dr} - W_r \phi^*_{rq} - \frac{1}{T_r} l_m i^*_{ds} \qquad (11)$$

$$V_{qreq} = \overset{*}{\phi}_{qr} + \frac{1}{Tr} \phi^*_{qr} + W_r \phi^*_{dr} - \frac{1}{T_r} l_m i^*_{qs}$$

V_{dreq} and V_{qreq} are components of the rotor voltage respectively. The stator currents sliding surface will be calculated based on the below equations:

$$S(i_{ds}) = \overset{*}{i}_{ds} - i_{ds}, S(i_{qs}) = \overset{*}{i}_{qs} - i_{qs} \qquad (12)$$

The reference rotor flux in the sliding mode regimen is determined by below equation:

$$\phi^*_{dr} = \frac{\sigma l_r}{W_s l_m} (\frac{r_s}{\sigma} i_{ds}^* - W_s i^*_{sq} - \frac{1}{\sigma} u - \frac{r_s}{\sigma w_s} i_{qs}^*) \qquad (13)$$

$$\phi^*_{qr} = \frac{\sigma l_r}{W_s l_m} (-\frac{r_s}{\sigma} i_{qs}^* - W_s i^*_{ds} - \frac{r_s}{\sigma w_s} i_{ds}^*)$$

where σ is the total leaking constant and determines as below: $\sigma = l_s (1 - \frac{l^2_m}{l_s l_r})$. Rotor voltage of references are defined as follow:

$$V^*_{qr} = V_{qreq} - V_{qrn}, V^*_{dr} = V_{dreq} - V_{drn} \qquad (14)$$

where n shows discrete components of the rotor voltage of reference. The designed control unit by MATLAB/Simulink software is shown in Figure 8.
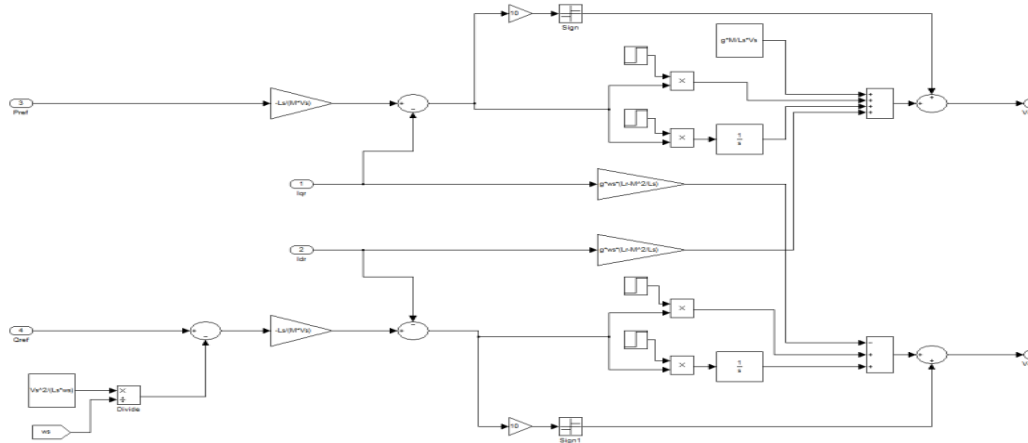
Figure 8: Diagram of the control strategy

A simple form of control operation is a relay function of sliding mode theory. Design of the control unit is expressed by use of Equation 15 which shows fusion of sliding control unites and PI.

$$U_{dq} = U_{PI} + K * sign(S_{dq}) \qquad (15)$$

6. SIMULATION RESULTS AND DISCUSSION

To verify the proposed method, simulation results of a DFIG generator sample as shown by MATLAB /Simulink software are presented in this section. Also, the performance of the DFIG system is analysed under grid voltage fluctuations. The wind turbine was of doubly fed induction generator type. The sliding mode controller was achieved based on the stator flux orientation reference in order to control the active and reactive powers by direct component and stator flows second degree and via desired power flow between grid and generator in the MATLAB environment (Figure 9).

Figures 10 to 15 show machine speed deviation per second; active power of rotor; reactive power of rotor; machine angle per second; DFIG terminal voltage; and DC link voltage under balanced grid, respectively.
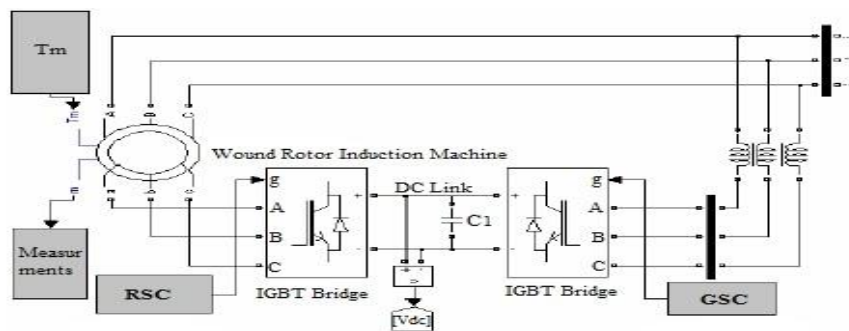

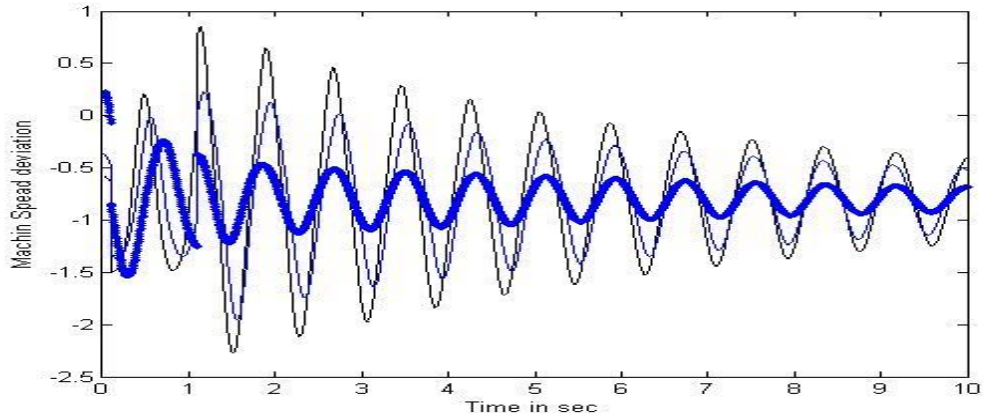*Figure 9: configuration of wind turbine and DFIG system with MATLAB*

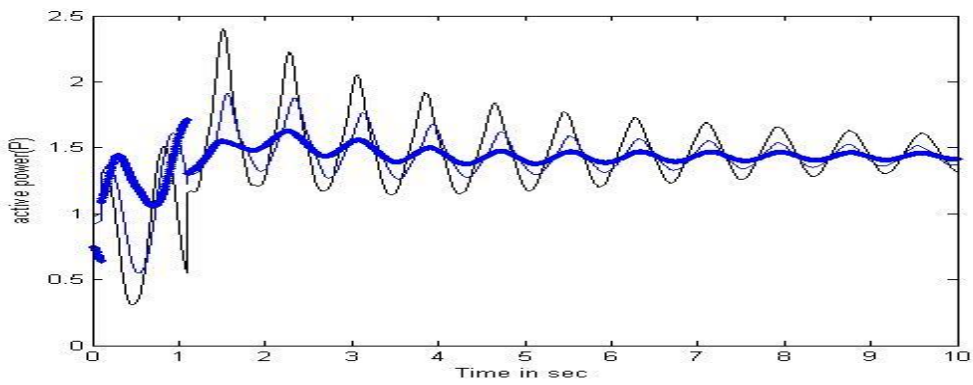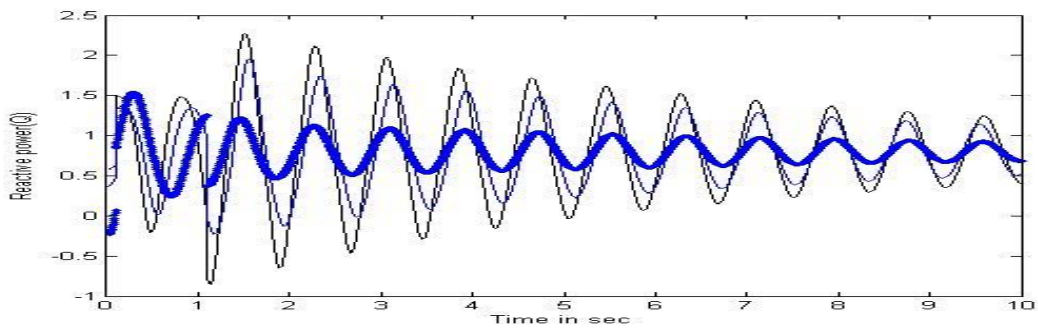*Figure10: Machine Speed Deviation per Sec*

Figure 11: Active power of rotor

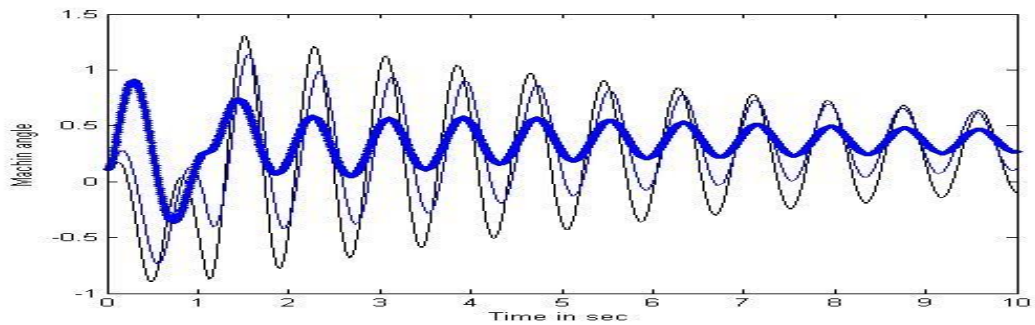*Figure 12: Reactive power of rotor*
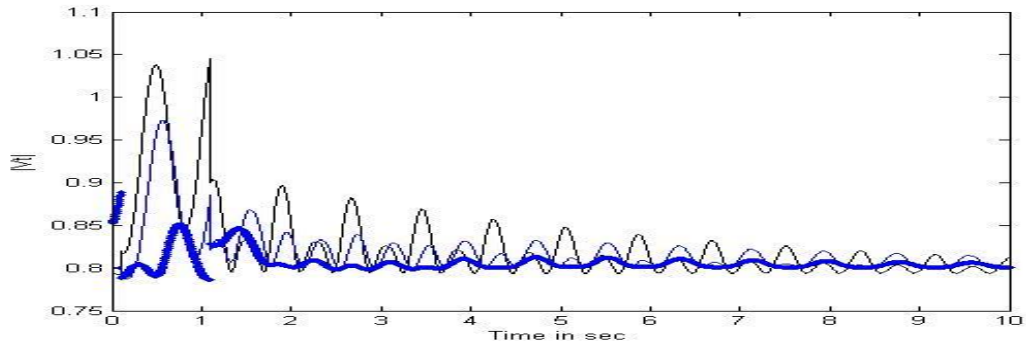

Figure 13: Machin angle per Sec
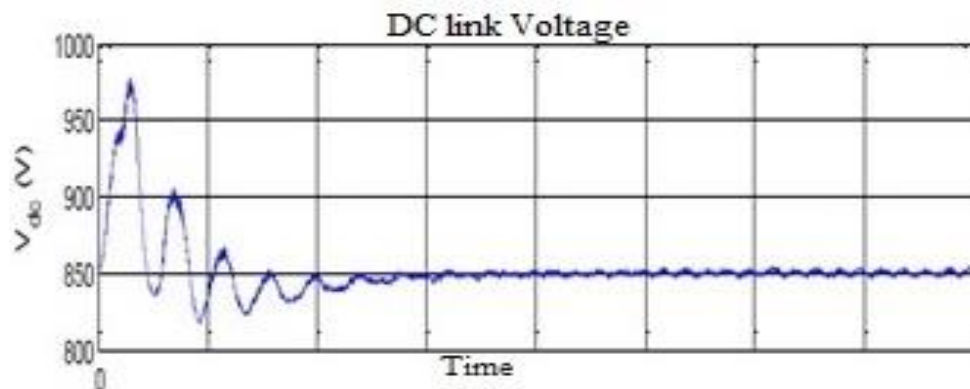
Figure 14: DFIG Terminal voltage

Figure 15: DC link Voltage under balanced grid

7. CONCLUSION

In this study a complete system for electrical energy production using a doubly fed induction generator (DFIG) with a wind turbine was simulated using the MATLAB/Simulink environment. The studied system consisted of a DFIG with stator and rotor, in which the stator was connected to the grid directly and rotor was connected to the grid via two converters: a machine converter and a grid converter. Control of the machine inverter provided a set of active and reactive powers exchanged between the grid and the machine. With the consideration of turbine variable velocity state and a design controller for DFIG in the form of a sliding mode, favourable results were reached in spite of the uncertainty of the system's active and reactive powers.

8. REFERENCES

Amimeur, H., Aouzellag, D., Abdessemed, R., Ghedamsi K., Sliding mode control of a dual-stator induction generator for wind energy conversion systems, Electrical Power and Energy Systems, Vol. 42, pp. 60-70, 2012.

Bekakra, Y., Attous, D.B., "Comparison study between SVM and PWM inverter in sliding mode control of active and reactive power control of a DFIG for variable speed wind energy", International Journal of Renewable Energy Research., Vol.2, No.3, 2012

Belgacem, Kh., Mezouar, A., Massoum, A., "Sliding Mode Control of a Doubly-fed Induction Generator for Wind Energy Conversion", International Journal of Energy Engineering 2013, 3(1): 30-36 DOI: 10.5923/ j.ijee.20130301.05.

Chen, W-L., Hsu, Y-Y., "Controller Design for an Induction Generator Driven by a Variable-Speed Wind Turbine", IEEE Transactions on Energy Conversion, Vol. 21. No. 3, pp.625–635, 2006.

Gaillard, A., Poure, P., Saadate, S., Machmoum, M., "Variable Speed DFIG Wind Ener gy System for Power Generation and Harmonic Current Mitigation, Renewable Ener gy 34,2009, pp 1545-1553

Gautam. D, Vittal. V, Harbour. T, "Impact of Increased Penetration of DFIG-Based Wind Turbine Generators on Transient and Small Signal Stability of Power Systems", IEEE Transactions on Energy Society, Vol. 24. No. 3, pp.1426-1434, 2009.

Hamane, B., Benghanem, M., Bouzid, A.M., Belabbes, A., "Control for Variable Speed Wind Turbine Driving a Doubly Fed Induction Generator using Fuzzy-PI Control" Energy Procedia Published by Elsevier Ltd, 18 (2012) 476 – 485

Han, A., Zhang, Z., Yin, X., "Study of Factors Affected the Rotor Over-Current of DFIG During The Three Phase Voltage Dip," IEEE, Third Int. Conf. on Elect. Utility, 2008

Harini. C, Kumari. NK, Raju. GS, 2011 "Analysis of wind turbine driven doubly fed induction generator", in International Conference on Electrical Energy Systems (ICEES), pp.246-251,

Huazhang H, Chung CY. "Coordinated damping control design for DFIG-based wind generation considering power output variation". IEEE Trans Power Syst 2012;27(4):1916–25.

Jadhav, H.T., Roy, R., A comprehensive review on the grid integration of doubly fed induction generator. Electrical Power and Energy Systems.49(2013)8-18

Junyent-Ferre, A., Gomis-Bellmunt, O., Sumper, A., Sala, M., Mata, M., "Modeling and control of the doubly fed induction generator wind turbine ", Simulation Modelling Practice and Theory 18 (2010) 1365–1381, Elsevier.

Lei, Y., Mullane, A., Lightbody, G., Yacamini, R.," Modeling of the Wind turbine with a doubly fed induction Generator for grid integration studies" IEEE transactions on energy conversion, Vol.21.NO1, March 2006

Poitiers, F., Bouaouiche, T., Machmoum, M., "Advanced control of a doubly-fed induction generator for wind energy conversion" Electric Power Systems Research 79 (2009) 1085–1096

Rao, Y.S., Laxmi, A.J., "Direct torque control of DFIG based wind turbine under voltage dips" International Journal in Advance in Engineering, 2012

Slottweg, J.G., Haan, S.W.H., Polinder, H., Kling, W.L., "General Model for Representing Variable Speed Wind Turbines In Power Systems, " Vol.18,No.1,2003, pp.144151,2003.

Tapia, G., Tapia, A., Ostolaza, J.X., "Modeling and control of wind turbine driven by doubly fed induction generator", IEEE Trans. Energy Conversion, Vol.18, No.2, pp.194-204, Nov. 2004.

Utkin, V., Variable structure systems with sliding modesa survey. IEEE Trans. Automat Control,; Vol. 22, N°. 2, pp. 212-222, 1977.

Yanhua. L, Zhang. Xu, Zhao, Dongmei. M, "Research on the Wind Farm Reactive Power Compensation Capacity and Control Target", in Asia Pacific Power and Energy Engineering Conference (APPEEC), pp.1-5, 2011.

Yin, M., Li, G., Zhou, M. "Study on the control of DFIG and it's Responses to grid disturbances" IEEE 2006.

#368: The relatıonshıp of sustaınabılıty and technology ın offıce ınterıors

Fatma Ceyda GÜNEY YÜKSEL[1], Füsun SEÇER KARIPTAŞ[2], Sennur HILMIOĞLU[3]

[1] Haliç University, Istanbul, fatmaceydayuksel@halic.edu.tr
[2] Haliç University, Istanbul, fusunsecer@halic.edu.tr
[3] Haliç University, Istanbul, sennurhilmioglu@halic.edu.tr

Abstract: It is possible to find various definitions of sustainability in different disciplines, such as sustainable economy and sustainable agriculture. Sustainability in design is handled a little differently from these general concepts; it needs to be interpreted outside of the usual definitions. The aim of this study was to consider sustainability, which has a popular place in today's design concept, within the scope of the design of office interiors and to interpret its effect on the design of these spaces. The concept of sustainability, which we can interpret as a tangible effect of the Industrial Revolution, has caused mankind to face the fact that the necessary resources are not infinite, regardless of space or product design. Developing technologies have made migration from rural areas to cities attractive. This situation also caused unconscious consumption of energy resources and made mankind question the production and consumption process again. Especially in new building systems, energy conservation and minimizing environmental pollution through sustainable design approaches come into play at this point, allowing the user to reach comfort conditions of the living space. The main function of offices is to continue the act of working and doing business. However, the concept of office, which developed over time, has allowed additional functions to be added to these office areas, with working areas, resting, socializing, eating areas etc. The office has turned into places where needs are also met. With changing conditions, office interior designs must also adapt to these conditions. It is important for office interiors to be sustainable, to adapt to changing conditions and to meet more demands with differing function needs. Within the scope of the study, control systems that create physical environmental conditions such as heating, ventilation, lighting in office interiors and criteria that can make the space sustainable such as flexible furniture, correct space organization, selection of materials and reinforcement elements will be discussed in detail. Technologically equipped applications required to create sustainable office interiors will be explained through selected examples.

Keywords: sustainability; office; interior design; technology

1. INTRODUCTION

The concept of sustainability has been one of the most researched, studied and touched upon issues of the 21st century, especially when we consider it in terms of design. To define it in a general framework, in the words of Çelik Erengezgin, sustainability is "… an effort to maintain life by taking everything into account, not in spite of everything" (Erengezgin, 2005). In this context, it is possible to think that sustainability emerged as a result of the effort to maintain the existing one. For example, many factors such as the continuity of existing energy, long-term use of natural resources, and the useful life of selected building material have been effective in the development of the sustainability of buildings.

The residence, which was the main space used for commercial and business activities in the past, has relinquished its place to the office where we now spend most of our time, continuing to interact both socially and spatially. This situation has revealed the necessity of completing some basic requirements in office design. The need for workspaces has gained more importance with the increase in the time allocated to the act of work. In general, offices are areas where people work individually or together, and also have social interaction. The main function of offices is to continue the act of working and doing business. However, the concept of office, which has developed over time, has allowed additional functions to be added to these areas, so offices can be used for resting, socializing, eating, etc., as well as working areas. It has turned into places where needs are also met. The most important parameter forming the basis of this change has been technology. The transformation of office spaces into areas that can serve different functions can be achieved by constructing the relationship in the context of technology and space. At the same time, this relationship allows for office designs to be made in accordance with comfort conditions for the user. This means providing a suitable environment to create a sustainable space. When designing a sustainable space, it is possible to create comfortable and harmonious spaces for the user, without requiring high costs, by adapting parameters such as flexibility, correct material selection, correct spatial organization, full-empty volume relationship, transformability, and simplicity in design. When we consider the design of office interiors in this direction, it will be possible to create spaces suitable for different needs with alternative space suggestions designed with technology, and to consider these spaces as sustainable spaces.

The aim of this study was to consider the relationship between sustainability and technology, which has a popular place in today's design concept, within the scope of the design of office interiors and to interpret the effect on the design of these spaces. Within the scope of the study, alternative design proposals for office interiors will be presented on the scale of the parameters created by the sustainable design criteria through flexible interior design and changes in the technological context. New systems developed with technology, ventilation, lighting suggestions and the effects of these suggestions on office interiors were considered. The contribution of flexible space design to the reorganization of office interiors will be discussed with the use of furniture and materials which have developed with technology and its reflection on office design in the context of spatial and working functionality will be evaluated.

2. SUSTAINABILITY AND TECHNOLOGY

The Industrial Revolution, then the oil crisis, global warming, etc., from the 1970s and 1980s were issues that forced people to face nature and themselves. In this context, sustainable architecture has gained a conceptual dimension, different from the ecological design approach. Sev defined sustainability as a design philosophy that tries to redefine the necessity of designing and using buildings with a sense of responsibility towards the environment and determining the limits of how to behave in this framework (Sev, 2009).

The concept of sustainability, which we can interpret as a tangible effect of the Industrial Revolution, has caused mankind to face the fact that the necessary resources are not infinite, regardless of space or product design. Developing technologies have made migration from rural areas to cities attractive. The emergence of different job opportunities and the rapid population growth in urban areas have also led to the problem of lack of resources over time. Accordingly, new building systems emerged as a result of technological development, with a resultant near-extinction for certain green areas. It has brought along rapid population growth and unplanned urbanization (Güney Yüksel and Seçer Kariptaş, 2019). While this situation also causes unconscious consumption of energy resources, it has made human beings question the production and consumption process again.

The concept of sustainability, which aims to eliminate environmental problems due to developing technology and economy, to raise environmental awareness and to use resources and energy efficiently, has been effective in shaping many building design processes. The adoption of approaches such as energy conservation and minimizing environmental pollution, especially in new building systems in the design process, has led to an effective effort to find solutions to the problems arising from the use of energy resources. For this reason, sustainability has been a system of thought that paved the way for the concept of "green technology".

In order to create a sustainable future, the use and enhancement of these technologies is of great importance. At this point, the philosophy of achieving maximum comfort with less energy has necessitated smart building designs and appropriate technologies. In sustainable development, technology has an important place in establishing a relationship with the environment. Although it is known how much technology contributes to the improvement of the life quality of users, it is an undeniable fact that sometimes it also has harmful effects on the environment. At this point, it is necessary to give importance to the use of technology in the phase of creating a sustainable future.

2.1. Sustainable approaches to the office interior

Technological developments and new construction methods that emerged in the 20th century allowed the emergence of different applications in office design. The Larkin Office Building in New York (Figure 1), designed by Frank Lloyd Wright in 1906, met the aesthetic values of the period. The working order and the spatial organization related to it has been an example that reflects the design concept in question (Tercan, 2014).
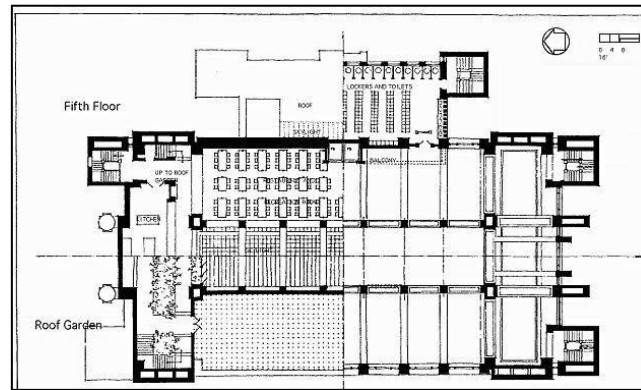

Figure 27: Larkin office building ground floor plan, Frank Llyoyd Wright, New York (Url 1)

Inclusion of computer systems in working life since 1980 brought a new direction to office designs with technology. Especially for heating-lighting-ventilation, new standards have been developed and supporting systems in this field have begun to be reflected in the design process (Güney Yüksel, Seçer Kariptaş and Kariptaş, 2022).

The use of technology, which has become a necessity in today's age, has reduced the need for physical space in offices compared to the past, and has brought with it the opportunity to use it away from the working. Especially with portable computers, working spaces have become much more flexible to design. The high user density shows how important resource and energy conservation is when designing office spaces. In this direction, it is clear that office buildings designed by considering sustainable design criteria support minimum energy use by considering user comfort conditions. It is known that a sustainable office building provides 40% energy efficiency compared to a standard office structure (Eşsiz and Özgen, 2004).

In order to minimize energy consumption in offices, the building should be designed in accordance with effective energy use. In other words, the building is expected to meet the features that will benefit from renewable energy sources such as wind energy and solar energy and support passive systems. At the same time, it is necessary to prefer building designs that require less mechanical systems and will not harm the ecosystem during construction, use and demolition stages. However, it is important for an energy efficient office building to consider many criteria such as climate data, sensitivity for the environment, and respect for material and water conservation.

When we consider energy efficiency in smart office buildings, depending on the air flow outside environment, the user can be informed to open or close the windows; systems that stop artificial lighting even when daylight is sufficient for lighting contribute to energy savings to a large extent. The said sensor systems have infrared, ultrasonic and acoustic sensor types that activate the lighting and air conditioning systems when users are detected. At this point, it will be possible to save 80% thanks to the user sensors placed indoors (Morhayim, 2003).

In the consumption of water resources, ensuring efficient water use is necessary to ensure sustainability. In office structures, water is needed for many purposes like drinking, cleaning, irrigation, etc. (Figure 2). It is necessary to keep the energy consumption needed in all processes such as the use, treatment, distribution and re-collection of water under control. At the same time, reducing the amount of water used and the rate of waste water are important criteria in this context. The reuse of water such as rain water, gray water (waste water used in sinks, dishwashers and washing machines) and their use in the same areas will reduce the rate of use of clean water, which is often of drinking water quality (Sözer, 2000).
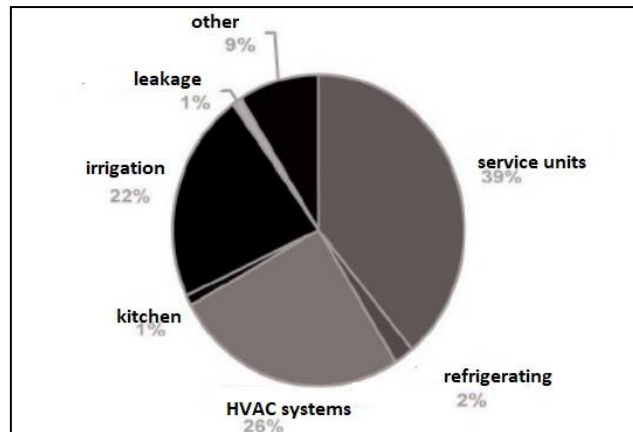
Figure 2: Water consumption diagram in office buildings (Tuğlu Karslı, 2008)

The basis of a sustainable approach requires choosing the one that respects nature. For this reason, in the selection of materials in office interiors, both the protection of natural resources and the selection of long-lasting, high-strength, easily replaceable materials are important. At the same time, the fact that the material is suitable for the function and usage conditions of the place where it will be used and that it does not need much maintenance is one of the most important elements in the design of a sustainable office.

The office interior is important for the health and comfort of the employees. Providing indoor comfort conditions at the desired level is of great importance in working environments. In this context, it is necessary to choose the right ventilation systems. Natural ventilation systems provide energy savings to be used in mechanical ventilation. The use of these two systems that support each other, the planning of the necessary technical and spatial arrangements in the design phase, are among the solutions that increase the indoor air quality in this context.

It is especially important for office workers to feel safe in their working environment in terms of the sustainability of the working system. In this context, the important thing is to adapt the offices to the design process by providing the determined systemic infrastructure and spatial arrangement. Thus, it will be possible to use sustainable offices in terms of both spatial and working system.

2.2. Technology effect

Today, with technology that has increased its place in our working life, in addition to applications in the field of informatics and information in the office, it contains elements such as heating, ventilation, lighting, filtration, effective material and resource use, which both contribute to sustainable design criteria and allow the creation of spaces suitable for the comfort conditions of users. Many technological applications such as cleaning and ventilation of offices and thermal heat control systems support the efficient use of workspaces in this process.

Since the 1980s, buildings that can respond to the demands of technology users have come to the fore. In particular, this process created a starting point with the use of smart buildings for the first time in the USA. The European Smart Building Group in the UK defines smart buildings as: enables resources to be managed efficiently throughout life thanks to equipment and tools with minimum cost (So and Chan, 1999).

Smart building systems, which are the products of smart technologies, are structures developed by considering multiple technologies together. Buildings are expected to take into account energy efficiency while providing safety and comfort conditions for their users. With the automation systems in smart buildings, it will be possible to determine the amount of energy and fuel consumed by systems such as ventilation, heating, cooling and lighting, which use a large proportion of energy consumption. Monitoring processes such as the maintenance, control and inspection of systems, when necessary, enables efficient use of energy in buildings.

In particular, it is seen that most of the buildings with smart building technology are in harmony with their surroundings. However, a building that is not related to its environment and is designed independently will damage both itself and the environment in time. The relationship between sustainable design and technology comes into play in this direction. An office structure that does not harm the environment, nature and resources, prefers the use of renewable resources, gives importance to the harmony of materials with nature and recycling in all processes such as design and construction, and offers sustainable smart building technology (Boduroğlu, Seçer, Kariptaş and Altuncu, 2009).

Conservation of energy as well as production and consumption are among the criteria that have a significant impact on the creation of sustainable office interiors. Energy conservation includes energy recovery with passive methods in the building and the selection of energy-saving equipment. Systems such as lighting, heating, cooling, air conditioning and ventilation are the highest energy consumers in offices. Office buildings are one of the building types with the highest usage frequency during the day. It is not possible for an office to be illuminated all year round with only natural light. At this point, lighting should be combined with artificial lighting, taking into account the evening hours and the hours when natural light is not effective during the day. It is necessary to have information about how much artificial lighting is needed and how daylight changes during the day or seasonally (Abdelatia et al., 2010). Controlled use of natural lighting and artificial lighting in office buildings provides energy savings.

For daylight systems used in office buildings, it is possible to minimize energy and resource consumption by the integration of automatic lighting control systems (Figure 3.) (Tuğlu Karslı, 2006).
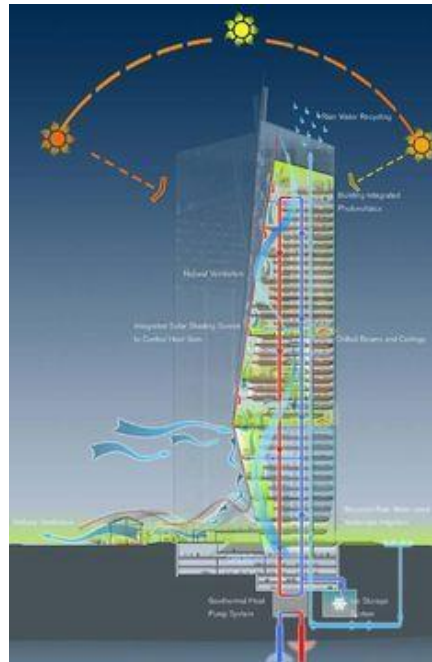

Figure 3: Daylight Diagram

Elements such as smart glass, light shelves and sky gardens can be used to benefit from natural lighting in office interiors. However, it is also important that the preferred lighting equipment is of high efficiency. At the same time, with smart automation systems, passive control facilities that will protect against unnecessary heat gain and loss in office buildings can be utilized. Passive systems reduce energy costs in office buildings with the help of factors such as orientation, insulation, window placement and design. There are 4 main components that make up these systems;

- Collector (windows, water tanks, dark walls)
- Sunlight
- Distribution (heating, natural circulation, simple circulation fans)
- Auxiliary systems (non-solar auxiliary heating or cooling systems, systems used when there is no sun or the stored energy is not sufficient) (Güngör, 1991).

It is possible to benefit from the systems installed in the office spaces to monitor the energy used in office buildings. These systems allow their users to monitor energy and instantly detect potential problems and inefficiencies. Lighting fixtures in office interiors ensure the conservation of the energy used and needed. Thus, the lighting power per square meter can be greatly reduced.

Conservation of water resources and efficiency in water use are at the forefront of resource conservation. It is necessary to use green tissue and irrigation strategies (reuse and recycling of water) that will not cause water waste in office interiors, and reduce the consumption of potable water. At the same time, water conservation can be ensured by making designs and applications that will reduce flood waters and waste water spilled into the sewerage system.

3. EXAMINING THE RELATIONSHIP OF SUSTAINABILITY AND TECHNOLOGY ON EXAMPLES

Applications regarding the relationship between sustainability and technology are encountered in today's office buildings. Although the offices were built in different periods, they have common points in terms of technology and sustainability. Analyzes were made on three different samples.

3.1. Turkey Is Bank headquarters building

One of the best examples of the period in which it was built, in terms of sustainability and technology, is the Türkiye Is Bank Headquarters Building (Figure 4). Located in Istanbul, the building consists of three office towers in total. When we consider the office structure in terms of sustainability and technology relationship, the applications we encounter are as follows (Tuğlu and Karslı, 2008):

- It is seen that lighting elements with high efficiency are preferred in all working places.
- Double skin applications such as low-e glass are used to prevent heat loss in the building.
- Energy conservation of the existing mechanical installation system is ensured by a computerized control system.
- Waste heat generated during mechanical heating in the building, water heating, etc. reusable in different functions.
- Systems used to collect rainwater allow the water to be stored and filtered, allowing its reuse in auxiliary functions such as garden irrigation.
- Equipment used in the plumbing system, such as pressurized reservoirs, waterless urinals, photocell taps, provides water savings.
- Sensors that can measure CO_2 in the office, adjust the appropriate temperature and humidity in the office interior, and balance the indoor air quality.
- Filters that prevent the spread of harmful bacteria are used in the ventilation system. Thanks to smart systems, maintenance can be performed at periodic intervals (Boduroğlu, Seçer, Kariptaş and Altuncu, 2009).

Figure 4: Türkiye Is Bank Headquarters Building (Url 2)

3.2. Palladium Tower

This building (Figure 5), located in Istanbul, was put into service in 2014 and consists of 42 office floors. The building's environmental awareness target is LEED Gold certificate and it was designed and built in accordance with the 'Gold', one of the upper levels of the LEED evaluation system (Kuran, 2014).

Within the scope of the project, energy modelling based on simulation was used. The indoor air quality of the building was created, and rainwater was stored and used in reservoir and for landscape irrigation. At the same time, emissions caused by transportation were minimized and thus, a healthy and efficient working area has been created for users. With the energy automation system, the energy consumption control of the building was ensured and energy savings achieved. The entire system is controlled by a computer system with 5,000 I/O capacity.

LED luminaires are used for lighting and the automation system used to minimize the energy consumption originating from lighting to help keep the consumption under control. In addition, cooling process in the office, free-

cooling is carried out through sensors; garden irrigation is done thanks to the gray irrigation system in the building; and controlled water use is ensured by means of aerators in the faucets.

Figure 5: Palladium Tower (Url 3)

3.3. Tekfen OZ Levent office building

The office building, which was completed in 2010, is located in Levent, Istanbul and is known as Turkey's first LEED field project in the commercial building category (Figure 6). The multi-storey car park, which was previously located at the location, was dismantled and parts of the building were used in the construction of the new office building (Url 4). The relationship between sustainability and technology can be listed as follows:

- The indoor air quality and, accordingly, the provision of sufficient oxygen in the space is ensured with the help of smart sensors in the building.
- In the sections of the building, heating and cooling can be controlled independently in every volume in line with the need.
- Energy recovery systems are used, thus, energy consumption is minimized.
- Within the framework of effective use of water, the water required for air conditioning and mechanical installations was provided from stored ground drainage water and rain water. At the same time, this water is used for garden irrigation.
- A central energy billing system has been established and meters have been placed on the floor distribution panels that feed the panels used by the tenants. Thus, it was possible to make separate measurements for each of them.
- All places without lighting control are centrally controlled by means of lighting automation. Dimmer system is preferred to provide light control.
- The automation system in the office structure is designed for the entire installation system. The automation system of the building is produced with microprocessor technology, which allows for renewal and development in terms of hardware and software (Mangan, 2006).
- Systems such as fire safety, lighting, ventilation, heating and cooling in the building are integrated into the automation system. If necessary, the systems automatically make the necessary changes in connection with each other.
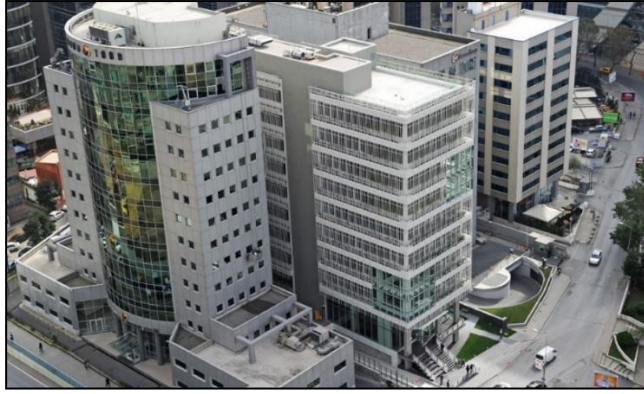
Figure 6: Tekfen OZ Levent Office Building (Url 5)

4. CONCLUSION

A building that does not harm the environment, nature and resources, attaches importance to recycling, and turns to renewable resources, together with the technology of its age, and structures designed in accordance with sustainable design needs are considered as smart buildings. Within the framework of the relationship between technology and sustainability, the source and way of using the energy used in smart buildings are important. For this reason, while the use of renewable energy sources is increasing, the use of systems that will be harmful to the environment should not be preferred.

Especially in smart building systems, active and passive systems are of great importance in ensuring energy efficiency. Along with the design process of the building, environmental factors should be taken into consideration and sustainable design criteria. At the same time, smart systems obtained with the help of technological possibilities contribute to the sustainability of buildings in this direction. It is seen that smart systems used in line with the examples discussed contribute to the sustainability of the buildings (Table 1).

Table 1: Relationship between sustainability and technology on examples

Criteria Providing the Sustainability-Technology Relationship	Turkey Is Bank headquarters building	Palladium tower	Tekfen OZ Levent office building
Indoor Quality	There are sensors in the office that can measure CO_2, adjust the appropriate temperature and humidity, and balance the indoor air quality.	Energy modeling based on simulation was used. The indoor air quality of the building has been created.	Ensuring sufficient oxygen in the space is provided with the help of smart sensors in the building.
Energy Conservation and Efficient Use of Energy	Energy conservation of the existing mechanical installation system is ensured by a computerized control system. Double wall applications such as low-e glass are used to prevent heat losses.	With the energy automation system, the energy consumption control of the building and energy savings were achieved. The entire system is controlled by a computer system with 5,000 I/O capacity.	A central energy billing system has been established and meters have been placed on the floor distribution panels that feed the panels used by the tenants. Systems such as fire safety, lighting, ventilation, heating and cooling are integrated into the automation system.
Efficiency in Water Use	Systems used to collect rainwater allow the water to be stored and filtered, allowing its reuse in auxiliary functions such as garden irrigation.	Garden irrigation is carried out thanks to the gray irrigation system.	The water required for air conditioning and mechanical installations was supplied from stored ground drainage water and rain water.

	Plumbing equipment, such as pressurized reservoirs, waterless urinals, photocell taps, saves water.	Controlled water usage is provided by means of aerators in taps.	Not Provided Effectively
Resource Conservation			
Environmental Relationship	Not Provided Effectively	Emissions caused by transportation are minimized.	Not Provided Effectively

While office buildings provide comfortable conditions due to the fact that they serve multiple and different users, it is expected that this technology will benefit much more from the balance of sustainability. It is quite clear that technology-centered office interior applications will be seen more frequently and the working order and operation will be carried out in this direction. For this reason, it is thought that all technology and sustainability-oriented solutions created in the office interior will be a part of the design and application in the following processes. It will be possible to implement all the arrangements made in the name of systemic, spatial and operation easily and to be developed in the light of technological data. Thus, in the future, the application and transfer of innovations and conveniences developed in different professions together with new technologies to the field of construction, will increase gradually.

5. REFERENCES

Abdelatia, B., Marenne, C., Semidor, C. 2010. Daylighting Strategy for Daylighting Schools: Case Study of Prototype Classrooms in Libya. Journal of Sustainable Development, 3, 60-67.

Boduroğlu, Ş, Seçer Kariptaş, F., Altuncu, D. 2009. Ecology-Technology Balance in Contemporary Turkish Architecture of the Last Ten Years, Symposium of the Last 10 Years of Planning and Architecture, 156-169.

Erengezgin, Ç., 2005. Energy Architecture. Ege University Solar Energy Institute 4th Renewable Energies Symposium and Industry Exhibition Abstracts.

Eşsiz, Ö. Özgen, A., 2004. "Double Shell Glass Facade Systems Reducing Energy Consumption in Office Buildings", Yapı Magazine, 97-104.

Güney Yüksel, F.C., Seçer Kariptaş, F., 2019. Sustainable approaches to residential interior. Near Architecture Magazine. 2 (2), 27-28.

Güney Yüksel, F.C., Seçer Kariptaş, F., Kariptaş, F., 2022. Reorganization of the office interior after the Covid-19 pandemic, bab Journal of FSMVU Faculty of Architecture and Design. 3 (1), 85- 102.

Güngör, A., 1991. Use of Solar Passive Systems for Natural Heating and Cooling of Buildings.

Kuran, A. 2014. Palladium Tower, Ae Magazine, 32, 10-14.

Lee, E., Selkowitz, S., Bazjanac, V., Inkarojrik, V., Kohler, C., 2002. High Performance Commercial Building Facades, Lawrence Berkeley National Laboratory, University of California, Berkeley, CA.

Mangan, S. D., 2006. Subsystem Evaluation in Smart Buildings: The Case of Istanbul, ITU FBE, Master Thesis.

Morhayim, L., 2003. Evaluation of Ecological Architectural Design Concept in the Example of High Office Buildings in Istanbul, Master Thesis, YTU Institute of Science and Technology, Istanbul.

Sev, A., 2009. "Sustainable Architecture", Building Industry Center, Yem Publishing.

So, At and Chan, WI 1999. Intelligent building Sysytems, Kluwer academic Publishers, USA.

Tercan, A., 2014. Design for a sustainable compromise in office buildings. Architect Magazine. 1 second, 62.

Tuglu Karsli, Hu., 2006. "Energy Conservation in Lighting", Installation Magazine, 126-137.

Tuglu Karsli, Hu., 2008. A Model Proposal for the Evaluation of Office Buildings and Environmental Performance Analysis in the Framework of Sustainable Architecture, MSGSU, Proficiency in Art Thesis.

Url 1: Great Buildings Drawing - Larkin Building

Url 2: https://archives.saltresearch.org/handle/123456789/204634

Url 3: https://www.tahincioglu.com/palladium-tower/galeri.php#

Url 4: https://www.akillisehirler.gov.tr/wp-content/uploads/kapasiteGelistım/Egitim_Pdf/Akilli_Yapilar.pdf p.105

Url 5: https://www.altensis.com/proje/tekfen-oz-levent-ofis-binasi-ilk-leed-certificate-ticari-office-binasi/

Url 2: https://archives.saltresearch.org/handle/123456789/204634

#371: Energy and exergy analyses of various wind turbine alternatives for a district

Nurdan Yıldırım[1], Levent Bilir[2]

[1*]*Faculty of Engineering, Department of Mechanical Engineering, Yasar University, 35100 Izmir Turkey, nurdan.yildirim@yasar.edu.tr*
[2]*Faculty of Engineering, Department of Energy Systems Engineering, Yasar University, 35100 Izmir Turkey, levent.bilir@yasar.edu.tr*

Abstract: Renewable energy power stations are becoming more popular even though their electricity production cost is higher than fossil fuel-based energy power stations. The reason behind this fact is that renewable energy sources have the advantage of sustainability and they provide fuel diversity to countries. Turkey is among the lucky countries for renewable energy sources with high wind energy potential. Generally, this high wind potential is exploited using large scale wind turbines although the use of small-scale wind turbines also offers a suitable use potential. In the present study, two different cases were taken into consideration for the wind turbine installation for a residential district, which consisted of 20 detached houses in İzmir city of Turkey. In the first case, the installation of individual small-scale wind turbines of 5-kW capacity for each house was considered. A single wind turbine with a 100-kW capacity was evaluated in the second case to meet the electricity needs of all the houses. The total turbine capacity for both cases were kept identical in order to make a comparison in terms of annual energy production. In addition, exergy efficiency values of the selected wind turbines were analysed in detail. The results of the study revealed that although the annual electrical energy needs of the houses could be covered in both cases, the case in which a single 100-kW wind turbine was installed was advantageous both in energy generation and exergetic efficiency aspects. Under the light of these results, it was concluded that for small communities or districts, the use of a single wind turbine with an adequate capacity was better than the use of individual residential-scale wind turbines.

1. INTRODUCTION

Worldwide renewable energy use is increasing rapidly due to environmental concerns. Although the production cost of electricity from renewable sources is still high compared to fossil-based fuels, the crucial advantages in sustainability and fuel diversity lead countries to install renewable power plants. Turkey has high renewable energy potential including solar, geothermal, wind energy etc. The high wind energy potential of Turkey has been exploited using generally large-scale wind turbines so far and 8 percent of the country's power is generated from wind energy currently. The present installed wind power plant capacity of around 6.5GW is planned to reach 20GW by 2023. Although the country has a considerable installed capacity on large-scale wind turbines, the use of small-scale turbines is not common. Possible installation of small-scale wind turbines can help to access the planned target for 2023. Additionally, these small turbines can provide local energy where it is needed. Energy analysis of wind turbines has been investigated in many studies. However, exergy analysis is also important in order to assess a system. The exergy efficiency along with the energy production of wind turbines have also been the subject of many investigations. Koroneos et al. (2003) performed exergy analysis of solar, wind and geothermal energy systems. They also compared the energy efficiency of the mentioned systems with non-renewable energy sources. Şahin et al. (2006) evaluated the energy and exergy performance of a 100kW wind turbine, which was operated in İstanbul, Turkey, for various wind speed values. Ozgener and Ozgener (2007) took a 1.5kW wind turbine, installed at Ege University campus area in İzmir, Turkey, into consideration. They calculated the capacity factor and exergy efficiency of the turbine using data collected from September 2002 to November 2003. The capacity factor was found to be 11.58% for the evaluated period and the exergy efficiency was found to be in the range of 0 to 48.72%.

Hepbasli and Alsuhaibani (2011) summarized the exergy and exergoeconomic analysis methods for a wind system and they provided a summary of previous studies in the field. They also proposed some improved indices and methods for exergy-based investigations. Redha et al. (2011) evaluated an 850kW wind turbine energy generation and exergy performance in UAE. They concluded that the exergy analysis was more useful to describe the irreversibility. Caliskan et al. (2013) examined the energy and exergy performance of a hybrid system based on hydrogen, electricity production and storage systems. They evaluated various subsystems such as geothermal, wind, photovoltaic panels and proton exchange membrane fuel cell. The overall exergy efficiency of the evaluated systems was found in the range of 5.838% and 5.865%, depending on the dead state temperature. Kalinci et al. (2017) focused on a hybrid system consisted of a photovoltaic array, wind turbines, an electrolyzer, a polymer electrolyte membrane fuel cell, a hydrogen tank and a converter. They made energy exergy analyses for the system, which was evaluated for a stand-alone island model. They used HOMER software for economic and energy load distributions. The energy and exergy efficiency of the wind turbine was reported to be 46% and 50.12%, respectively. Lamas (2017) presented the irreversibilities throughout a wind power system. The evaluation of a wind turbine exergetic values was performed and economic analysis of the system was also accomplished. Mohammadi et al. (2017) analysed energy and exergy efficiency of a combined cooling, heating and power system coupled with a wind turbine and compressed air energy storage system. They concluded that the maximum exergy destruction occurred in wind turbine, combustion chamber and compressed air energy storage system. Aghbashlo et al. (2018) examined the exergetic performance of a wind power plant in Iran. The exergy efficiency of the plant was found to be 63.82% and 15.76% according to standard exergy and extended exergy accounting analyses.

In this study, two wind turbine installation alternatives for a residential district of 20 detached houses in Izmir, Turkey were taken into account. The first alternative was the installation of individual residential scale (5kW) wind turbine for each house. As a second alternative the installation of a single unit wind turbine having the same total installed capacity (100kW) was evaluated for the district. The alternatives were compared according to their annual energy production. Additionally, exergy efficiencies of both systems were demonstrated. The results showed that the single 100kW wind turbine was advantageous both in energy production and exergy efficiency aspects.

2. SYSTEM DESCRIPTION

A district consisting of 20 detached, single-storey houses was the focus of the present study. In order to meet the electricity needs of each house, two alternative wind energy systems were evaluated. In Case 1, a 5kW individual wind turbine installation for each house was considered, while in Case 2, a single 100kW wind turbine installation, which supplied the electricity needs of all the houses, was evaluated. A schematic view of Case 1 is illustrated in Figure 1. Similarly, the schematic view of Case 2 is given in Figure 2.
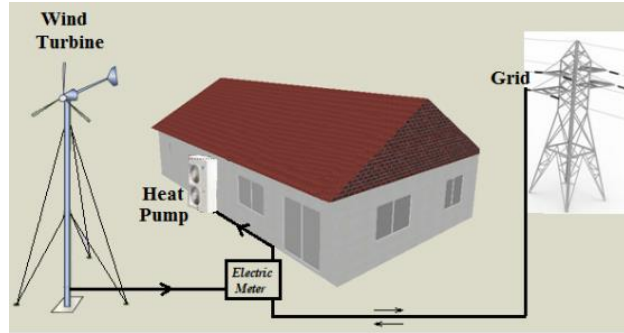
Figure 28: Schematic view of a single 5 kW wind turbine and the evaluated house (Case 1)
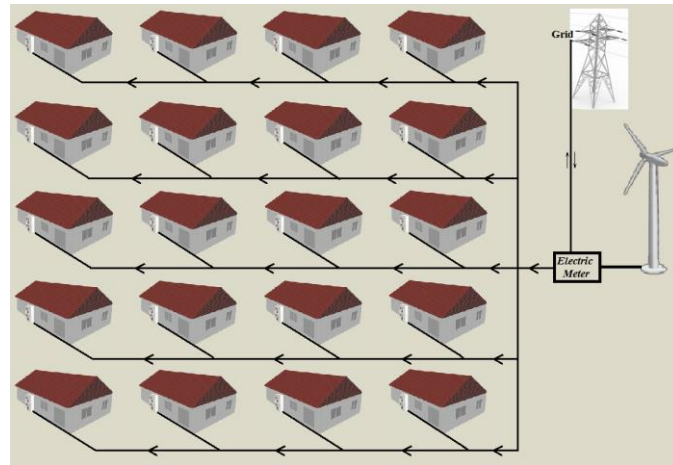

Figure 2: Schematic view of a single 100 kW wind turbine and 20 houses (Case 2)

Each considered single-storey house had 117 m² floor area and its construction components with their overall heat transfer coefficients (U) are presented in Table 1.

Table 1: Overall heat transfer coefficient (U) for construction components

U-Values (W/m²K)			
Wall	Roof/Ceiling	Floor	Window
0.70	0.45	0.70	2.4

Four people were assumed to live in the considered house and the occupancy and operation schedules were taken as the default values determined in DesignBuilder software (Design builder, 2022). The design temperature of the inside air was taken as 20°C and 26°C for winter and summer, respectively. The change of outside air and the frequency of different temperatures for İzmir, taken from Meteonorm software (Meteonorm, 2022), are illustrated in Figure 3.
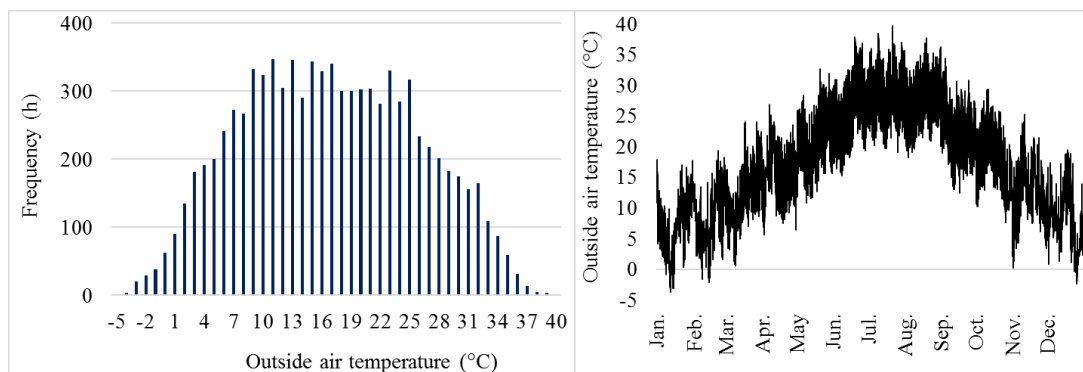

Figure 3: Outside temperature for İzmir, Turkey.

The electrical energy need of a single house was targeted to be met by a 5kW wind turbine in Case 1, while the needs of all 20 houses was to be met by a single 100kW wind turbine in Case 2. The characteristic properties of two wind turbines are listed in Table 3.

Table 3: Wind turbine characteristics (Front Generator Wind Turbine-a, b, 2022)

Specification	Unit	Case 1	Case 2
Rated Power	kW	5	100
Cut-In Speed	m/s	3	3
Rated Speed	m/s	12	12
Cut-Out Speed	m/s	25	25
Hub Height	m	12	18
Rotor Diameter	m	6.4	20.8
Swept Area	m^2	32.17	339.8

3. POWER GENERATION OF A WIND TURBINE

The hourly wind speed values for İzmir, taken from Meteonorm software were used in order to calculate the hourly electricity generation of selected wind turbines. The following procedure, also summarized in Figure 4, was implemented in the calculation:

- The wind turbine did not generate any power when the wind speed was below cut-in or above cut-out wind speed for the wind turbine;
- Wind turbine generation increased with the increasing wind speed when the wind speed was between cut-in and rated wind speed values of the wind turbine.
- The wind turbine generated maximum (rated) power when the wind speed was between rated and cut-out wind speed values for the wind turbine.

As the wind speed measurements were made at a height of 10m, wind speed values at turbine hub heights (12m for 5kW wind turbine and 18m for 100kW wind turbine) were calculated using Hellmann relation, given by Equation (1) (Hepbasli and Alsuhaibani, 2011)

Equation 8: wind speed
$$v = v_{ref} \times \left[\frac{z}{z_a}\right]^{\mu}$$

Where:

- v = wind speed values at turbine hub heights (m/s)
- v_{ref} = wind speed values at measurement heights (m/s)
- Z = wind turbine hub height (m)
- z_a = height of wind speed measurement (m)
- μ = Hellmann exponent

The Hellmann exponent (μ) is related to terrain type and it was taken as 0.3 in the present study for a region which was inhabited (small town with some trees and shrubs) (Ruedas et al., 2011).
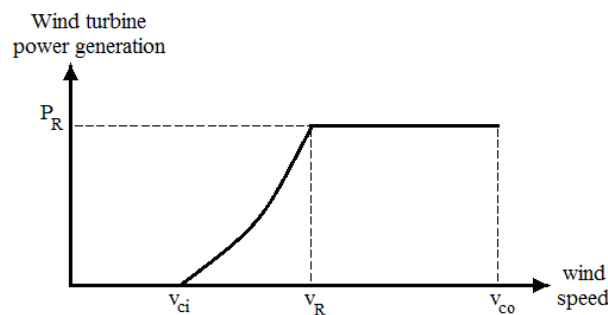

Figure 4: Power generation of a wind turbine

The mathematical expression of the given procedure is given with Equation (2) (Johnson, 2006):

Equation 2: Power generation

$$P = \begin{cases} 0 & when\ v < v_{ci} \\ a + bv^k & when\ v_{ci} \le v \le v_R \\ P_R & when\ v_R \le v \le v_{co} \\ 0 & when\ v > v_{co} \end{cases}$$

Where:

$$a = \frac{P_R v_{ci}^k}{v_{ci}^k - v_R^k} \text{ and } b = \frac{P_R}{v_R^k - v_{ci}^k}$$

- P = power (kW)
- v_{ci} = cut-in wind speed (m/s)
- v_{co} = cut-out wind speed (m/s)
- v_R = rated wind speed (m/s)
- P_R = rated power (kW)
- k = shape parameter (-)

The shape parameter (k) of Weibull distribution function, given by Equation (3) is needed in power generation calculations.

Equation 3: Weibull distribution function

$$f(v) = \left(\frac{k}{c}\right)\left(\frac{v}{c}\right)^{k-1} exp\left[-\left(\frac{v}{c}\right)^k\right]$$

Where:

- c = scale parameter (m/s)

Measured wind speed values at 10m height were used and the maximum likelihood method, given by Equation (4) (Bilir et al., 2015), was implemented to find the shape parameter:

Equation 4: shape parameter

$$k = \left[\frac{\sum_{i=1}^{n} v_i^k \ln(v_i)}{\sum_{i=1}^{n} v_i^k} - \frac{\sum_{i=1}^{n} \ln(v_i)}{n}\right]^{-1}$$

Where:

- $n = \dfrac{[0.37 - 0.088 \times lnc_a]}{\left[1 - 0.088 \times ln\left(\frac{z_a}{10}\right)\right]}$

After the determination of the shape parameter, the scale parameter (c) was calculated by Equation (5):

Equation 5: scale parameter

$$c = \left(\frac{1}{n}\sum_{i=1}^{n} v_i^k\right)^{1/k}$$

Since the hub height of the evaluated wind turbines were different than 10m, the shape and scale parameters at the wind turbine hub heights were calculated with Equations 6 and 7 (Tar, 2008):

Equation 6 & 7: the shape and scale parameters at the wind turbine hub heights

$$k_z = k_a \times \frac{\left[1 - 0.088 \times ln\left(\frac{z_a}{10}\right)\right]}{\left[1 - 0.088 \times ln\left(\frac{z}{10}\right)\right]}$$

$$c_z = c_a \times \left(\frac{z}{z_a}\right)^n$$

Where:

- c_a = scale parameter at measurement height (-)
- c_z = scale parameter at wind turbine hub height (-)
- k_a = shape parameter at measurement height (-)
- k_z = shape parameter at wind turbine hub height (-)

Wind turbine power generation calculations were accomplished with the hourly wind speed values and Weibull distribution function parameters obtained for the hub height of the relevant wind turbine.

4. EXERGY EFFICIENCY OF A WIND TURBINE

Exergy analysis of any system is employed to evaluate the thermodynamic imperfection of the system. For this reason, exergy efficiency of the selected wind turbines was also calculated as well as their energy generation. Exergy efficiency for a wind turbine can be written as given in Equation (8) (Hepbasli and Alsuhaibani, 2011):

Equation 8: Exergy efficiency

$$\varepsilon = \frac{\dot{E}x_{out}}{\dot{E}x_{in}}$$

Where:

- ε = exergy efficiency (%)
- $\dot{E}x_{in}$ = input exergy rate (kW)
- $\dot{E}x_{out}$ = output exergy rate (kW)

The output exergy of the wind turbine is the electrical power it generates and the input exergy rate for the wind turbine can be calculated by Equation (9) if the air is assumed to be a perfect gas (Hepbasli and Alsuhaibani, 2011):

Equation 9: input exergy rate

$$\dot{E}x_{in} = \dot{m} \times \left\{c_{p,a} \times \left[T_{in} - T_0 - T_0 \times ln\left(\frac{T_{in}}{T_0}\right)\right] + R_a \times T_0 \times ln\left(\frac{P_{in}}{P_0}\right)\right\}$$

Where:

- $\dot{m}$ = mass flow rate (kg/s)
- $c_{p,a}$ = specific heat of air (kJ/kgK)
- P_{in} = inlet pressure (kPa)
- P_0 = dead state pressure (kPa)
- R_a = gas constant (kJ/kgK)
- T_{in} = inlet temperature (°C)
- T_{out} = dead state temperature (°C)

The inlet temperature values in Equation (9) were calculated as wind chill temperature given by Hepbasli and Alsuhaibani (2011). Temperature and wind speed values in Equation (10) were taken in °F and mph, respectively.

Equation 10: wind chill temperature

$$T_{windch} = 35.74 + 0.6215 \times T_a - 35.75 \times (v)^{0.16} + 0.4274 \times T_a \times (v)^{0.16}$$

Where:

- T_{windch} = wind chill temperature (°C)
- T_a = air temperature (°F)
- v = wind speed (mph)

The inlet pressure value in Equation (11) is determined as (Sahin et al., 2006):

Equation 11: inlet pressure

$$P_{in} = P_0 + \frac{v^2}{2}$$

The atmospheric (dead state) pressure (P_0) and temperature (T_0) were taken as 101.325 (kPa) and 25 (°C) in this study.

5. RESULTS AND DISCUSSION

The heating and cooling energy needs of the evaluated house and domestic hot water was calculated with Design Builder software on a monthly basis and is summarized in Table 4.

The house was assumed to be air conditioned with a heat pump and domestic hot water was also assumed to be supplied by the heat pump. The coefficient of performance value of the heat pump was taken as 4 in heating and 3 in cooling. Additionally, the lighting and other equipment electricity requirements were added in the total electrical energy needs of the house. The electricity was assumed to be supplied by the wind turbine as long as its generation was sufficient to cover the demand. If the wind turbine electricity supply was not sufficient, additional energy could be taken from the grid. Conversely, if the energy generation of the wind turbine was excessive, the surplus energy can be fed into the grid. The monthly and annual electrical energy demand of the house was determined by the explained assumptions and presented in Table 5. It can be seen from Table 5 that the maximum electricity need in January was 360.5 kWh, while a minimum 195.2 kWh electricity requirement was present in October. The annual electrical energy need of a single house was determined as 3,360.6 kWh.

Table 4: Heating and cooling energy needs of the evaluated house

Month	Heating Need (kWh)	Cooling Need (kWh)
January	698.6	0.0
February	650.0	0.0
March	416.7	0.0
April	132.3	0.0
May	6.5	59.6
June	0.0	294.5
July	0.0	358.7
August	0.0	332.4
September	0.0	169.2
October	36.2	0.0
November	405.3	0.0
December	691.1	0.0
Annual	**3,036.8**	**1,214.3**

Table 5: Electrical energy need of a single house and twenty houses

Month	Electrical Energy Need (kWh)	
	Single House	Twenty Houses
January	360.5	7,210
February	331.0	6,620
March	291.6	5,832
April	213.2	4,264
May	207.3	4,146
June	279.8	5,596
July	305.4	6,108
August	297.5	5,950
September	237.3	4,746
October	195.2	3,904
November	282.2	5,644
December	359.4	7,188
Annual	**3,360.6**	**67,212**

5.1. Energy analysis of the wind turbines and coverage ratio values

The present study aimed to evaluate how much of the electrical energy need of the evaluated twenty houses could be met by the proposed wind turbines. The hourly power and energy generation of the wind turbines were calculated and their monthly generation is given in Table 6, for simplicity. The values are also presented in Figure 5 in order to make the comparison of two systems easier.

Table 6: Electrical energy generation of the proposed wind turbines

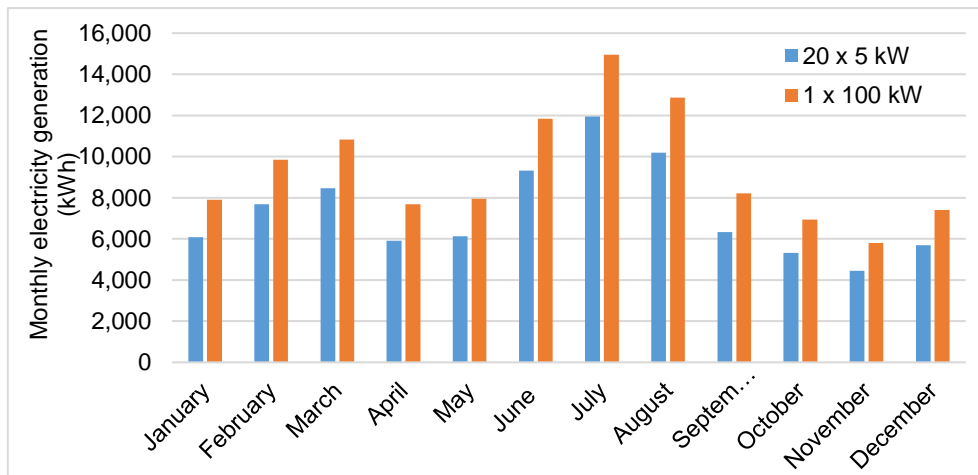| Month	Electrical Energy Generation (kWh)	
	20 x 5 kW wind turbines	1 x 100 kW wind turbine
	(Case 1)	(Case 2)
January	6,086.1	7,907.3
February	7,684.6	9,839.6
March	8,459.7	10,829.7
April	5,907.7	7,687.8
May	6,133.1	7,953.1
June	9,313.3	11,832.9
July	11,944.3	14,944.3
August	10,193.5	12,872.9
September	6,333.1	8,207.9
October	5,320.6	6,940.6
November	4,446.3	5,808.7
December	5,691.0	7,409.0
Annual	**87,513.3**	**112,233.8**

Figure 5: Electrical energy generation of twenty 5 kW turbines and a single 100 kW turbine

It can be easily seen that both wind turbine systems could supply the whole electrical energy need of the district composed of twenty houses and could even generate surplus energy. The monthly and annual coverage ratio of the required electrical energy of the district is summarized in Table 7.

Table 7: Electrical energy need coverage for Case 1 and Case 2

Month	Electrical Energy Need of 20 Houses (kWh)	Electrical Energy Generation of Wind Turbine(s) (kWh)		Coverage Ratio (%)	
		Case 1	Case 2	Case 1	Case 2
January	7,210	6,086.1	7,907.3	84.4	109.7
February	6,620	7,684.6	9,839.6	116.1	148.6
March	5,832	8,459.7	10,829.7	145.1	185.7
April	4,264	5,907.7	7,687.8	138.5	180.3
May	4,146	6,133.1	7,953.1	147.9	191.8
June	5,596	9,313.3	11,832.9	166.4	211.5
July	6,108	11,944.3	14,944.3	195.6	244.7
August	5,950	10,193.5	12,872.9	171.3	216.4
September	4,746	6,333.1	8,207.9	133.4	172.9
October	3,904	5,320.6	6,940.6	136.3	177.8
November	5,644	4,446.3	5,808.7	78.8	102.9
December	7,188	5,691.0	7,409.0	79.2	103.1
Annual	**67,212**	**87,513.3**	**112,233.8**	**130.2**	**167.0**

The single 100kW wind turbine was found to generate 24,720.5 kWh more energy than twenty individual 5kW wind turbine. Additionally, the single 100kW wind turbine generated sufficient electricity for the district across all months. However, the single 5kW wind turbines were found to be insufficient for January, November and December. As a result the use of a single wind turbine was more efficient and profitable for the district in an energy generation aspect.

5.2. Exergy efficiency analysis of the wind turbines

The exergy efficiency of a 5kW and a 100kW wind turbine, defined by Equation 8, were calculated with the wind speed values and outside temperature values obtained from Meteonorm software. The results are presented in Figure 6.
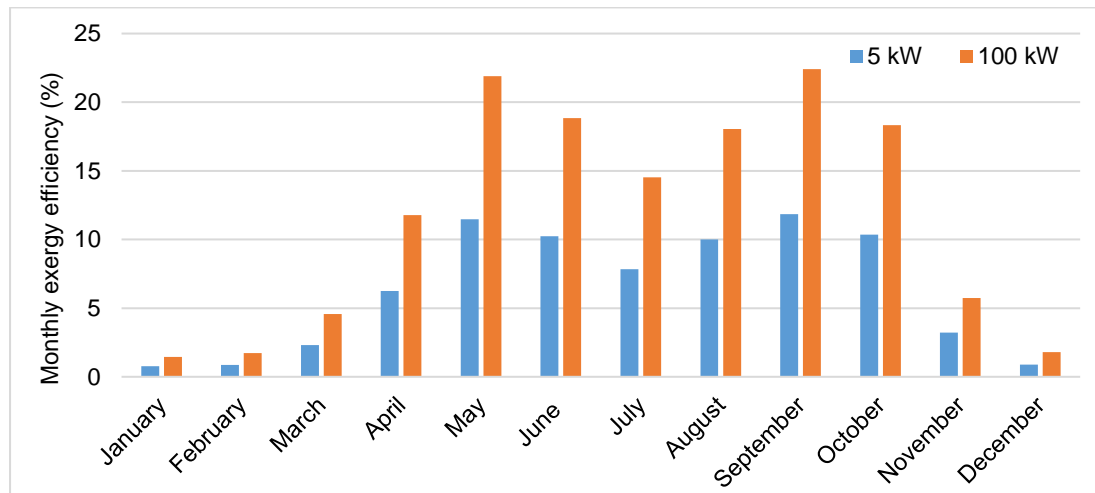

Figure 6: Exergy efficiency of a 5 kW turbine and a 100 kW turbine

The results showed that the single 100kW wind turbine was also superior than a 5kW wind turbine exergetically. A maximum 22.41% exergy efficiency was observed in September for the 100kW wind turbine and the minimum exergy efficiency of this turbine was found to be 1.44% in January. Nevertheless, for the 5kW wind turbine, the maximum and minimum exergy efficiencies were 11.84% and 0.76% for the same months, respectively. The exergy efficiency was found to be higher in May, June, August, September and October in both cases, while very low exergy efficiency values were encountered in January, February and December in both cases.

6. CONCLUSION

A district, consisted of twenty identical single-storey houses, each with a 117 m² floor area, was taken into consideration in this study. The heating, cooling and domestic water heating values of the houses were computed using Design Builder software. The heating and cooling were assumed to be performed by a heat pump with a COP value of 4 in heating and 3 in cooling. Consequently, the electrical energy needs of the house with a heat pump was calculated. The total electrical energy needs of the house was determined by adding lighting and other equipment usage. As the houses were identical, the electricity needs of a single house was multiplied by twenty in order to determine the district electrical energy needs. Two cases were proposed to supply the district with electricity. In Case 1, a 5kW wind turbine installation for each house was considered, while in Case 2, a single 100kW wind turbine was evaluated to cover the electricity needs of the whole district. The characteristics of these turbines were equal except the rated power and hub height values. Although the annual electrical energy needs of the district was covered for both cases, the results showed that the use of single 100kW wind turbine was advantageous both energetically and exergetically. In addition, it was found that when a single 100kW wind turbine was used, the total electrical energy need of the district could be met for all months. However, in the case of individual 5kW wind turbine use, the necessary electrical energy could not be fully met in January, November or December. The exergy efficiency of the 100kW turbine was also found to be higher than the exergy efficiency of the 5kW turbine for all months. Under the light of these results, it was concluded that for small communities or districts, the use of a single wind turbine with an adequate capacity was better that the use of individual residential scale wind turbines.

7. REFERENCES

Aghbashlo, M., Tabatabaei, M., Hosseini, S. S., Dashti, B. B., Soufiyan, M. M., 2018. Performance Assessment of a Wind Power Plant Using Standard Exergy and Extended Exergy Accounting (EEA) Approches, Journal of Cleaner Production, Vol. 171, pp 127-136.

Bilir, L., İmir, M., Devrim, Y., Albostan, A., 2015. Seasonal and Yearly Wind Speed Distribution and Wind Power Density Analysis Based on Weibull Distribution Function, International Journal of Hydrogen Energy, Vol. 40, pp 15301-15310.

Caliskan, H., Dincer, I., Hepbasli, A., 2013. Energy, Exergy and Sustainability Analyses of Hybrid Renewable Energy Based Hydrogen and Electricity Production and Storage Systems: Modelling and Case Study, Applied Thermal Engineering, Vol. 61, pp 784-798.

Design Builder & Energy Plus software programs, 2022. Design Builder Software Ltd., United Kingdom. Design Builder& Energy Plus software library, https://www.designbuilder.co.uk/, (access in 2022).

Front Generator Wind Turbine-a, 2022. 5 kW wind turbine web site http://www.allwindturbine.com/products_info/H6-4-5kw-grid-tied-wind-generator-system-130620.html (access in 2022).

Front Generator Wind Turbine-b, 2022. 100 kW wind turbine web site http://www.allwindturbine.com/products_info/H19-2-100KW-Grid-Tied-Wind-Turbine-230239.html (access in 2022).

Hepbasli, A., Alsuhaibani, Z., 2011. Exergetic and Exergoeconomic Aspects of Wind Energy Systems in Achieving Sustainable Development, Renewable and Sustainable Energy Reviews, Vol. 15, pp 2810-2825.

Johnson, G.L. 2006. Wind Energy Systems. University Reprints.

Kalinci, Y., Dincer, I., Hepbasli, A., 2017. Energy and Exergy Analyses of a Hybrid Hydrogen Energy System: A Case Study for Bozcaada, International Journal of Hydrogen Energy,   Vol. 42, pp 2492-2503.

Koroneos, C., Spachos, T., Moussiopoulos, N., 2003. Exergy Analysis of Renewable Energy Sources, Renewable Energy, Vol. 28, pp 295-310, 2003.

Lamas, W. Q. 2017. Exergo-Economic Analysis of a Typical Wind Power System, Energy,   Vol. 140, pp 1173-1181.

Meteonorm, 2022. Global Meteorological Database Version 7 Software and Data for Engineers, Planers and Education, http://www.meteonorm.com/ (access in 2022).

Mohammadi, A., Ahmadi, M. H., Bidi, M., Joda, F., Valero, A., Uson, S., 2017. Exergy Analysis of a Combined Cooling, Heating and Power System Integrated with Wind Turbine and Compressed Air Energy Storage System, Energy Conversion and Management, Vol. 131,   pp 69-78.

Ozgener, O., Ozgener, L., 2007. Exergy and Reliability Analysis of Wind Turbine Systems: A Case Study, Renewable and Sustainable Energy Reviews, Vol. 11, pp 1811-1826.

Redha, A. M., Dincer, I., Gadalla, M., 2011. Thermodynamic Performance Assessment of Wind Energy Systems: An Application, Energy, Vol. 36, pp 4002-4010.

Ruedas, F. B., Camacho, C. A., Marcuello, S. R., 2011. Wind Farm - Technical Regulations, Potential Estimation and Siting Assessment, edited by Suvire, G. A., in Chapter 4, InTech. (https://www.intechopen.com/books/wind-farm-technical-regulations-potential-estimation-and-siting-assessment/methodologies-used-in-the-extrapolation-of-wind-speed-data-at-different-heights-and-its-impact-in-th)

Şahin, A. D., Dincer, I., Rosen, M. A., 2006. Thermodynamic Analysis of Wind Energy, International Journal of Energy Research, Vol. 30, pp 553-566.

Tar, K., 2008. Some Statistical Characteristics of Monthly Average Wind Speed at Various Heights, Renewable and Sustainable Energy Reviews, Vol. 12, pp 1712-1724.